THE UNIVERSITY OF OKLAHOMA

GRADUATE COLLEGE

GEOLOGICAL AND PALEONTOLOGICAL INVESTIGATIONS OF THE UPPER JURASSIC MORRISON FORMATION AT THE BASIN MARGINS OF CENTRAL MONTANA AND THE WESTERN PANHANDLE OF OKLAHOMA

A DISSERTATION

SUBMITTED TO THE GRADUATE FACULTY

in partial fulfillment of the requirements for the

Degree of

DOCTOR OF PHILOSOPHY

By

DEAN ROBERT RICHMOND
Norman, Oklahoma

2020

GEOLOGICAL AND PALEONTOLOGICAL INVESTIGATIONS OF THE UPPER JURASSIC MORRISON FORMATION AT THE BASIN MARGINS OF CENTRAL MONTANA AND THE WESTERN PANHANDLE OF OKLAHOMA

A DISSERTATION APPROVED FOR THE

SCHOOL OF GEOSCIENCES

BY THE COMMITTEE CONSISTING OF

Richard Lupia II, Chair

John Pigott

Matthew Pranter

Richard Cifelli

Judith Totman Parrish

TABLE OF CONTENTS

ABSTRACT

During the past century, the research focus area of the Morrison Formation has been the Colorado Plateau. There are two main reasons for the research emphasis in the region. First, the Colorado Plateau contains world-class exposures of the formation. Second, the majority of Morrison Formation vertebrate sites (dinosaur quarries) are located within its boundaries. Due to the emphasis where the formation is well-exposed, the geology and paleontology of the Morrison Formation at the basin margins has not received much attention from researchers. The focus of this project is to investigate two different regions of the Morrison foreland basin margin and research the geology and paleontology of these areas.

Exposures of the Morrison Formation are limited in central Montana. Relatively recent dinosaur discoveries in the northern portion of the basin resulted in an investigation of the formation in the region. The investigation led to the discovery, description, and first confirmed occurrences of the fossil wood *Xenoxylon meisteri* in the Upper Jurassic of North America. In addition to the fossil wood *Xenoxylon*, numerous carbonate mound springs were discovered and are described. These carbonate tufa deposits are the first recorded occurrences for the Morrison Formation and are some of the oldest tufa deposits in North America. The presence of *Xenoxylon* and the carbonate mound springs have paleoclimatic significance for the northern basin margin. Whereas climate models for the Morrison Formation on the Colorado Plateau suggest that it was hot and dry, the presence of *Xenoxylon* and the mound springs in central Montana indicate a higher precipitation rate and likely cooler temperatures than more southern regions.

The second basin margin investigated was the western panhandle of Oklahoma. The Morrison Formation in the western portion of the state is divided into three newly formed members (Cimarron, Boise, and Kenton) that likely correlate with the three main members of the Colorado

Plateau (Tidwell, Salt Wash, and Brushy Basin). The three Oklahoma Morrison members are the lateral distal depositional facies of each of the members of the Colorado Plateau. The depositional facies and climatic proxies (e.g. *Xenoxylon*) of the new members of the Morrison Formation in Oklahoma each recorded a distinct climatic interval. Overall, the climate of the Morrison Formation in Oklahoma was more temperate and wetter than the Colorado Plateau.

ACKNOWLEDGMENTS

The research project was supported by the Sam Noble Museum of Natural History and the Oklahoma University School of Geosciences. I extend my gratitude to my committee members, Dr. Richard Lupia, Dr. Richard Cifelli, Dr. John Pigott, Dr. Matthew Pranter (University of Oklahoma), and Dr. Judith Totman Parrish (University of Idaho emerita), for their time, support, and guidance during this process. I extend warm appreciation to my co-authors, Marc Philippe, Tyler Hunt, Michael Behm, and Jason Klimek. Each of you made indispensable contributions to this research. Thank you.

I am grateful to Nate Murphy of the Judith River Dinosaur Institute for his friendship and never-ending support. I enjoyed our many hours discussing the Morrison Formation of central Montana by the campfire. I wish to thank David and Rosalie Hein for their lifelong friendship and their continued support and interest in the Morrison Formation research of central Montana. I am grateful to the many ranchers in the remote area of the Oklahoma panhandle for access to their lands to perform this geologic evaluation. In particular, I sincerely thank Monty Joe and Vickie Roberts of Kenton, Oklahoma for their friendship and support during this project. Finally, I cannot adequately express my appreciation and gratitude for the support and patience of my loving wife, Deana Richmond, and my children; without their support, this goal could not have been achieved.

CHAPTER 1: INTRODUCTION

The Upper Jurassic Morrison Formation has been studied intensely since the first discovery of dinosaurs in the newly opened American West. These fascinating animals have captured the imagination of fossil hunters, scientists, and the general public for more than a century. The Morrison Formation is an expansive formation with surface exposures in many states of the U.S. intermountain west. Late Jurassic dinosaurs have been discovered in every U.S. state where the Morrison Formation is exposed. Since the Bone Wars of the 1870's, scientific research has focused on numerous aspects of the dinosaurs and the formation to understand the fauna, flora, stratigraphy, depositional facies, tectonics, paleoclimate, age of the formation, etc. The formation is well exposed on the Colorado Plateau in Utah, Colorado, Arizona, and New Mexico. This same region contains the majority of dinosaur excavation sites. Additional excavations are scattered throughout the intermountain west in central New Mexico, the western Oklahoma panhandle, eastern Colorado and Wyoming, southwestern South Dakota, and central Montana (fig. 1).

The Morrison Formation is composed of terrestrial sediments deposited into a foreland basin. The Morrison foreland basin is the product of an orogenic belt that formed along the western North American plate boundary during the Jurassic Period. The tectonics and timing of the northward prograding orogenic belt, and the sediments derived from the event, remain the topic of research. In general, the stratal depositional packages of the formation are thickest in the west and thin toward the basin margins. At the eastern basin periphery, the Morrison Formation is only present in the subsurface. It is difficult to determine if the basin margin's zero-edge was from depositional onlap onto the craton or a product of post depositional uplift and erosion based on the interpretation of the well log data.

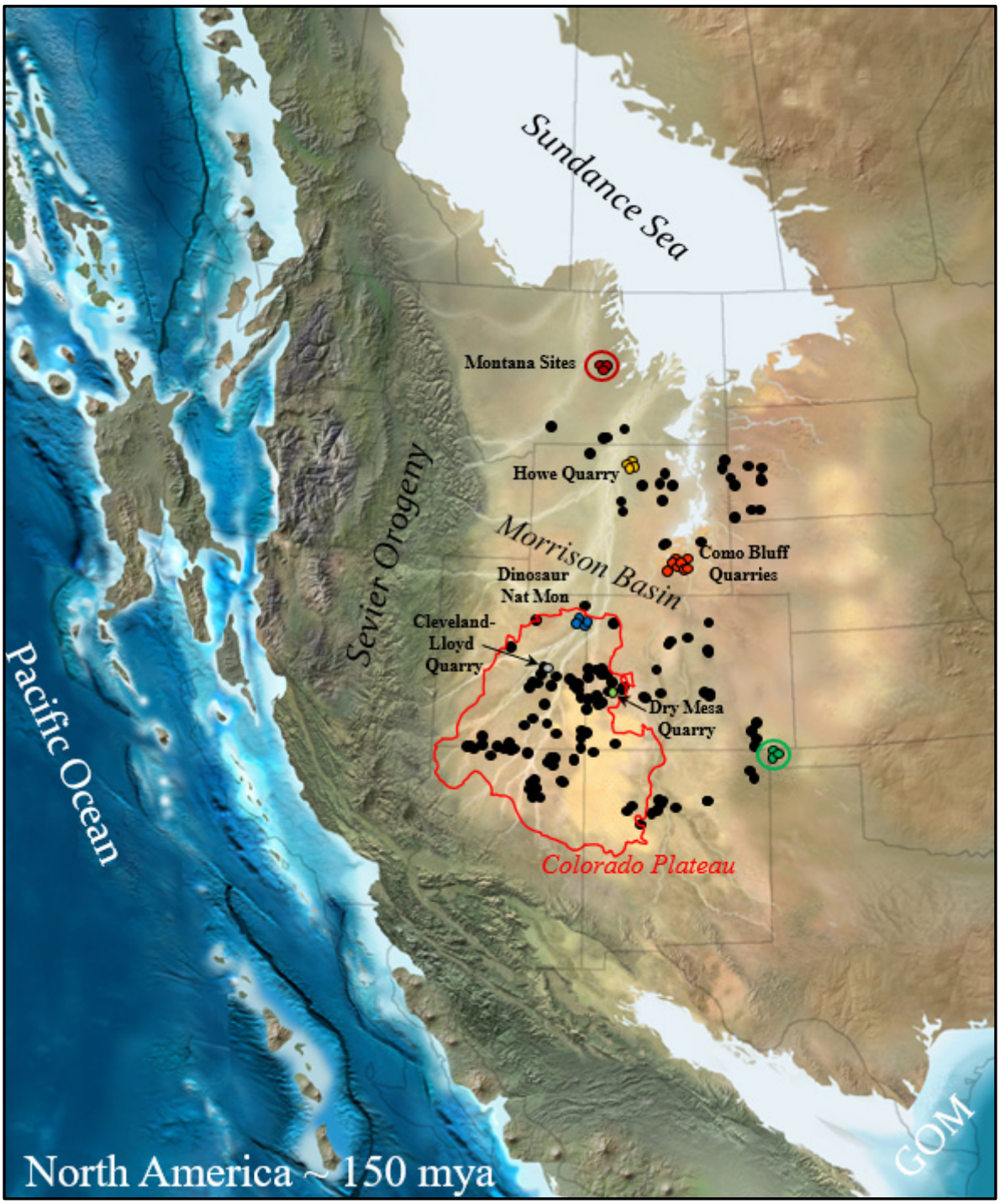

Figure 1. Map of the Late Jurassic of North America showing numerous dinosaur sites of the Morrison Formation. A few prominent quarries have been highlighted. The research areas of central Montana and western Oklahoma are circled red and green, respectively. Each research area is located at a distinctly different margin of the Morrison Formation foreland basin. Image modified from R. Blakey.

The recent discovery of dinosaur bones in the Morrison Formation of central Montana sparked research interest in the area. Preliminary investigations into the geology, paleontology, and paleobotany revealed the formation was distinctive from that of the Colorado Plateau. Initial paleontological evaluations suggest that some dinosaurs may represent different genera than those typically found in more southern regions. The abundance of petrified wood and the discovery of carbonate buildups (mound springs) in the formation implies that the climate was wetter than the Colorado Plateau.

Whereas the Morrison strata in central Montana are some of the northernmost exposures of the formation, the strata present in the western panhandle of Oklahoma are some of the easternmost surface outcrops of the formation. In contrast to the recently discovered dinosaurs of Montana, the dinosaur fossils of the western panhandle of Oklahoma were discovered during the early 1930's. However, since the Oklahoma fossil discoveries the Morrison Formation in the panhandle has received negligible attention from researchers.

Purpose of Study

Both areas (central Montana and western Oklahoma) provide the prospect of comparing and contrasting the Morrison Formation of the Colorado Plateau to the basin periphery. The Colorado Plateau has been intensively studied due to its distinct well-exposed strata. Therefore, the Colorado Plateau region is often used as the standard by which many of the aspects of the formation are interpreted. This research project is composed of three seemingly unrelated projects, but together add to the knowledge base of the Morrison Formation at the basin periphery. These chapters, each a complete project, are also a foundation for supplemental research to further unravel the geological, paleontological, and paleoclimatic history of these unique basin regions.

Chapter 2 presents the results of an investigation of the petrified wood *Xenoxylon meisteri*, discovered in the Morrison Formation of central Montana. This new discovery is the first representation of the genus and species in the Jurassic Period of North America. Six samples of the wood are quantitively described and compared to all other referenced "*Xenoxylon*" wood from North America. Paleoclimate implications are discussed.

Chapter 3 summarizes the geological investigation of 99 unusual terrestrial carbonate buildups. The buildups are sampled, mapped, and analyzed to determine their origin. Their paleoclimatic implications are discussed.

Chapter 4 relates the study of the Morrison Formation in the western panhandle of Oklahoma and is a review of the stratigraphy, sedimentology, depositional facies, and vertebrate taphonomy with paleoclimatic inferences based on the geology and taphonomy. Three new formation members are named and described. The Morrison depositional facies at the eastern basin margin are related to the coeval facies of the Colorado Plateau.

CHAPTER 2

First occurrence of the boreal fossil wood *Xenoxylon meisteri* from the Jurassic of North America: Morrison Formation of central Montana, USA

Dean Richmond [a], Richard Lupia [b], Marc Philippe [c], Jason Klimek [d]

[a] *ConocoPhillips School of Geology and Geophysics, Sarkeys Energy Center Suite 710, University of Oklahoma, Norman, OK 73019*
[b] *Sam Noble Museum, University of Oklahoma, 2401 Chautauqua Avenue, Norman, OK 73072*
[c] *Université Lyon 1, CNRS, UMR 5023 LEHNA, F-69622 Villeurbanne, France*
[d] *Department of Geological Sciences, S389 Eyring Science Center, Brigham Young University, Provo, UT 84602*

Published: Review of Palaeobotany and Palynology, August 2019
https://doi.org/10.1016/j.revpalbo.2019.05.001

ABSTRACT

Six specimens of the fossil wood *Xenoxylon meisteri* were discovered in the Upper Jurassic Morrison Formation of central Montana and are described herein. The discovery represents the first confirmed occurrence of the species *X. meisteri* in North America. In addition, we review all occurrences of petrified wood attributed to *Xenoxylon* from North America. Early to Late Jurassic *X. phyllocladoides* specimens of Greenland are accepted. Previously reported occurrences of *Xenoxylon* from the Lower Jurassic Navajo Sandstone of Utah, *Xenoxylon morrisonense* Medlyn and *X. moorei* Tidwell from the Upper Jurassic Morrison Formation of Utah, and fossil woods reported from the Lower Cretaceous Cloverly (Wyoming) and McMurray Sandstone (Alberta, Canada) formations have secondary xylem characteristics incongruous with the genus and are discounted. The remaining accepted specimens are Cretaceous in age from the Canadian Arctic (Valanginian) and the North Slope of Alaska (Albian and Maastrichtian). Thus, these new Montana specimens of *Xenoxylon* are the earliest and southernmost occurrences of the genus in continental North America. Global distribution and paleoecology strongly imply *Xenoxylon* was constrained to

cool/wet climates. Thus, these lower latitude North American occurrences corroborate other proxies indicating a cooler wetter climate, at least locally/briefly, in the northern portion of the Upper Jurassic Morrison foreland basin.

1. Introduction

Xenoxylon was first described by Gothan (1905) for Late Jurassic wood from the Norwegian archipelago of Svalbard (Arnold, 1952; Suzuki and Terada, 1992). Distinctive anatomical features of the genus are the contiguous obround radial bordered pits with one, rarely two, pits in the fenestriform cross-field (Oh et al., 2015). The occurrence of sequences of flattened pits is considered an apomorphic character by Philippe (1993); accordingly, the genus *Xenoxylon* may be regarded as monophyletic. Thirty-three species of *Xenoxylon* have been proposed from across the northern hemisphere (Zheng et al., 2008; Philippe et al., 2013; Feng et al., 2015; Wan et al., 2016). Most species and occurrences are restricted to Far East Asia (Oh et al., 2015). In 2013, Philippe et al. created three informal sub-generic morphogroups ("*latiporosum*", *phyllocladoides*", and "*meisteri*") and reduced the number to 11 valid species. *Xenoxylon* is known from fossil secondary xylem without known extant relatives (Philippe and Thévenard, 1996). No fossil foliage or reproductive structures have yet been found connected to the wood (Oh et al., 2015). However, *Xenoxylon* is regularly associated with isolated foliage of the Miroviaceae family (Manum et al., 2000; Marynowski et al., 2008). The phylogenetic position of the genus is uncertain (Philippe and Thévenard, 1996; Ding et al., 2000; Marynowski et al., 2008), but geochemical analysis designates a closer affinity to Podocarpaceae than to Pinaceae or Araucariaceae (Marynowski et al., 2008).

The genus is reported from Late Triassic through Late Cretaceous deposits (Oh et al., 2011; Oh et al., 2015). The earliest occurrences of *Xenoxylon* are from Triassic-age formations of the Far

East (Kim et al., 2005; Oh et al., 2011; Tian et al., 2016; Wan et al., 2016), implying *Xenoxylon* evolved in the region during the Triassic (Khudaiberdyev, 1993) and spread to other areas of the world during the Jurassic (Khudaiberdyev, 1993; Morgans, 1999; Tian et al., 2015) and Cretaceous periods (Parrish and Spicer, 1988; Terada et al., 2011; Afonin and Philippe, 2014). The genus is abundant and widespread in Europe and Asia, but is scarce in North America (Arnold, 1952; Parrish and Spicer, 1988; Spicer and Parrish, 1990; Selmeier and Grosser, 2011). Based on global compilations of generic occurrences, co-occurring (wood) taxa and sedimentological proxies, the presence of *Xenoxylon* is a strong indicator of a cool and wet climate in the northern hemisphere during the Mesozoic (Philippe and Thévenard, 1996; Philippe et al., 2009; Tian et al., 2016, Philippe et al., 2017).

2. Material and methods

The fossil wood specimens, one from a preserved log (West Tufa specimen) and the others from discrete accumulations of petrified wood fragments, were collected by the senior author and cut transversely, tangentially, and radially for thin-section observation. Thin sections prepared by Wagner Petrographic (Lindon, Utah) were examined under a light microscope for anatomical features. Images were captured using a Nikon Rebel T1i on an Olympus BX-50 microscope and brightness and contrast adjusted as necessary in Adobe Photoshop v6.0. Some sections were slightly oblique and Helicon Focus v7.0.1 was used to stack several images to improve focus over the depth of field. Measurements were produced using JMicroVision v1.27 from the digital images. Using the transverse section, 100 tracheids were measured for perimeter (μm) and area (μm^2) for both earlywood and latewood for a total of 200 measurements to illustrate the general size of tracheids for each group. In the tangential section, the heights of 100 rays were measured (μm) and

a cell count was performed for each ray. The diameter of 40 tangential bordered pits were measured, except for samples PW21 and SQTR. Due to preservation only 20 tangential bordered pits were measured for these two samples. In the radial section, 300 bordered pits were measured (μm) to calculate height to width ratio. Stratigraphic measurements were made using accepted geological methods and surveyed using a Nikon DTM-322 total station.

3. Geological setting

The Upper Jurassic Morrison Formation is a sequence of terrestrial strata deposited over much of western North America following the northward retreat of the shallow epicontinental Sundance Sea (Foster, 2007a). In Montana, the Morrison Formation is underlain by the marine Swift Formation, which recorded the final regression of the Sundance Sea (Imlay, 1954; Khalid, 1990; Fuentes et al., 2011) developing a planation surface. The Morrison Formation consists of conglomerates, sandstones, siltstones, mudstones, and limestones and is famous for its paleobiota including dinosaurs, non-dinosaurian vertebrates, invertebrates, and plant fossils (Turner and Peterson, 1999; Chure et al., 2006). The formation extends over a million square kilometers of the intermountain west of the United States (Dodson, et al., 1980; Lockley, et al., 1986; Hotton and Baghai-Riding, 2010). Age-equivalent rocks are found in western Canada and have yielded plant fossils, but vertebrate fossils have yet to be discovered. The Brushy Basin Member is the most widespread of the ten formally named members of the formation (Turner and Peterson, 1999). In Montana, the formation has not been formally subdivided into members; however, based upon biostratigraphy of invertebrate microfauna the sediments are age-equivalent to the Salt Wash and lower Brushy Basin Member (Turner and Peterson, 1999; Richmond et al., 2017). Stratigraphically overlying the formation are the terrestrial sediments of the Lower Cretaceous Kootenai Formation (Fisher, 1908; Calvert, 1909; Suttner, 1969).

The main study area (fig. 1) of the Upper Jurassic Morrison Formation in central Montana is where the formation is exposed along the flanks of Spindletop Dome, a small Laramide-age orogenic anticlinal structure. Numerous freshwater tufa-like carbonate build-ups (Richmond et al., 2018) have been discovered in the mudstone beds between 40 and 53 m above the base of the formation. Several localized clusters of carbonate build-ups have been identified. They measure from one to three meters across and a meter high.

A cluster of 17 build-ups was found approximately 42–44 meters above the underlying Jurassic Swift Formation in the southwest corner of the study area. Petrified wood fragments were recovered from the surface of two of the build-ups (PW20, PW21). Another cluster of 61 build-ups is located 1.9 kilometers to the southeast of the first. The build-ups of the second cluster are stratigraphically approximately 42–46 meters above the underlying Jurassic Swift Formation, in the southeast corner of the study area. Three discrete accumulations of petrified wood fragments (SQTR, PW5 and PW6) were found 240 meters west but stratigraphically equivalent to the southeast cluster of build-ups (fig. 1). Additionally, three build-ups were found 1.1 kilometers to the northwest of the first cluster. These build-ups are stratigraphically 51 meters above the underlying Swift Formation. A slightly compressed 6-meter long calcified log (West Tufa specimen; fig. 2) is partially encased by carbonate in one of these build-ups.

4. Systematics

All specimens from the Morrison Formation in central Montana described herein are reposited in the Paleobotany and Micropaleontology (OPC, locality number followed by specimen number provided) of the Sam Noble Museum at the University of Oklahoma, Norman, Oklahoma. To relocate illustrated features, X/Y stage coordinates of image centers are reported in millimeters

on an Olympus BX-50 (s/n 9H14094). The specimens are described in stratigraphic order, lowest to highest (fig. 1).

Genus: *Xenoxylon* Gothan, 1905

Species: *Xenoxylon meisteri* Palibin et Jarmolenko, 1932

4.1 PW20 specimen (Plate I)

Locality: OPC 2281, Fergus County, Montana, USA

Material: OPC 2281–31621 through OPC 2281–31632: blocks of petrified wood, billets and slides

A tracheidoxyl with growth rings expressed as narrow abrupt transitions from earlywood to latewood, type D of Brison et al. (2001) (Plate I, 1). In transverse section, tracheids are irregular polygons. Tracheids in earlywood have a median perimeter of 179 μm with a median area of 2157 μm^2. Latewood comprises one to two tracheid rows maximum width of 63 μm. Latewood tracheids have a median perimeter of 100 μm with a median area of 543 μm^2. Latewood cells display a reduction in perimeter of 44% and area of 75%. No axial parenchyma, axial resin canals, nor idioblasts were observed (Plate I, 1). In tangential section, medullary rays are uniseriate to partially biseriate, never entirely biseriate nor triseriate (Plate I, 2). Ray heights vary from 26 μm to 448 μm with a median height of 67 μm. In a random 100-ray count, the number of cells per ray varies from 1–18 cells (median = 2, variance = 14.6); maximum observed out-of-count was 32 cells high (table 1). Median ray cell vertical diameter is 26 μm (Plate I, 2). Bordered pits on the tracheid tangential walls are circular, 15.8 μm in diameter; pits are separate or contiguous (Plate I, 3), usually uniseriate, occasionally offset to subopposite (Plates I, 3, 4).

In radial section, the pitting on the tracheid radial walls is xenoxylean, uniseriate, with long chains of contiguous flattened, obround pits (Plate I, 5). The median radial bordered pit width is 30

μm with a median height of 16 μm yielding a median height to width ratio of 0.51. Occasionally radial bordered pits align adjacent or with alternate spacing (Plate I, 6). Bordered pit apertures are usually round with a diameter of 5 μm. Cross-field pitting is fenestriform with a single large oopore (Plate I, 7). Two pits present in a cross-field are rare (Plate I, 7).

4.2 PW21 specimen (Plate II)

Locality: OPC 2282, Fergus County, Montana, USA

Material: OPC 2282–31633 through OPC 2282–31653: blocks of petrified wood, billets and slides

A tracheidoxyl with growth rings expressed as narrow abrupt transitions from earlywood to latewood, type D of Brison et al. (2001) (Plate II, 1, 2). In transverse section, tracheids are asymmetrical polygons. Tracheids in earlywood have a median perimeter of 197 μm and median area of 2607 μm^2. Latewood comprises a minimum of one tracheid row with a maximum of four rows and a maximum width of 127 μm. The tracheids of latewood have a median perimeter of 93 μm and a median area of 467 μm^2. Latewood cells display a reduction in perimeter of 53% and area of 82%. No axial parenchyma, axial resin canals, nor idioblasts were observed (Plate II, 1).

In tangential section, medullary rays are uniseriate, never biseriate nor triseriate. Ray heights vary from 29 μm to 827 μm with a median height of 135 μm. In a random 100-ray count, the number of cells per ray varies from 1–27 cells (median = 4, variance = 37.6); maximum observed out-of-count was 52 cells high (table 1). Median ray cell vertical diameter is 30 μm (Plate II, 3). Bordered pits on the tracheid tangential walls are circular, 20.6 μm in diameter; pits are separate or contiguous (Plate II, 3), uniseriate in narrow tracheids and frequently subalternate to opposite in wider tracheids (Plate II, 4).

In radial section, the pitting on the tracheid radial walls is xenoxylean, uniseriate, with long chains of contiguous flattened, obround pits (Plates II, 5). The median radial bordered pit width is 32 μm with a median height of 17 μm yielding a median height to width ratio of 0.52. Noncontiguous radial bordered pits are usually round and are concentrated at the ends of the tracheids near cross-fields (Plate II, 6). Apertures are usually round with a diameter of 5 μm. Cross-field pitting is fenestriform with a single large oopore (Plate II, 7). Two pits present in a cross-field are rare.

4.3 PW6 specimen (Plate III)

Locality: OPC 2267, Fergus County, Montana, USA

Material: OPC 2267–31605 through OPC 2267–31620: blocks of petrified wood, billets and slides

A tracheidoxyl with growth rings expressed as narrow abrupt transitions from earlywood to latewood, type D of Brison et al. (2001) (Plate III, 1). In transverse section, tracheids are rounded irregular polygons. Tracheids in earlywood have a median perimeter of 163 μm with median area of 1711 μm^2. Latewood comprises a minimum of two row of tracheids with a maximum of eight rows with a maximum width of 225 μm. The tracheids of latewood have a median perimeter of 77 μm and median area of 335 μm^2. Latewood cells display a reduction in perimeter of 53% and area of 80%. No axial parenchyma, axial resin canals, nor idioblasts were observed (Plate III, 1).

In tangential section, medullary rays are uniseriate to partially biseriate, never entirely biseriate nor triseriate (Plate III, 2). Ray heights vary from 25 μm to 774 μm with a median height of 205 μm. In a random 100-ray count, the number of cells per ray varies from 1–29 cells (median = 7, variance = 29.4); maximum observed out-of-count was 52 cells high (table 1). Median ray cell vertical diameter is 28 μm (Plate III, 2). Bordered pits on the tracheid tangential walls are circular, 12.5 μm in diameter; pits are separate and uniseriate (Plate III, 3).

In radial section, the pitting on the tracheid radial walls is xenoxylean, uniseriate, with long chains of contiguous flattened, obround pits (Plates III, 4). The median radial bordered pit width is 24 μm with a median height of 15 μm yielding a median height to width ratio of 0.60. Noncontiguous radial bordered pits are usually round and are concentrated at the ends of the tracheids near cross-fields (Plate III, 5). Apertures are usually round with a diameter of 5 μm. Cross-field pitting is fenestriform with a single large oopore (Plate III, 6). Two pits present in a cross-field are rare.

4.4 SQTR specimen (Plate IV)

Locality: OPC 2259, Fergus County, Montana, USA

Material: OPC 2259–31565 through OPC 2259–31576: blocks of petrified wood, billets and slides

A tracheidoxyl with growth rings expressed as narrow abrupt transitions from earlywood to latewood, type D of Brison et al. (2001) (Plate IV, 1). In transverse section, tracheids are squarish polygons, occasionally round. Tracheids in earlywood have a median perimeter of 148 μm with a median area of 1477 μm^2. Latewood comprises a minimum of one tracheid row with a maximum of four rows with a maximum width of 96 μm. The tracheids of latewood have a median perimeter of 74 μm and median area of 381 μm^2. Latewood cells display a reduction in perimeter of 50% and area of 74%. No axial parenchyma, axial resin canals, nor idioblasts were observed (Plate IV, 1).

In tangential section, medullary rays are nearly homogenous although often have one or more notably different cells; they are uniseriate, never biseriate nor triseriate (Plate IV, 2). Ray heights vary from 56 μm to 425 μm with a median height of 176 μm. In a random 100-ray count, the number of cells per ray varies from 2–18 cells (median = 7, variance = 11.7); maximum observed out-of-count was 37 cells high (table 1). Median ray cell vertical diameter is 26 μm

(Plate IV, 2). Bordered pits on the tracheid tangential walls are circular, 14.3 μm in diameter; pits are separate and uniseriate to slightly offset (Plate IV, 3).

In radial section, the pitting on the tracheid radial walls is xenoxylean, uniseriate, with long chains of contiguous flattened, obround pits (Plates IV, 4, 5). The median bordered pit width is 30 μm with a median height of 17 μm yielding a median height to width ratio of 0.56. Noncontiguous radial bordered pits are usually round and are concentrated at the ends of the tracheids near cross-fields (Plate IV, 5). Apertures are usually round with a diameter of 5 μm. Cross-field pitting is fenestriform with a single large oopore (Plate IV, 6). Two pits present in a cross-field are rare.

4.5 PW5 specimen (Plate V)

Locality: OPC 2266, Fergus County, Montana, USA

Material: OPC 2266–31577 through OPC 2266–31604: blocks of petrified wood, billets and slides

A tracheidoxyl with growth rings expressed as narrow abrupt transitions from earlywood to latewood, type D of Brison et al. (2001) (Plate V, 1). In transverse section, tracheids are square to rounded irregular polygons. Tracheids in earlywood have a median perimeter of 128 μm with a median area of 987 μm^2. Latewood comprises a minimum of two row of tracheids with a maximum of six rows with a maximum width of 125 μm. The tracheids of latewood have a median perimeter of 60 μm and median area of 168 μm^2. Latewood cells display a reduction in perimeter of 53% and area of 73%. No axial parenchyma, axial resin canals, nor idioblasts were observed (Plate V, 1).

In tangential section, medullary rays are nearly homogenous although often have one or more notably different cells; they are uniseriate, never entirely biseriate nor triseriate (Plate V, 2). Ray heights vary from 25 μm to 679 μm with a median height of 130 μm. In a random 100-ray count, the number of cells per ray varies from 1–25 cells (median = 5, variance = 23.8); maximum

observed out-of-count was 42 cells high (table 1). Median ray cell vertical diameter is 28 μm (Plate V, 2). Bordered pits on the tracheid tangential walls are circular, 22.7 μm in diameter; pits are separate and uniseriate to slightly offset (Plate V, 3).

In radial section, the pitting on the tracheid radial walls is xenoxylean, uniseriate, with long chains of contiguous flattened, obround pits (Plate V, 4). The median radial bordered pit width is 26 μm with a median height of 16 μm yielding a median height to width ratio of 0.61. Noncontiguous radial bordered pits are usually round and are concentrated at the ends of the tracheids near cross-fields (Plate V, 5). Apertures are usually round with a diameter of 5 μm. Cross-field pitting is fenestriform with a single large oopore (Plate V, 6). Two pits present in a cross-field are rare.

4.6 West Tufa specimen (Plate VI)

Locality: OPC 2256, Fergus County, Montana, USA

Material: OPC 2256–31550 through OPC 2256–31564: blocks of petrified wood, sections and slides

A petrified log positioned partially encased by a carbonate build-up (fig. 2) has growth rings expressed as narrow abrupt transitions from earlywood to latewood, type D of Brison et al. (2001) (Plate VI, 1). In transverse section, tracheids are rounded polygons; occasionally square. Tracheids in earlywood have a median perimeter of 189 μm with a median area of 2566 μm^2. Latewood comprises two to three cell rows with a maximum width of 75 μm. The tracheids of latewood have a median perimeter of 106 μm and median area of 752 μm^2. Latewood cells display a reduction in perimeter of 44% and area of 71%. No axial parenchyma, axial resin canals, nor idioblasts were observed (Plate VI, 1).

In tangential section, medullary rays are nearly homogenous although though often have one or more notably different cells; they are uniseriate, never biseriate nor triseriate (Plate VI, 2). Ray heights vary from 66 μm to 529 μm with a median height of 218 μm. In a random 100-ray count, the number of cells per ray varies from 2–21 cells (median = 9, variance = 17.0); maximum observed out-of-count was 46 cells high (table 1). Median ray cell vertical diameter is 26 μm (Plate VI, 2). Bordered pits on the tracheid tangential walls are circular, 14.0 μm in diameter; pits are separate and uniseriate to subopposite (Plate VI, 3).

In radial section, the pitting on the tracheid radial walls is xenoxylean, uniseriate, with long chains of contiguous flattened, obround pits (Plates VI, 4). The median radial bordered pit width is 29 μm with a median height of 17 μm yielding a median height to width ratio of 0.57. Noncontiguous radial bordered pits are usually round and are concentrated at the ends of the tracheids near cross-fields (Plate VI, 5). Apertures are usually round with a diameter of 5 μm. Cross-field pitting is fenestriform with a single large oopore (Plate VI, 6). Two pits present in a cross-field are rare.

4.7 Discussion

Xenoxylon was originally given a clear circumscription by Gothan (1905) but the genus was expanded later by Kräusel (1949). Recent work and review of reposited specimens by Philippe and Thévenard (1996) and Philippe et al. (2013) has affirmed Gothan's usage and developed a set of characters that clearly delineate *Xenoxylon* from all other Mesozoic woods. The first of these is the occurrence, at least locally, in the earlywood, of uniseriate radial border pits with a markedly obround shape (wider than tall). Although most uniseriate radial pits tend toward circular when separate, contiguous uniseriate pits of "araucarian" type tend to be more obround (flattened;

Philippe and Bamford, 2008). Philippe et al. (2013) measured 34 radial pits from the *Xenoxylon* type specimen and determined a mean height to width ratio of 0.57 with a standard deviation of 0.05. They concluded a height to width ratio of 0.60 or less is rare in woods of "araucarian" type and informally designated 0.60 as the criterion for any individual pit (in a contiguous series) to be considered a "xenoxylean" radial pit. Figure 3 illustrates the distribution of measured ratios for each of the six specimens with 44–90% of radial pits falling below this criterion; PW5 and PW6 have medians and means just higher, between 0.604 to 0.613, with all other specimens below 0.60. The second required characteristic of the genus *Xenoxylon* is fenestriform cross-field pitting in earlywood tracheids, with a single pit per field, occupying the whole field or—rarely—two where walls divide a cross-field. All our specimens show this feature (Plates I–VI). Based on our assessment of these two characters, all six specimens may be confidently assigned to the genus *Xenoxylon*.

Philippe et al. (2013) recognized three informal species groups within *Xenoxylon*. The three groups are *latiporosum*-type, *meisteri*-type, and *phyllocladoides*-type. The *latiporosum*-type is named after *X. latiporosum* (Cramer) Gothan; it is characterized by uniformly obround radial bordered pits, and "rare, uniseriate, spaced" (Philippe et al., 2013, table 2) tangential bordered pits. The *meisteri*-type is named after *X. meisteri* Palibin et Jarmolenko and has pitting similar to the *latiporosum*-type, but "close observation reveals biseriate pitting and/or pits clusters" as well as "tracheid portions [that] appear unpitted" (Philippe et al., 2013, p.130). The *meisteri*-type species also show "frequent to abundant tangential pitting" that are "commonly bi-tri-seriate with crowded alternate" tangential bordered pits (Philippe et al., 2013, p. 130–131). The *phyllocladoides*-type is named after *X. phyllocladoides* Gothan and is characterized by occasional obround radial bordered pits among mostly round pits in discrete clusters which are also sometimes biseriate and opposite.

The tangential bordered pits in *phyllocladoides*-type are "rare, uniseriate, spaced" (Philippe et al., 2013, table 2). All six of our specimens conform to the *meisteri*-type. All of our specimens possess small-to-large clusters of uniseriate obround radial bordered pits separated by gaps without any pits, especially near ray fields, and abundant tangential bordered pits.

Philippe et al. (2013) suggested species-level distinctions below group-level are not useful because species are based on minor variations (e.g., ray height). Nevertheless, Philippe et al. (2013) retained 11 valid species pending actual viewing of types and developed a key to these species. All of our specimens key out as either *Xenoxylon meisteri* or *X. japonicum* based on uniseriate radial pitting in untraumatized wood and the length of the radial pit clusters. *X. meisteri* and *X. japonicum* are distinguished primarily on the number of cells that make up rays with rays of *X. meisteri* having between 1 and 18 (usually 3–8) and rays of *X. japonicum* having up to 40–50. Table 1 shows the ray heights for each of our specimens. Based on a count of 100 rays, the median number for four specimens fall within the *X. meisteri* range and PW20, at 2, and West Tufa, at 9, are slightly separate from the normal range. However, the maximum number within-count exceeds the usual range for *X. meisteri* in four specimens. Furthermore, the maximum number out-of-count ($\approx$ 6 cm^2, >1,000 rays examined) for four specimens meets the criterion for inclusion in *X. japonicum*. In their discussion of *X. japonicum*, Philippe et al. (2013) noted the designated lectotype does not have tangential pitting and another specimen had 2–11 (mean = 4.22) cells in its rays. Philippe et al. (2013) noted the fossil wood species *X. meisteri* and *X. japonicum* frequently co-occur and postulated they might originate from the same tree species. In view of the low observed median and mean values of ray heights in our specimens and of the indistinct delimitation of *X. meisteri* and *X. japonicum* based on counts—median/mean, range, and maximum, we assign all six of our specimens to *Xenoxylon meisteri*.

5. Review of North American *Xenoxylon* specimens

5.1 Xenoxylon *from Lower Jurassic of central Utah*

A poorly preserved fossil wood from the Lower Jurassic Navajo Sandstone of central Utah was assigned to the genus *Xenoxylon* by Parrish and Falcon-Lang (2007). The lack of vessels indicated an affinity to Coniferales. The wood was compared to *Xenoxylon morrisonense* Medlyn (Medlyn and Tidwell, 1975) and assigned to the same genus with reservation. The radial section was rescanned using ultraviolet induced autofluorescence imaging to show the attributes of the bordered pits more clearly (Wilkens et al., 2005; Wilkens, 2008). Although the bordered pits are contiguous and uniseriate, they were shown to be uniformly circular rather than flattened (Wilkens, 2008). Therefore, this wood from the Navajo Sandstone is not a valid occurrence of the genus *Xenoxylon* (fig. 4).

5.2 Xenoxylon *from the Lower and Upper Jurassic of Greenland*

Specimens from several Jurassic-aged formations (Pliensbachian to Portlandian/ Kimmeridgian) of Jameson Land, eastern Greenland were reported in the supplemental material to Oh et al. (2015). Oh et al. (2015) assigned these specimens geographically to Europe, but they properly belong to North America. The identifications were made by M. Philippe from unpublished specimens belonging to Mathiesen's collection in the Copenhagen Geological Museum. All specimens were assigned to *X. phyllocladoides* and are accepted herein (fig. 4).

5.3 Xenoxylon *from the Upper Jurassic of Utah*

A 56-centimeter diameter petrified log embedded in a pebble conglomerate from Upper Jurassic Morrison Formation of Garfield County, Utah was described by Medlyn and Tidwell (1975) as *Xenoxylon morrisonense* (fig. 4). The type material (BYU926) of *X. morrisonense* was

reexamined and imaged at the Brigham Young University Earth Science Museum. Although the radial bordered pits are "vertically flattened" as originally described (Plates VII, 1, 2), the median height to width ratio (n = 300) is 0.91 and none fall at or below the 0.6 cut-off for xenoxylean bordered pits (fig. 3). The thin sections are presently very dark. Although the cross-fields have one or sometimes two unbordered pits per cross-field, the pits have small, subcircular to oblique elliptical apertures and do not fill the cross-field (Plates VII, 3–5). In addition, the pitting of the horizontal walls of the ray parenchyma could not be confirmed. Although a wavy appearance was noted, the "pitting" seems due to preservation—interruptions in dark staining of the walls—rather than perforations and is not observed in all rays (Plate VII, 4, black arrow). All other features described in the original published description were confirmed, including axial parenchyma (Plate VII, 1, arrow). Medlyn and Tidwell (1975) assigned their specimen to the genus *Xenoxylon* prior to the recent work completed by Philippe and Thévenard (1996) and Philippe et al. (2013). Philippe and Thévenard (1996) and Philippe et al. (2013) considered the placement of *X. morrisonense* in the genus invalid on the attribute of several pits per cross-field. In our reinvestigation of the type, we observed a single pit per cross-field was far more common than two, and more than two pits per cross-field were never observed. However, assignment to *Xenoxylon* remains invalid on the basis of the absence of both fenestriform cross-field pitting and xenoxylean radial pitting.

Tidwell et al. (1998) named a second species, *Xenoxylon moorei*, from the Upper Jurassic Morrison Formation for fossil wood collected from Mygatt-Moore Dinosaur Quarry in west-central Colorado and from another locality in Castle Dale, Utah, both from the Brushy Basin Member (Foster, 2007b). We reinvestigated the type specimen (BYU 5110) and paratypes (MWC 2194 and 2170) and observed only a few radial pits and those pits were more circular than obround. Tidwell et al. (1998) also stated the cross-field pitting has one, rarely two pores with slight borders. We

could not observe any cross-field pitting in the type material due to poor preservation and very dark coloration. *X. moorei* has been considered misassigned to *Xenoxylon* due to the number and shape the pits in the cross-field as described in the protologue (Philippe and Thévenard, 1996; Philippe et al., 2013). Our observations based on presently visible features of the type material do not refute this conclusion.

5.4 Invalid Lower Cretaceous Xenoxylon

Gordon (1932) described fossil woods from bituminous sands of the McMurray Formation in Alberta, Canada from the Late Barremian to Aptian age (fig. 4). The woods from the formation have been identified as *Xenoxylon*, *Sciadopitys*, and *Keteleeria* (Ells, 1931; Gordon, 1932; Carrigy, 1959). Gordon (1932) described two of her samples with a distinct affinity to *Xenoxylon*. The first (her axis 25) is a badly crushed specimen with an abrupt earlywood to latewood transition. No parenchyma, or resin canals are present. The rays are uniseriate. Rounded bordered pits are sometimes separate and close, but never touch. The wood apparently exhibits one large fenestriform pit per cross-field (Gordon, 1932; plate VI), but based on her text and drawing (op.cit., p. 51 and fig. 4) cross-field pitting, appears to be at least locally, cupressoid. The second specimen (her axis 26) displays a gradual transition from earlywood to latewood. No parenchyma, or resin canals are present. The rays are uniseriate. The tracheid radial pitting is assigned to the abietinean type with rounded bordered pits that are separate with instances where the pits touch, but never horizontally flattened. Cross-fields consists of one ray cell per field. The microphotograph given in her plate IX is strongly reminiscent of *Xenoxylon*, but again her text and drawing (Gordon, 1932, p. 55, fig. 5) describe bordered phyllocladoid cross-field pits. As long as this material has not been

reappraised to resolve these conflicts, it is probably more prudent to consider that these fossil woods do not belong to the genus *Xenoxylon*.

Fossil logs found in the Lower Cretaceous Cloverly Formation north of Shell, Wyoming were described as *Xenoxylon* and *Mesembrioxylon* by Murphy et al. (2005) (fig. 4). Murphy et al. (2005) made thin sections of the transverse and tangential views, but not the radial view for the samples. The senior author sought new samples in the field in hopes of obtaining additional thin sections, but the search was unsuccessful. We had thin sections from the original cut billets prepared for examination in hopes that areas of distorted wood might reveal missing characters. We observed no radial features. In the absence of a radial section, the features necessary to assign this taxon to any genus are missing; therefore, we provisionally discount this attribution to *Xenoxylon*.

5.5 Valid Lower/Upper Cretaceous Xenoxylon

Arnold (1952) described an occurrence of *X. latiporosum* from the Chandler Formation (renamed the Nanushuk Formation, Mull et al., 2003) of northern Alaska (fig. 4). The Nanushuk Formation is Albian and Cenomanian age, consisting of marine, transitional, and nonmarine deposits exposed on the North Slope of Alaska (Mull et al., 2003). In their discussion of *X. japonicum*, Philippe et al. (2013) note that Arnold's (1952) specimen might belong to *X. japonicum*; Vogellehner (1968) previously mentioned Arnold's material in his discussion of *X. japonicum* but postponed discussion for another paper that was never published. In addition to fenestriform cross-fields and strongly obround radial pitting, Arnold described radial pits in groups of 2–30 separated by unpitted spaces, rays composed of 2–12 cells and "considerable" tangential pitting on latewood tracheids. Taken together, these characters are consistent with circumscription

of *X. meisteri* rather than *X. latiporosum*. We requested loan of the type material from University of Michigan Museum of Paleontology, but due to relocating to a new facility, all the collections are presently boxed and unavailable (R. Burnham, pers. comm., 2018). At present, Arnold's material is affirmed as *Xenoxylon* based on the clear published illustrations, but it is possible that, on reexamination, his material will be shown to be another, and strictly the first reported, occurrence of *X. meisteri* in North America. Parrish and Spicer (1988) also identified *X. latiporosum* from the Nanushuk Formation on the North Slope of Alaska. Again, in addition to fenestriform cross-fields and strongly obround radial pitting, Parrish, and Spicer (1988) note radial pits are "in groups of variable number separated by more or less smooth tracheid walls (p. 20)." They reported the rays are uniseriate and commonly contain 12–25 cells, although cell count can vary from 1–30 cells, and tangential pits were rare (Parrish and Spicer, 1988). We requested loan of this material and Dr. J. T. Parrish provided all the transverse sections, but we were unable to obtain the remainder from Dr. R. A. Spicer. It is unclear if this material may be assignable to *X. meisteri* (rare tangential pitting) without further study, but it is clearly assignable to *Xenoxylon* based on published description and illustrations.

Selmeier and Grosser (2011) studied fossil wood from several locations in the Sverdrup Basin of the Arctic. The wood from the Deer Bay Formation (Valanginian) was identified as *Dacrydioxylon*. The genus *Dacrydioxylon* is considered invalidly published (Philippe et al., 1999) and the material was reassigned to *Xenoxylon hopeiense* (Philippe et al., 2013). We requested a loan of this material from the State Office for Mining, Energy, and Geology in Hannover which curates the collection. They do not loan glass slides but were willing to loan associated numerous raw wood fragments; unfortunately, those fragments are not curated to pair with the identified slides (C. Heunisch, pers. comm, 2017). This wood is accepted as *Xenoxylon* on basis of

fenestriform cross-field pitting and scattered obround radial bordered pits (Selmeier and Grosser, 2011, plate 6, figure 2).

Six taxa of plant megafossils were found in the terrestrial sediments of the Upper Cretaceous Prince Creek Formation (Late Campanian age, Mull et al., 2003) of the North Slope of Alaska (Spicer and Parrish, 1990) (fig. 4). Only a general description of each was provided. Spicer and Parrish (1990) identified one specimen as *X. latiporosum*. The fossil wood has bordered pits which are uniseriate, contiguous, and obround (25 μm wide and 15–18 μm high). Cross-field pits are fenestriform and rays are "generally short (usually less than 22 cells high) (p. 230)." No mention is made of clustering of radial pits or of tangential pitting. However, this occurrence is considered to have been correctly identified as *Xenoxylon* (Oh et al., 2015).

5.6 Review of North American woods assigned to Xenoxylon*: Conclusions*

All the reported North American occurrences of *Xenoxylon* were reviewed. All previously described Jurassic-aged specimens of *Xenoxylon* are invalid representations except for *X. phyllocladoides* specimens from Early to Late Jurassic of Greenland (Oh et al., 2015). Only occurrences reported as *Xenoxylon latiporosum* from Alaska and Arctic Canada (Arnold, 1952, Parrish and Spicer, 1988; Selmeier and Grosser, 2011) are valid occurrences of the genus in the Cretaceous of North America. Therefore, our six specimens from Montana constitute the first Jurassic occurrence of *Xenoxylon* in continental North America and the earliest occurrence of *Xenoxylon meisteri* in North America even if the material identified as *X. latiporosum* in both Arnold (1952) and Parrish and Spicer (1988) is actually *X. meisteri* (fig. 4).

The geographic extent of the Morrison Formation from New Mexico to Canadian border renders a uniform age improbable and more likely represents a time-transgressive sequence

(Harris, 2005). Formational absolute dates fall within the Kimmeridgian to Tithonian Stages (156 to 149 Ma) and are derived from sediments from the Four Corners area of the Colorado Plateau where the formation is well exposed (Kowallis et al., 1991; Hurd et al., 2006; Eichler, et al., 2007; Kowallis et al., 2007; Bradshaw and Kowallis, 2009; Trujillo, et al., 2014, Trujillo and Kowallis, 2015; Galli, et al., 2018). Based upon palynology and detrital zircons, Fuentes et al. (2011) provide a latest Oxfordian to Kimmeridgian age for the Morrison Formation in northwestern Montana. Invertebrate biostratigraphy in the research area (Richmond et al., 2017) places the formation in Charophyte/Ostracod Biozone 3 of Kimmeridgian age (Schudack et al., 1998; Turner and Peterson, 1999).

Busby et al. (2005) reviewed North American magnetostratigraphy and established a paleolatitude range for Montana during the Kimmeridgian between 40 and 50^{o} north. Dickinson (2018) generated a North American plate latitude reconstruction for 154 Ma; using his reconstruction, we position our *Xenoxylon* occurrences in Montana between 49–50° N paleolatitude. The location of our specimens is the southernmost North American occurrence of *Xenoxylon* in the Jurassic or Cretaceous (fig. 4) and fills the gap in the genus' geographic range noted previously by researchers (Philippe and Thévenard, 1996; Philippe et al., 2009; Tian et al., 2016; Philippe et al., 2017). Moreover, our occurrences, and those of Arnold (1952) and Parrish and Spicer (1988) if confirmed, would attest to the long-term persistence of *X. meisteri* in North America.

6. Paleoclimatic implications

6.1 Morrison Formation paleoclimatic overview

Based upon climate models and climate proxies many researchers have proposed the Morrison foreland basin experienced a semiarid to arid climate (Parrish et al., 1982, Parrish and

Peterson, 1988; Turner and Fishman, 1991; Valdes and Sellwood, 1992; Demko and Parrish, 1998; Richmond and Morris, 1998; Parrish et al., 2004). By the Late Jurassic, North America's northward movement fragmented the Triassic monsoonal climate pattern, resulting in a low-pressure cell over the continent (Parrish and Doyle, 1984; Parrish and Peterson, 1988). Late Jurassic modeled temperatures for the western North America range from 5° C (winter) to > 36° C (summer) which would be about 5° C warmer than at present (Demko and Parrish, 1998). Temperature independently does not account for the aridity of western North America during the Late Jurassic. The aridity was likely generated by several factors including the latitudinal position in the subtropical dry belt, the Sevier orogenic belt acting as a rain shadow (Demko and Parrish, 1998) and oceanic upwelling driven by coastal wind patterns (Parrish and Peterson, 1988). Based on palynological studies, Hotton (1986) derived an arid climate for the formation. Given the modeled arid conditions, Peterson and Turner-Peterson (1987) suggested the presence of narrow but extensive riparian environments that supported abundant plant life to sustain the large herbivorous dinosaurs which roamed the Morrison basin. Similarly, Parrish et al. (2004) concluded the vegetation was primarily riparian, at least in the southern extent of the Morrison Formation.

In contrast, other climate proxies indicate a generally wet climate. Perennial fluvial, paludal, and lacustrine facies in the Morrison basin (Lockley et al., 1984; Lockley, et al., 1986; Dunagan, 1999; Dunagan and Turner, 2004; Gorman II, et al., 2008) support this interpretation. Several paleolakes have lacustrine ooid facies (Lockley et al., 1984; Lockley et al., 1986). Ooids can take over a thousand years to form (Neese and Pigott, 1987) suggesting a long-term presence for these paleolakes. The presence of aquatic vertebrates, e.g., crocodiles (Hups et al., 2006; Hunt and Richmond, 2018), turtles (Gaffney, 1979), lungfish (Kirkland, 1987), bony fish (Small et al., 2007, Gorman II et al., 2008), and amphibians (Hecht and Estes, 1960) indicate perennial lakes and

rivers were present in the Morrison basin (Gorman II, et al., 2007, 2008). Aquatic invertebrates have specific environments in which they live (Evanoff et al., 1998; Schudack et al., 1998; Dunagan, 1999; Good, 2004; Richmond et al., 2017) and usually require clean perennial lakes and rivers to survive. Aquatic invertebrates are present throughout the Morrison basin (Evanoff et al., 1998). According to Tidwell (1990) the abundance of plant fossils indicates a humid, tropical climate (although not necessarily if plants were confined to river-margins; Peterson and Turner-Peterson, 1987; Parrish et al., 2004).

Latitudinal differentiation in climate (in space and time) is supported by several studies. Busby et al. (2005) found paleomagnetic evidence of a rapid 13° northward shift after the onset of Morrison deposition and before deposition of the Brushy Basin member. Busby et al. (2005) further argued for wetter climates as North America drifted into these temperate latitudes based on evidence for "wet" ignimbrite eruptions. Baghai-Riding and Hotton (2009) and Hotton and Baghai-Riding (2010) investigated palynological samples along a south-to-north transect from New Mexico to Wyoming and proposed wet conditions increased with latitude in the basin. In the Morrison Formation of central Montana, the highest deposits, just below the contact with the overlying Kootenai Formation, are comprised of extensive coal beds (Calvert, 1909; Fisher, 1909; Harris, 1966; Silverman and Harris, 1967). Myers et al. (2014) used the chemical index of alteration minus potassium, and the calcium and magnesium weathering index of paleosols, to estimate paleorainfall for the Morrison Formation in south-central Montana; their data reconstructed a 1000–1200 mm/year paleorainfall (equivalent to a sub-humid climate) for this region with lower paleorainfall values southward. Parrish et al. (2004) suggested cooler temperatures, and hence less evaporation rather than increased precipitation, might be sufficient to explain the wetter conditions in the northern Morrison Basin.

6.2 Xenoxylon *as a proxy for Morrison climate in Montana*

Based on the distribution of occurrences and on correlative lithological climate proxies, the presence of *Xenoxylon* has been used to indicate cool and wet/humid terrestrial climate conditions in the northern hemisphere of the Mesozoic (Philippe and Thévenard, 1996; Marynowski et al., 2008; Philippe et al., 2009; Tian et al., 2016; Philippe et al., 2017). Based on growth ring characteristics, Harland (2005) concluded *Xenoxylon* was an evergreen tree with a leaf retention time of more than five years—a duration typical of cold to temperate climate vegetation (Wright et al., 2004; Harland et al., 2007; Philippe et al., 2009). Therefore, our identification of *Xenoxylon* indicates the Morrison Formation in central Montana was deposited under a cool and wet/humid temperate climate. This adds additional support to the previous studies cited above that found cool and wet/humid conditions characterized the northern Morrison Basin.

7. Conclusions

Six specimens found in central Montana mark the first occurrences of the genus *Xenoxylon* in the Upper Jurassic of continental North America. The specimens are stratigraphically separated by 10 meters indicating *Xenoxylon* was part of the paleoflora in the northern portion of the Morrison foreland basin. All specimens are here identified as *X. meisteri* marking the first confirmed occurrence of this species in North America and the oldest and southernmost occurrence of the genus in North America. The presence of *Xenoxylon* in the Morrison Formation of Montana supports the inference that the northern portion of foreland basin experienced a wet or wet/cool climate as opposed to the drier climatic regime recognized for the more southern regions.

Acknowledgments

We express appreciation to the D. Hein family for access to their Montana ranch and for donating the *Xenoxylon meisteri* specimens to the University of Oklahoma Sam Noble Museum for research. We want to extend a special appreciation to N. Murphy of Judith River Dinosaur Institute for all his support during the many field seasons in Montana. We want to thank the following people for their assistance with the project: B. Schatzke of Rocky College, Billings, Montana for her research assistance; J. Totman-Parrish, University of Idaho, emerita; B. Bodenbender of Hope College, Holland, Wisconsin for providing billets for the Big Horn Basin *Xenoxylon* material and E. Clites for directing us to the Cloverly Formation collection sites. And finally, we thank J. Andersen for access to his ranch near Shell, Wyoming.

References (formatted for Review of Palaeobotany and Palynology)

Afonin, M., Philippe, M., 2014. Fossil woods from the Lower Cretaceous (Albian) of Kamchatka Peninsula, Russian Far East. Cretaceous Research 50, 110–119.

Arnold, C.A., 1952. Silicified plant remains from the Mesozoic and Tertiary of western North America. II. Some fossil woods from northern Alaska. Papers of the Michigan Academy of Science 28, 9–20.

Baghai-Riding, N.L., Hotton, C.L., 2009. Palynological evidence for conifer dominance and arid climate in the Late Jurassic Morrison Formation, U.S.A. The Geological Society of America, Abstr. Prog. 41, 40.

Bradshaw, R.W., Kowallis, B.J., 2009. U-Pb dating of zircons from the Salt Wash Member of the Morrison Formation near Capitol Reef National Park, Utah. The Geological Society of America, Abstr. Prog. 42, 11.

Brison, A.-L., Philippe, M., Thévenard, F., 2001. Are Mesozoic wood growth rings climate induced? Paleobiology 27, 531–538.

Busby, C.J., Bassett, K.N., Steiner, M.B., Riggs, N.R., 2005. Climatic and tectonic controls on Jurassic intra-arc basins related to northward drift of North America. The Geological Society of America Special Paper 393, 359–376.

Calvert, W.R., 1909. Geology of the Lewistown Coal Field Montana. United States Geological Survey Bulletin 390, 83.

Carrigy, M.A., 1959. Geology of the McMurray Formation Part III General Geology of the McMurray Area. Research Council of Alberta Geological Division Memoir 1, 130.

Chure, D.J., Litwin, R., Hasiotis, S.T., Evanoff, E., Carpenter, K., 2006. The fauna and flora of the Morrison Formation: 2006. *In* Foster, J.R., Lucas, S.G., (eds), Paleontology and Geology of the Upper Jurassic Morrison Formation. New Mexico Museum of Natural History and Science Bulletin 36, 233–249.

Demko, T.M., Parrish, J.T., 1998. Paleoclimatic setting of the Upper Jurassic Morrison Formation. Modern Geology 22, 283–296.

Dickinson, W.R., 2018. Tectonosedimentary relations of Pennsylvanian to Jurassic strata on the Colorado Plateau. The Geological Society of America, Special Paper 553, 184.

Ding, Q.-H., Zheng, S-L., Zhang, W., 2000. Mesozoic fossil woods of genus *Xenoxylon* from Northeast China and its palaeoecology. Acta Palaeontologica Sinica 39, 237–249.

Dodson, P., Behrensmeyer, A.K., Bakker, R.T., McIntosh, J.S., 1980. Taphonomy and paleoecology of the dinosaur beds of the Jurassic Morrison Formation. Paleobiology 6, 208–232.

Dunagan, S.P., 1999. Paleosynecology and taphonomy of freshwater carbonate lakes and ponds from the Upper Jurassic Morrison Formation (Western Interior, U.S.A.). The Geological Society of America, Abstr. Prog. 31, 365.

Dunagan, S.P., Turner, C.E., 2004. Regional paleohydrologic and paleoclimatic settings of wetland/lacustrine depositional systems in the Morrison Formation (Upper Jurassic), Western Interior USA. Sedimentary Geology 167, 269–296.

Eichler, C.M., Hurd, O.V., Dickinson, W.R., Gehrels, G.E., McGraw, J.L., Amar, J.R., Anderson, C.E., Ojha, J., 2007. U-Pb ages of detrital zircons from sandstone of the Upper Jurassic Morrison Formation on the Colorado Plateau. The Geological Society of America, Abstr. Prog. 39, 148.

Ells, S.C., 1931. Fossil wood discovered in Alberta bituminous sands. Canadian Mining Journal 52, 171–172.

Evanoff, E., Good, S.C., Hanley, J.H., 1998. An overview of the freshwater mollusks from the Morrison Formation. Modern Geology 22, 423–450.

Feng, Z., Wei, H.-B., Wang, C.-L., Chen, Y.-X., Shen, J.-J., Yang, J.-Y., 2015. Wood decay of *Xenoxylon yunnanensis* Feng sp. nov. from the Middle Jurassic of Yunnan Province, China. Palaeogeography, Palaeoclimatology, Palaeoecology 433, 60–70.

Fisher, C.A. 1908. Southern extension of the Kootenai and Montana coal-bearing formations in northern Montana. Economic Geology 3, 77–99.

Fisher, C.A., 1909. Geology of the Great Falls Coal Field Montana. Unites States Geological Survey Bulletin 356, 1–85.

Foster, J., 2007a. Jurassic West, The dinosaurs of the Morrison Formation and their world. Indiana University Press, 387.

Foster, J., 2007b. Taphonomy of the Mygatt-Moore Quarry, a large dinosaur bone bed in the Upper Jurassic Morrison Formation of western Colorado. The Geological Society of America, Abstr. Prog. 39, 400.

Fuentes, F., DeCelles, P.G., Constenius, K.N., Gehrels, G.E., 2011. Evolution of the Cordilleran foreland basin system in northwestern Montana, USA. The Geological Society of America Bulletin 124, 507–533.

Galli, K.G., Buchwaldt, R., Lucas, S.G., Tanner, L., 2018. New chemical abrasion thermal ionization mass spectrometry dates from the Brushy Basin Member, Morrison Formation, western Colorado: Implications for dinosaur evolution. The Journal of Geology, 126, 473–486.

Gaffney, E.S., 1979. The Jurassic turtles of North America. Bulletin of the American Museum of Natural History 162, 135.

Good, S.C., 2004. Paleoenvironmental and paleoclimatic significance of freshwater bivalves in the Upper Jurassic Morrison Formation, Western Interior, USA. Sedimentary Geology 167, 163–176.

Gordon, A.G., 1932. The anatomical structure of Mesozoic plants from the bituminous sands of the McMurray Formation. Unpublished M.Sc. Thesis, University of Alberta, CA, 116.

Gorman II, M.A, Miller, I.M., Small, B.J., Pardo, J.D., 2007. A lacustrine Late Jurassic flora in the Morrison Formation. The Geological Society of America, Abstr. Prog. 39, 89.

Gorman II, M.A, Miller, I.M., Pardo, J.D., Small, B.J., 2008. Plants, fish, turtles, and insects from the Morrison Formation; A Late Jurassic ecosystem near Canon City, Colorado. The Geological Society of America Field Guide 10, 295–310.

Gothan, W., 1905. Zur Anatomie lebender und fossiler Gymnospermen-Hölzer. Abhandlungen preußische geologische Landesanstalt 44, 1–108.

Harland, M. 2005. Cretaceous polar conifer forests: Composition, leaf life-span and climate significance. Unpublished PhD dissertation University of Leeds, UK, 220 p.

Harland, M., Francis, J.E., Brentall, S.J., Beerling, D.J., 2007. Cretaceous (Albian–Aptian) conifer wood from Northern Hemisphere high latitudes: Forest composition and palaeoclimate. Review of Palaeobotany and Palynology 143, 167–196.

Harris, J.D., 2005. A review of Morrison Formation paleogeography and tests for time-transgression and faunal provincialism. The Geological Society of America, Abstr. Prog. 37, 13.

Harris, W.L., 1966. The stratigraphy of the Upper Jurassic–Lower Cretaceous rocks in the Great Falls-Lewiston Coal Field, central Montana. Billings Geological Society 17th Annual Field Conference, 164–177.

Hecht, M.K., Estes, R., 1960. Fossil amphibians from Quarry Nine. Postilla, Yale Peabody Museum of Natural History 46, 1–19.

Hotton, C.L., 1986. Palynology of the Morrison Formation. The Geological Society of America, Abstr. Prog. 4, A20.

Hotton, C.L., Baghai-Riding, N.L., 2010. Palynological evidence for conifer dominance within a heterogeneous landscape in the Late Jurassic Morrison Formation, USA. *In*, Gee, C.T. (ed.), Plants in Mesozoic time; morphological innovations, phylogeny, ecosystems, 295–328.

Hunt, T.C., Richmond, D.R., 2018. The aquatic vertebrate community of a bone-dry pond: The historic Stovall Quarry 8, Morrison Formation in the panhandle of Oklahoma. The Society of Vertebrate Paleontology, Abstr. Prog., 152–153.

Hups, M.K., Lockley, M.G., Foster, J.R., 2006. A partial skeleton of *Goniopholis* from the Brushy Basin Member of the Morrison Formation (Upper Jurassic), Cactus Park, Colorado, and distribution of large neosuchians. *In* Foster, J.R., Lucas, S.G., (eds), Paleontology and Geology of the Upper Jurassic Morrison Formation. New Mexico Museum of Natural History and Science Bulletin 36, 107–108.

Hurd, O.V., McGraw, J.L., Dickinson, W.R., 2006. U-Pb ages of detrital zircons in the Upper Jurassic Morrison Formation (Salt Wash and Westwater Canyon Members) of the Four Corners Regions, Southwest USA. The Geological Society of America, Abstr. Prog. 38, 34.

Imlay, R.W., 1954. Marine Jurassic formations in the Pryor Mountains and northern Bighorn Mountains, Montana. Billings Geological Society Fifth Annual Field Conference Guidebook, 54–64.

Khalid, M.E.A., 1990. Sedimentology of the Swift Formation (Jurassic) in the Little Rocky Mountains of Montana. Unpublished M.Sc. Thesis, University of Saskatchewan, CA, 107 p.

Khudaiberdyev, R., 1993. Fossil woods of the genus *Xenoxylon* and their development in the Mesozoic of Middle Asia. *In* Lucas, S.G., Morales, M. (eds), The Nonmarine Triassic: New Mexico Museum of Natural History & Science Bulletin 3, 229–231.

Kim, K., Jeong, E.K., Kim, J.H., Paek, S.D., Suzuki, M., Philippe, M., 2005. Coniferous fossil woods from the Jogyeri Formation (Upper Triassic) of the Nampo Group, Korea. IAWA Journal 26, 253–265.

Kirkland, J.I., 1987. Upper Jurassic and Cretaceous lungfish tooth plates from the Western Interior, the last dipnoan faunas of North America. Hunteria 2, 1–16.

Kowallis, B.J., Christiansen, E.H., Deino, A.L., 1991. Age of the Brushy Basin Member of the Morrison Formation Colorado Plateau, western USA. Cretaceous Research 12, 483–493.

Kowallis, B.J., Britt, B.B., Greenhalgh, B.W., Sprinkel, D.A., 2007. New U-Pb zircon ages from an ash bed in the Brushy Basin Member of the Morrison Formation near Hanksville, Utah. Central Utah: Diverse Geology of a Dynamic Landscape, Utah Geological Association, 75–80.

Kräusel, R., 1949. Die fossilen Koniferen-Hölzer (Unter Ausschluß von *Araucarioxylon* Kraus). II: Kritische Untersuchungen zur Diagnostik lebender und fossiler Koniferen-Hölzer. Palaeontographica Abt. B 89, 83–203.

Lockley, M.G., Prince, N.K., Houck, K., Carpenter, K., 1984. Reconstruction of a Late Jurassic lacustrine ecosystem. The Geological Society of America, Abstr. Prog. 16, 228.

Lockley, M.G., Houck, K.J., Prince, N.K., 1986. North America's largest dinosaur trackway site: Implications for Morrison Formation paleoecology. The Geological Society of America Bulletin, 97, 1163–1176.

Manum, S.B., Van Konijnenburg-VanCittert, J.H.A., Wilde, V., 2000. *Tritaenia* Maegdefrau et Rudolf, Mesozoic '*Sciadopitys*-like' leaves in mass accumulations. Review of Palaeobotany and Palynology 109, 255–269

Marynowski, L., Philippe, M., Zaton, M., Hautevelle, Y., 2008. Systematic relationships of Mesozoic wood genus *Xenoxylon*: integrative biomolecular and palaeobotanical approach. Neues Jahrbuch für Geologie und Paläontologie-Abhandlungen 247, 177–189.

Medlyn, D.A., Tidwell, W.D., 1975. Conifer wood from the Upper Jurassic of Utah. I *Xenoxylon morrisonense* nov. spec. American Journal of Botany 62, 203–208.

Myers, T.S., Tabor, N.J., Rosen, N.A., 2014. Multiproxy approach reveals evidence of highly variable paleoprecipitation in the Upper Jurassic Morrison Formation (western United States), Geological Society of America 126, 1105–1116.

Morgans, H.S., 1999. Lower and Middle Jurassic woods of the Cleveland Basin (North Yorkshire), England. Palaeontology 42, 303–328.

Murphy, J., Clites, E., Demko, T.M., Bodenbender, B.E., 2005. Fluvial sedimentology and plant taphonomy of a dinosaur site and associated strata, Upper Jurassic Morrison and Lower Cretaceous Clovery Formations, Bighorn Basin, WY. The Geological Society of America Abstr. Prog. 37, 32.

Mull, C.G., Houseknecht, D.W., Bird, K.J., 2003. Revised Cretaceous and Tertiary Stratigraphic Nomenclature in the Colville Basin, Northern Alaska. U.S. Geological Survey Professional Paper 1673, 51.

Neese, D.G., Pigott, J.D., 1987. Ooid genesis at Brown's Cay, Bahamas: *In situ* diurnal observations. 8th Bathhurst Meeting of Carbonate Sedimentologists, Papers with programs.

Oh, C., Legrand, J., Kim, K., Philippe, M., Paik, I.S., 2011. Fossil wood diversity gradient and Far-East Asia palaeoclimatology during the Late Triassic–Cretaceous interval. Journal of Asian Earth Sciences 40, 710–721.

Oh, C., Philippe, M., Kim, K., 2015. *Xenoxylon* synecology and palaeoclimatic implications for the Mesozoic of Eurasia. Acta Palaeontologica Polonica 60, 245–256.

Palibin, I.V., Jarmolenko, A.V., 1932. Novyi vid iskopayemoy drevesiny s Vitimskogo ploskogorya. Izvestiya Vsesoyuznogo geologo-razvedyvatel'nogo obyedineniya (Trudy VGRO) 51, 177–179

Parrish, J.T., Ziegler, A.M., Scotese, C.R., 1982. Rainfall patterns and the distribution of coals and evaporites in the Mesozoic and Cenozoic. Palaeogeography, Palaeoclimatology, Palaeoecology 40, 67–101.

Parrish, J.T., Doyle, J.A., 1984. Predicted evolution of global climate in Late Jurassic–Cretaceous time. International Organization of Paleobotany Conference, Abstract with programs 2.

Parrish, J.T., Peterson, F., 1988. Wind directions predicted from global circulation models and wind directions determined from eolian sandstone of the western United States – a comparison, *In* Kocurek, G. (ed.), Late Paleozoic and Mesozoic Eolian Deposits of the Western Interior of the United States. Sedimentary Geology 56, 261–282.

Parrish, J.T., Spicer, R.A., 1988. Middle Cretaceous wood from the Nanushuk Group, central North Slope, Alaska. Palaeontology 31, 19–34.

Parrish, J.T., Peterson, F., Turner, C.E., 2004. Jurassic "savannah"; plant taphonomy and climate of the Morrison Formation (Upper Jurassic, Western USA). Sedimentary Geology 167, 137–162.

Parrish, J.T., Falcon-Lang, H.J., 2007. Coniferous trees associated with interdune deposits in the Jurassic Navajo Sandstone Formation, Utah, USA. Palaeontology 50, 829–843.

Peterson, F., Turner-Peterson, C.E., 1987. The Morrison Formation of the Colorado Plateau: Recent advances in sedimentology, stratigraphy, and paleotectonics. Hunteria 2, 1–18.

Philippe, M., 1993. *Xenoxylon* as a Protopinaceae? New xylological and palaeoecological evidence. 15º International Botany Conference, Abstr. Prog.

Philippe, M., Thévenard, F., 1996. Repartition and palaeoecology of the Mesozoic wood genus *Xenoxylon*: palaeoclimatological implications for the Jurassic of Western Europe. Review of Palaeobotany and Palynology 91, 353–370.

Philippe, M., Zijlstra, G. Barkacka, M., 1999. Greguss's Morphogenera of Homoxylous Fossil Woods: A Taxonomic and Nomenclatural Review. Taxon, 48, 667-676.

Philippe, M., Bamford, M.K., 2008. A key to morphogenera used for Mesozoic conifer-like woods. Review of Palaeobotany and Palynology 148, 184–207.

Philippe, M., Jiang, H-E., Kim, K., Oh, C., Gromyko, D., Harland, M., Paik, I.-S., Thévenard, F., 2009. Structure and diversity of the Mesozoic wood genus *Xenoxylon* in Far East Asia: Implications for terrestrial palaeoclimates. Lethaia 42, 393–406.

Philippe, M., Thévenard, F., Nosova, N., Kim, K., Naugolnykh, S., 2013. Systematics of palaeoecologically significant boreal Mesozoic fossil wood genus, *Xenoxylon* Gothan. Review of Palaeobotany and Palynology 193, 128–140.

Philippe, M., Puijalon, S., Suan, G., Mousset, S., Thévenard, F., Mattioli, E., 2017. The paleolatitudinal, distribution of fossil wood genera as a proxy for European Jurassic terrestrial climate. Palaeogeography, Palaeoclimatology, Palaeoecology 466, 373–381.

Richmond, D.R., Morris, T.H., 1998. Stratigraphy and cataclysmic deposition of the Dry Mesa Dinosaur Quarry, Mesa County, Colorado. Modern Geology 22, 121–143.

Richmond, D.R., Lukens, M.W., Celestino, S.M., 2017. Upper Jurassic Morrison Formation clams on the half shell, central Montana. The Geological Society of America, 49.

Richmond, D.R., Behm, M., Lupia, R, Hein, D.G., 2018. Tufa-like carbonate build-ups imaged through electrical resistivity tomography: A case study from the Morrison Formation of central Montana. The Geological Society of America, 50.

Schudack, M.E., Turner, C.E., Peterson, F., 1998. Biostratigraphy, paleoecology, and biogeography of charophytes and ostracodes from the Upper Jurassic Morrison Formation, Western Interior, USA. Modern Geology 22, 379–414.

Selmeier, A., Grosser, D., 2011. Lower Cretaceous conifer drift wood from Sverdrup Basin, Canadian Arctic Archipelago. Zitteliana 51, 19–35.

Silverman A.J., Harris, W.L., 1967. Stratigraphy and economic geology of the Great Falls-Lewistown coal field central Montana. State of Montana Bureau of Mine and Geology Bulletin 56, 1–20.

Small, B.J., Gorman, M.A., Pardo, J., Smith, D., 2007. A Late Jurassic lacustrine biota from the Morrison Formation of Colorado. The Geological Society of America, Abstr. Prog. 39, 400.

Spicer, R.A., Parrish, J.T., 1990. Latest Cretaceous woods of the central North Slope, Alaska. Palaeontology 33, 225–242.

Suttner, L.J., 1969. Stratigraphic and petrographic analysis of Upper Jurassic–Lower Cretaceous Morrison and Kootenai Formations, southwest Montana. The American Association of Petroleum Geologist Bulletin 53, 1391–1410.

Suzuki, M., Terada, K., 1992. *Xenoxylon* fossil woods from the Lower Cretaceous Akaiwa subgroup of Shiramine, central Japan. Journal of Phytogeography and Taxonomy 40, 91–97.

Terada, K., Nishida, H., Sun, G., 2011. Fossil woods from the Upper Cretaceous to Paleocene of Heilongjang (Amur) River area of China and Russia. Global Geology 14, 192–208.

Tian, N., Xie, A.-W., Wang, Y.-D., Jiang, Z.-K, Li, L.-Q., Yin, Y.-L., Zhu, Z-P.., Wang, J.-J., 2015. New records of Jurassic petrified wood in Jianchang of western Liaoning, China and their palaeoclimate implications. Science China Earth Science 58, 2154–2164.

Tian, N., Wang, Y.-D., Philippe, M., Li, L.-L. Xie, X.-P., Jiang, Z.-K., 2016. New record of fossil wood *Xenoxylon* from the Late Triassic in the Sichuan Basin, southern China and its paleoclimatic implications. Palaeogeography, Palaeoclimatology, Palaeoecology 464, 65–75.

Tidwell, W.D., 1990. Preliminary report on the mega flora of the Upper Jurassic Morrison Formation. Hunteria 2, 3–12.

Tidwell, W.D., Britt, B.B., Ash, S.R., 1998. Preliminary floral analysis of the Mygatt-Moore Quarry in the Jurassic Morrison Formation, west-central Colorado. Modern Geology 22, 341–378.

Trujillo, K.C., Foster, J.R., Hunt-Foster, R.K., Chamberlain, K.R., 2014. A U/Pb age for the Mygatt-Moore Quarry, Upper Jurassic Morrison Formation, Mesa County, Colorado. Volumina Jurassica 2, 107–114.

Trujillo, K.C., Kowallis, B.J., 2015. Recalibrated legacy $^{40}Ar/^{39}Ar$ Ages for the Upper Jurassic Morrison Formation, Western Interior, U.S.A. Geology of the Intermountain West 2, 1–8.

Turner, C.E., Fishman, N.S., 1991. Jurassic Lake T'oo'dichi': A large alkaline, saline lake, Morrison Formation, eastern Colorado Plateau. The Geological Survey of America Bulletin 103, 538–558.

Turner, C.E., Peterson, F., 1999. Biostratigraphy of dinosaurs in the Upper Jurassic Morrison Formation of the Western Interior, U.S.A. Utah Geological Survey Miscellaneous Publication 99-1, 77–114.

Valdes, P.J., Sellwood, B.W., 1992. A palaeoclimatic model for the Kimmeridgian. Palaeogeography, Palaeoclimatology, Palaeoecology 95, 47–72.

Vogellehner, J., 1968. Zur anatomie und phylogenie mesozoischer gymnospermenhölzer, beitrag 7: Prodromus zu einer Monographie der Protopinaceae. II. Die Protopinoiden Hölzer des Jura. Palaeontographica B 124, 125–162.

Wan, M., Zhou, W., Tang, P., Liu, L., Wang, J., 2016. *Xenoxylon junggarensis* sp. nov., a new gymnospermous fossil wood from the Norian (Triassic) Huangshanjie Formation in northwestern China, and its palaeoclimatic implications. Palaeogeography, Palaeoclimatology, Palaeoecology 441, 679–687.

Wilkens, N.D., Farmer, J., Pigg, K., 2005. Exceptional paleobotanical remains preserved in Navajo Sandstone interdune deposits near Moab, Utah. The Geological Society of America Abstr. Prog. 37, 527.

Wilkens, N.D., 2008. Paleoecology of Early Jurassic Navajo Sandstone interdune deposits. Unpublished PhD dissertation University of Arizona, Tucson, AZ, 417 p.

Wright, I.J., Reich, P.B., Westoby, M., et al. 2004. The worldwide leaf economics spectrum. Nature 428, 821–827.

Zheng, S.-L., Li, Y., Zhang, W., Li, N., Wang, Y.-D., Yang, X.-J., Yi, T.-M., Yang, J.-J., Fu, X.-P., 2008. Fossil wood of China. China Forestry Publishing House, Beijing, 356.

Figures

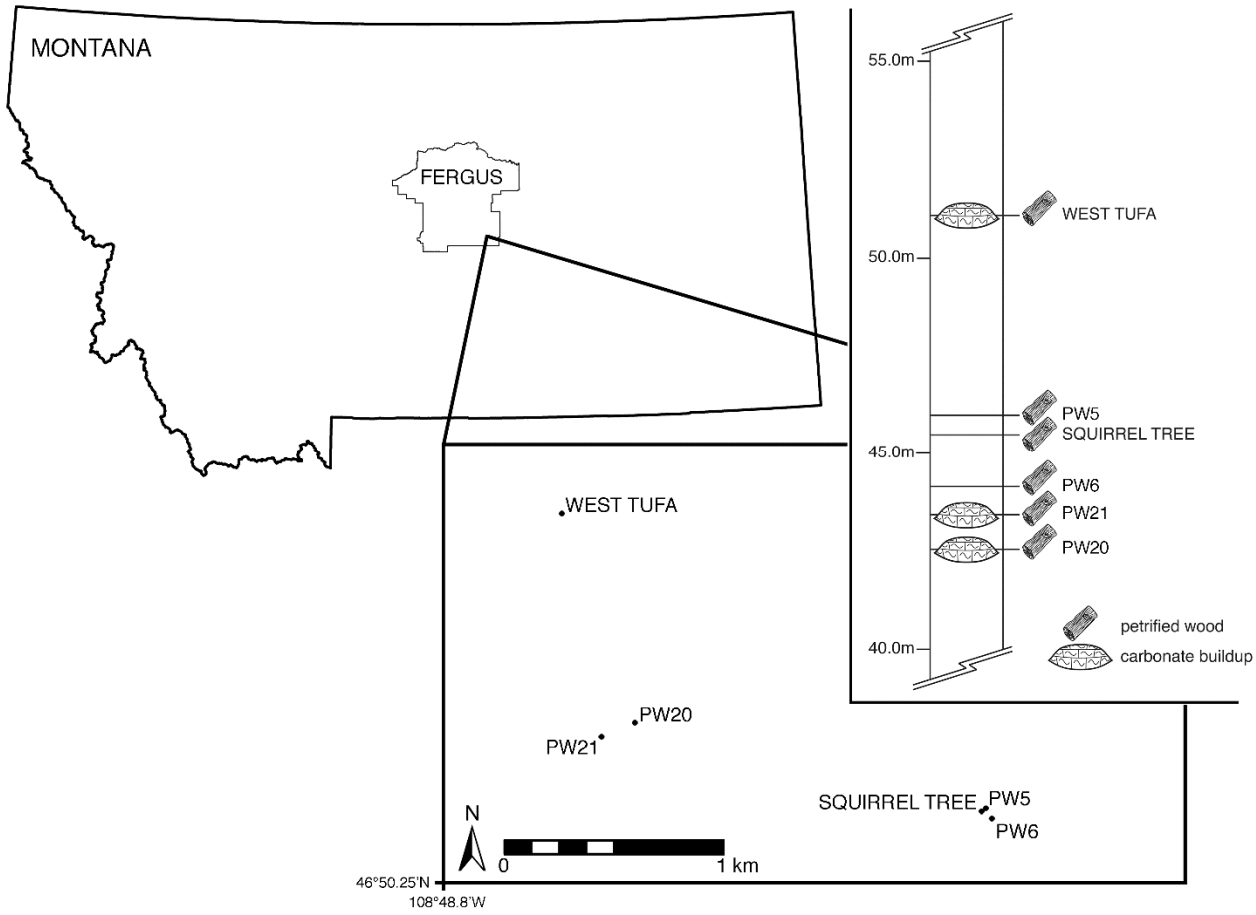

Figure 1. Geographic and stratigraphic distribution of localities from which petrified wood of *Xenoxylon* has been identified in Fergus County, Montana. Height in composite stratigraphic section reported as meters above the conformable Swift/Morrison formational contact.

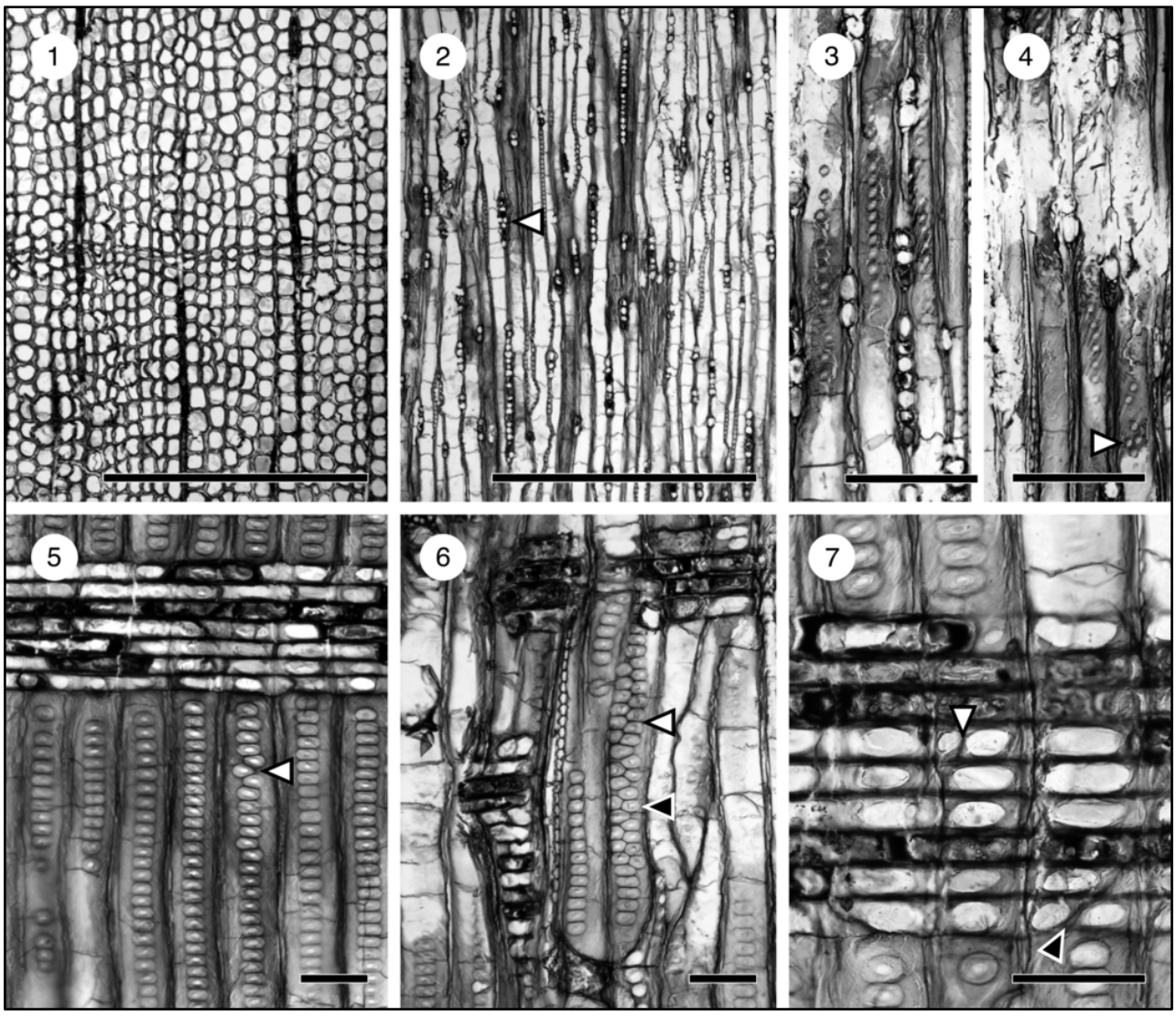

Plate 1. Petrified wood specimen PW20. **1**. Transverse section showing abrupt growth ring 1–2 cells wide; OPC 2281–31626, 146.7 x 33.8, scale bar = 1 mm. **2**. Tangential section showing medullary rays and septa in tracheids. Rays are usually uniseriate, but some rays are partially biseriate (arrow); OPC 2281–31628, 120.2 x 27.5, scale bar = 1 mm. **3**. Tangential section showing tangential bordered pits in late wood. Pitting is dispersed or continuous; OPC 2281–31628, 144.7 x 7.9, scale bar = 100 µm. **4**. Tangential section showing tangential bordered pits in late wood. Pitting is usually uniseriate but rarely subopposite (arrow); OPC 2281–31628, 143.0 x 8.4, scale bar = 100 µm. **5**. Radial section showing xenoxylean radial bordered pits in mostly long, uniseriate, contiguous series. Frequently shorter series and even isolated pits appear (lower left) and very rarely subalternate pits are observed (arrow); OPC 2281–31630, 127.7 x 13.6, scale bar = 100 µm. **6**. Radial section showing biseriate, alternate (white arrow) to subopposite (black arrow) pitting in disturbed wood; OPC 2281–31630, 125.6 x 8.4, scale bar = 100 µm. **7**. Radial section showing fenestrate cross-field pits. Usually only one pit occupies cross-field, but two occur where two ray cells overlap a tracheid (white arrow) or where two tracheids overlap a ray cell (black arrow); OPC 2281–31630, 130.7 x 41.0, scale bar = 100 µm.

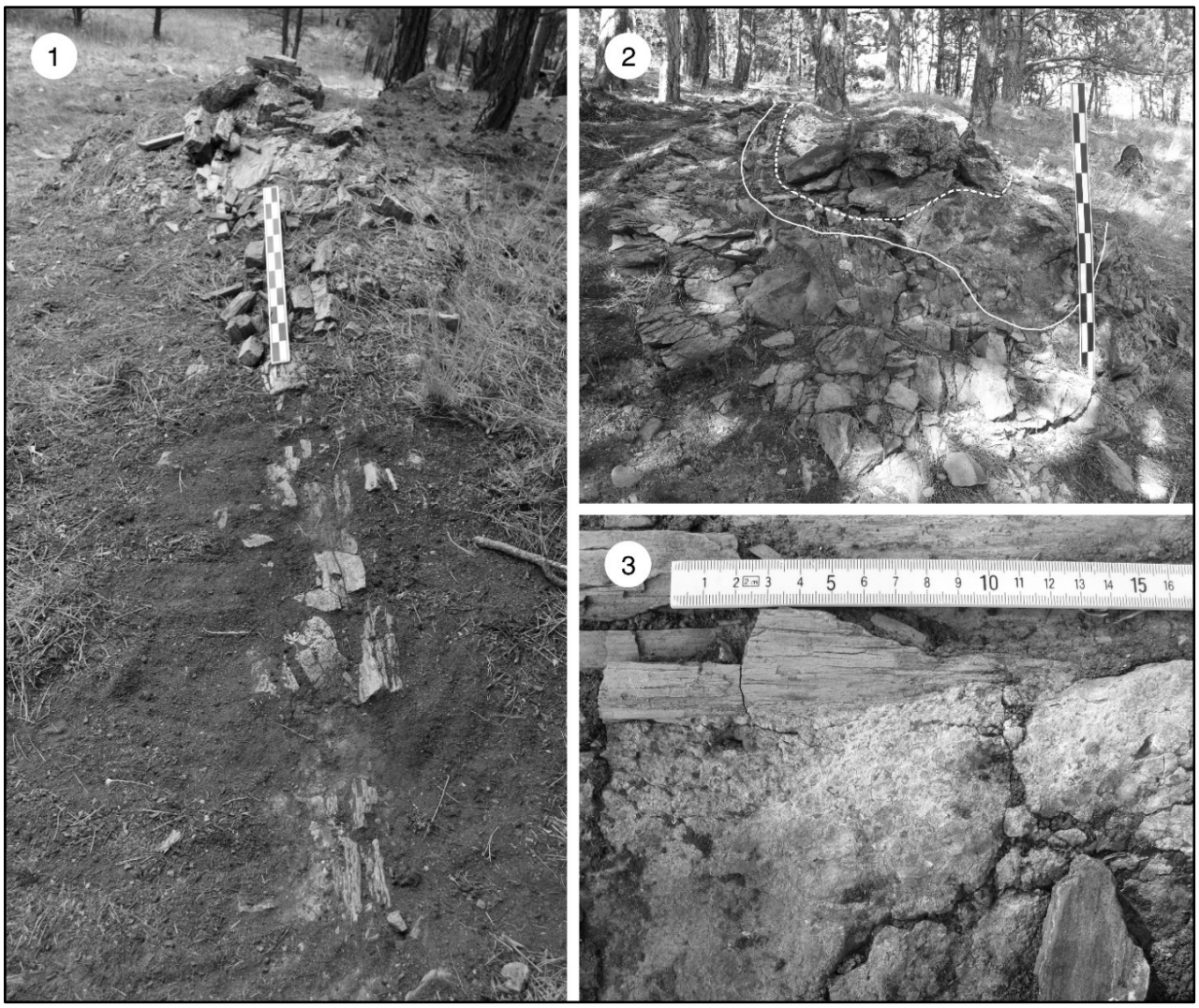

Figure 2. **1**. Image of petrified log of *Xenoxylon* Gothan, 1905 found in a carbonate build-up at the West Tufa locality, Fergus County, Montana. Scale is one meter. **2**. Image of petrified log and build-up in cross section illustrating approximate boundaries of log (dashed line) and the carbonate. Scale is one meter. **3**. Closeup image of petrified log in, and partially covered by, a spheroidal/ spherulitic carbonate. Scale is in centimeters.

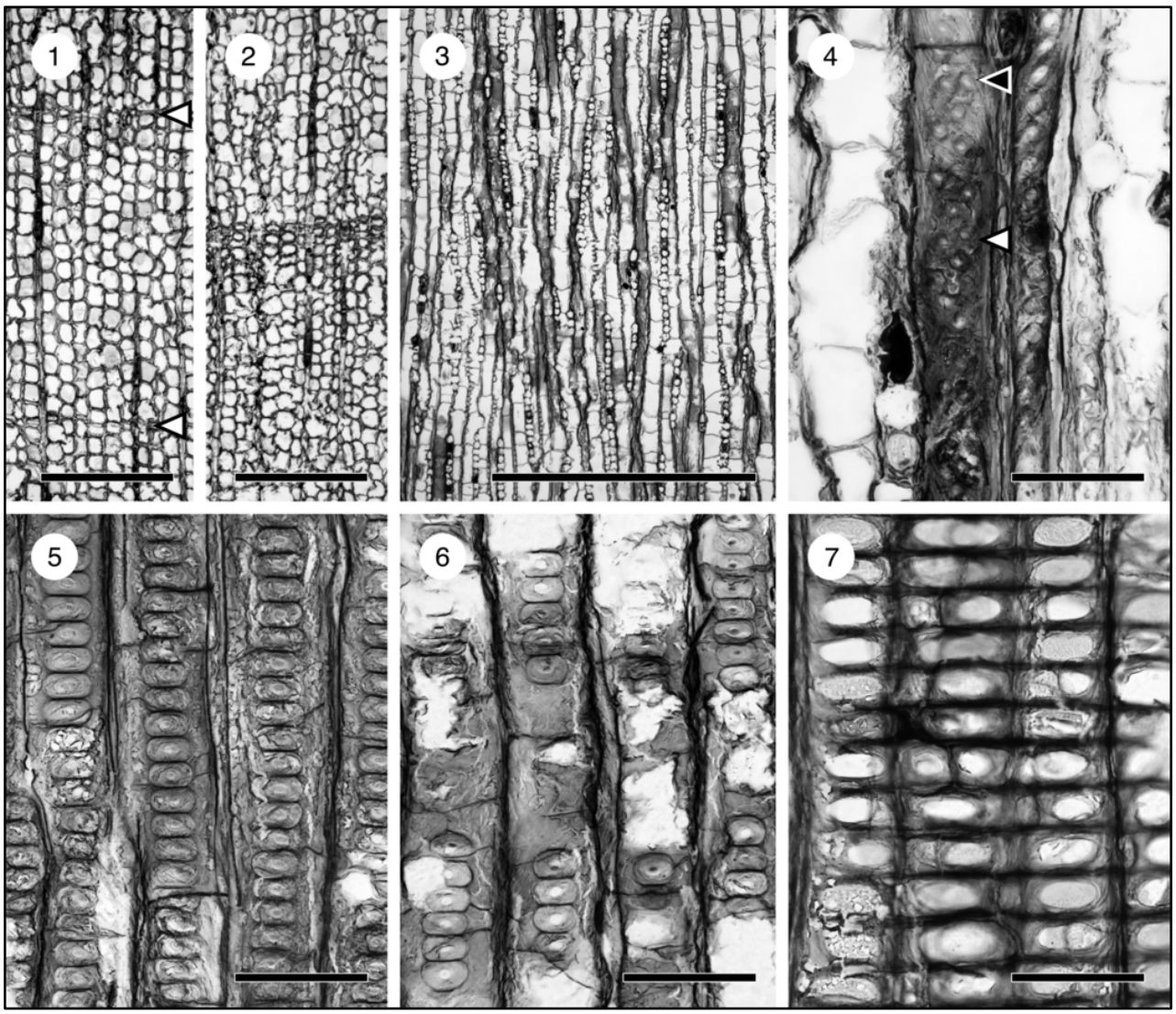

Plate 2. Petrified wood specimen PW21. **1**. Transverse section showing two abrupt growth rings 1–2 cells wide (arrows); OPC 2282–31640, 137.7 x 11.8, scale bar = 500 µm. **2**. Transverse section showing semi-abrupt growth ring 3–5 cells wide; OPC 2282–31640, 143.2 x 13.7, scale bar = 500 µm. **3**. Tangential section showing uniseriate medullary rays and septa in tracheids; OPC 2282–31643, 137.6 x 31.9, scale bar = 1 mm. **4**. Tangential section showing tangential bordered pits in late wood. Pitting is usually uniseriate but frequently subalternate (white arrow) to subopposite (black arrow). OPC 2282–31643, 143.0 x 8.4, scale bar = 100 µm. **5**. Radial section showing xenoxylean radial bordered pits in long, uniseriate, contiguous series; OPC 2282–31649, 132.0 x 25.1, scale bar = 100 µm. **6**. Radial section showing gaps and short series of radial bordered pits; OPC 2282–31649, 132.5 x 20.7, scale bar = 100 µm. **7**. Radial section showing fenestrate cross-field pits. Two pits occur where two rays' cells overlap a tracheid; OPC 2282–31649, 139.8 x 38.2, scale bar = 100 µm.

	Ray Height (number of cells)					
Specimen	Minimum	Median	Mean	Maximum	Variance	Maximum out-of-count
PW20	1	2	4.6	18	14.6	32
PW21	1	4	7.0	27	37.6	52
PW6	1	7	8.1	29	29.4	52
Squirrel Tree	2	7	7.5	18	11.7	37
PW5	1	5	6.0	25	23.8	42
West Tufa	2	9	9.2	21	17.0	46

Table 1. Comparison of ray heights, measured as the number of cells, for each of the six specimens of *Xenoxylon* described from Fergus County, Montana. Values, except for "maximum out-of-count" are based on 100 rays selected at random. Value for maximum out-of-count is based on scanning one entire tangential section (≈ 12 cm^2). For partially biseriate rays, count was made along both sides and minimum value recorded.

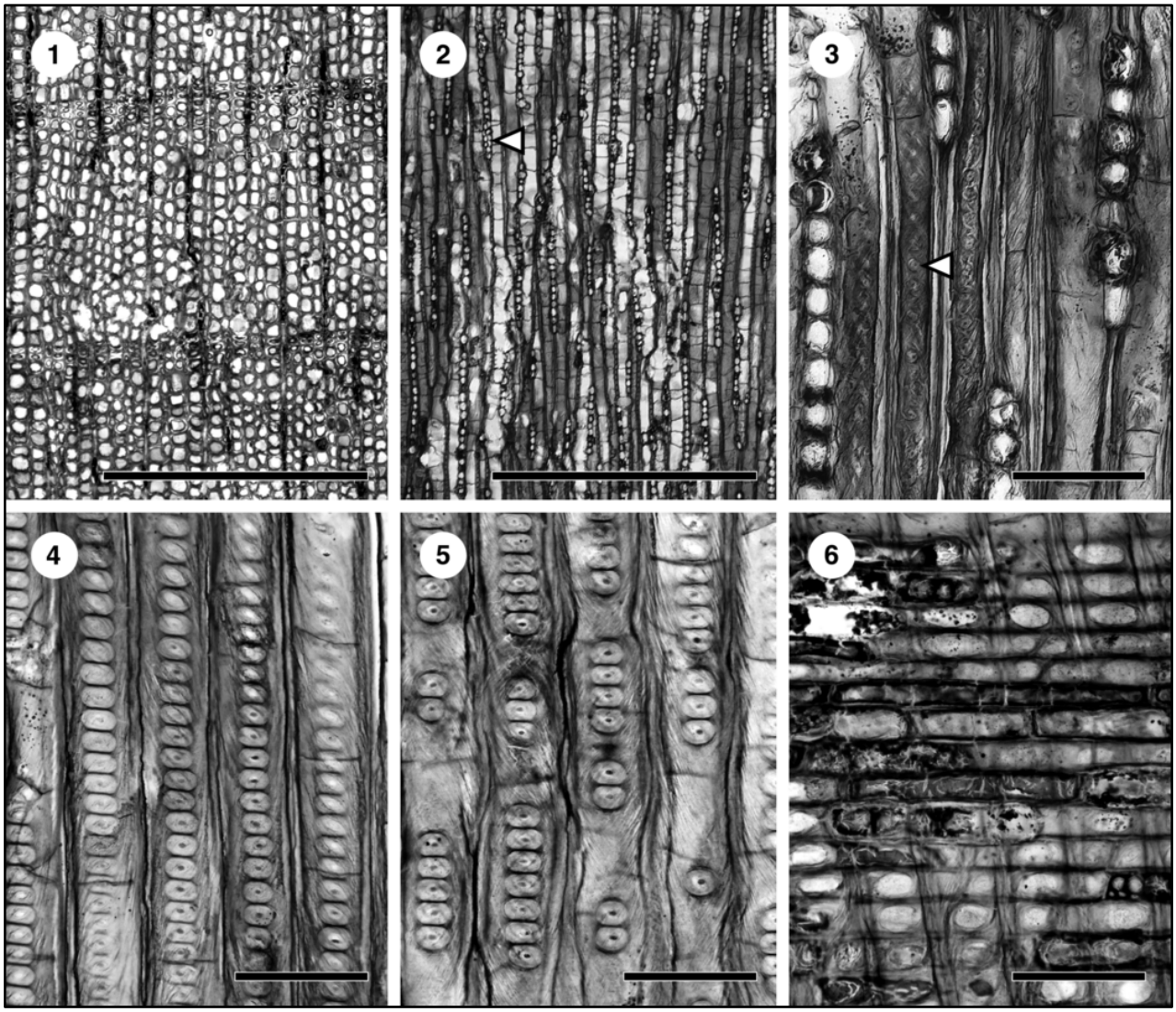

Plate 3. Petrified wood specimen PW6. **1**. Transverse section showing two semi-abrupt growth rings of 4–5 cells, OPC 2267–31607, 157.3 x 7.8, scale bar = 1 mm. **2**. Tangential section showing medullary rays and septa in tracheids. Rays are usually uniseriate, but some rays are partially biseriate (arrow); OPC 2267–31617, 156.1 x 35.7, scale bar = 1 mm. **3**. Tangential section showing tangential bordered pits (arrow) in late wood. OPC 2267–31617, 148.5 x 45.1, scale bar = 100 µm. **4**. Radial section showing xenoxylean radial bordered pits in long, uniseriate, contiguous series; OPC 2267–31619, 142.7 x 29.1, scale bar = 100 µm. **5**. Radial section showing gaps and short series of radial bordered pits; OPC 2267–31619, 134.3 x 12.1, scale bar = 100 µm. **6**. Radial section showing fenestrate cross-field pits. Two pits occur where two rays' cells overlap a tracheid. Ray cell walls usually perpendicular, sometimes oblique; OPC 2267–31619, 154.6 x 11.8, scale bar = 100 µm.

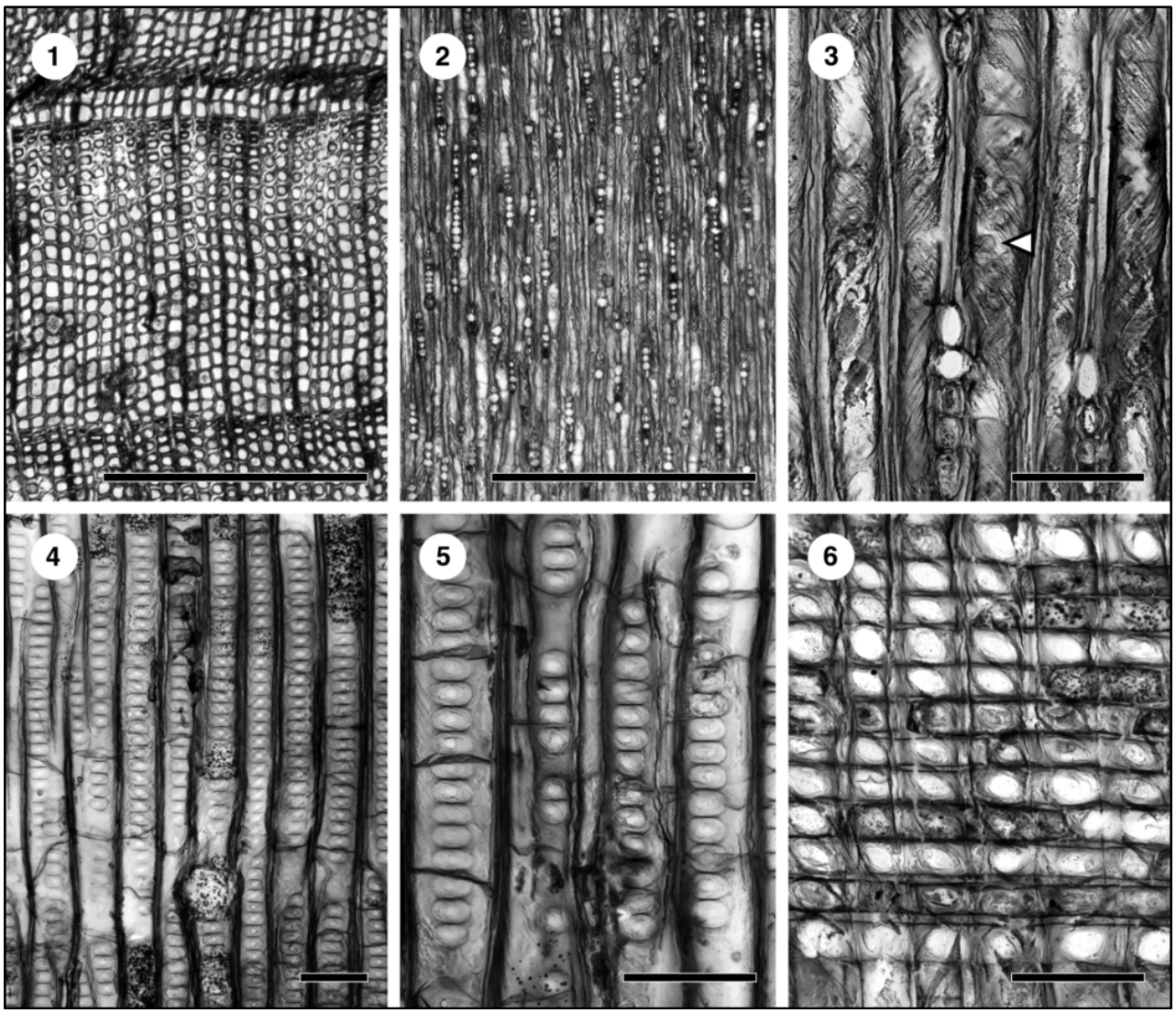

Plate 4. Petrified wood specimen Squirrel Tree. **1**. Transverse section showing two semi-abrupt growth rings of 2–5 cells, OPC 2259–31570, 157.9 x 32.2, scale bar = 1 mm. **2**. Tangential section showing uniseriate medullary rays; OPC 2259–31575, 157.7 x 23.5, scale bar = 1 mm. **3**. Tangential section showing discontinuous tangential bordered pits in late wood, not always in straight series (arrow). Note spiral checking. OPC 2259–31575, 164.0 x 29.9, scale bar = 100 µm. **4**. Radial section showing xenoxylean radial bordered pits in long, uniseriate, contiguous series with local gaps. Pits appear alternate (lower left) due to overlap of two tracheids; OPC 2259–31573, 114.9 x 35.2, scale bar = 100 µm. **5**. Radial section showing gaps and short series of radial bordered pits as wells as septa; OPC 2259–31573, 151.7 x 25.6, scale bar = 100 µm. **6**. Radial section showing fenestrate cross-field pits. Cross-field pits appear oblique and pointed due to spiral checking compared to cross-field with wide or no checking (arrow); OPC 2259–31573, 112.4 x 38.1, scale bar = 100 µm.

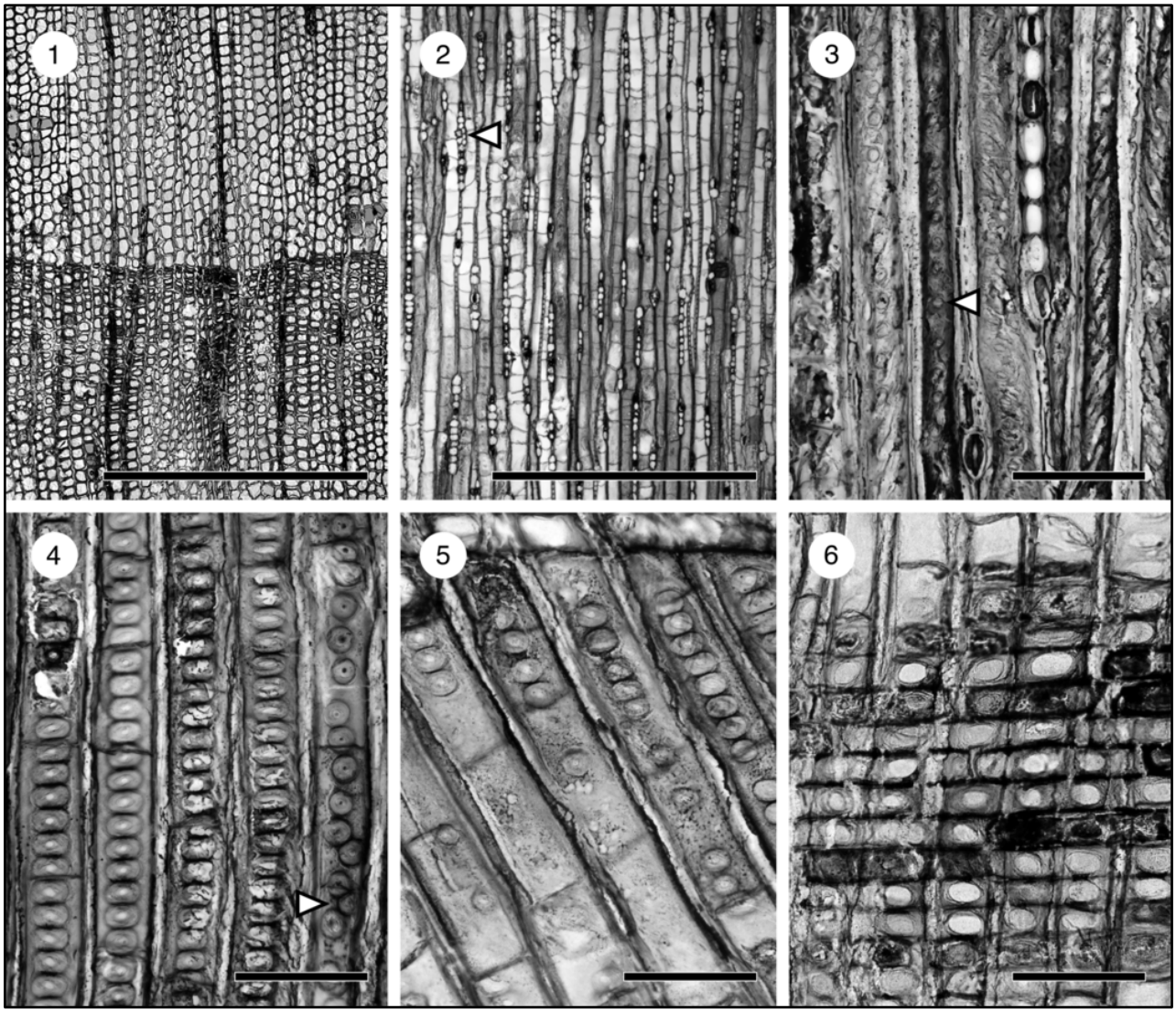

Plate 5. Petrified wood specimen PW5. **1**. Transverse section showing semi-abrupt growth rings of 1–6 cells, OPC 2266–31593, 117.2 x 30.4, scale bar = 1 mm. **2**. Tangential section showing uniseriate medullary rays, occasionally partially biseriate (arrow), and septa; OPC 2266–31599, 143.9 x 36.9, scale bar = 1 mm. **3**. Tangential section showing discontinuous tangential bordered pits in late wood. Note spiral checking; OPC 2266–31599, 153.5 x 22.4, scale bar = 100 µm. **4**. Radial section showing xenoxylean radial bordered pits in long, uniseriate, contiguous series and loose, semi-alternate series (arrow). Pits appear alternate (lower left) due to overlap of two tracheids; OPC 2266–31603, 144.6 x 29.6, scale bar = 100 µm. **5**. Radial section showing gaps and short series of radial bordered pits; OPC 2266–31603, 128.7 x 43.1, scale bar = 100 µm. **6**. Radial section showing fenestrate cross-field pits; OPC 2266–31603, 154.5 x 26.7, scale bar = 100 µm.

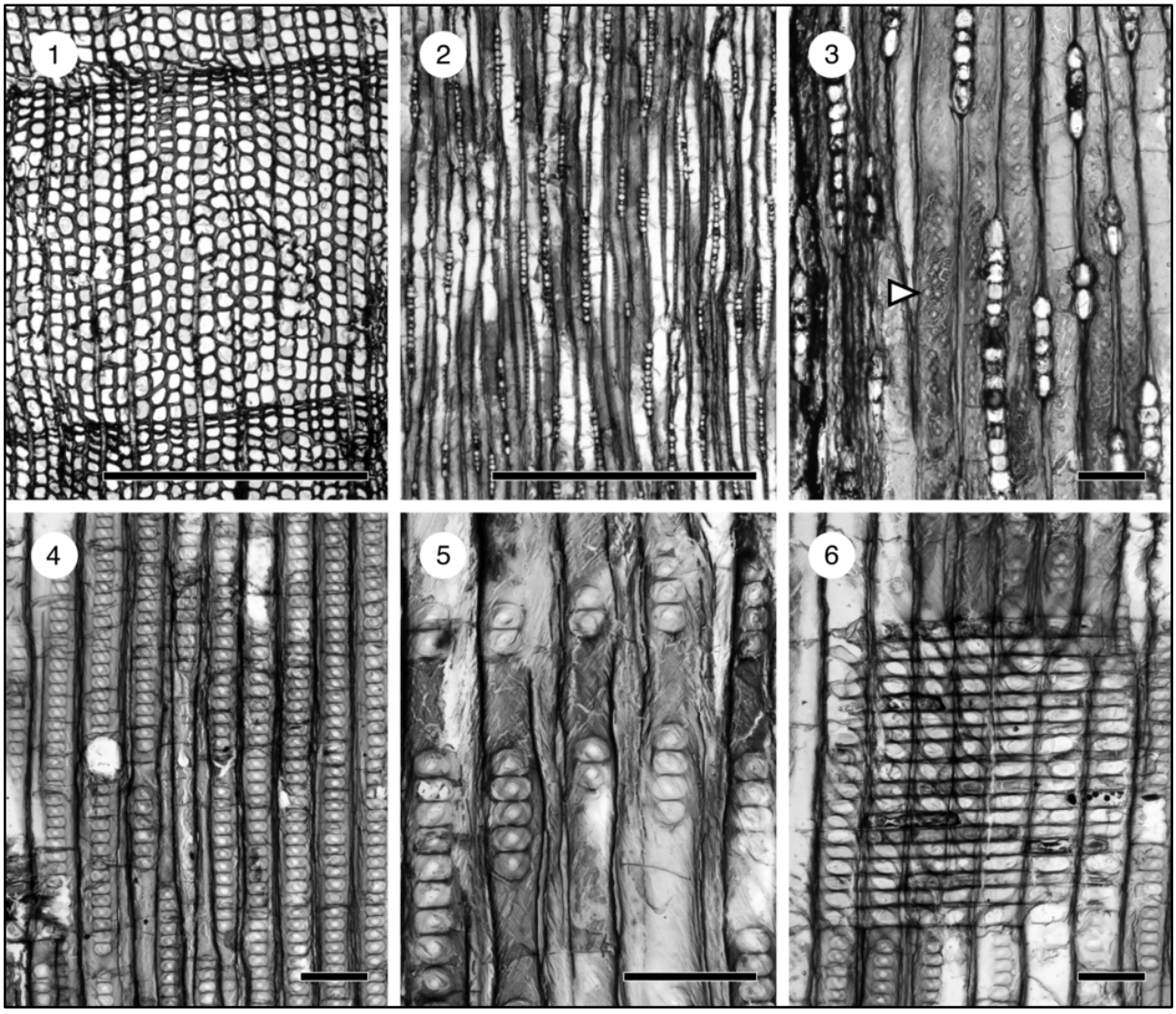

Plate 6. Petrified wood specimen West Tufa. **1**. Transverse section showing two abrupt to semi-abrupt growth rings of 1–5 cells, OPC 2256–31559, 117.1 x 15.1, scale bar = 1 mm. **2**. Tangential section showing uniseriate medullary rays and septa; OPC 2256–31561, 119.4 x 32.4, scale bar = 1 mm. **3**. Tangential section showing contiguous and discontinuous tangential bordered pits in late wood, some subopposite (arrow); OPC 2256–31561, 120.9 x 18.3, scale bar = 100 µm. **4**. Radial section showing xenoxylean radial bordered pits in long, uniseriate, contiguous series with few gaps; OPC 2256–31553, 124.6 x 24.5, scale bar = 100 µm. **5**. Radial section showing gaps and short series of radial bordered pits. Note spiral checking; OPC 2256–31553, 150.0 x 26.5, scale bar = 100 µm. **6**. Radial section showing fenestrate cross-field pits appearing oblique and pointed due to checking; OPC 2256–31553, 121.7 x 38.0, scale bar = 100 µm.

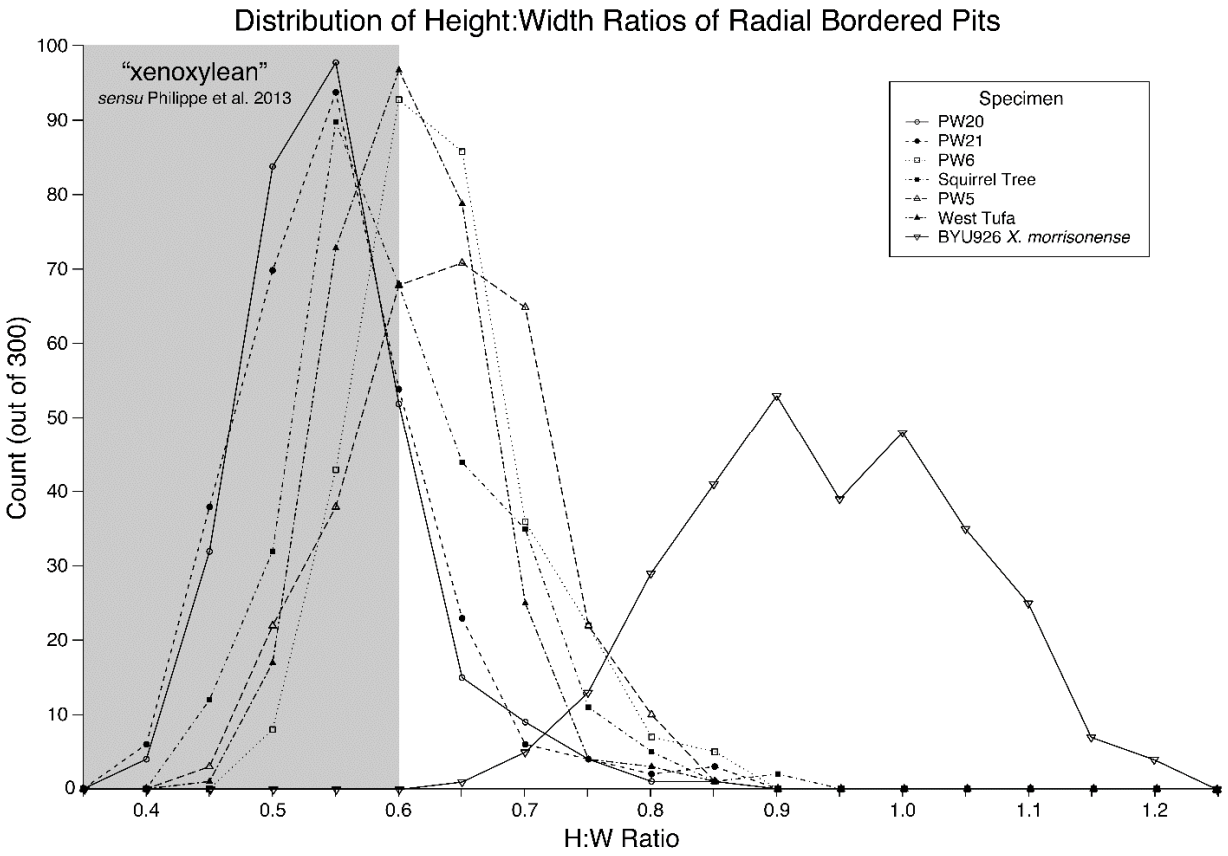

Figure 3. Distribution of height to width ratios of radial bordered pits for seven specimens of *Xenoxylon.* Each point is the number of measurements in a bin of width 0.05 plotted at the included upper bin limit. Measurements were made for 300 radial bordered pits from each of the six specimens of *Xenoxylon* described herein, plus the type specimen of *Xenoxylon morrisonense* Medlyn et Tidwell (BYU 926). Gray area denotes height to width ratios less than 0.6 that characterize "xenoxylean" pits as designated by Philippe et al. (2013).

Figure 4. Distribution and status of published *Xenoxylon* occurrences in North America. Occurrences are grouped by formation but divided by time and/or species following Oh et al. (2015, and its supplementary material). **1**. *X. phyllocladoides*, Pleinsbachian (Oh et al., 2015 suppl.); **2**. *X. phyllocladoides*, Toarcian (Oh et al., 2015 suppl.); **3**. *X.* sp., Pleinsbachian–Toarcian (Parrish and Falcon-Lang, 2007); **4**. *X. phyllocladoides*, Aalenian (Oh et al., 2015 suppl.); **5**. *X. phyllocladoides*, Callovian (Oh et al., 2015 suppl.); **6**. *X. phyllocladoides*, Kimmeridgian–Tithonian (Oh et al., 2015 suppl.); **7**. *X. morrisonense*, Kimmeridgian–Tithonian (Medlyn and Tidwell, 1975); **8**. *X. moorei*, Kimmeridgian–Tithonian (Tidwell et al., 1998); **9**. *X. meisteri*, Kimmeridgian–Tithonian (this paper); **10**. *Dacrydioxylon* sp. (= *X. hopeiense* per Philippe et al., 2013), Valanginian (Selmeier and Grosser, 2011); **11**. Axis 25 and Axis 26 (= *X. phyllocladoides* group per Oh et al., 2015 suppl.), Barremian–Aptian (Gordon, 1932); **12**. *X. latiporosum*, Albian–Cenomanian (Arnold, 1952, but see text for discussion); **13**. *X. latiporosum*, Albian–Cenomanian (Parrish and Spicer, 1988); **14**. *X.* sp., Albian–Cenomanian (Murphy et al., 2005); **15**. *X. latiporosum*, Campanian (Spicer and Parrish, 1990); **16**. *X. latiporosum*, Maastrichtian (Spicer and Parrish, 1990).

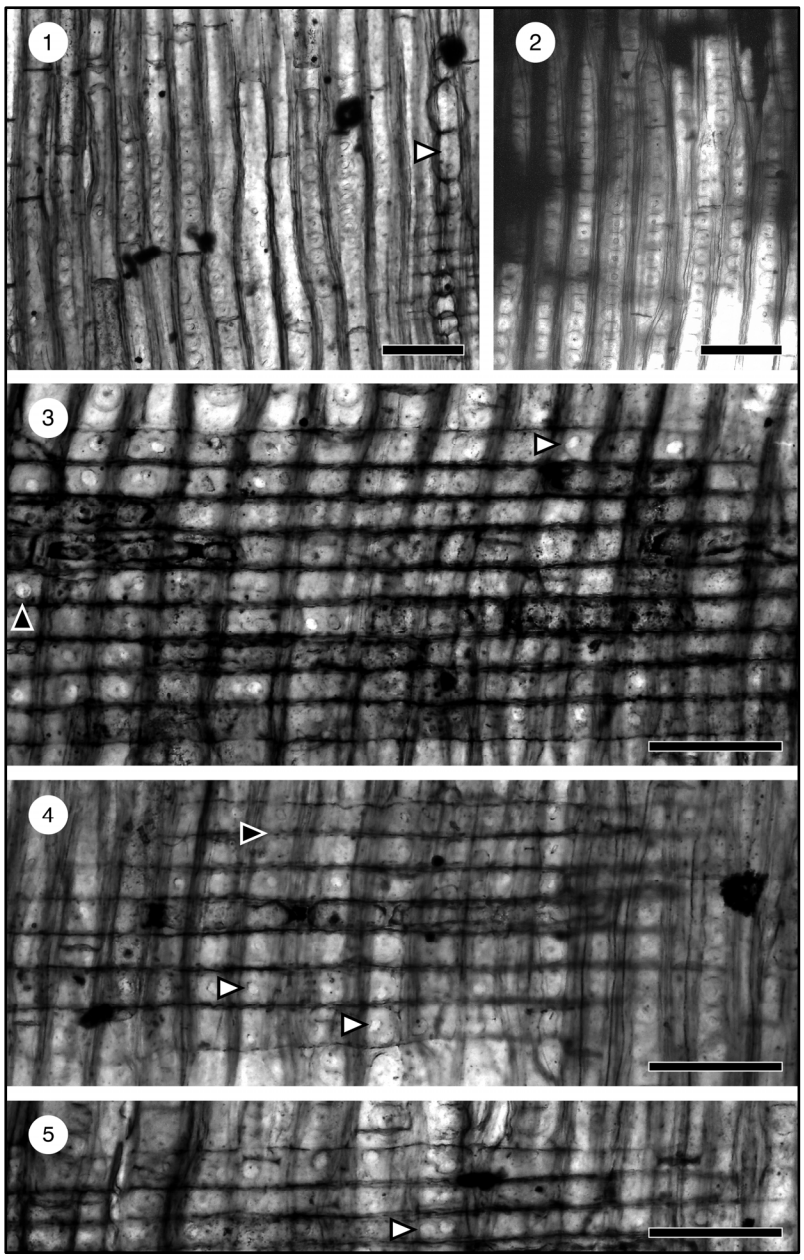

Plate 7. Type specimen of *Xenoxylon morrisonense* Medlyn et Tidwell, 1975 (BYU 926). **1**. Radial section showing radial bordered pits in long, uniseriate, contiguous series. Note nearly circular outlines and swollen, bulbous axial parenchyma (arrow). **2**. Radial section showing radial bordered pits in long, uniseriate, contiguous series with blue filter to decrease contrast in thick area of specimen. **3**. Radial section showing cross-field pitting consisting of a single simple pit that is oblique and pointed (white arrow) or nearly circular (black arrow). Pits vary in size but never fill cross-field. **4**. Radial section showing cross-field pitting consisting of a single simple, oblique pits (arrows). Undulating ray cell walls are evident here (black arrow) but appear to be due preservation rather than structural indentations as concluded by Medlyn and Tidwell. **5**. Radial section showing cross-field pitting consisting of two, simple, nearly circular pits (arrow). Pairs of cross-field pits are proportionally rare compared to single pits. All scale bars = 100 μm.

CHAPTER 3

Carbonate mound springs of the Upper Jurassic Morrison Formation of central Montana and their paleoclimatic significance for the northern foreland basin

Dean Richmond [a], John Pigott [a], Richard Lupia [b], Michael Behm [a], and David Hien [c]

[a] *School of Geosciences, University of Oklahoma, Sarkeys Energy Center Suite 710, Norman, Oklahoma 73019, USA*
[b] *Sam Noble Museum, University of Oklahoma, 2401 Chautauqua Avenue, Norman, OK 73072*
[c] *Billings, Montana, USA*

ABSTRACT

Recent investigations of the Morrison Formation in central Montana resulted in the discovery of 99 small (< 3 m diameter) carbonate buildups in close geographic and stratigraphic proximity. The buildups may be divided into two groups by dominant mineralogic composition: siderite versus calcium carbonate. The siderite buildups display prominent cone-in-cone structures whereas several calcium carbonate buildups encase trunks of silicified wood. The buildups are found in five distinct spatial clusters on the southern and western flanks of Spindletop Dome and are distributed in association with, and alignment to, the Jurassic-aged structural lineaments in the region. The buildups are distributed stratigraphically between 40–52 m above the base of the Morrison Formation. Interpretation of electrical resistivity tomography surveys indicate that additional buildups are present in the subsurface. Carbonate-rich groundwater migrated up the fractures to the capillary fringe or to the surface. The siderite buildups likely formed in the subsurface near the capillary springs and were subartesian, with low surface discharge rates. The bulk rock negative δ13C values demonstrate the buildups were produced by meteoric waters in a continental setting. The presence of the mound spring tufa deposits scattered throughout a 12 m portion of the Morrison section indicate that the region experienced extended periods of increased rainfall.

1. Introduction

The Upper Jurassic Morrison Formation, an expansive sequence of terrestrial sediments deposited in foreland basins formed by the North America Cordilleran orogenic system, covers approximately 1.5 million km^2 of the intermountain west (Dodson et al., 1980). The formation has been intensely studied for uranium (Turner-Peterson and Fishman, 1986), coal (Harris, 1966; Silverman and Harris, 1966), oil and gas (Johnson, 2005) and dinosaurs (Foster, 2007). Since the dinosaur Bone Wars of Othniel Charles Marsh and Edward Drinker Cope during the 1870's in the newly opened American West, dinosaurs have been the focus of research and imagination. Jurassic dinosaurs have been discovered in every U.S. state where the Morrison Formation is exposed (Turner and Peterson, 1999). Age equivalent rocks are found in southcentral Canada but have only yielded plant fossils; vertebrate fossils have yet to be discovered (Brown, 1946; Rouse, 1959; Jansa, 1972).

The relatively recent discovery and ongoing excavation of dinosaurs in the northernmost portion of the Morrison foreland basin prompted research to discern the stratigraphic placement of the dinosaur quarries and to provide insight into the depositional facies and paleoecology. This geological investigation led to the discovery of numerous fossil wood sites in the research area (Richmond et al., 2019; Richmond et al., 2019a; Richmond et al., 2019b). Petrified wood was found in proximity to, and encased in, strange hemisphere-shaped terrestrial carbonate buildups (Richmond et al., 2019). The discovery of numerous previously unidentified terrestrial carbonate buildups initiated this project to ascertain their origin and significance. These are the first terrestrial carbonates buildups reported for the Morrison Formation. The purpose of this paper is to document the surface and near-subsurface spatial configuration of the buildups, place them into a

stratigraphic framework, compare them to other terrestrial carbonates and draw conclusions as to the environmental conditions that led their development, and to understand their paleoclimatic significance.

2. Methods

2.1 Geological data collection

Stratigraphic measurements were made using accepted geological methods and surveyed using a Nikon DTM-322 total station. Samples retrieved were then thin sectioned by Wagner Petrographic (Lindon, Utah) and subsequently were examined under a Zeiss petrographic microscope. The spatial position of each buildup was determined by a handheld Garmin GPS. The buildups appear to have a linear component to them, therefore best fit lines were drawn for the spatial latitude and longitude data.

2.2 Geochemical Analysis

A Thermo Scientific Niton XL3t Ultra Analyzer X-ray Fluorescence gun was used to measure the elemental abundance of the carbonates. The device measured each sample for 210 seconds cycling from Main Range, High Range, Low Range, and Light Range. The Main, High, and Low Ranges ran for 30 seconds, the Light Range ran for 90 seconds. The order was repeated to complete the full 210-second reading. Forty-one elements were measured using the XRF tool; 28 of these elements provide useful insight into the rock's lithologic composition. Only the highest percentages of elements are shown for this study.

Carbonate samples were prepared for x-ray diffraction (XRD) with accepted methods (Moore and Reynolds, 1997). Powder XRD analyses were performed at the University of

Oklahoma School of Geosciences using a Rigaku Ultima IV diffractometer. Cu-K-alpha radiation (40 kV, 44 mA) was used with a scintillation detector. Data analysis was completed using Jade 2010 software with the ICDD (International Centre for Diffraction Data) PDF4+ database.

2.3 Isotopic data collection

Stable isotopic analyses of oxygen and carbon in calcium carbonate were performed using a Thermo Electron Kiel IV automated carbonate preparation device connected to a Thermo MAT 253 stable isotope ratio monitoring mass spectrometer. The system is equipped with a dual inlet system and is housed in the Stable Isotope Geoscience Facilities (SIGF) at Texas A&M University. Isotope values are reported in delta notation relative to the Vienna Pee Dee Belemnite (VPDB‰) isotopic standard. The long-term average precision of the isotopic reference material NBS19 measured within sample runs to monitor instrumental precision is 0.06‰ for $\delta^{18}O$ (±1σ) and 0.03‰ for $\delta^{13}C$ (±1σ) for the SIGF Kiel IV and MAT 253.

2.4 Geophysical Data Collection

Electrical resistivity tomography (ERT) data were acquired using an ARES-II system with stainless steel electrodes at a 1-m and 2-m spacing. All four profiles were measured using a dipole electrode configuration, sensitive to both lateral and vertical changes in resistivity. The ERT data were processed and inverted using AGI EarthImagerTM 2D resistivity inversion and modeling software. The inversion algorithm is based on an iterative damped least square method which is dependent on several constraints. Among them, the choices of the initial model and of the damping factor usually have the largest effects. Based on initial tests, the apparent resistivity distributions (pseudo-sections) were selected as the initial models and the same damping factor was applied for

all profiles. Overall, a relatively moderate to low data misfit (< 6 %) was achieved after removing data outliers with a small number of iterations. Finally, the resistivity models were cut off at depth at a sensitivity threshold. Owing to the pronounced difference of low-resistivity mudstone and high-resistivity limestone, ERT is a promising tool for characterizing carbonates in the investigated area. Challenges do arise in interpreting ERT measurements when pronounced heterogeneity resulting from varying fracture density, karstification, or thin layering occurs below the resolution threshold (e.g. Everett, 2013; Loke et al., 2013). Furthermore, electrical resistivity is largely governed by water content within the soil profile and greatly depends on primary and secondary porosity of the rocks and soil.

It should be noted that, due to the intrinsic limited resolution of the ERT method, the images of the resistivity distribution represent averages over wider areas and tend to be smeared, e.g., high-resistivity zones of small extent will show up as larger blotches with intermediate resistivities. Further, the imaging capabilities decrease with depth and deep high-resistivity zones are likely to be underestimated in value.

3. Geologic setting and regional structural complexity

The main study area (fig. 1) is in southeastern Fergus County, Montana, where the Morrison Formation is exposed along the flanks of the Spindletop Dome. Based on field stratigraphic measurements and well log data, the Morrison Formation in central Montana is approximately 72 m in thickness (unpublished research). The formation is bounded by the underlying Upper Jurassic Swift Formation and the overlying Lower Cretaceous Kootenai Formation. The Swift Formation consists of shallow marine shelfal sandstone deposits which accumulated through the final transgressive-regressive marine sequence during mid–late Oxfordian

time (Imlay, 1954; Khalid, 1990; Fuentes et al., 2011). The northward retreat of the seaway established a planation surface on which the northern Morrison sediments were deposited (Richmond et al., 2019). In central Montana, the Morrison Formation is conformable with the underlying marine sandstone beds of the Swift Formation. The J5 unconformity (Pipiringos and O'Sullivan, 1978), present at the base of the Morrison Formation in more southern states, is absent in central Montana (This study; Imlay, 1954; Uhlir et al., 1988; Khalid, 1990; Meyers and Schwartz, 1994; Fuentes, et al., 2011). The overlying Lower Cretaceous (Aptian) Kootenai Formation is an alluvial and fluvial sequence comprised of deposits of coarse- to medium-grained fluvial sandstone beds, overbank deposits of mudstone, and calcrete paleosols, with the formation capped by interstratified lacustrine limestone and dolomite units (Dupree, 2009).

The Morrison Formation is undifferentiated in central Montana and consists of a mudstone-dominated section with fine-grained anastomosing fluvial channel and thin crevasse splay sandstone beds. The formation can be divided into lower and upper informal members based upon depositional facies and e-log characteristics. The lower portion of the Morrison Formation consists of red illitic mudstone with small anabranching distributary channel beds. This lower unit is interpreted to represent a stranded muddy tidal flat that formed on the residual sandy tidal flat parasequence of the retreating Sundance Sea (Swift Formation). A sharp demarcation can be observed between the reddish illitic mudstones of the lower unit and the variegated illitic mudstones and isolated anastomosing fluvial channel and thin splay sandstone beds of the upper unit. The upper member represents the subsequent progradation of the Morrison fluvial distributary system to central Montana. The stranded tidal flat of the lower unit lacks fossils, whereas the upper fluvial floodplain facies contains fossil invertebrates (Richmond et al., 2017), dinosaurs (Saitta, 2015; Richmond and Murphy, 2017), and petrified wood (Richmond et al., 2019).

There is a hypothetical relationship between the structural components of central Montana and the development of the Morrison carbonate buildups, therefore a brief summary of the structural features of the region is presented. The present-day structure of the central Montana region is complex (Porter et al., 2002) as verified by fracture swarms, compressional, and extensional faulting. The structure of central Montana, and the majority of the state, is related to Precambrian laterally extensive basement faults that trend at approximately 50° azimuth from southwestern to northeastern Montana (Sims et al., 2004). Reactivation of these Precambrian zones of crustal weakness during the Laramide orogenic event of the Late Cretaceous and Early Paleogene likely formed many of the present-day structures of central Montana, including the anticlinal structures of the Big and Little Snowy Mountains, Spindletop Dome, Flat Willow and the Cat Creek anticlines and many other local anticlinal features (Gardner, 1950). There are two orthogonal major lineaments present in the Montana Rocky Mountains and the adjacent plains (Maughan, 1993). The northeast-southwest lineaments (Great Falls, Greenhorn, Snake River-Yellowstone, and Greybull) strike between 45–50° azimuth and correlate to the Precambrian basement faults. The major northwest-southeast lineaments (Bridger, Chadron, and Cedar Creek) strike between 320–325° azimuth, (Maughan, 1993; fig. 2). In central Montana, this broad zone of northeast-southwest trending structures controlled depositional patterns for some Paleozoic and Mesozoic sedimentary rocks (O'Neill and Lopez, 1993). Steeply dipping basement faults which strike northeast-southwest and southeast-northwest in Fergus, Petroleum, and Garfield counties have been mapped in central Montana are thought to have been reactivated through geologic time (Nelson, 1995).

The southern flank of Spindletop Dome is marked by an eastward-dipping normal fault with a strike of 295º azimuth. Numerous local drainages with linear coulees are acute to the normal fault and trend northwest between 332–340º azimuth. Subordinate drainages abruptly turn from the northwest-trending coulee and trend northeast at approximately 45º azimuth (fig. 3). The modern drainage patterns track these regional fracture patterns. In some local coulees, the basal Kootenai sandstone bed (locally called the Cat Creek 3 sandstone bed) displays sheer sandstone 30 m high.

During the Late Jurassic, Sevier orogenic thrusting occurred along large north-trending folds in southwestern Montana (Hutsinpiller and Parry, 1985). A paleogeographic/paleotectonic high called "Belt Island" in north-central Montana (Porter, 2011) was likely the result of reactivation of Precambrian basement faults in the plate interior. However, there are no known plutonic emplacements in central Montana related to these Jurassic regional paleostresses. The earliest granitic plutonism occurred during the Late Cretaceous between 74 and 69 Ma in west-central Montana in the Big and Little Belt Mountains (Snee et al., 2002).

On the southern and western flanks of Spindletop Dome the Morrison Formation buildups can be separated into five geographic distinct areas designated from local coulee dams or other surface features (fig. 4). The names of the clusters moving west to east: Kootenai Ridge cluster (SW ¼, SE ¼, Sec 28, T13N R23E), Homestead cluster (NE ¼, SE ¼, Sec 33, T13N R23E), East Blue Dam cluster (SE ¼, NE ¼, and NE ¼, SE ¼, Sec 33, T13N R23E), West Ralph Dam cluster (NW ¼, SW ¼, Sec 34, T13N R23E), and Prairie Dog Dam cluster (SW ¼, SW ¼, Sec 35, T13N R23E). Prairie Dog Dam cluster has the highest number of siderite and carbonate buildups (fig. 4).

4. Description of Morrison Formation buildups

The buildups are stratigraphically between 40–52 m above the base of the Morrison Formation. The majority of the buildups are small hemisphere-shaped features a meter in height above the ground surface elevation and up to 3 m in diameter. The buildups are divided into two classes: siderite ($FeCO_3$) and carbonate ($CaCO_3$) buildups. At present, 34 siderite and 65 carbonate buildups have been discovered. The buildups occur in 5 clusters and 10 carbonate buildups have petrified wood associated with them. All of the buildups are encased in a variegated illitic mudstone matrix with no associated fluvial or lacustrine facies. Some of the designated buildups have siderite present beneath and on the flanks of the central carbonate dome. The contact between the siderite and carbonate is always sharp and distinct where these siderite-carbonate buildups occur.

4.1. Siderite buildups

The Morrison Formation siderite buildups are typically found in clusters (e.g. Prairie Dog Dam cluster) but solitary siderite buildups are present (fig. 4). The homogenous siderite buildups can be several meters in length but are less than half a meter in height (fig. 5A). There are no sandstone beds, horizontal carbonate strata, or fossils associated with the siderite buildups. The buildups are more elongate than circular, and the uppermost surfaces are irregular from the protrusion of cone-in-cone apices (figs. 5B, C). Cone-in-cone structures are common in the siderite buildups (figs. 6A, B). In thin section, the siderite is homogenous displaying ghost traces of the cone-in-cone crystalline growth (fig. 6C).

XRD results on three siderite samples (SM 20, CM 40, CM 52) indicate the buildups are composed of 48.7% calcium carbonate ($CaCO_3$), 16.7% quartz (SiO_2), 16.0% siderite/ankerite ($CaFe(CO_3)$/$CaMgFe(CO_3)_2$), 10.5% illite, 7.3% kaolinite and 0.9% pyrite (FeS_2).

XRF was performed on five different siderite buildups (SM 12, 18, 19, 32, 33). The three major elements for each siderite buildup are calcium (Ca), iron (Fe), and silica (Si). The analysis demonstrates a percentage variation in these three main elements as well as the trace elements (K, Mg, Ti, Mn, Al, P, S, Cl, Sr) (fig. 7).

4.2. Carbonate buildups

In contrast to the siderite buildups, the majority of the carbonate buildups are not found in close proximity to one another, but small clusters of carbonate buildups are present (fig. 4). The homogenous carbonate buildups vary in length and height. The buildups are generally hemisphere-shaped, are typically a meter in diameter and less than a meter in height although larger buildups are present (figs. 8A, B). A large broad buildup (CM 40; fig. 8C) with siderite overlain by carbonate is a meter in height with a 7-meter diameter. Carbonate buildups do not have macroscale cone-in-cone features. The encasing sediments of the carbonate buildups consists of illitic variegated or organic-rich mudstones. There are no sandstone beds or other terrestrial carbonate beds associated with the carbonate buildups. Some carbonate buildups have siderite on the flanks and/or beneath an overlying carbonate buildup (e.g. CM 40 and CM 52; fig. 4). These peripheral siderites have small cone-in-cone ridges present (fig. 6D).

The majority of the carbonate buildups are composed of orthochemical micrite. Clastic detrital grains common in many terrestrial carbonates (e.g. travertines, tufas, calcretes, etc.) are absent. In general, allochems are rare. Few macro fossils are present with the carbonate buildups.

Ten carbonate buildups have petrified wood in close proximity to the buildup but only three have petrified logs incorporated into the buildup (CM 13, 31, 52). Typical macrophyte debris (leaves or twigs), hydrophytes, or charophytes are generally absent. Only two microscopic woody macrophyte fossil fragments were discovered. The first is unidentifiable woody debris (fig. 9A), the second is a partial tangential fragment of a homoxylous wood (fig. 9B). In addition to the woody fragments, partial bryophyte leaves (liverworts; Philippe writ. comm., 2020) are preserved in several buildups (CM 13, 17, 35; fig. 9C). An organic fabric was discovered in buildup CM 13 and might be the tufa-associated green algae *Oocardium stratum* (fig. 9 D). Fossil freshwater invertebrates such as ostracods or gastropods were not observed. Biogenic laminae from cyanobacteria, typical of many terrestrial carbonates, were not observed. No trace fossils have been found.

Petrographic features of the carbonates include long dogtooth calcite crystals. Some dogtooth crystals appear to be coated with microbial films (fig. 10A). A very distinctive texture observed in some carbonate buildups are spherulites (figs. 10B, C). The spherulites have a radiating array of crystalline fibers which developed from a nucleus (Beck and Andreassen, 2010). Interestingly, the spherical crystal growth appears to have pushed organic material to the rim. Organic material is concentrated to the interstitial space between proximal spherules. Occasionally organic material is encompassed by the spherule's mineral growth. The organic material is likely residual microphytes (algae) or bacteria (Chafetz and Folk, 1984).

Many terrestrial carbonates have primary porosity. Primary porosity in the carbonate buildups is limited to intergranular spaces between the spherulites and the porous structures of macrophytes. In addition to the primary orthochemical micrite and radial-fibrous spherulites, many buildups have late diagenetic fractures annealed with sparry calcite.

XRD analysis was run on several carbonate buildups (CM 13, 38, 64, and 52). The data indicate that the buildups are composed of 98% calcium carbonate and 2% carbon. XRF was executed on eight different carbonate buildups and two carbonate peripheral siderites (SM 40.1, 40.2; figs. 7 and 11). The three major elements are calcium (Ca), iron (Fe) in minor amounts, and silica (Si). Variation in the three main elements as well as the trace elements (K, Mg, Ti, Mn, Al, P, S, Cl, Sr) (fig. 11) indicates the geochemistry for each buildup was distinct. Two carbonate buildups (CM 13 and CM 52) were analyzed with XRF on a cm-scale cross-section from the bottom of a large cut slab of the buildup moving upward (figs. 12, 13). CM 13 and CM 52 are stratigraphically separated by 5 m (fig. 1). Both buildups incorporate petrified wood, *Circoporoxylon* and *Xenoxylon,* respectively. The most noticeable variation for CM 13 is the percentage of Mg (fig. 12; letters C, G, S, T).The CM 52 data displays a more consistent chemistry with only minor differences (fig 13). The petrified wood (*Xenoxylon*; letters L-WD and M-WD) has a very distinct chemistry from the buildup and implies wood preservation may involve nonmetals (Si, P, S, and Cl; fig. 13).

Three carbonate buildups (CM 13, 35, 52) were selected for standard isotopic analyses. The analysis on each buildup was measured three times per sample for verification. The $\delta^{18}O$ for all three buildups shows relatively low variability, ranging from –15.48‰ to –16.89‰. The $\delta^{13}C$ also shows a low variability ranging from –4.27‰ to –6.51‰ (table 1). The $\delta^{13}C$ values are similar to the pre-industrial revolution atmospheric value of meteoric water precipitated calcite (–6.5‰; NOAA data; Sharp, 2007).

4.3. Electrical resistivity tomography

Four localized electrical resistivity tomography (ERT) surveys were conducted to better understand the structure and potential subsurface continuation of the surface buildups (fig. 3), as previously applied to delineate the subsurface continuation of a fossil tufa outcrop in northeast Spain (Huerta et al., 2016). On average, the obtained resistivities range from 20–200 Ω-m. Based on the correlation with outcrops and surface geology, two lithologies are interpreted to be present in the subsurface. Lithology 1 (limestone) resistivities range from 150–300 Ω-m with thickness that range from 0.5 to al east 1.5 m. Lithology 2 (mudstone) resistivities range 10–70 Ω-m. The lowest resistivities associated with lithology 2 are attributed to the increased moisture content of some surface areas (dark blue) (fig. 14).

ERT profile *A–A'* (fig. 14A) was run parallel to Prairie Dog Dam (PDD) eastern array (fig 4). Although we attempted to pass over several carbonate buildups, the ERT profile only shows high resistivity (> 150 Ω-m) at the distal ends of the profile. The northeastern buildup is about 6 meters across. The profile does not show any additional high resistivity carbonates in the subsurface.

ERT profile *B–B'* (fig. 14B) was oriented perpendicular to profile *A–A'* trending northwest (Fig 4.) and crossing the western, central, and eastern PDD arrays. The surface high resistivity (> 150 Ω-m) at profile marker 58 m crosses over a small surface carbonate buildup (fig. 4). The ERT profile crosses many of the siderite buildups of the PDD central array between 86–100 m. This profile section displays low resistivities (< 25 Ω-m). Although the profile crosses over several siderite buildups, the mounds are not discernible in the profile. There are several potential reasons why the siderite buildups are not seen in the profile. The topographic low where the siderite buildups reside may have had a higher water saturation (ephemeral creek bed). The siderite

buildups are highly fractured, and those fractures can hold conductive water. It is also possible that the siderite buildups are thin surface features which would make them indiscernible in the ERT since electrical current prefers conductive pathways. In contrast, the profile does discern a small carbonate buildup from PDD western array at 116–118 m. In the subsurface between 36–60 m is a high resistivity (110–200 Ω-m) zone interpreted to be a large buildup or possibly two buildups separated stratigraphically.

ERT profile *C–C'* (fig. 14C) was run parallel to the East Blue Dam Cluster over the largest observed surface carbonate buildup (CM 40; fig. 4). The hemispherical buildup (CM 40) is 13 m long and 2 m thick and is underlain by a thin siderite bed. Underlying the entire structure is a low resistivity zone (28–15 Ω-m) interpreted to be a ≈ 2 m thick mudstone bed. Beneath this mudstone bed is high resistivity zone (150–300 Ω-m) interpreted to be a significantly sized carbonate buildup in the subsurface. The lateral extent of this buildup may range from 15 to 41 m. The suggested minimum thickness is around 1.5 m, as ERT images tend to blur vertically with depth. Near the end of the profile, the carbonate subsurface layers appear disjointed and stratigraphically higher. This may be interpreted as representing different smaller carbonate buildup. Given the inherent low resolution of ERT imaging, however, this interpretation is speculative.

ERT profile *D–D'* (fig. 14D) was oriented perpendicular to profile *C–C'* (fig. 4). The high resistivities (150–200 Ω-m) at profile maker 18.2 m represent a small surface buildup. Underlying the high resistivity zone (carbonate buildup) is a lower resistivity zone (30–20 Ω-m). Similar to profile *C–C'*, below the lower resistivity zone is a subsurface high resistivity zone (150–200 Ω-m). This zone is interpreted to represent a significantly sized buildup, or possibly two coeval buildups. The lateral extent of this buildup is at least 24 m and may extend beyond the profile. The estimated thickness is 1–1.5 m. It should be noted the large *D–D'* profile subsurface buildup(s) has a different

subsurface elevation than the large *C–C'* profile subsurface buildup. They are therefore are not stratigraphically equivalent.

The four ERT surveys help to define the lateral extent of the surface buildups and the relative stratigraphy of several previously unknown carbonate buildups in the subsurface. The surface buildups and subsurface carbonates are decoupled by a thin low-resistivity zone that represent the encasing illitic mudstone. The ERT data indicate the presence of additional large stratigraphically isolated carbonate buildups in the subsurface.

5. Comparisons with other terrestrial carbonates

Abiotic carbonate precipitation can occur through precipitation from evaporation, an increase in temperature, or a reduction in carbon dioxide (CO_2) pressure. Biogenetic carbonates include those manufactured by animals and plants, fungi, and bacterial generated carbonates (Castanier et al., 2000). Both processes can result in precipitation of carbonates in terrestrial environments. A review of terrestrial carbonates is provided to facilitate the identification/origin of these unusual Morrison carbonate buildups.

5.1. Concretions

Vast numbers of papers have been written describing concretions throughout geologic time (Mozley and Burns, 1993 and references therein). Concretions grow by two different means: concentric or pervasive growth. Concentric growth occurs as successive layers of cement or cemented material are added increasing the radius in time. The concentric growth layers of isopachous cement can be viewed petrographically (Potter et al., 2011; Potter-McIntyre, 2013, Potter-McIntyre et al., 2014). Pervasive growth is where the cement crystals grow concurrently

with little to no increase in the radius of the concretion. Carbonate concretions typically grow by concentric expansion, whereas siderite concretions develop by pervasive growth (Raiswell and Fisher, 2000). Concretion formation is understood to occur during early diagenesis, with growth taking thousand to millions of years depending on geochemical conditions and the size of the concretion (Berner, 1968; Boles et al., 1985). The duration of concretion formation is difficult to determine and may be mineral dependent. It was originally proposed that the large Moeraki carbonate septarian concretions of New Zealand took anywhere from 140,000 to 65 million years to form (Boles et al., 1985). Reevaluation of the Moeraki concretions using isotopic data revealed the concretions took about 3 million years to form (Thyne and Boles, 1989). Yoshida et al. (2018) stated that concretions form very rapidly during early diagenesis; much faster than previous estimates.

Carbonate concretions characteristically form in several depositional environments: marine (Mozley and Burns, 1993), marginal marine (Middleton and Nelson, 1996), marsh (Allison and Pye, 1994; Daun et al., 1996), lacustrine (Cronan and Thomas, 1993; Park, 1995), and terrestrial (Chan et el., 2006; Chan et al., 2012). Concretions form in a variety of lithologies but are characteristically enriched in carbonate forming a solid mineral mass having sharp boundaries with encasing sediments. Concretions can initiate nucleation from the reduction of organic material by microbes (Raiswell and Fisher, 2000; Mozley and Davis, 2005; Potter-McIntyre, 2013; Thomka and Lewis, 2013; Yoshida et al., 2018). They form in diagenetic microenvironments and often have well-preserved fossils at their centers (Park, 1995; Potter-McIntyre, 2013; McCoy, 2015; Vitkus, 2015; Cotroneo et al., 2016; Yoshida et al., 2018). Concretion geometries vary, but include spheres, pipes, and irregular shapes. Concretion diameters can vary from millimeters to several

meters (Levy, et al., 1998; Abdel-Wahab and McBride, 2001; Pratt, 2001; McBride and Milliken, 2006; Thomka and Lewis, 2013; Potter-McIntyre et al., 2014).

Carbonate concretions are common in the marine environment (Mozley and Burns, 1993, and references therein; Pratt, 2001; Loyd et al., 2012; Thomka and Lewis, 2013). Most marine concretions form on the continental shelf (Mozley and Burns, 1993) but can also form in deeper marine environments (Loyd et al., 2012). Commonly the host rock is organic-rich shales and to a lesser degree sandstone (Mozley and Burns, 1993). Marine carbonate concretions vary greatly in size (Gregory et al., 1989; Pratt, 2001; Baumann et al., 2016) but usually are in the centimeter range. Marine concretions can also be very large (as evidenced by the sizes (> 2 m) of the Paleocene Moeraki boulders of New Zealand). The large concretions are highly variable in size although many of the small concretions may have been collected as novelties since their discovery in the 1850's (Boles et al., 1985). Very large concretions (> 9 m) can also form by diagenetic cementation of porous sandstones (Biek, 1994; Abdel-Wahab and McBride, 2001; McBride and Milliken, 2006; Wanas, 2008; Arribas et al., 2012).

Terrestrial concretions are often associated with lacustrine facies (Harriss and Troup, 1970; Cronan and Thomas, 1972; Tyler and Buckney, 1980; Williams and Owen, 1992; Park, 1995; Vitkus, 2015). Concretions of the Lake T'oo'dichi' lacustrine complex (Turner and Fishman, 1991) of the Upper Brushy Basin Member of the Morrison Formation of southeastern Utah and southwestern Colorado were studied (Potter-McIntyre, 2013, Potter-McIntyre et al., 2014). Three types of concretions were noted from the Lake T'oo'dichi' sediments: calcite, iron (oxyhydr)oxide, and phosphate. Carbonate concretions are most common in reduced lacustrine facies, they are spheroidal and < 120 mm in diameter. Iron (oxyhydr)oxide concretions are circular and < 500 mm in diameter. Phosphate concretions are also spherical and are < 70 mm in diameter (Potter-McIntyre,

2013, Potter-McIntyre et al., 2014). These concretions are interpreted to have formed during early diagenesis in a reducing lacustrine environment.

Terrestrial concretions, excluding lacustrine-formed concretions, are commonly small (mm–cm scale) oxidized iron-rich concretions (Chan et al., 2004; Chan et al., 2006; Potter and Chan, 2007; Potter et al., 2011). These small concretions form when iron-rich fluids interact with oxidizing groundwater (Chan et al., 2004).

The Morrison Formation buildups of central Montana are not considered to be concretions. The siderite and carbonate buildups do not have either pervasive or concentric layers of cementation typical of concretions. They do exhibit sharp contacts with the encasing sediments, but the encasing mudstones are not generally organic-rich. The buildups are not spheres, pipes, or amorphous shapes. The Morrison buildups are significantly larger than previously described terrestrial carbonate concretions. Although several buildups have petrified wood associated with them, the fossils do not appear to be related to carbonate formation.

5.2. Calcretes

Calcretes are customarily divided into two types: pedogenic and groundwater. Travertines, tufas, or lacustrine/palustrine carbonates are not included in this classification. Pedogenic calcretes (caliche; also referred to as aridisols–Retallack, 1993 or calcisols–Mack et al., 1993) are a laterally extensive surface terrestrial carbonate-cemented duricrust formed in the soil profile (Wright and Tucker, 1991; Horn et al., 2013). Pedogenic calcretes usually develop in warm, semiarid climates (Machette, 1985; Alonso-Zarza, 2003; Pentecost, 2005; Horn et al., 2013) where high evaporation and evapotranspiration are favorable for inorganic carbonate precipitation (Alonso-Zarza and Wright, 2010). Cementation of pedogenic calcretes was once thought to be related to groundwater

fluctuations but is now considered to be sourced from bicarbonate (HCO_3) from atmospheric precipitation (Alonso-Zarza and Wright, 2010). Partial pressure of CO_2 in the soil is a significant variable of calcite precipitation (Wright and Tucker, 1991). The precipitation of carbonate in the soil and its interaction with the biota is a complex process (Wright and Tucker, 1991; Alonso-Zarza and Wright, 2010).

Pedogenic calcretes are generally less than a few meters in thickness (Pentecost, 2005) and are controlled by the host rock and the duration of subaerial exposure (Alonso-Zarza, 2003). Well-documented modern calcretes require long periods of time to form (Machette, 1985; Wright and Tucker, 1991). A typical calcrete profile consists of host material of any type of composition or texture and may include several horizons present including the transitional, chalky, nodular, platy, hardpan, and a pisolithic horizon. Pisoliths are sand or gravel micrite-coated grains. The grain may be coated entirely or only on the underside. For a more detailed review of the pedogenic soil profiles refer to Esteban and Klappa (1983), Wright and Tucker (1991), Alonso-Zarza (2003) and Alonso-Zarza and Wright (2010).

Calcretes have numerous varied large-scale features and microfabrics. Large-scale features include rhizoliths, structures produced by roots; laminar calcretes, that may be abiotically or biotically formed by cyanobacteria or root mats; coated grains (pisoliths); teepee structures; and argillipedoturbation, which is the shrinking and swelling of smectitic clays resulting in 50 cm vertical cracks (Wright and Tucker, 1991). Microfabrics can be separated into alpha and beta calcretes. Alpha calcretes consists of dense micritic fabric that include nodules, large rhombic euhedral calcite crystals, floating or etched host silicate grains, and complex microfractures including circular, granular or desiccation cracks. Nodules may be concentric or amorphous and microcrystalline (Horn et al., 2013). Beta calcretes are dominated by biogenic features including

tubules, fibrous calcite, calcified pellets, and/or microbial coatings (Wright and Tucker, 1991; Alonso-Zarza, 2003; Alonso-Zarza and Wright, 2010; Horn et al., 2013) Biogenic fabrics can also include rhizoliths, alveolar septal structures, interpreted as calcified fungal filaments, and micrite-coated grains produced by fungi and cyanobacteria (Alonso-Zarza, 2003). Additional larger scale biogenic structures may be formed by insects, such as beetles, bees, wasps, ants, or termites, or by other burrowing invertebrates (Hasiotis and Demko, 1996; Hasiotis and Kirkland, 1998; Alonso-Zarza, 2003; Hasiotis, 2004; Hasiotis et al., 2007).

Groundwater calcretes form below the soil profile in the vadose zone or at the capillary fringe (Wright and Tucker, 1991; Alonso-Zarza and Wright, 2010). Groundwater calcrete formation is dependent on the permeability of the host sediments, the availability of the water in the vadose zone and the carbonate supplied by the phreatic zone. The microfabric is alpha-dominated; lacks vertical root traces and peds. Beds have sharp basal and upper contacts with bed thicknesses generally greater than 3 meters but can be as thick as 10 meters (Jutras et al., 2007). Bed morphology mimics the topography or channel-fill deposits (Alonso-Zarza and Wright, 2010). Groundwater calcretes also commonly form in arid to semiarid climates (Alonso-Zarza and Wright, 2010).

Morrison Formation calcretes are common, particularly in the Brushy Basin Member of the Colorado Plateau (Demko et al., 2004, Tanner et al., 2014). Commonly, Morrison calcretes have abundant root traces and vertic structures, which are desiccation cracks, wedge-shaped peds, slickensides. The features form from the from swelling and shrinking of the encasing smectitic mudstones. Brushy Basin nodular horizons have a limited lateral extent of several hundred meters and may have either distinct or indistinct boundaries (Tanner et al., 2014). Brushy Basin paleosols of the Colorado Plateau signify either a variable climate alternating between arid and humid

(VanDeVelde, 2006; VanDeVelde et al., 2006; Tanner et al., 2014) or a predominately semiarid climate with seasonal precipitation (Demko et al., 2004). Most Morrison Formation calcretes formed in floodplain/overbank or marginal lacustrine environments in a semiarid climatic regime (Demko et al., 2004; VanDeVelde et al., 2006).

In southeastern Wyoming, where the Morrison Formation is undifferentiated, there are several calcrete layers that consist of pebble-sized carbonate nodules. A laterally extensive calcrete layer at 42–43 m above the base of the formation is locally widespread and has been used for stratigraphic correlation. This calcrete layer has been referred to as the "boundary caliche" (Allen, 1996) is composed of lacustrine and palustrine carbonates that became exposed and desiccated during a prolonged period of aridity (Gallagher, 2010).

In the study area, the only duricrust with a discernible B horizon observed is a 20-cm thick silcrete layer present stratigraphically 23 m above base of the Morrison Formation. The silcrete XRF data indicates silica percentages are between 72–88% with minor percentages of calcium (fig. 15). No Morrison calcrete beds were observed in the research area. However, calcrete horizons are present in the overlying Lower Cretaceous Kootenai Formation.

The carbonate buildups are not considered to be pedogenic or groundwater calcretes due the lack of horizonal lateral extent, lack of any pedogenic profiles or large-scale pedogenic features. The spherulites are not micrite-coated grains (pisoliths). Although the buildups are micritic, they do not display the alpha or beta microfabric characteristics. The characteristics of the carbonate buildups do not correspond with those of calcretes and therefore are rejected as such.

5.3. Groundwater-fed carbonate deposits

Groundwater-fed carbonate deposits include travertine, tufas, sinters, and speleothems (Chafetz and Folk, 1984; Steinen, et al., 1987; Pedley, 1990; Golubic et al., 1993; Koban and Schweigert, 1993; Ford and Pedley, 1996; Pentecost and Coletta, 2007; Capezzuoli et al., 2014; Della Porta, 2015; Mohammadi et al., 2019). The classification of groundwater-fed carbonate deposits has a diverse history (see Jones and Renaut, 2010). Modern freshwater springs are categorized by the mean water temperature at the vent, where temperatures range from cold to boiling (Jones and Renaut, 2010). With such a large spectrum of water temperatures, a mean water temperature higher than the mean air temperature has been proposed for referring to thermal springs (Pentecost et al., 2003). Thermal waters are further divided into warm (20–40ºC), mesothermal (40–60ºC), and hyperthermal (> 60ºC) (Renaut and Jones, 2000).

Sinters can be siliceous or carbonaceous and are usually associated with hot springs or geysers in active volcanic terrains where mineral charged geothermal fluids discharge at the surface (Campbell et al., 2015; Munoz-Saez et al., 2016). Sinters are low porosity carbonate buildups where biotic carbonate generation is very minimal (Koban and Schweigert, 1993). However, Jones and Renaut (2010) recommend the term sinter be restricted to high temperature silica spring deposits. At the other end of the temperature spectrum, speleothems deposits form in caves by evaporation of cool mineral-enriched waters.

Pedley (1990) and Ford and Pedley (1996) use water temperature to delineate between travertine and tufa deposits, but the determinant condition is the ambient water temperature. Herein we follow the general classification of Pedley (1990), but further define tufas as being precipitated under cooler water temperatures (< 20ºC) whereas travertines as being precipitated under thermal conditions (> 20ºC; Barilaro, et al., 2012). Additional parameters that control carbonate

precipitation are climate, discharge rates, rate of CO_2 degassing, and the presence or absence of biota (Jones and Renaut, 2010).

Commonly, travertines and tufas are characterized by banding from cyanobacteria growth discontinuities. The banding couplets are typified by alternating light and dark calcite related to seasonal changes in carbonate precipitation (Jones and Renaut, 2010). Cyanobacteria trichomes (e.g. cell rows) are surrounded by a mucilaginous sheath made up of polysaccharides called a filament and calcify when carbonate is precipitated in association with the organism. The filaments also trap sediments in the stromatolitic bands (Merz, 1992) and often include cemented hydrophytes, semiaquatic macrophytes, and a diverse invertebrate fauna.

An important characteristic of groundwater-fed carbonate deposits is primary porosity (Steinen, et al., 1987; Golubic et al., 1993; Koban and Schweigert, 1993; Barilaro, et al., 2012; Guo and Chafetz, 2012; Mohammadi et al., 2019). Porosity forms from the degassing of CO_2 (Pentecost and Coletta, 2007; Barilaro, et al., 2012), microporous micritic laminae (Mohammadi et al., 2019), moldic porosity from crust formation on organic debris (Golubic et al., 1993; Koban and Schweigert, 1993), and the dissolution of ostracod and gastropod tests (Mohammadi et al., 2019). Primary porosity for both travertines and tufas range between 14–17% (Sopaci and Akgün, 2015; Yetkin et al., 2017). Secondary porosity can be biomoldic or vuggy dissolution, or can form from fractures (Barilaro, et al., 2012).

Travertines are usually considered abiotic due to the hydrothermal water conditions that prohibit the existence of higher organisms (Chafetz and Folk, 1984; Koban and Schweigert, 1993; Ford and Pedley, 1996; Evans, 1999). Different invertebrates, plants, mosses, protozoa, algae, fungi, and bacteria have different tolerances of high-water temperature (Renaut and Jones, 2000). As discharged thermal waters flow away from the vent and cool, biota with differing temperature

tolerances begin to inhabit these varying temperature zones. The preservation of temperature-adapted organisms in fossil groundwater-fed deposits can be used as a guide to paleothermometry. Characteristic proximal travertine facies include irregular high macroscopic porosity, dendritic microbes or calcitic shrubs (Chafetz and Folk, 1984), laminar microbial mats, peloidal layers, and coated gas bubble layers from degassing CO_2 from the decarbonation of limestone (Chafetz and Folk 1984; Koban and Schweigert, 1993; Pedley, 2009). Travertine is enriched in ^{13}C and often contains high levels of sulfur (Pedley, 2009). Travertines tend to show less macrofacies diversity than tufa systems on account of their relatively limited lateral extent and biota (Ford and Pedley, 1996).

Cool water tufa carbonate precipitation occurs at ambient temperatures (< 20^{o}C) and is usually associated with proximal paludal or lacustrine depositional facies (Pedley, 1990; Ford and Pedley, 1996). These tufas are characterized by the presence of heterotrophic bacteria, cyanobacteria, microphytes (algae), hydrophytes, macrophytes, and freshwater invertebrates (Kerney, 1959; Pedley, 1990; Ford and Pedley, 1996, Koban and Schweigert, 1993; Evans, 1999; Capezzuoli et al., 2014). Vertebrate fossils can also be associated with tufa deposits (Kerney, 1959; Springer et al., 2017). Inorganic precipitation (e.g., degassing CO_2) and organic microbial activity are important factors for carbonate precipitation in tufa environments. Tufa deposits have been further divided into allochthonous and autochthonous deposits (Pedley, 1990). Allochthonous tufas consists either cemented phytoclasts, intraclasts of silt- and sand-sized clasts sourced from tufas, micritic tufa material or peloids and are usually associated with fluvial depositional systems (Pedley, 1990). Autochthonous tufas are cemented by cyanobacteria (stromatolites). The stromatolitic horizontal laminations relate to seasonal growth patterns of the cyanobacteria (Janssen et al., 1999).

6. Discussion: Morrison Formation mound springs

6.1 Siderite buildups

Siderite is the product of the interaction of numerous dynamic inorganic and organic systems. Groundwater chemistry is the summation of meteoric and subsurface water interactions with the local geology, aquifer lithologies, and soils. Availability and solubility of iron in soils is partly a byproduct of the decomposition of organic matter. Ferrous carbonate (siderite/ankerite) and ferric hydroxide (goethite and polymorphs) precipitate at a circumneutral pH (Hedrich et al., 2011). If the pH is low (< 4) the iron and carbonate ($CaCO_3$) will remain in solution if the pH is high (> 9) bicarbonate (HCO_3) precipitates and releases CO_2. To form siderite, the complexing agent $CaCO_3$ binds with the ferrous/ferric iron at a circumneutral pH (Blöthe and Roden, 2009).

Iron-rich microbial ecosystems have played a major role in the biogeochemistry of the Earth from the Archean and Early Proterozoic Eons and continues to the present (Roden et al., 2012; Vuillemin et al., 2019). In modern neutral pH freshwater environments iron-oxidizing phylum proteobacteria govern iron redox reactions (Blöthe and Roden, 2009; Hedrich, et al., 2011; Roden et al., 2012). Iron redox states are interconnected to inorganic compounds in soils and sediments. Microorganisms play a fundamental function in iron redox reactions (Blöthe and Roden, 2009). Betaproteobacteria are the most common microbes in modern circumneutral pH freshwater environments including soil horizons (Roden et al., 2012). These lithotrophic iron-oxidizing bacteria often colonize in the soil transition zone between the anaerobic and aerobic subsurface environments (Roden et al., 2004). The position of the anaerobic/aerobic transition zone (e.g. the capillary fringe) in the subsurface can vary by precipitation, the upward migration of groundwater, or the deoxygenation of groundwater by microorganisms feeding on dissolved organic material leached from the overlying soil profiles.

Cone-in-cone features are common world-wide, known from every geologic age, and usually form in calcite, gypsum, or quartz (Cobbold et al., 2013). They commonly form in low-permeability sedimentary rocks such as shale or mudstone. Cobbold et al. (2013) advocates that cone-in-cone features develop from fracturing with a vertical dilation that is coeval with fiber growth. The fractures are formed either by the force of crystallization, or fluid over-pressurization. Selles-Martinez (1994) agrees that crystalline fibers grow in over-pressured regimes where fractures are induced by a decrease in pore pressure between sediments having dissimilar mechanical properties. Cone-in-cone crystallization forms before complete lithification as the siderite dislodges the encasing mudstone upward against gravity (Hooker and Cartwright, 2015).

Terrestrial siderites form in humid continental environments where precipitation exceeds evaporation. Siderites typically accumulate in poorly drained/anoxic wetland soils (Sheldon and Tabor, 2009; Ludvigson et al., 2013; Fernandez et al., 2014). The Morrison siderites formed from precipitation-fed groundwater that infiltrated local mudstone sediments raising the phreatic zone in paleotopographic lows or by moving up small fractures as a slow subsurface seep into the vadose zone. This groundwater then interacted with the organic- and iron-rich forest soils and aided by iron-oxidizing betaproteobacteria, which reside near the capillary fringe, resulting in siderite precipitation. Fluid overpressurization in the subsurface allowed for the formation of large cone-in-cone structures during precipitation. The chemical variabilities of the siderite buildups as show by the XRF data (fig. 7) likely resulted from the homogenous groundwater interacting with localized variable soil chemistries.

6.2 Carbonate mound springs

The carbonate buildups are also the product of inorganic and organic interactions. In contrast to the groundwater interaction in the subsurface, the groundwater is precipitating calcium carbonate on the surface. The carbonate buildups lack the many characteristics that are recognized to define modern groundwater-fed terrestrial deposits such as travertine and tufas. Modern groundwater-fed carbonate deposits are separated by vent water temperature and the presence or absence of biota. Additional data must be utilized to determine the carbonate classification of fossil groundwater-fed carbonate deposits. The Morrison carbonate buildups are composed of orthochemical micrite, are generally abiotic, show low primary porosity, display no cyanobacterial laminae, and fossil allochems are rare. These general characteristics suggest the carbonate buildup represent travertine deposits. However, there are no known hydrothermal sources to have created groundwater-fed carbonate buildups with water temperatures in excess of 20^{o} C. Carbon dioxide degassing is an important component of travertine deposition with the bubbles being preserved in the carbonate. These primary porosity structures were not observed in the field, nor in thin section for any of studied Morrison carbonate buildups. This suggests CO_2 degassing was not violently occurring at the surface during precipitation and therefore the buildup was likely not hydrothermally sourced.

Additional evidence from fossil and standard isotopic data indicate the carbonate buildups are tufa deposits. The incorporation of the microscopic woody macrophyte fossil fragments, homoxylous wood, bryophyte leaves (liverworts; fig. 9), and the logs of *Circoporoxylon* and *Xenoxylon* into the carbonate buildups indicated that plants were in growing near the mounds. Although different plants can have varying water temperature tolerances, the close proximity to such a small diameter buildup suggest an ambient water temperature. The fossilized microphyte

fabric which may be the eukaryotic microalgae (Zygnematophyceae) *Oocardium stratum* Nägeli (Pfiester, 1976) also provides an indication of the water temperature. The calcifying desmid *O. stratum* is a colonial freshwater green alga commonly associated with modern tufas (Pentecost, 1991, 2005; Linhart and Schagerl, 2011). The desmid develops branching calcite tubes with unicells located on the top of the tube of calcite. A halo of mucus surrounds the top algal cell (Golubic and Marcenko, 1958; Golubic et al., 1993). The biocrystals can grow up to 10 mm annually (Sanders and Rott, 2009). *O. stratum* is known for the manner in which it becomes encrusted in freshwater carbonate-depositing sites (Pentecost, 1991; Ibarra et al., 2014). The pore diameter of the Morrison fossil microphyte is ≈ 30µ, whereas the pore diameter the calcite tubes of modern *O. stratum* are between 17–20µ (Ibarra and Sanon, 2019). The algae *O. stratum* is known from waters with a temperature range from 7–13º C but can exist in cooler (4º C; Tran et al., 2019) or warmer water temperatures with an optimum water temperature of 13ºC (Pentecost, 1991; Sanders and Rott, 2009; Linhart and Schagerl, 2011; Rott et al., 2012; Ibarra et al., 2014). Additional observed niche conditions for modern *O. stratum* include carbonate supersaturation, gradual CO_2 degassing, and circumneutral pH 7–8 spring waters (Rott et al., 2012). Associated with the *O. stratum* are two 142µ diameter pores which may represent the stems of hydrophytes growing in association with the algae. If the fossil is *O. stratum*, its presence preserved in the carbonates indicates pH-neutral water with ambient temperatures (i.e. < 20º C).

The radial-fibrous spherulites are found in outcrop at the upper surface of the carbonate buildups. Spherulites are thought to develop in thermogenic spring settings (Muir and Walton, 1957; Steinen et al., 1987) although other researchers disagree with this interpretation (Walkden et. al., 1994). Spherulites are a common feature of fossil and modern tufa deposits (Guo and Chafetz, 2012). The modern Sitting Bull Falls tufa near Carlsbad, New Mexico also displays

spherulites. Bacterially-precipitated vaterite and calcite in marine and terrestrial environments are well-documented (Boquet et al., 1973; Chafetz and Folk, 1984; Merz, 1992; Castanier et al., 2000; Braissant et al., 2003; Párraga et al., 2004; Ronholm et al., 2014; Baumann et al., 2016). Chafetz and Folk (1984) suggest bacterial carbonate precipitation may account for 90% of a buildup's framework grains. The spherulites likely formed by the secretion of biofilms (e.g. glycocalyx) from a betaproteobacteria such as *Ralstonia eutropha* H16 (Braissant et al., 2003), or a Jurassic variant. *R. eutropha* H16 is a chemolithoautotrophic bacterium able to grow within organic substrates under aerobic conditions (Müller et al., 2013). The modern bacterium *R. eutropha* H16 has an identical XRD diffractogram as calcium carbonate (Braissant et al., 2003). The bacterial formation of spherulites also indicates an ambient temperature, aerobic environment.

The standard isotopic data of the carbonate buildup also indicate that they are tufas. The $\delta^{18}O$ values are the product of meteoric water isotopic fractionation from latitude, elevation, precipitation and evaporation, seasonal variation and temperature, and the precipitation of calcite (Dansgaard, 1964; Sharp, 2007). Seasonal temperature variations are related to an increase in latitude resulting in a greater range in seasonal isotopic values, but in general, the mean $\delta^{18}O$ value decreases with an increase with latitude (Sharp, 2007).

The mean $\delta^{18}O$ value derived from marine shell carbonates during the Late Jurassic (150 Ma) is –1‰ VPDB (Veizer et al., 1999). Based on isotopic analysis of pedogenic carbonates and fossils, $\delta^{18}O$ values for paleometeoric waters of the Morrison Formation were highly depleted (Ekart and Cerling, 1996). $\delta^{18}O$ values derived from fossil crocodile teeth and turtle scutes for four locations in the Morrison Formation show comparable values. From south to north the fossil localities are Kenton, OK; Fruita, CO; Nine Mile Hill, WY (central WY), and Upton, WY

(northern WY) with the respective $\delta^{18}O$ values –16.14‰, –20.30‰, –16.31‰, and –16.94‰ (Brundridge, 2013). The central Montana values are isotopically heavier (table 1).

In general, freshwater carbonates have negative $\delta^{13}C$ values, but these values can become even lighter if there are significant contributions of organic carbon (Sharp, 2007). Paleo $\delta^{13}C$ values requires a correction due to secular variation of the $\delta^{13}C$ throughout geologic time (Mackenzie and Pigott, 1981). The total dissolved carbon in the oceans has changed through geologic time. Variations in oceanic dissolved inorganic carbon is related to tectonism, erosion, productivity and carbonate deposition (Sharp, 2007). During the Late Jurassic (150 Ma), the secular variation was near +2‰ VPDB (Veizer et al., 1999).

For terrestrial environments, the $\delta^{13}C$ of the freshwater carbonate is controlled by the dissolved inorganic carbon in the groundwater and its interaction with the soil. Carbonates precipitated at lower altitudes (the Morrison planation surface of central Montana) where vegetation productivity is generally higher, should have lighter $\delta^{13}C$ values due a greater contribution of ^{12}C from C_3 plants. At higher elevations where plant productivity is poor $\delta^{13}C$ will have isotopically heavier values.

Isotopic data of the Morrison tufa deposit (table 1) $\delta^{18}O$ values are similar to the present weight annual $\delta^{18}O$ global distribution for comparable latitudes, suggesting minimal diagenetic alteration (Darling et al., 2006). The central Montana $\delta^{18}O$ values are slightly heavier than more southern Morrison Formation $\delta^{18}O$ values signifying minor input from the retreating Sundance seaway, perhaps due to changes in atmospheric circulation during the winter months. The $\delta^{13}C$ data indicate the dissolved inorganic carbon was derived from atmospheric CO_2 and the groundwater had short resident time with minor interactions with organic matter in the soil (Darling et al., 2006; Sharp, 2007). Woody plants (C_3) are enriched in ^{12}C with values of $\delta^{13}C \approx$ –25‰ (Park and

Epstein, 1961; Sharp, 2007; Bacon et al., 2011) and the soils they produce have similar values (Diochon and Kellman, 2008). The $\delta^{13}C$ values indicate these are not pedogenic carbonates. Pedogenic carbonates $\delta^{13}C$ values are dominated by the isotopic signal of plant communities (Sharp, 2007).

The standard isotopic data from the Morrison carbonate buildups was plotted on a cartesian graph with $\delta^{18}O$ on the *x*-axis and $\delta^{13}C$ on the *y*-axis (fig. 16). Fluvial and lacustrine tufas both have low negative $\delta^{18}O$ values. In contrast, lacustrine tufas have a positive $\delta^{13}C$ values, whereas fluvial tufas have negative $\delta^{13}C$ values. The Morrison carbonate buildup data have both negative $\delta^{18}O$ and $\delta^{13}C$ values. The Morrison isotopic data plots in the range of the oldest North America tufas, those associated with the Navajo Sandstone (Parrish et al., 2019). Thermogenic waters have positive $\delta^{13}C$ values. The positive values reflect an increase in dissolved inorganic carbon as a result of deep subsurface circulation and longer residence times in limestone aquifers (Andrews, 2006). Thermogenic waters have negative $\delta^{18}O$ values indicating a meteoric source (Gandin and Capezzuoli, 2008; Della Porta, 2015).

The negative isotopic values for the Morrison Formation buildups reveal that they were produced by meteoric waters in a continental setting (Andrews, 2006; Sharp, 2007). Drier climates, which increase the groundwater's residence time owing to decreased recharge, also results in isotopically heavier $\delta^{13}C$ values (Tanner, 2010). The difference between the positive Late Jurassic oceanic values (+2 ‰) and the negative values of the Morrison Formation of central Montana (–5.3‰ average) suggest the region had a low attitude with high plant productivity, and a wet climate.

The Morrison carbonate tufa buildups are similar to the artesian mound springs of the Great Artesian Basin (GAB) in the Lake Eyre South region of Southern Australia (Keppel, 2011; 2012).

The GAB mound springs acquired their name for their hemispherical shape that forms by the accretion of sediment around the spring outlet. The outlet gradually rises in elevation forming a dome- or shield-shaped cone and are typically between 2–5 m in height (Williams and Homes, 1978, Keppel, 2011; fig. 17). Many GAB mound springs do not consist of the characteristic calcareous mound but either emerge at ground level, or consist of soft, silty mounds. There are more than 5000 springs distributed among 169 spring groups in the southern GAB (Keppel et al., 2020). The GAB mound springs form under a semiarid to arid climate (Harris, 1981). The GAB-associated paludal environments are limited in size due to the high rates of evaporation (> 10 mm/day; Holmes et al., 1981). GAB mound spring formation is related directly to a low flow rate (Ponder, 1986). Springs with higher flow rates have associated channels (e.g. spring tails) which distribute the discharged fluids away from the spring vent, whereas decreased flow rates allow for the precipitation at the vent, resulting in the building up of the mound. Estimated discharge from a small spring in the GAB is 200 l/hr. With solute concentrations of 4 g/l, the spring would deposit 170 t of carbonate to build a 3-m high mound in about 1000 years (Williams and Homes, 1978). The GAB mound springs are composed of eolian sand, plant debris, and mud and sand carried up through fractures by the spring discharge (Ponder, 1986). According to Stokes law, a discharge rate of greater than 4 cm/s is required to lift fine sand up a fracture (Williams and Homes, 1978).

The Morrison mound springs are similar in shape to the GAB mound springs but have a subartesian component (fig. 17). No detrital sand or clay has been found in the Morrison mound springs suggesting discharge rates were < 4 cm/s. Low flow rates facilitated the building of the mound. The lack of associated fluvial, paludal or lacustrine facies supports the interpreted low surface discharge rate. The spatial distribution of the siderite and carbonate buildups in proximity to Late Jurassic faults or fractures corresponds to the azimuth orientation of the present-day major

Montana lineaments (fig. 18). The mound springs were sourced by an increase in local groundwater from precipitation, raising the near-surface vadose zone and resulting in movement up fractures to discharge at the surface.

Similarly, local modern fractures through the Swift, Morrison, and Kootenai Formations permit the discharge of groundwater to the surface as seeps and small springs (Richmond pers obs., 2017–2019). Discharge rate is controlled by Montana's yearly variable rainfall. Ponderosa pines dominate the highland landscapes, but where springs or seeps reach the surface on these uplands, small groves of the mesophytic quaking aspen are present. Some of these seeps do not have discharge tails.

6.3 Montana Morrison forest ecology and soils

The flora form the Morrison Formation of central Montana is important to understanding the geochemistry of the siderite buildups and the negative $\delta^{13}C$ values of the mound springs. Each is the product of the groundwater interaction with decomposing organic carbon during its relatively short residence time. Numerous petrified woods including partial logs have been discovered stratigraphically between 25–63 m, with the majority of the fossil woods between 35–55 m. The carbonate mound springs are within the same stratigraphic section as the majority of the petrified wood samples.

Modern plant diversity and productivity are highest in equatorial regions and decrease toward the poles. In contrast, during the Late Jurassic plant diversity and productivity was greatest in the midlatitudes (45^{o} latitude; Rees et al., 2000; Rees et al., 2004). Based on the spatial distribution and the numerous specimens discovered, it is probable that the Jurassic tree spacing constituted a forest (> 10 trees/0.01 km^2). Paleoecology of this northern forest was likely similar to

a temperate coniferous forest with narrow crowns, a semi-closed canopy, and limbless shade-pruned trees. The northern forest of the Morrison Formation was likely three tiered with an overstory, an understory, and groundcover. A tree's wood growth is the product of latitude, altitude, solar input and geography of the growth site (Creber and Chaloner, 1984). Presently, three gymnosperm genera have been identified *Xenoxylon* (Richmond et al., 2019), *Piceoxylon* (Richmond et al., 2019a), and *Circoporoxylon* (Richmond et al., 2019b). *Xenoxylon* is a boreal wood known for its affinity for cool and wet climates (Philippe and Thévenard, 1996; Philippe et al., 2009; Tian et al., 2016; Philippe et al., 2017). *Piceoxylon* is also a boreal genus, but *Circoporoxylon* had an affinity for warm temperate climates (Chinnappa and Rajanikanth, 2016). Specimens of *Circoporoxylon* from the study area display narrow growth rings and numerous false rings, suggesting that the genus was near its northernmost range. According to Copenheaver et al. (2006) false growth rings in gymnosperms are often caused by dry spells. However, the false rings of *Circoporoxylon* may reflect temperature variations rather than moisture dependence.

Additional Coniferales from the Morrison Formation of central Montana include *Podozamites lanceolatus*, *Pityophyllum lindstromi*, *Pityocladus* sp., and *Pagiophyllnm* sp. (Brown, 1972). Based on palynology, other genera of the families Pinaceae and Podocarpaceae were also present (Hotton and Baghai-Riding, 2010). Subdominant understory woody plants included Cycadales (*Zamites arcticus)*, Ginkgoales (*Ginkgoites marginatus*, *Ginkgoites pluripartita*), and Bennettitales (*Cycadolepis* sp., *Nilssonia compta*, and *Weltrichia* sp.) (Brown, 1972). The groundcover in the Late Jurassic of central Montana was comprised of fungi, the sphenophyte *Equisetum lateralis*, the pteridophytes *Hausmannia fisheri*, *Coniopteris hymenophylloides, Adiantites montanensis*, *Cladophlebis alberta*, *Cladophlebis heterophylla*, and *Cladophlebis virginiensis*, and the pteridosperm *Sagenopteris elliptica* (Brown, 1972). These groundcover genera

prefer terrestrial wet floodplains. Based on the Morrison Formation in northern Wyoming, bryophytes and pteridophytes (lycopsids, sphenophytes, and ferns) comprised 20% of the palynological sample (Hotton and Baghai-Riding, 2010). According to Hotton and Baghai-Riding (2010) their palynological data support increasing humidity and higher water tables northward in the Morrison basin. Several mudstone beds from the Morrison Formation of central Montana were processed for palynomorphs and yielded bisaccate pollen and trilete and fungal spores. Additional genera include the gymnosperms *Alisporites*, and *Monosulcites*/*Cycadopites, Eucommiidites*? and *Classopollis*? The additional pollen and fern genera, fungal spores, and homoxylous woods suggest high humidity and a high-water table for the Morrison Formation of central Montana.

The accumulation of organic materials of the forest floor is chiefly a function of the annual litterfall minus decomposition. The largest proportion of allochthonous organic matter is from foliage, seeds, branches, and bark. The main litterfall contribution is from the overstory with understory plants supplying about 10 percent (Binkley and Fisher, 2019). Storms can accelerate litterfall volumes whereas elevated temperatures and soil moisture can hasten decomposition rates. Conversely, ground fires can consume forest floor organic materials. Annual litter production can be related to latitude. During the Late Jurassic central Montana was at a paleolatitude of 50^{o} north (Richmond et al., 2019). Most modern conifer forests have an annual litterfall of 1975–5900 kg/hectare/year (Binkley and Fisher, 2019); however, a cool temperate forest at 50^{o} north latitude generates 3700 kg/hectare/year (Bray and Gorham, 1964).

The rate of organic decay depends on the interaction of physical factors, water chemistry, and biological agents. Decomposition can be rapid with turnover rates varying between 1–3 years for cool temperate climates (Binkley and Fisher, 2019). Litterfall on the forest floor is fragmented by arthropod and annelid decomposers, then consumed by rotifers and pervasive microbes. The top

organic soil layer consists of undecomposed litter which overlies the fermentation layer where decomposition occurs. This layer overlies the humus layer where decay is nearly complete.

In these habitats, nutrient turnover is slow. Potassium and sodium are quickly leached from the soil. Nitrogen, phosphorus, sulfur, and magnesium are released into the soil after a longer period. Iron, zinc, and copper are left accumulated in the litter material (Staaf, 1980). Plants require iron for the production of chlorophyll, for respiratory and photosynthetic enzyme systems, and the reduction of nitrates and sulfates. Gymnosperms contain between 60–200 ppm iron (Landis et al., 2005). Most gymnosperms prefer a moderately acidic soil with a pH of 5.5. Acid soils usually occur in regions where annual precipitation > 600–800 mm (Havlin, 2005). Natural acid soils form when high temperatures and high precipitation rates leach basic cations (Na, Ca, Mg, and K) and carbonates, leaving acidic iron and aluminum oxides minerals (Artiola et al., 2019). Soils are also acidified by the breakdown of metal sulfides and the decomposition of acidic organic material. Acid soils increase the solubility of iron. Under acidic conditions, Fe^{0} readily oxidizes to Fe^{2+}, and Fe^{2+} to Fe^{3+} as the pH increases above 5 (Lindsay, 1991). Therefore, the forest floor soils and the interaction with the groundwater induced the precipitation of the siderite in the subsurface.

The Morrison floral productivity in central Montana is a manifestation of a low attitude and the precipitation rates. The floral productivity resulted in abundant decomposing organic carbon on the forest floor and in the shallow subsurface. The precipitation and groundwater geochemically interacted with the organic carbon to produce more negative $\delta^{13}C$ values. The high productivity of the region (Rees et al., 2000, Rees et al., 2004), and the low negative $\delta^{13}C$ values suggests that the groundwater had a relatively short residence time in the subsurface otherwise the $\delta^{13}C$ values would have been substantially isotopically lighter (≈ –25‰).

7. Paleoclimatic significance

The Pangean megamonsoon system of western North America sustained an unusually humid climate in an otherwise protracted arid interval during the Late Paleozoic through the Middle Mesozoic (Nordt et al., 2015). During the Triassic, the mean annual precipitation rapidly transitioned from a warm temperate humid climate (225 Ma) to a cool temperate arid climate (210 Ma) (Nordt et al., 2015). This trend for the North American southwest continued into the Jurassic as signified by the numerous widespread Middle Jurassic eolian deposits (e.g. Wingate, Navajo, Entrada, and their lateral equivalent formations; Peterson, 1988; Clemmensen et al., 1989; Nation, 1990; Chan and Archer, 2000). The arid climatic trend continued into the Late Jurassic, as represented by the eolian lithologic units of the Morrison Formation: the Bluff Sandstone, the Unkpapa Sandstone, Junction Creek, and Recapture Members and the gypsiferous sediments of the Tidwell Member (Szigeti and Fox, 1981; Peterson, 1988; Parrish and Peterson, 1988; Bernier and Chan, 2006). These eolian and gypsiferous members are stratigraphically in the lower half of the formation (Demko and Parrish, 1998).

A zonal climate model applied by Parrish et al. (1982) predicted low rainfall patterns for much of the Morrison basin. The aridity was likely generated by several factors, including the latitudinal position in the subtropical dry belt, the Sevier orogenic belt acting as a rain shadow (Demko and Parrish 1998), and oceanic upwelling driven by coastal wind patterns (Parrish and Peterson 1988). Peterson and Turner-Peterson (1987) suggested the presence of narrow but extensive riparian environments that supported abundant plant life to sustain the large herbivorous dinosaurs which roamed the Morrison basin. Many researchers agree that foreland basin sediments of the Morrison Formation were deposited and formed in a semiarid to arid climate (Parrish et al., 1982; Hotton, 1986; Parrish and Peterson 1988; Turner and Fishman 1991; Valdes and Sellwood

1992; Demko and Parrish 1998; Parrish et al., 2004) with seasonal precipitation (Demko et al., 2004).

Dodson et al. (1980) suggested a strong seasonal climate based upon dinosaurian fauna and taphonomy. However, Jurassic dinosaurs are assumed to have been migratory (Fricke et al., 2011; Bronzo et al., 2017). Therefore, their presence or absence from a region should not be used for evidence to infer paleoclimate. Many of the fluvial channels of the Morrison basin were ephemeral, signifying seasonal or episodic precipitation with sufficient fluid flow to transport sediments (and large dinosaur bones, Morris et al., 1996).

In contrast to the arid or variable climate models and lithologic proxies, other lithologic and paleontological proxies indicate a perennial wet climate. Perennial fluvial, palustrine, and lacustrine facies in the Morrison basin support this conclusion (Lockley et al., 1984; Lockley et al., 1986; Dunagan 1999; Dunagan and Turner 2004; Gorman II et al., 2008). The presence of aquatic and semi-aquatic vertebrates (Hecht and Estes, 1960; Gaffney 1979; Kirkland, 1987; Hups et al., 2006; Small et al., 2007; Gorman II et al., 2008; Hunt and Richmond 2018) and aquatic invertebrates (Evanoff et al., 1998; Schudack et al., 1998; Dunagan, 1999; Good, 2004; Richmond et al., 2017) indicate the presence of perennial lakes and rivers in the Morrison basin.

In addition to the aquatic fauna, the flora also indicates a wet climate (Tidwell, 1990; Tidwell and Medlyn, 1992, 1993; Gee et al., 2019; Richmond et al., 2019). However, Demko and Parrish, (1998) suggested that plants only represent a small spatial and stratigraphic portion of the formation and are inconsequential to the overall climatic interpretation. The apparent lack of plant fossils in the more southern regions of the Morrison Formation may be due to a taphonomic megabias. Fossil bones and plants generally require different pH environments for preservation. Acidic environments favor the preservation of plant material, whereas more basic environments

promote bone preservation (Gordon and Buikstra, 1981; Ballhaus at al., 2012; Manifold, 2012). The abundance of fossil bones stratigraphically and spatially in the formation implies a depositional bias toward oxidizing environments.

Similar to modern continentality, the proximity of the northward-retreating Sundance Sea during the Late Jurassic likely created cool and wet coastal climates in central Montana in contrast to the more southern inland continental regions. Palynological research over the Morrison basin shows the paleoclimate transitioned from arid in the southern latitudes (Hotton and Baghai-Riding, 2010) to a more humid climate in the northern clines (Baghai-Riding et al., 2015). The new discovery of the boreal wood *Xenoxylon* in the Morrison Formation of central Montana corroborates a wet climate in the northern basin latitudes (Richmond et al., 2019). The newly discovered partial bryophyte leaves with their chambers occupied by cyanobacteria also provide some insights into the paleoclimate. Bryophytes live in a wide variety of habitats; however, they prefer moist environments (Schuster, 1966; Shaw and Renzaglia, 2004). They do not favor excessively dry environments, nor high levels of direct solar radiation. In forest ecosystems, bryophytes regulate soil temperature and moisture (Deane-Coe and Sparks, 2016). Their preservation in a mound springs indicate they were in proximity to the outlet.

If the microphyte fabric is *Oocardium stratum* or a close relative, then its presence in association with the Morrison carbonate mound springs provides additional insight into the paleoclimate of the Morrison Formation of central Montana. Modern *O. stratum* is present in warm- and cool-temperate climates (Pentecost, 1990; 2005), but is more prevalent in regions where summer temperatures exceed 25ºC (Pentecost, 1991). It is also common in modern cooler mountainous terrains (Sanders and Rott, 2009; Linhart and Schagerl, 2011; Rott et al., 2012; Tran et al., 2019).

Semi-arid conditions are incapable of sustaining the perennial highwater table necessary for continuous discharge to form tufa deposits (Pedley, 1990). The presence of carbonate mound springs indicates a sufficiently high phreatic zone close to the surface for groundwater to migrate up microfractures in the impermeable Morrison mudstones to the ground surface. Warm to temperate, humid climates appear to be most favorable for freshwater tufa development, whereas cold conditions inhibit tufa growth (Pedley, 1990). Consequently, regions with higher rainfall and temperatures promote tufa formation (Ford and Pedley 1996). An average annual temperature between 5–15ºC is suggested to be the most favorable to tufa formation and growth (Pentecost, 1991; Ibarra et al., 2014). The occurrence of mound springs in the Morrison Formation in central Montana suggests a cool temperate climate.

Stable isotope data from the mound springs have a negative $\delta^{18}O$ signals (more O^{16}) verifies that during the Late Jurassic central Montana was a high latitude (between 40–50º; Richmond et al., 2019) and that an area experienced increased rainfall. Tufas generally occur in regions characterized by an annual rainfall in excess of 500 mm/year (Pentecost, 1991; Ibarra et al., 2014). Tufas with *Oocardium* commonly have rainfall than exceeds 1000 mm/year (Ibarra et al., 2014). Using the elemental analyses to calculate the calcium and magnesium weathering index (CALMAG) of paleosol B horizons in the Upper Jurassic Morrison Formation of south-central Montana Myers et al. (2014) estimated a mean annual rainfall for the region ≈ > 1200 mm/year. The occurrence of the tufas and a varied paleoflora, and the CALMAG data of Myers et al. (2014) indicate that during the Late Jurassic central Montana experienced a warm temperate (Rees et al., 2004) to cool temperate climate with dry warm summers and with increased precipitation during the cool winter months.

The ERT data display the presences of larger mounds in the subsurface, with mudstone strata between the surface and the subsurface mounds. These subsurface views provide two inferences about the buildups. First, the larger buildups record a prolonged period of increased precipitation. Second, the environmental conditions required for the buildups were not continuous. The separation of the subsurface and surface by mudstone deposition suggests that there were dry periods with insufficient precipitation to create buildups. The numerous carbonate mound springs, and their variable stratigraphic positions within the formation (40–52 m), suggest a long-term wet cycle during the Late Jurassic of central Montana, interspersed with drier periods of undetermined length.

8. Conclusions

The discovery of numerous mound springs represents the first observed occurrence of tufa deposits in the Morrison Formation and represent some of the oldest tufa deposits recorded for North America (Dorney et al., 2017; Parrish et al., 2017; Parrish et al., 2019). The spatial data demonstrate a linear relationship to the buildups, and they were likely sourced by carbonate-rich water from fractures along Jurassic-aged lineaments. The siderite buildups, with their cone-in-cone structures, formed in the subsurface near the capillary fringe. In the subsurface the groundwater interacted with iron-rich soils of the forest floor. XRF data of the various siderite buildups show a variable chemistry which may have been caused by the groundwater interacting with local soils. Betaproteobacteria might have advanced the precipitation of the iron carbonates in the subsurface. The carbonate mound springs formed from groundwater surface seeps leaking up fractures. Spring flow rates are interpreted to have been low, as there are no connecting fluvial or lacustrine facies. The precipitation of the carbonates mounds was inorganic and organic. The presence of the

spherulites shows that the betaproteobacteria played a part in some carbonate precipitation. The mound spring waters discharged at the surface is interpreted to have been cool based on the isotopic data, the lack of evidence for CO_2 degassing at the vent, low sulfur percentages, and the associated plant material (e.g. *Oocardium*).

The presence of the algal material in the spherulites and algal films on the dogtooth calcite crystals, the incorporation of *Oocardium*, bryophyte leaves and homoxylous wood of gymnosperm logs into the mounds indicate the mound springs formed at the surface with plants living in close proximity to the springs.

The isotopic $\delta^{13}C$ data indicate that the groundwater was sourced by meteoric in origin, occurring in a low elevation continental setting that experienced high rainfall. The stratigraphic sections and the ERT subsurface data of the mound springs imply repeated periods of increased precipitation separated by drier periods. This wet climate for Morrison Formation of central Montana is in contrast to the climate models and interpretations of the more southern regions.

Acknowledgments

I especially thank the Hein family for access to their ranch and their wonderful support during this research project. I am grateful to Nate Murphy of Judith River Dinosaur Institute, Billings Montana, for his continuous field support and use of field equipment.

References (formatted for submittal to Paleogeography, Paleoclimatology, Paleoecology)

Abdel-Wahab, A., McBride, E.F., 2001. Origin of giant calcite-cemented concretions, Temple Member, Qasr El Sagha Formation (Eocene), Faiyum Depression, Egypt. J. Sediment Res. 71, 70–81.

Allen, A., 1996. Morrison Formation stratigraphy between the classic Como Bluff and Thermopolis area, Wyoming. Paleoenvironments of the Jurassic: Field Conference, Tate Museum, Casper College, WY, p. 19–28.

Allison, P.A., Pye, K., 1994. Early diagenetic mineralization and fossil preservation in modern carbonate concretions. PALAIOS 9, 561–575.

Alonso-Zarza, A.M., 2020. Palaeoenvironmental significance of palustrine carbonates and calcretes in the geological record. Earth-Sci. Rev. 60, 261–298.

Alonso-Zarza, A.M., Wright, V. P., 2010. Palustrine carbonates. Develop. Sediment. 61, 103–131.

Andrews, J.E., 2006. Palaeoclimatic records from stable isotopes in riverine tufas: Synthesis and review. Earth-Sci. Rev. 75, 85–104.

Arribas, M.E., Rodríguez-López, J.P., Meléndez, N., Soria, A.R., de Boer, P.L., 2012. Giant calcite concretions in aeolian dune sandstones; sedimentological and architectural controls on diagenetic heterogeneity, mid-Cretaceous Iberian Desert System, Spain. Sediment. Geol. 243, 130–147.

Artiola, J.F., Walworth, J.L., Musil, S.A., Crimmins, M.A., 2019. Soil and land pollution. *In* Brusseau, M.L., Pepper, I. L., Gerba, C.P., (eds), Environment and Pollution Science 3rd Edition, Academic Press, p. 219–235.

Bacon, K.L., Belcher, C.M., Hesselbo, S.P., McElwain, J.C., 2011. The Triassic–Jurassic boundary carbon isotope excursions expressed in taxonomically identified leaf cuticles. PALAOIS 26, 461–469.

Baghai-Riding, N., Hotton, C.L., Davis, K., Davidson, T., 2015. Palynological evidence for a latitudinal moisture gradient in the Late Jurassic Morrison Formation. Geol. Soc. Am. Abstr. Prog. 47, 143.

Ballhaus, C., Gee, C.T., Bockrath, C., Greef, K., Mansfeldt, T., Rhede, D., 2012. The silicification of trees in volcanic ash–An experimental study. Geochim. et Cosmochim. Acta 84, 62–74.

Barilaro, F., Della Porta, G., Capezzuoli, E., 2012. Depositional geometry and fabric types of hydrothermal travertine deposits (Albegna Valley, Tuscany, Italy). Rend. Online Soc. Geol. It. 21, 1024–1025.

Baumann, L.M.F., Birgel, D., Wagreich, M., Peckmann, J., 2016. Microbially-driven formation of Cenozoic siderite and calcite concretions from eastern Austria. Austrian J. Earth Sci. 109, 211–232.

Beck, R., Andreassen, J.-P., 2010, Spherulitic growth of calcium carbonate. Crystal growth and design 10, 2934-2947.

Berner, R.A., 1968. Rate of concretion growth. Geochim. et Cosmochim. Acta 32, 477–483.

Bernier, J.C., Chan, M.A., 2006. Sedimentology, depositional environments, and paleoecological context of an Early Late Jurassic sauropod, Tidwell Member, Upper Jurassic Morrison Formation, east-central Utah. Mount. Geol. 43, 313–332.

Biek, B., 1994, Concretions and nodules in North Dakota: Cannonballs, logs, and other oddities. North Dakota Geol. Surv. 21, 6–11.

Binkley, D., Fisher. R.F., 2020. Ecology and Management of Forest Soils, 5th Ed., John Wiley and Sons, p. 1–456.

Blöthe, M., Roden, E. E., 2009. Microbial iron redox cycling in a circumneutral-pH groundwater seep. Appl. Environ. Microbiol. 75, 468–473.

Boles, J.R. Landis, C.A. Dale, P., 1985. The Moeraki Boulders; anatomy of some septarian concretions. J. Sediment. Pet. 55, 398–406.

Boquet, E., Boronat, A., Ramos-Cormenzana, A., 1973. Production of calcite (calcium carbonate) crystals by soil bacteria is a general phenomenon. Nature 246, 527–528.

Braissant, O., Cailleau, G., Dupraz, C., Verrecchia, E. P., 2003. Bacterially induced mineralization of calcium calcite in terrestrial environments: The role if exopolysaccharides and amino acids. J. Sediment. Res. 73, 485–490.

Bray, J.R., Gorham, E., 1964. Litter production in forests of the world. Adv. Ecolog. Res. 2, 101–157.

Bronzo, K.M., Fricke, H., Hoerner, M.E., Lundstrom, C., 2017. Using oxygen, carbon and strontium isotope ratios of tooth enamel from dinosaurs to infer patterns of movement over the Late Jurassic Landscape of CO, UT, and WY. Geol. Soc. Am. Abstr. Prog. 49, 4.

Brown, J.T., 1972. The flora of the Morrison Formation (Upper Jurassic) of central Montana (Doctoral dissertation). University of Montana, Missoula, MT, 59 p.

Brown, R.W., 1946. Fossil plants and Jurassic–Cretaceous boundary in Montana and Alberta. Am. Assoc. Pet. Geol. Bull. 30, 238–248.

Brundridge, K., 2013, Assessing latitudinal variations in climate of the Jurassic Morrison Formation from oxygen isotopes from aquatic vertebrates. (Master's thesis). University of Texas at San Antonio, San Antonio, TX, 65 p.

Campbell, K.A., Guido, D. M., Gautret, P., Foucher, F., Ramboz, C., Westall, F., 2015. Geyserite in hot-spring siliceous sinter: Window on Earth's hottest terrestrial (paleo)environment and its extreme life. Earth-Sci. Rev. 148, 44–64.

Capezzuoli, E., Gandin, A., Pedley, M., 2014. Decoding tufa and travertine (fresh water carbonates) in the sedimentary record: The state of the art. Sediment. 61, 1–21.

Castanier, S., Le Métayer-Levrel, G., Perthuisot, J.-P., 2000. Bacterial roles in the precipitation of carbonate minerals. *In* Riding R.E., Awramik S.M. (eds), Microbial Sediments, Springer-Verlag, Berlin, p. 32–39.

Chafetz, H.S., Folk, R. L., 1984. Travertines: Depositional morphology and the bacterially constructed constituents. J. Sediment. Pet. 54, 289–316.

Chan, M.A., Archer, A. W., 2000. Cyclic Eolian Stratification on the Jurassic Navajo Sandstone, Zion National Park: Periodicities and Implications for Paleoclimate. *In* Sprinkel, D.A., Chidsey, T.C., Jr., Anderson, P.B., (eds), Geology of Utah’s Parks and Monuments. Utah Geol. Assoc. Pub. 28, 1–11.

Chan, M.A., Beitler, B. Parry, W.T., Ormö, J. Komatsu, G., 2004. A possible terrestrial analogue for haematite concretions on Mars. Nature 429, 731–734.

Chan, M.A., Johnson, C.M., Beard, B.L., Bowman J.R., Parry, W.T., 2006. Iron isotopes constrain the pathways and formation mechanisms of terrestrial oxide concretions: A tool for tracing iron cycling on Mars? Geosphere 2, 324–332.

Chan, M.A., Potter, S. L., Bowen, B.B., Parry, W. T., Barge, L. M., Seiler, W., Petersen, E. U., Bowman, J.R., 2012. Characteristics of terrestrial ferric oxide concretions and implications for Mars. Sediment. Geol. 102, 253–270.

Chinnappa, C., Rajanikanth, A., 2016. A new species of *Circoporoxylon* from the Kota Formation (Jurassic), Pranhita-Godavari Basin, India, and palaeobiogeography of the genus. Ameghiniana 53, 675–684.

Clemmensen, L.B., Olsen, H., Blakey, R. C., 1989, Erg-margin deposits in the Lower Jurassic Moenave Formation and Wingate Sandstone, southern Utah. Geol. Soc. Bull. 101, 759–773.

Cobbold, P.R., Zanella, A., Rodrigues, N., Løseth, H., 2013. Bedding-parallel fibrous veins (beef and cone-in-cone): Worldwide occurrence and possible significance in terms of fluid overpressure, hydrocarbon generation and mineralization. Marine Pet. Geol. 43, 1–20.

Copenheaver, C.A., Pokorski, E.A., Currie, J.E., Abrams, M.D., 2006. Causation of false ring formation in *Pinus banksiana*: A comparison of age, canopy class, climate and growth rate. For. Ecol. Manag. 236, 348–355.

Cotroneo, S., Schiffbauer, J.D. McCoy, V.E., Wortmann, U.G., Darroch, S.A.F., Peng, Y., Laflamme, M., 2016. A new model of the formation of Pennsylvanian iron carbonate concretions hosting exceptional soft-bodied fossils in Mazon Creek, Illinois. Geobiol. 14, 543–555.

Creber, G.T., Chaloner, W.G., 1984. Influence of environment factors on the wood structure of living and fossil trees. Botant. Rev. 50, 358–390.

Cronan, D.S., Thomas, R.L., 1972. Geochemistry of ferromanganese oxide concretions and associated deposits in Lake Ontario. Geol. Soc. Am. Bull. 83, 1493–1502.

Darling, G.W., Bath, A.H., Gibson, J.J., Rozanski, K., Isotopes in water. *In* Leng M.J. (ed) Isotopes in Palaeoenvironmental Research. Developments in Paleoenvironmental Research 10, 1–66.

Dansgaard, W., 1964. Stable Isotopes in Precipitation. Tellus 16, 437–468.

Daun, W.M., Hedrick, D.B., Pye, K., Coleman, M.L., White, D.C., 1996. A preliminary study of the geochemical and microbiological characteristics of modern sedimentary concretions. Limnol. Oceanogr. 41, 1404–1414.

Deane-Coe, K.K., Sparks, T.P., 2016. Cyanobacteria associations in temperate forest bryophytes revealed by $\delta^{15}N$ analysis. Torrey Botan. Soc. 143, 50-57.

Della Porta, G., 2015. Carbonate build-ups in lacustrine, hydrothermal, and fluvial settings: comparing depositional geometry, fabric types and geochemical signature. *In* Bosence, D.W.J., Gibbons, K.A., Le Heron, D.P., Morgan, W.A., Pritchard, T., Vining, B.A. (eds), Microbial carbonates in space and time: Implications for global exploration and production. Geol. Soc. London Spec. Pub. 418, 17–68.

Demko, T. M.; Currie, B. S.; and Nicoll, K. A. 2004. Regional paleoclimatic and stratigraphic implications of paleosols and fluvial/overbank architecture in the Morrison Formation (Upper Jurassic), Western Interior, USA. Sediment. Geol. 167:115–135.

Demko, T.M., Parrish, J.T., 1998. Paleoclimatic setting of the Upper Jurassic Morrison Formation. Mod. Geol. 22, 283–296.

Diochon, A., Kellman, L., 2008. Natural abundance measurements of ^{13}C indicate increased deep soil carbon mineralization after forest disturbance. Geophys. Res. Let. 35, L14402, 1–5.

Dodson, P., Behrensmeyer, A.K., Bakker, R.T., McIntosh, J.S., 1980. Taphonomy and paleoecology of the dinosaur beds of the Jurassic Morrison Formation. Paleobiol. 6, 208–232.

Dorney, L.J., Parrish, J.T., Chan, M.A., Hasiotis, S. T., 2017. Petrography and environmental interpretation of tufa mounds and carbonate bed in the Jurassic Navajo Sandstone of southeastern Utah, U.S.A. J. Sediment. Res. 87, 967–985.

Dunagan, S.P., 1999. Paleosynecology and taphonomy of freshwater carbonate lakes and ponds from the Upper Jurassic Morrison Formation (Western Interior, U.S.A.). Geol. Soc. Am. Abstr. Prog. 31, 365.

Dunagan, S.P., Turner, C.E., 2004. Regional paleohydrologic and paleoclimatic settings of wetland/lacustrine depositional systems in the Morrison Formation (Upper Jurassic), Western Interior USA. Sediment. Geol. 167, 269–296.

Dupree, R.T., 2009. Provenance of Lower Kootenai (Lower Cretaceous) fluvial sandstone bodies, Sandy Hollow/Big Hole River area, southwestern Montana (Master's thesis). University of Louisiana, Lafayette, LA, 84 p.

Dworkin, S.I., Nordt, L., Atchley, S., 2005. Determining terrestrial paleotemperatures using the oxygen isotopic composition of pedogenic carbonate. Earth Planet. Sci. Let. 237, 56–68.

Ekart, D.D., Cerling, T.E., 1996. pCO_2 during deposition of the Late Jurassic Morrison Formation and other paleoclimatic/ecologic data as inferred by stable carbon and oxygen isotope analyses. Geol. Soc. Am., Abstr. Prog. 28, 2.

Esteban, M., Klappa, C.F., 1983. Subaerial exposure environment. Am. Assoc. Pet. Geol. Mem. 33, 1–54.

Evanoff, E., Good, S.C., Hanley, J.H., 1998. An overview of the freshwater mollusks from the Morrison Formation. Mod. Geol. 22, 423–450.

Evans, J.E., 1999. Recognition and implications of Eocene tufas and travertines in the Chadron Formation, White River Group, Badlands of South Dakota. Sediment. 46, 771–789.

Everett, M.E., 2013., Near-Surface Applied Geophysics. Cambridge University Press, 403 p.

Fernandez, A., Tang, J., Rosenheim, B.E., 2014. Siderite 'clumped' isotope thermometry: A new paleoclimate proxy for humid continental environments. Geochim. Cosmochim. Acta 126, 411–421.

Ford, T.D., Pedley, H.M., 1996. A review of tufa and travertine deposits of the world. Earth-Sci. Rev. 41, 117–175.

Foster, J., 2007. Jurassic West: The dinosaurs of the Morrison Formation and their world. Indiana University Press, p. 1–389.

Fricke, H.C., Hencecroft, J., Hoerner, M.E., 2011. Lowland–upland migration of sauropod dinosaurs during the Late Jurassic epoch. Nature 480, 513-515.

Fuentes, F., DeCelles, P.G., Constenius, K.N., Gehrels, G.E., 2011. Evolution of the Cordilleran foreland basin system in northwestern Montana, U.S.A. Geol. Soc. Am. Bull, 123, 507–533.

Gaffney, E.S., 1979. The Jurassic turtles of North America. Am. Mus. Nat. Hist. Bull. 162, 135.

Gallagher, T.M., 2010. Origin of Jurassic carbonate nodules in southeastern Wyoming (Bachelor's thesis) University of Pittsburgh, Pittsburgh, PA, 35 p.

Gandin, A., Capezzuoli, E., 2008. Travertine versus calcareous tufa: distinctive petrologic features and stable isotope signatures. Ital. J. Quaternary Sci. 21:125–136.

Gardner, L.S., 1950, Geology of the Button Butte-Forestgrove area, Fergus County, Montana. U.S. Geol. Surv. Oil and Gas Invest. Map OM-106.

Gee, C.T., Sprinkel, D.A., Bennis, M.B., Gray, D.E., 2019. Silicified logs of *Agathoxylon hoodii* (Tidwell et Medlyn) comb. nov. from Rainbow draw near Dinosaur National Monument, Uintah County, Utah, USA, and their implications for araucariaceous conifer forests in the Upper Jurassic Morrison Formation. Geol. Intermount. West 6, 77–92.

Golubic, S., Marcenko, E. 1958. Zur kenntnis der morphologie and taxonomie der gattung *Oocardium* (On morphology and taxonomy of the genus *Oocardium* – desmids). Schweiz. Z. Hydrol., 20, 177–185.

Golubic, S., Violante, C., Ferreri, V. D'Argenio, B., 1993. Algal control and early diagenesis in Quaternary travertine formation (Rocchetta a Volturno, central Apennines). Bollettino della Soc. Paleon. Italiana 1, 231–247.

Good, S.C., 2004. Paleoenvironmental and paleoclimatic significance of freshwater bivalves in the Upper Jurassic Morrison Formation, Western Interior, USA. Sediment. Geol. 167, 163–176.

Gordan, C.C., Buikstra, J.E., 1981. Soil pH, bone preservation, and sampling bias at mortuary sites. Amer. Antiq. 46, 566–571.

Gorman II, M.A., Miller, I.M., Pardo, J.D., Small, B. J., 2008. Plants, fish, turtles, and insects from the Morrison Formation; A Late Jurassic ecosystem near Cañon City, Colorado. Geol. Soc. Am. Field Guide 10, 295–310.

Gregory, R.T., Douthitt, C.B., Duddy, I.R., Rich, P.V., Rich, T.H., 1989. Oxygen isotopic composition of carbonate concretions from the Lower Cretaceous of Victoria, Australia: implications for the evolution of meteoric waters on the Australian continent in a paleopolar environment. Earth Planet. Sci. Letters 92, 27–42.

Guo, X., Chafetz, H.S., 2012. Large tufa mounds, Searles Lake, California. Sediment. 59, 1509–1535.

Harris, C., 1981. Oases in the desert: the mound springs of northern South Australia. Proceed. Royal Geograph. Soc. Australasia, S. Australian Branch 81, 26–39.

Harris, W.L., 1966. The stratigraphy of the Upper Jurassic-Lower Cretaceous rocks in the Great Falls-Lewistown coal field, central Montana. Billings Geol. Soc. 17th Ann. Field Conf., 164–177.

Harriss, R.C., Troup, A.G., 1970. Chemistry and origin of freshwater ferromanganese concretions. Limnol. Oceangraph. 15, 702–712.

Hasiotis, S.T. 2004. Reconnaissance of Upper Jurassic Morrison Formation ichnofossils, Rocky Mountain Region, USA: paleoenvironmental, stratigraphic, and paleoclimatic significance of terrestrial and freshwater ichnocoenoses. Sediment. Geol. 167, 177–268.

Hasiotis, S.T., Demko, T.M. 1996. Terrestrial and freshwater trace fossils, Upper Jurassic Morrison Formation, Colorado Plateau. *In* Morales, M. (ed) The Continental Jurassic, Mus. N. Arizona Bull. 60, 355–370.

Hasiotis, S.T., Kirkland, J.I. 1998. Crayfish fossils and burrows (Decapoda: Cambaridae) Upper Jurassic Morrison Formation, Colorado Plateau, U.S.A. *In* Carpenter, K., Kirkland, J., Chure, D., (eds), The Upper Jurassic Morrison Formation: An interdisciplinary study, Mod. Geol. 22, 481–491.

Hasiotis, S.T., Kraus, M.J., Demko, T.M., 2007. Climate controls on continental trace fossils. *In* Miller, W. III, (ed), Trace Fossils—Concepts, Problems, Prospects. Elsevier Press, Amsterdam, p. 172–195.

Havlin, J.L., 2005. Fertility. In Hillel, D., Rosenzweig, C., Powlson, D., Scow, K., Singer, M., Sparks, D., (eds), Encyclopedia of Soils in the Environment 2. Academic Press, p. 10–19.

Hecht, M.K., Estes, R., 1960. Fossil amphibians from Quarry Nine. Postilla, Yale Peabody Mus. Nat. Hist. 46, 1–19.

Hedrich, S., Schlömann, M., Johnson, D. B., 2011. The iron-oxidizing proteobacteria. Microbiol. 157, 1551–1564.

Holmes, J.W., Williams, A.F., Hall, J.W., Henschke, C.J., 1981. Measurements of discharges from some of the mound springs in the desert of northern south Australia. J. Hydrol. 49, 329–339.

Hooker, J.N., Cartwright, J.A., 2015. Kinematics of cone-in-cone growth, with implications for timing and formation mechanism. Am. Geophys Union, Abstr. Prog., MR41B–2639.

Horn, B.L.D., Pereira, V.P., Schultz, C.L., 2013. Calcretes of the Santa Maria Supersequence, Middle Triassic, Rio Grande do Sul, Brazil: Classification, genesis and paleoclimatic implications. Palaeogeo., Palaeoclim., Palaeoecol. 376, 39–47.

Hotton, C.L., 1986, Palynology of the Morrison Formation. Proceed. Fourth N. Am. Paleon. Conv., A20.

Hotton, C. Baghai-Riding, N., 2010. Palynological evidence for conifer dominance within a heterogeneous landscape in the Late Jurassic Morrison Formation, U.S.A. *In* Gee, C., (ed) Plants in Mesozoic Time, , Indiana University Press, p. 295–328.

Huerta, P., Armenteros, I., Tomé, O.M., Gonzálvez, P.R., Silva, P.G., González-Aguilera, D., Pedro Carrasco-García, P., 2016. 3-D modelling of a fossil tufa outcrop. The example of La Peña del Manto (Soria, Spain). Sediment. Geol. 333, 130–146.

Hunt, T.C., Richmond, D.R., 2018. The aquatic vertebrate community of a bone-dry pond: The historic Stovall Quarry 8, Morrison Formation in the panhandle of Oklahoma. Soc. Vert. Paleon. Abstr. Prog., 152–153.

Hups, M.K., Lockley, M.G., Foster, J.R., 2006. A partial skeleton of *Goniopholis* from the Brushy Basin Member of the Morrison Formation (Upper Jurassic), Cactus Park, Colorado, and distribution of large neosuchians. *In* Foster, J.R., Lucas, S.G., (eds) Paleontology and geology of the Upper Jurassic Morrison Formation. New Mexico Mus. Nat. Hist. Sci. Bull. 36, 107–108.

Hutsinpiller, A., Parry, W.T., 1985. Geochemistry and geothermometry of spring water from the Blackfoot reservoir region, southwestern Idaho. J. Volcan. Geotherm. Res. 26, 275–296.

Ibarra, Y., Corsetti, F.A., Cheetham, M.I., Feakins, S. J., 2014. Were fossil spring-associated carbonates near Zaca Lake, Santa Barbara, California deposited under an ambient or thermal regime? Sediment. Geol. 301, 15–25.

Ibarra, Y., Sanon, S., 2019. A freshwater analog for the production of *Epiphyton*-like microfossils. Geobiol. 17, 510–522.

Imlay, R.W., 1954. Marine Jurassic formation in the Pryor Mountains and northern Bighorn Mountains, Montana. Billings Geol. Soc. 5th Ann. Field Conf. p. 54–64.

Jansa, L., 1972. Depositional history of the coal-bearing Upper Jurassic–Lower Cretaceous Kootenay Formation, southern Rocky Mountains, Canada. Geol. Soc. Am. Bull. 83, 3199–3222.

Janssen, A., Swennen, R., Podoor, N., Keppens, E., 1999. Biological and diagenetic influence in Recent and fossil tufa deposits from Belgium. Sediment. Geol. 126, 75–95.

Johnson, E.A., 2005. Geologic assessment of undiscovered oil and gas resources in the Phosphoria total petroleum system, southwestern Wyoming province, Wyoming, Colorado, Utah. U.S. Geol. Surv. Digit. Data Series, DDS-69-D, p. 1–46.

Jones, B., Renaut, R.W., 2010. Calcareous spring deposits in continental settings. *In* Carbonates in continental settings facies, environments, and processes, Alonso-Zarza, A.M., Tanner, L.H., (eds), Developments in Sedimentology 61, 177–224.

Jutras, P., Utting, J., McLeod, J., 2007. Link between long-lasting evaporitic basins and the development of thick and massive phreatic calcrete hardpans in the Mississippian Windsor and Perce groups of eastern Canada. Sediment. Geol. 201, 75–92.

Keppel, M.N., Clarke, J.D.A., Halihan, T., Love, A.J., Werner, A.D., 2011. Mound springs in the arid Lake Eyre South region of South Australia: A new depositional tufa model and its controls. Sediment. Geol. 240, 55–70.

Keppel, M.N., Karlstrom, K., Crossey, L., Love, A.J., Priestley, S., 2020. Evidence for intra-plate seismicity from spring-carbonate mound springs in the Kati Thanda–Lake Eyre region, South Australia: implications for groundwater discharge from the Great Artesian Basin. Hydrogeol. J. 28, 297–311.

Keppel, M.N., Post, V.E.A., Love, A.J., Clarke, J.D.A., Werner, A.D., 2012. Influences on the carbonate hydrochemistry of mound spring environments, Lake Eyre South region, South Australia. Chem. Geol. 296–297, 50–65.

Kerney, M.P., 1959. An interglacial tufa near Hitchin, Hertfordshire. Proceed. Geol. Assoc. 70, 322–337.

Khalid, M.E.A., 1990. Sedimentology of the Swift Formation (Jurassic) in the Little Rocky Mountains (Master's thesis). University of Saskatchewan, CA, 107 p.

Kirkland, J.I., 1987. Upper Jurassic and Cretaceous lungfish tooth plates from the Western Interior, the last dipnoan faunas of North America. Hunteria 2, 1–16.

Koban, C.G., Schweigert, G., 1993. Microbial origin of travertine fabrics-Two examples from southern Germany (Pleistocene Stuttgart travertines and Miocene Riedöschingen travertine). Facies 29, 251–264.

Landis, T.D., Hasse, D.L., Dumroese, R.K., 2005. Plant nutrient testing and analysis in forest and conservation nurseries. Nat. Proceed. Forest Conserv. Nursery Assoc. 2004, p.76–83.

Levy, L.B., Jull, A.J.T., Werner, A., 1998. Interpreting the carbonate concretions of glacial Lake Hitchcock. Geol. Soc. Am., Abstr. Prog. 30, 331.

Lindsay, W.L., 1991. Iron oxide solubilization by organic matter and its effect on iron availability. Plant and Soil 130, 27–34.

Linhart, C. and Schagerl, M., 2011, Autecology of the rare tufa-forming desmid *Oocardium stratum* Naeg. (Doctoral dissertation) University of Vienna, AT, 86 p.

Lockley, M.G., Houck, K.J., Prince, N.K., 1986. North America's largest dinosaur trackway site: Implications for Morrison Formation paleoecology. Geol. Soc. Am. Bull. 97, 1163–1176.

Lockley, M.G., Prince, N.K., Houck, K., Carpenter, K., 1984. Reconstruction of a Late Jurassic lacustrine ecosystem. Geol. Soc. Am., Abstr. Prog. 6, 228.

Loke, M.H., Chambers, J.E., Rucker, D.F., Kuras, O., Wilkinson, P.B. 2013. Recent developments in the direct-current geoelectrical imaging method. J. Appl. Geophys. 95, 135–156.

Loyd, S.J., Berelson, W.M., Lyons, T.W., Hammond, D.E., Corsetti, F.A., 2012. Constraining pathways of microbial mediation for carbonate concretions of the Miocene Monterey Formation using carbonate-associated sulfate. Geochim. et Cosmochim. Acta 78, 77–98.

Ludvigson, G.A., González, L.A., Fowle, D.A., Roberts, J.A., Driese, S.G., Villarreal, M.A., Smith, J.J., Suarez, M.B., 2013. Paleoclimatic application and modern process studies of pedogenic siderite. SEPM New Frontiers in paleopedology and terrestrial paleoclimatology: Paleosols and soil surface analog systems 104, 79–87.

Machette, M.M., 1985. Calcic soils of the southwestern United States. Geol. Soc. Am. Spec. Pap. 203, 1–21.

Mack, G.H., Calvin, J.W., Curtis, M.H., 1993. Classification of paleosols. Geol. Soc. Am. Bull. 105, 129–136.

Mackenzie, F.T., Pigott, J.D., 1981. Tectonic controls of Phanerozoic sedimentary rock cycling. J. Geol. Soc. London 138, 183–196.

Manifold, B.M., 2012. Intrinsic and extrinsic factors involved in the preservation of non-adult skeletal remains in archaeology and forensic science. Bull. Int. Assoc. Paleodont. 6, 51–69.

Maughan, E.K., 1993. Stratigraphic and structural summary for central Montana. Montana Geological Society 1993 Field Conference Guidebook: Old Timers' Rendezvous Edition: Energy and mineral resources of central Montana, p. 3–20.

McBride, E.F., Milliken, K.L., 2006. Giant calcite-cemented concretions, Dakota Formation, central Kansas, USA. Sediment. 53, 1161–1179.

McCoy, V.E., 2015. The Formation of Concretions and their Role in Fossilization (Doctoral dissertation). Yale University, New Haven, CT, 256 p.

Merz, M.U.E., 1992. The biology of carbonate precipitation by cyanobacteria. Facies 26, 81–102.

Meyers, J.H., Schwartz, R.K., 1994. Summary of depositional environments, paleogeography, and structural control on sedimentation in the Late Jurassic (Oxfordian) Sundance foreland basin, western Montana. SEPM Mesozoic systems of the Rocky Mountain Region, USA, p. 331–350.

Middleton, H.A., Nelson, C.S. 1996. Origin and timing of siderite and calcite concretions in late Palaeogene non- to marginal-marine facies of the Te Kuiti Group, New Zealand. Sediment. Geol. 103, 93–115.

Mohammadi, Z., Capezzuoli, E., Claes, H., Alipoor, R., Muchez, P. Swennen, R., 2019. Substrate geology controlling different morphology, sedimentology, diagenesis and geochemistry of adjacent travertine bodies: A case study from the Sanandaj-Sirjan zone (western Iran). Sediment. Geol. 389, 127–146.

Moore, D.M., and Reynolds, R.C., Jr. 1997. X-ray diffraction and the identification and analysis of clay minerals. Oxford University Press, New York, 378 p.

Morris, T.H.; Richmond, D.R.; and Grimshaw, S.C. 1996. Orientation of dinosaur bones in riverine environments: Insights into sedimentary dynamics and taphonomy. *In* Morales, M. (ed), The Continental Jurassic. Mus. N. Arizona Bull. 60:521–530.

Mozley, P.S., Burns, S.J., 1993. Oxygen and carbon isotopic composition of marine concretions: An overview. J. Sediment. Pet. 63, 73–83.

Mozley P.S., Davis J.M., 2005. Internal structure and mode of growth of elongate calcite concretions: Evidence for small-scale, microbially induced, chemical heterogeneity in groundwater. Geol. Soc. Am. Bull. 117, 1400–1412.

Muir, R.O., Walton, E.K., 1957. The East Kirkton Limestone. Trans. Geol. Soc. Glasgow 12, 157–168.

Müller, J., MacEachran, D., Burd, H., Sathitsuksanoh, N., Bi, C., Yeh, Y.-C., Lee, T.S., Hillson, N.J., Chhabra, S.R., Singer, S.W., Bellerb, H.R., 2013. Engineering of *Ralstonia eutropha* H16 for autotrophic and heterotrophic production of methyl ketones. Appl. Environ. Microbiol. 79, 4433–4439.

Munoz-Saez, C., Saltiel, S., Manga, M., Nguyen, C., Gonnermann, H., 2016. Physical and hydraulic properties of modern sinter deposits: El Tatio, Atacama. J. Volcan. Geotherm. Res. 325, 156–168.

Myers, T.S., Tabor, N.J., Rosenau, N.A., 2014. Multiproxy approach reveals evidence of highly variable paleoprecipitation in the Upper Jurassic Morrison Formation (western United States). Geol. Soc. Am. Bull. 126, 1105–1116.

Nation, M.J., 1990. Analysis of eolian architecture and depositional systems in the Jurassic Wingate Sandstone, central Colorado Plateau (Master's thesis). Northern Arizona University, Flagstaff, AZ, 222 p.

Nelson W.J., 1995. Basement control of recurrent faulting, central Montana. *In* Ojakangas, R.W., Dickas, A.B., Green, J.C. (eds) Basement Tectonics 10:265–282.

Nordt, L., Atchley, S., Dworkin, S., 2015. Collapse of the Late Triassic megamonsoon in western equatorial Pangea, present-day American Southwest. Geol. Soc. Am. Bull. 127, 1798–1845.

O'Neill, J.M., Lopez, D.A., 1983. Great Falls Lineament, Idaho and Montana. Am. Assoc. Pet. Geol. Abstr. Prog. 8:1350–1351.

Park, L.E., Geochemical and paleoenvironmental analysis of lacustrine arthropod-bearing concretions of the Barstow Formation, southern California. PALAIOS 10, 44–57.

Park, R., Epstein, S., 1961. Metabolic fractionation of C^{13} and C^{12} in plants. Plant Physiol. 36, 133–138.

Párraga, J., Rivadeneyra, M. A., Martín-García, J.M., Delgado, R., Delgado. G., 2004. Precipitation of carbonates by bacteria from a saline soil, in natural and artificial soil extracts. Geomicrobiol. J. 21, 55–66.

Parrish, J.T., Hasiotis, S.T., Chan, M.A., 2017. Carbonate deposits in the Lower Jurassic Navajo Sandstone, southern Utah and northern Arizona U.S.A. J. Sediment. Res. 87, 740–762.

Parrish, J.T., Hyland, E.G., Chan, M.A., Hasiotis, S.T., 2019. Stable and clumped isotopes in desert carbonate spring and lake deposits reveal palaeohydrology: A case study of the Lower Jurassic Navajo Sandstone, south-western USA. Sediment. 66, 32–52.

Parrish, J.T., Peterson, F., 1988. Wind directions predicted from global circulation models and wind directions determined from eolian sandstones of the western United States–A comparison. Sediment. Geol. 56, 261–282.

Parrish, J.T., Peterson, F., Turner, C.E., 2004. Jurassic ‘‘savannah’’–plant taphonomy and climate of the Morrison Formation (Upper Jurassic, Western USA). Sediment. Geol. 167, 137–162.

Parrish, J.T., Ziegler, A.M., Scotese, C. R., 1982. Rainfall patterns and the distribution of coals and evaporite in the Mesozoic and Cenozoic. Palaeogeo. Palaeoclim., Paleoecol. 40, 67–101.

Pedley, H.M., 1990. Classification and environmental models of cool freshwater tufas. Sediment. Geol. 68, 143–154.

Pedley, H.M., 2009. Tufas and travertines of the Mediterranean region: a testing ground for freshwater carbonate concepts and developments. Sediment. 56, 221–246.

Pentecost, A., 1990. The algal-flora of travertine: an overview. *In* Hermon, J.S., Hubbard, D.A. (eds) In Travertine-marl: Spring deposits in Virginia. Virginia Div. Min. Res. Publ. 101, 117–128.

Pentecost, A., 1991. A new and interesting site for the calcite-encrusted desmid *Oocardium stratum* Naeg. in the British Isles. British Phycol. J. 26, 297–301.

Pentecost, A., 2005. Travertine. Springer-Verlag Berlin Heidelberg, p. 1–445.

Pentecost, A., Coletta, P., 2007. The role of photosynthesis and CO_2 evasion in travertine formation: a quantitative investigation at an important travertine-depositing hot spring, Le Zitelle, Lazio, Italy. J. Geol. Soc. 164, 843–853.

Pentecost, A., Jones, B., Renaut, R.W., 2003. What is a hot spring? Canadian J. Earth Sci. 40, 1443–1446.

Peterson, F., 1988. Pennsylvanian to Jurassic eolian transportation systems in the western United States. Sediment. Geol. 56, 207–260.

Peterson, F., Turner-Peterson, C.E., 1987. The Morrison Formation of the Colorado Plateau Recent advances in sedimentology, stratigraphy, and paleotectonics. Hunteria 2, 1–18.

Pfiester, L.A., 1976. *Oocardium stratum* a rare (?) desmid (Chlorophyceae). J. Phycol. 12, 134.

Philippe, M., Jiang, H.-E., Kim, K., Oh, C., Gromyko, D., Harland, M., Paik, I.-S., Thévenard, F., 2009. Structure and diversity of the Mesozoic wood genus *Xenoxylon* in Far East Asia: implications for terrestrial palaeoclimates. Lethaia 42, 393–406.

Philippe, M., Puijalon, S., Suan, G., Mousset, S., Thévenard, F., Mattioli, E., 2017. The paleolatitudinal, distribution of fossil wood genera as a proxy for European Jurassic terrestrial climate. Palaeogeo., Palaeoclim., Palaeoecol. 466, 373–381.

Philippe, M., Thévenard, F., 1996. Repartition and palaeoecology of the Mesozoic wood genus *Xenoxylon*: palaeoclimatological implications for the Jurassic of Western Europe. Rev. Palaeobot. Palynol. 91, 353–370.

Pipiringos, G.N., O'Sullivan, R.B., 1978. Principal unconformities in Triassic and Jurassic rocks, Western Interior United States–A preliminary survey. U.S. Geol. Surv. Prof. Pap. 1035A, 1–29.

Ponder, W.F., 1986. Mound Springs of the Great Artesian Basin. Limnology of Australia, p. 403–420.

Porter, J.R., 2011. Stratigraphic analysis of the Jurassic Ellis Group and paleotectonics in north-central Montana: Deciphering the historically enigmatic "Belt Island" (Master's thesis). Montana State University, Bozeman, MT, 133 p.

Porter, K., Wheaton, J., Miller, M., 2002. Potential for a Public Water Supply from the Madison Limestone in the Eastern Big Snowy Mountains and Little Snowy Mountains, Montana. Montana Bur. Mines Geol. Open File Rep. 449, 1–25.

Potter, S.L., Chan, M.A., Petersen, E.U., Dyar, M.D., Sklute, E., 2011. Characterization of Navajo Sandstone concretions: Mars comparison and criteria for distinguishing diagenetic origins. Earth Planet. Sci. Let. 301, 444–456.

Potter-McIntyre, S.L., 2013. Biochemical signatures in iron (oxyhydr)oxide diagenetic precipitates: Chemical, mineralogical, and textural markers (Doctoral dissertation). University of Utah, Salt Lake City, UT, 188 p.

Potter-McIntyre, S.L., Chan, M.A., McPherson, B. J., 2014. Concretion formation in volcaniclastic host rocks; evaluating the role of organics, mineralogy, and geochemistry on early diagenesis. J. Sediment. Res. 84, 875–892.

Pratt, B.R., 2001. Septarian concretions: internal cracking caused by synsedimentary earthquakes. Sediment. 48, 189–213.

Raiswell, R., Fisher, Q.J., 2000. Mudrock-hosted carbonate concretions: a review of growth mechanisms and their influence on chemical and isotopic composition. J. Geol. Soc. 157, 239–251.

Rees, P.M., Noto, C.R., Parrish, M.J., Parrish, J.T., 2004. Late Jurassic climates, vegetation, and dinosaur distributions. J. Geol. 112, 643–653.

Rees, P.M., Ziegler, A.M., Valdes, P.J., 2000. Jurassic phytogeography and climates: new data and model comparisons. *In* Huber, B.T., Macleod, K.G., Wing, S.L. (eds) Warm climates in earth history. Cambridge University Press, Cambridge, p.297–318.

Renaut, R.W., Jones, B., 2000. Microbial precipitates around continental hot springs and geysers. *In* Riding R.E., Awramik, S. M. (eds) Microbial Sediments. Springer, Berlin, p. 187–195.

Retallack, G.J., 1993. Classification of paleosols: discussion. Geol. Soc. Am. Bull. 105, 1635–1636.

Richmond, D. R., Lukens, M.W., and Celestino, S.M., 2017, Upper Jurassic Morrison Formation clams on the half shell, central Montana. Geol. Soc. Am. Abstr. Prog. 49, 4.

Richmond, D.R., Lupia, R., Philippe, M., and Klimek, J. 2019. First occurrence of the boreal fossil wood *Xenoxylon meisteri* from the Jurassic of North America: Morrison Formation of central Montana, USA. Rev. Palaeobot. Palynol., 267:39–53.

Richmond, D.R., Lupia, R., Philippe, M., 2019a, First report of the fossil wood *Piceoxylon* from the North American Jurassic (Morrison Formation, central Montana). Geol. Soc. Am. Abstr. Prog. 51, 38.

Richmond, D.R., Lupia, R., Philippe, M., 2019b, *Circoporoxylon* from the Upper Jurassic Morrison Formation of central Montana. Geol. Soc. Am. Abstr. Prog. 51, 271.

Richmond, D.R., Murphy, N., 2017, Beach front property in central Montana: The Upper Jurassic Morrison Formation in the northern portion of the foreland basin. Am. Assoc. Pet. Geol. Abstr. Prog. 90301.

Roden, E.E., McBeth, J.M., Blöthe, M., Percak-Dennett, E.M., Fleming, E.J., Holyoke, R.R., Luther, G. W. III, Emerson, D., Schieber, J., 2012. The microbial ferrous wheel in a neutral pH groundwater seep. Front. Microbiol. 3, 1–18.

Roden, E.E., Sobolev, D., Glazer, B., Luther, G.W., 2004. Potential for microscale bacterial Fe redox cycling at the aerobic-anaerobic interface. Geomicrobiol. J. 21, 379–391.

Ronholm, J., Schumann, D., Sapers, H.M., Izawa, M., Applin, D., Berg, B., Mann, P., Vali, H., Flemming, R. L., Cloutis, E. A., Whyte, L.G., 2014. A mineralogical characterization of biogenic calcium carbonates precipitated by heterotrophic bacteria isolated from cryophilic polar regions. Geobiol. 12, 542–556.

Rott, E., Hotzy, R., Cantonati, M., Sanders, D., 2012. Calcification types of *Oocardium stratum* Nägeli and microhabitat conditions in springs of the Alps. Freshwater Sci. 31, 610–624.

Rouse, G.E., 1959. Plant microfossils from Kootenay coal-measures strata of British Columbia. Micropaleon. 5, 303–324.

Saitta, E.T., 2015. Evidence for sexual dimorphism in the plated dinosaur *Stegosaurus mjosi* (Ornithischia, Stegosauria) from the Morrison Formation (Upper Jurassic) of western USA. PLoS One 10. e0123503.doi:10.1371/journal.pone.0123503.

Sanders, D., Rott, E., 2009. Contrasting styles of calcification by the micro-alga *Oocardium stratum* Naegeli 1849 (Zygnematophyceae) in two limestone-precipitating spring creeks of the Alps. Austrian J. Earth Sci. 102, 34–49.

Schudack, M.E., Turner, C.E., Peterson, F., 1998. Biostratigraphy, paleoecology and biogeography of charophytes and ostracodes from the Upper Jurassic Morrison Formation, Western Interior, USA. Mod. Geol. 22, 379–414.

Schuster, R. M. 1966. The Hepaticae and Anthocerotae of North America Vol. I. Columbia University Press, New York, p. 1–801.

Selles-Martinez, J., 1994. New insights in the origin of cone-in-cone structures. Carbonates and Evaporites 9, 172–186.

Sharp, Z., 2007. Principles of stable isotope geochemistry. Pearson Ed., 344 p.

Shaw, J., Renzaglia, K., 2004. Phylogeny and diversification of bryophytes. Am. J. Bot. 91, 1557–1581.

Sheldon, N.D., Tabor, N.J., 2009. Quantitative paleoenvironmental and paleoclimatic reconstruction using paleosols. Earth-Sci. Rev. 95, 1–52.

Silverman, A., Harris, W.L., 1966. Economic geology of the Great Falls-Lewistown coal field west-central Montana. Billings Geol. Soc. 17th Ann. Field Conf. 149–163.

Sims, P.K., O'Neill, J.M., Bankey, V., Anderson, E., 2004, Precambrian basement geologic map of Montana–An interpretation of aeromagnetic anomalies. U.S. Geol. Surv. Sci. Invest. Map 2829.

Small, B.J., Gorman, M.A., Pardo, J., Smith, D., 2007. A Late Jurassic lacustrine biota from the Morrison Formation of Colorado. Geol. Soc. Am. Abstr. Prog. 39, 400.

Snee, L.W., Reynolds, M.W., Miggins, D.P., 2002. Late Cretaceous and Tertiary plutonism, west-central Montana; pins in the end of compression and the beginning of extension. Geol. Soc. Am. Abstr. Prog. 34, 43.

Sopaci, E., Akgün, H., 2015. Geotechnical assessment and engineering classification of the Antalya tufa rock, southern Turkey. Engineer. Geol. 197, 211–224.

Springer, K.B., Pagati, J.S., Scott, E., 2017. Geology and vertebrate taphonomy of Tule Spring Fossil Beds National Monument Nevada, USA. Geol. Soc. Am. Field Guide 45, 1–30.

Staaf, H., 1980. Release of plant nutrients from decomposing leaf litter in a south Swedish beech forest. Holarctic Ecol., 129–136.

Steinen, R.P., Gray, N.H., Mooney, J., 1987. A Mesozoic carbonate hot-spring deposit in the Hartford Basin of Connecticut. J. Sediment. Pet. 57, 319–326.

Szigeri, G.J., Fox, J.E., 1981. Unkpapa Sandstone (Jurassic), Black Mills, South Dakota: An eolian facies of the Morrison Formation. SEPM Spec. Publ. 31, 331–349.

Tanner, L.H., 2010. Continental carbonates as indicators of paleoclimate. Dev. Sediment. 62, 179–214.

Tanner, L.H., Galli, K.G., Lucas, S.G., 2014. Pedogenic and lacustrine features of the Brushy Basin Member of the Upper Jurassic Morrison Formation in western Colorado: Reassessing the paleoclimatic interpretations. Volumina Jurassica X11, 115–130.

Thomka, J.R., Lewis, R.D., 2013., Siderite concretions in the Copan crinoid lagerstätte (Upper Pennsylvanian, Oklahoma): Implication for interpreting taphonomic and depositional processes in mudstone successions. PALAIOS 28, 697–709.

Thyne, G.D., Boles, J.R., 1989. Isotopic evidence for origin of the Moeraki septarian concretions, New Zealand. J. Sediment. Pet. 59, 272–279.

Tian, N., Wang, Y.-D., Philippe, M., Li, L.-L., Xie, X.-P., Jiang, Z.-K., 2016. New record of fossil wood *Xenoxylon* from the Late Triassic in the Sichuan Basin, southern China and its paleoclimatic implications. Palaeogeo., Palaeoclim., Palaeoecol. 464, 65–75.

Tidwell, W.D., 1990. Preliminary report on the megafossil flora of the Upper Jurassic Morrison Formation. Hunteria 2, 1–11.

Tidwell, W.D., Medlyn, D.A., 1992, Short shoots from the Upper Jurassic Morrison Formation, Utah, Wyoming, and Colorado, USA. Rev. Palaeobot. Palynol. 71, 219–238.

Tidwell, W.D., Medlyn, D.A., 1993. Conifer wood from the Upper Jurassic of Utah, USA Part II: *Araucarioxylon hoodii* sp. nov. Palaeobot. 42, 1–7.

Tran, H., Rott, E., Sanders, D., 2019. Exploring the niche of a highly effective biocalcifier: calcification of the eukaryotic microalga *Oocardium stratum* Nägeli 1849 in a spring stream of the Eastern Alps. Facies 65, 1–24.

Turner, C.E., and Peterson, F., 1999. Biostratigraphy of dinosaurs in the Upper Jurassic Morrison Formation of the Western Interior, U.S.A. Utah Geol. Surv. Misc. Pub. 99–1, 77–114.

Turner, C.E., and Fishman, N.S. 1991. Jurassic Lake T'oo'dichi': A large alkaline, saline lake, Morrison Formation, eastern Colorado Plateau. Geol. Soc. Am. Bull. 103:538–558.

Turner-Peterson, C.E., Fishman, N.S., 1986. Geologic synthesis and genetic models for Uranium mineralization in the Morrison Formation, Grants Uranium Region, New Mexico. Am. Assoc. Pet. Geol. Stud. 22, 357–388.

Tyler, P.A., Buckney, R.T., 1980. Ferromanganese concretions in Tasmanian lakes. Australian J. Marine Freshwater Res. 31, 525–531.

Uhlir, D.M., Akers, A., Vondra. C.F., 1988. Tidal inlet sequence, Sundance Formation (Upper Jurassic), north-central Wyoming. Sediment. 35, 739–752.

Valdes, P.J., Sellwood, B.W., 1992. A palaeoclimate model for the Kimmeridgian. Palaeogeo., Palaeoclim., Palaeoecol. 95, 47–72.

VanDeVelde, D.M., 2006. Interpretation of the depositional environment and paleoclimate of dinosaur sites, Brushy Basin Member of the Jurassic Morrison Formation, east-central Utah (Master's thesis). College of Bowling Green State University, Bowling Green, OH, 158 p.

VanDeVelde, D.M., Evans, J.E., Lewandowski, S.A., 2006. Paleosols as climate indicators for dinosaur sites, Brushy Basin Member of the Jurassic Morrison Formation, east-central Utah. Geol. Soc. Am. Abstr. Prog. 38, 63.

Veizer, J., Ala, D., Azmy, K., Bruckschen, P., Buhl, D., Bruhn, F., Carden, G.A.F., Diener, A., Ebneth, S., Godderis, Y., Jasper, T., Korte, C., Pawellek, F., Podlaha, O.G. and Strauss, H., 1999. $^{87}Sr/^{86}Sr$, $\delta^{13}C$ and $\delta^{18}O$ evolution of Phanerozoic seawater. Chem. Geol. 161, 59–88.

Vitkus, A. R., 2010. Unusual, fossiliferous concretions from the Lower Jurassic Moenave Formation in St. George, Utah, USA: Implications for ancient fish mass mortalities (Master's Thesis). University of Colorado, Boulder, CO, 56 p.

Vuillemin, A., Wirth, R., Kemnitz, H., Schleicher, A.M., Friese, A., Bauer, K.W., Simister, R., Nomosatryo, S., Ordoñez, L., Ariztegui, D., Henny, C., Crowe, S.A., Benning, L.G., Kallmeyer, J., Russell, J.M., Bijaksana, S., Vogel, H., Towuti Drilling Project Science Team, 2019. Formation of diagenetic siderite in modern ferruginous sediments. Geol. 47, 540–544.

Walkden, G.M., Irwin, J.R., Fallick, A.E., 1994, Carbonate spherules and botryoids as lake floor cements in the East Kirkton Limestone of West Lothian, Scotland. Trans. Royal Soc. Edinburgh: Earth Sci. 84, 213–221.

Wanas, H.A., 2008. Calcite-cemented concretions in shallow marine and fluvial sandstones of the Birket Qarun Formation (Late Eocene), El-Faiyum depression, Egypt: Field, petrographic and geochemical studies: Implications for formation conditions. Sediment. Geol. 212, 40–48.

Williams, A.F., Holmes, J.W., 1978, A novel method of estimating the discharge of water from mound springs of the Great Artesian Basin, central Australia. J. Hydrol. 38, 263–272.

Williams, T.M., Owen, R.B., 1992. Geochemistry and origins of lacustrine ferromanganese nodules from the Malawi Rift, Central Africa. Geochim. et Cosmochim. Acta 56, 2703–2712.

Wright, V.P., Tucker, M.E., 1991. Calcretes. Blackwell Scientific Publications, Oxford, England, 325 p.

Yetkin, M.E., Kahraman, B., M, K.O., Şengün, B., Şimşir, F., 2017. Determination of travertine samples porosity using image analysis method. Indian J. Engineer. 14, 227–235.

Yoshida, H., Yamamoto, K., Minami, M. Katsuta, N., Sin-ichi, S., Metcalfe, R., 2018. Generalized conditions of spherical carbonate concretion formation around decaying organic matter in early diagenesis. Sci. Rep. 8, 6308.

Figures

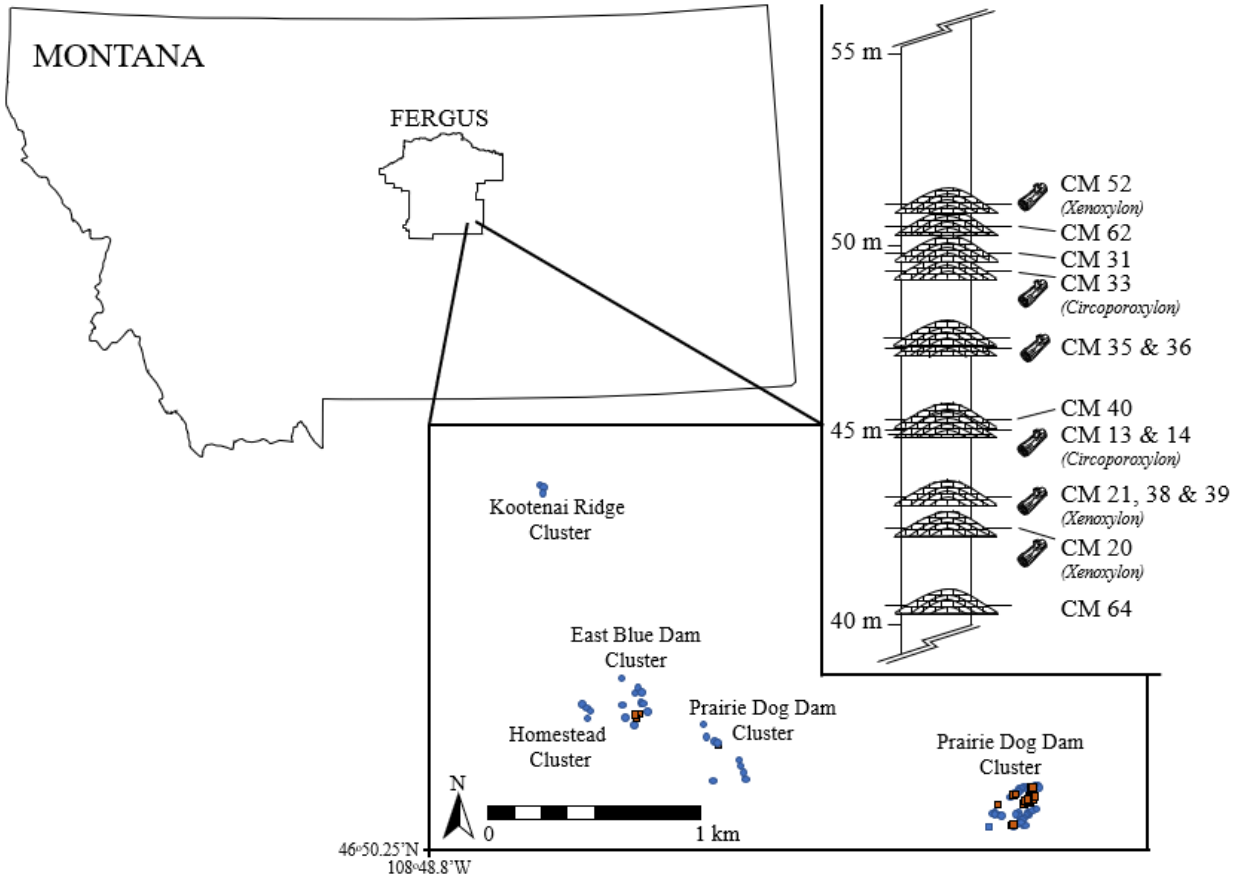

Figure 1. Geographic distribution for carbonate (blue circles) and siderite (orange squares) buildups in southeastern Fergus County, Montana. The buildups are separated into five different clusters. Only a sample of the 99 buildups are represented in the stratigraphic section. Some of the carbonate buildups have associated petrified wood, as indicated. Height in the stratigraphic section is reported in meters above the conformable Swift/Morrison formational contact.

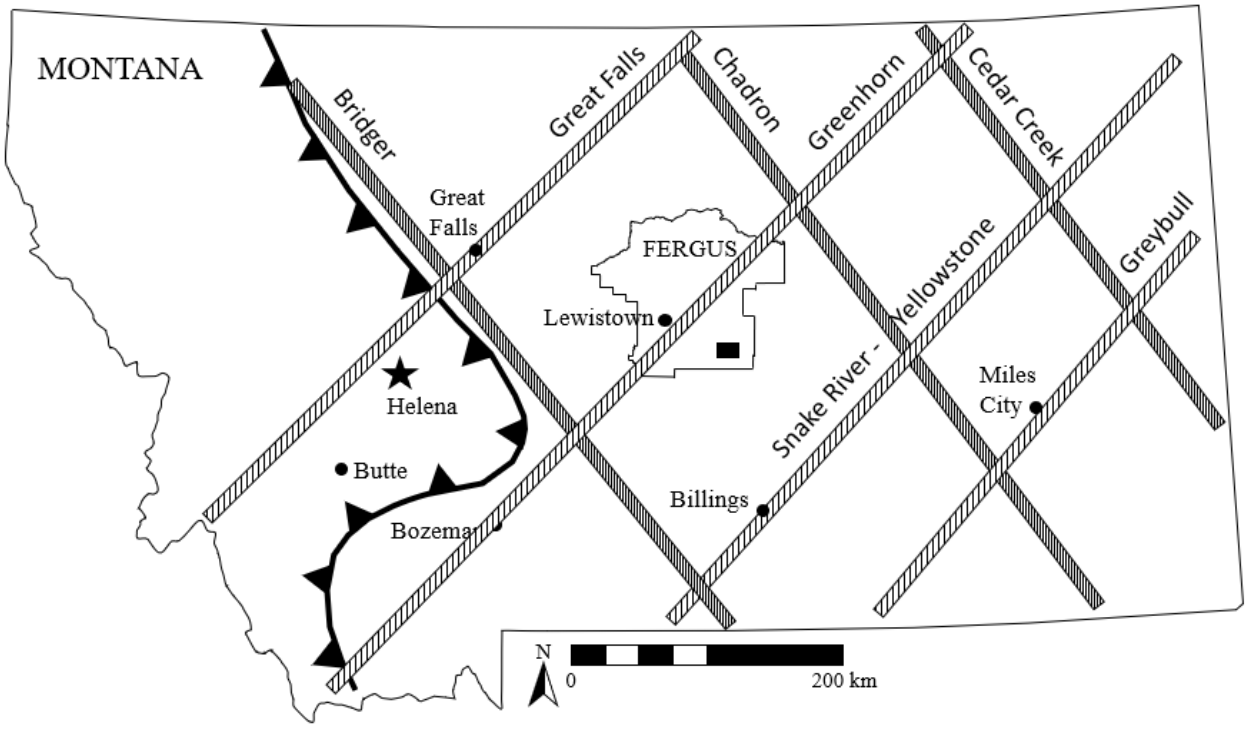

Figure 2. Regional stress lineaments for the central Rocky Mountains have a prolonged geologic history. The latest reactivation occurred during the Laramide orogenic event. The major northwest-southeast lineaments (Bridger, Chadron, and Cedar Creek) strike between 320–325º azimuth, whereas the northeast-southwest lineaments (Great Falls, Greenhorn, Snake River-Yellowstone, and Greybull) strike between 45–50º azimuth. The lineaments are an important component to the development of the Morrison Formation carbonate buildups. Figure modified from Maughan (1993).

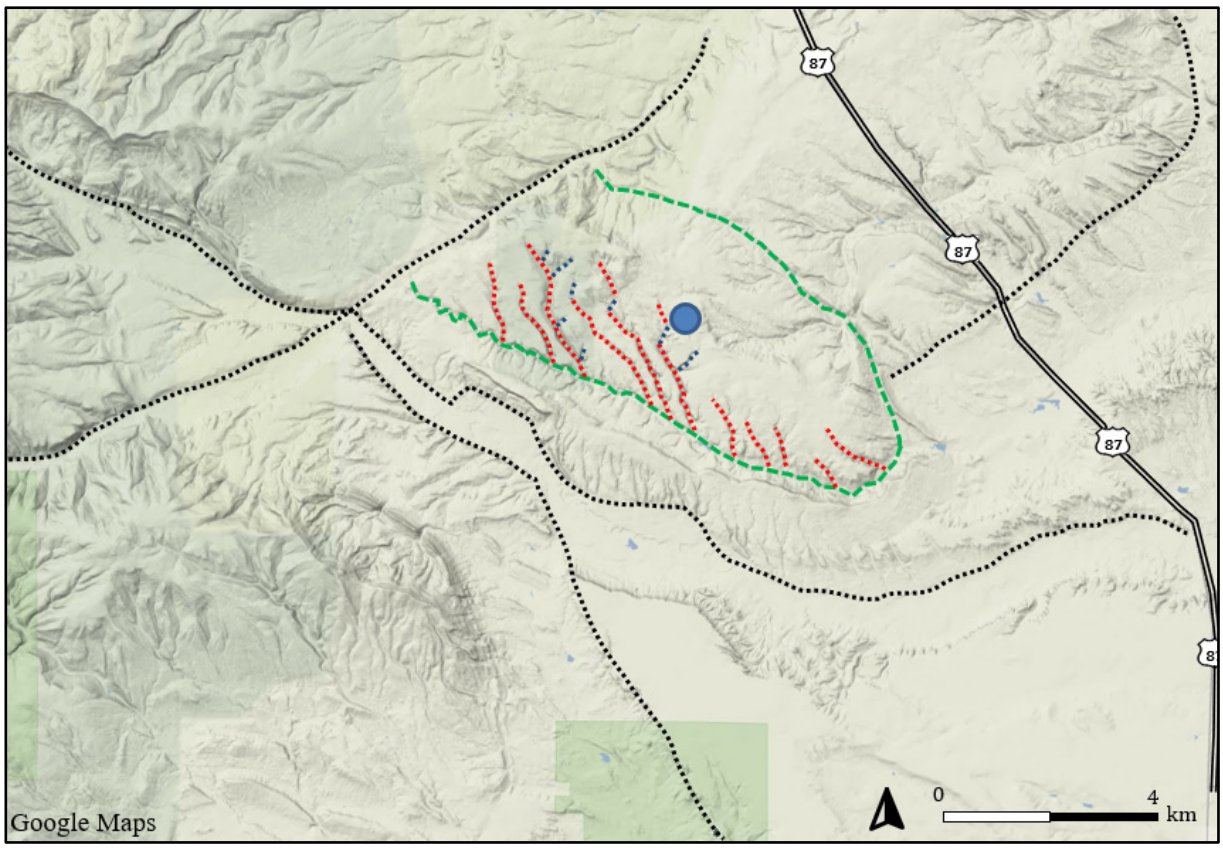

Figure 3. Physiographic map of the study area 20 km south of Grass Range, MT. The green dashed line represents the outline of Spindletop Dome. The black dotted line represents large faults. The trunk coulee drainages follow the northwest–southeast lineaments (red dashed lines). Subsidiary drainages turn abruptly and follow the northeast–southwest lineaments (blue dashed lines). The blue circle represents the general surface location of the carbonate buildups.

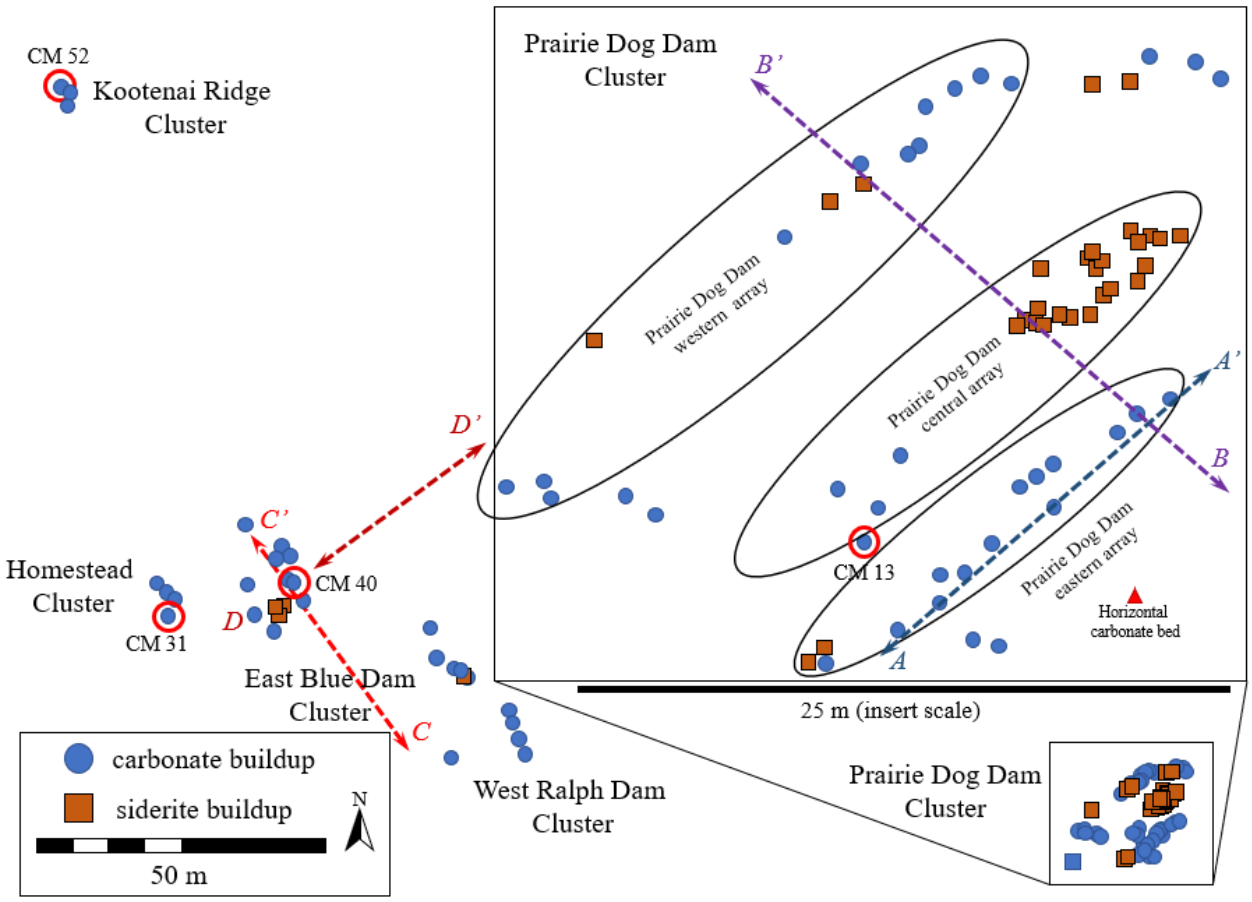

Figure 4. Spatial map of the carbonate and siderite buildups. The buildups are divided into clusters that are named based on local surface features. The Prairie Dog Cluster is subdivided into arrays (insert). The dashed lines *A–A'*, *B–B'*, *C–C'*, and *D–D'* represent the electrical resistivity tomography (ERT) profiles herein described. The four carbonate buildups highlighted by the red circles are specifically referred to herein.

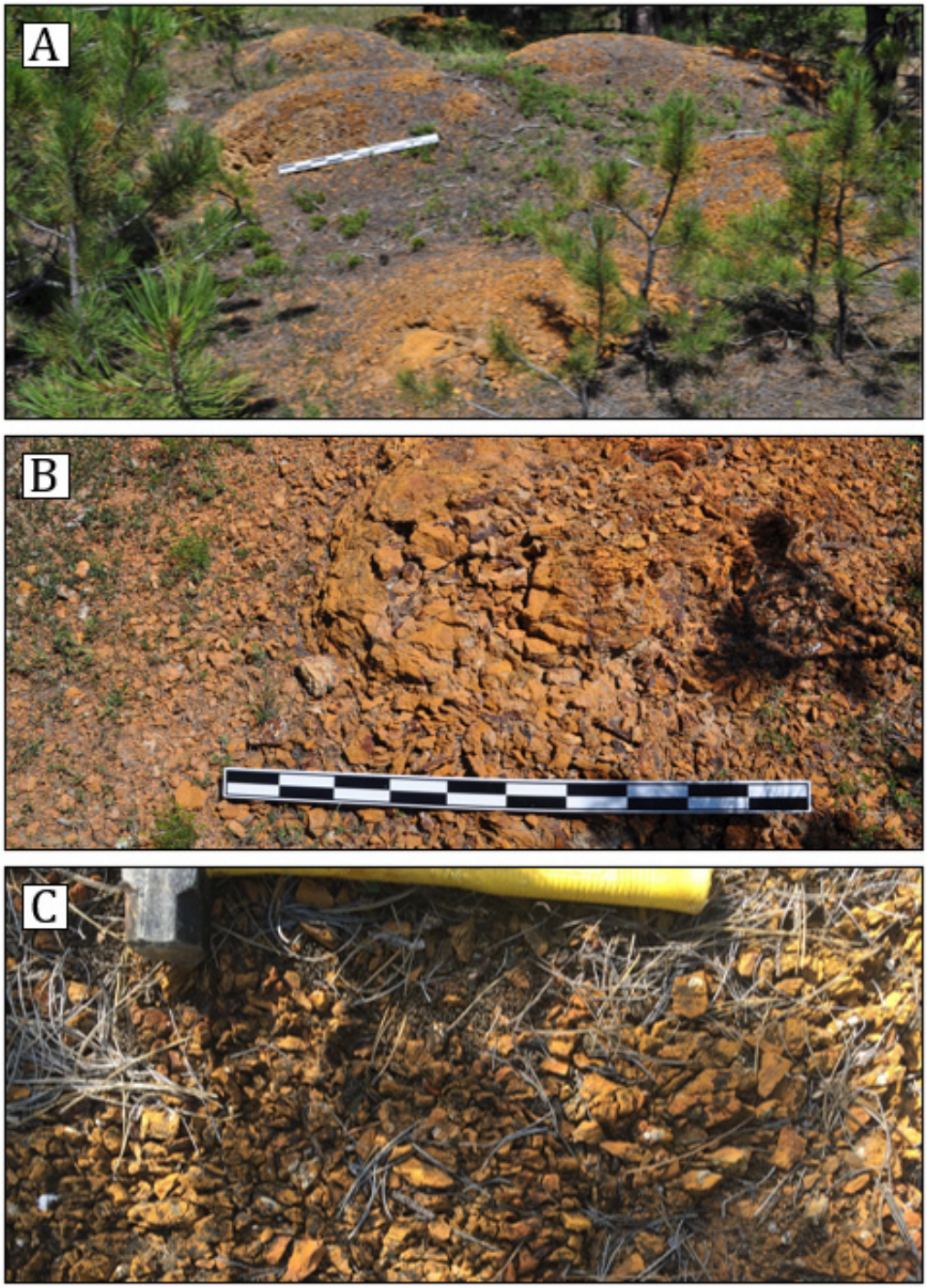

Figure 5. Field images of the siderite buildups. **A**. Siderite buildups can be a few meters long but are less than 50 cm high. They can be isolated or found in clusters. **B**. and **C**. Closeup views of the siderite buildup's upper surfaces disrupted by cone-in-cone apices. Meter stick and hammer used for scale.

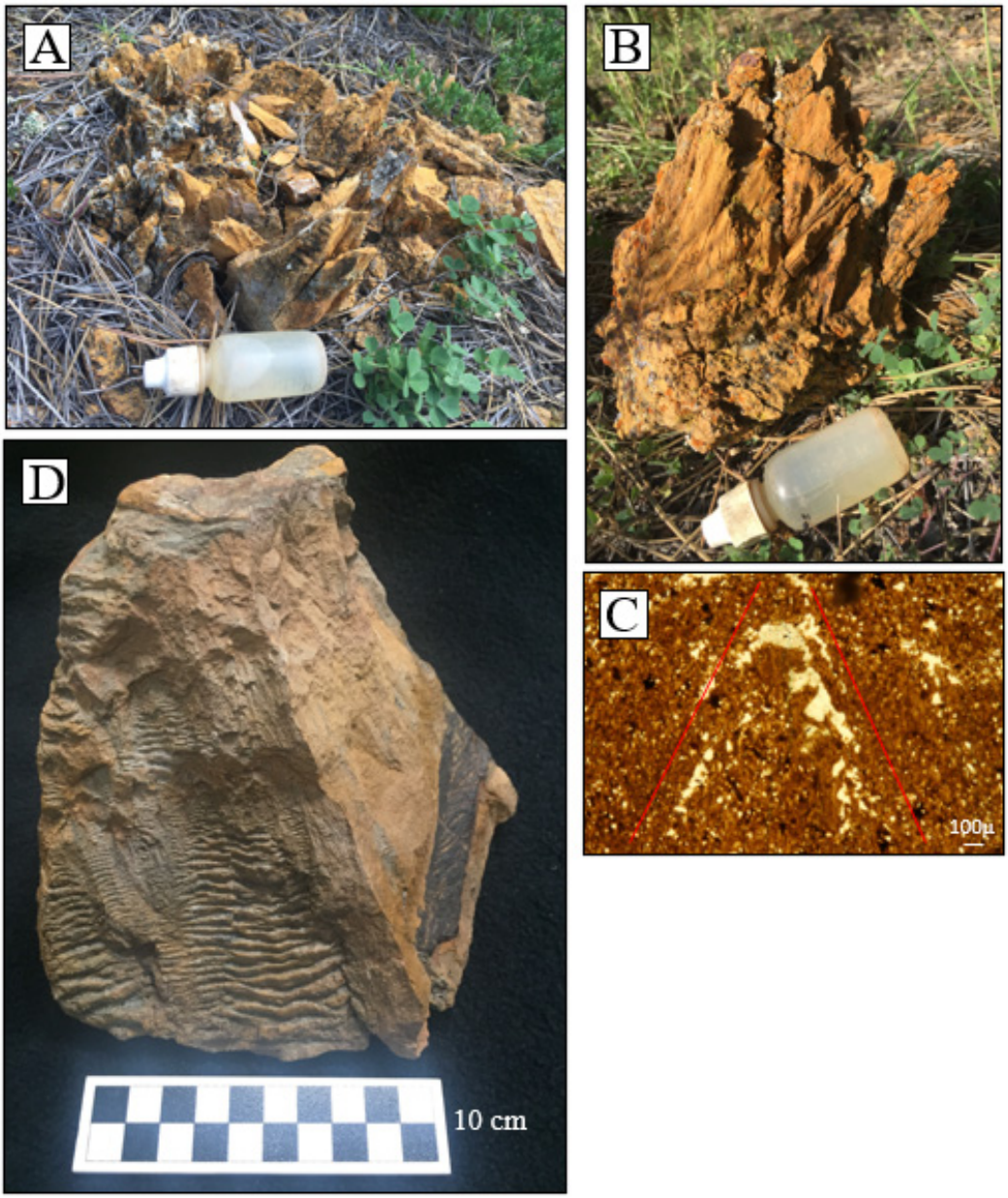

Figure 6. Images of cone-in-cone features of the siderite buildups. **A**. Siderite cone-in-cone feature in place. **B**. The same cone-in-cone feature as shown in A. This has been removed from the buildup to display the large size of the cone-in-cone feature. Acid bottle used for scale. **C**. Photomicrograph of a cone-in-cone feature from a siderite buildup. The cone-in-cone feature (red lines) is difficult to differentiate in the micritic matrix. **D**. Along the flanks or underlying some carbonate buildups (e.g. CM 52) are pale yellowish orange–dark yellow orange siderites. These are referred to as peripheral siderites and exhibit small cone-in-cone ridges.

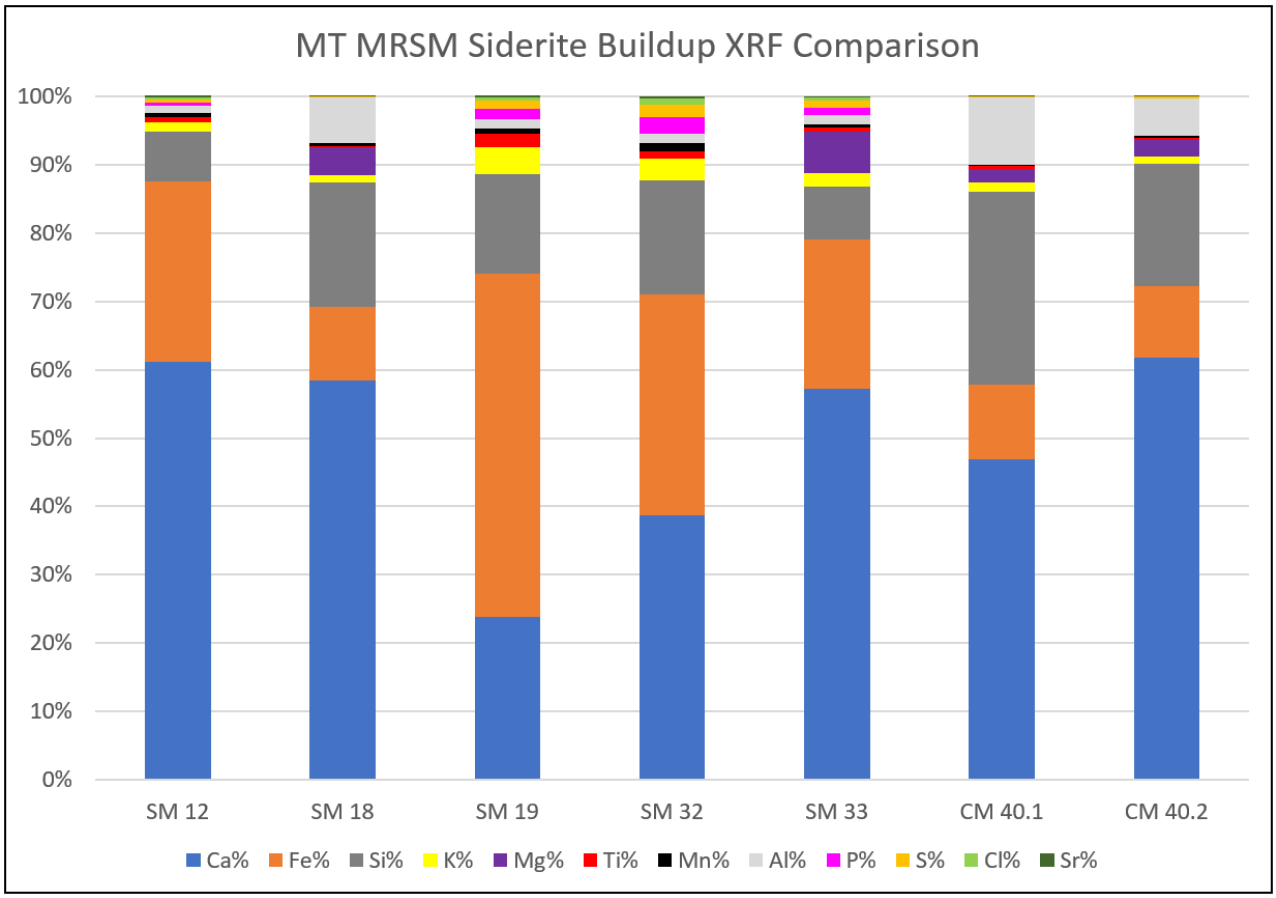

Figure 7. XRF comparison of several siderite buildups and two peripheral siderites (CM 40.1 and CM 40.2). The geochemical variability exhibited in the different buildups is thought to be the result of interaction of the groundwater with different local soil chemistries during development of the siderite buildup.

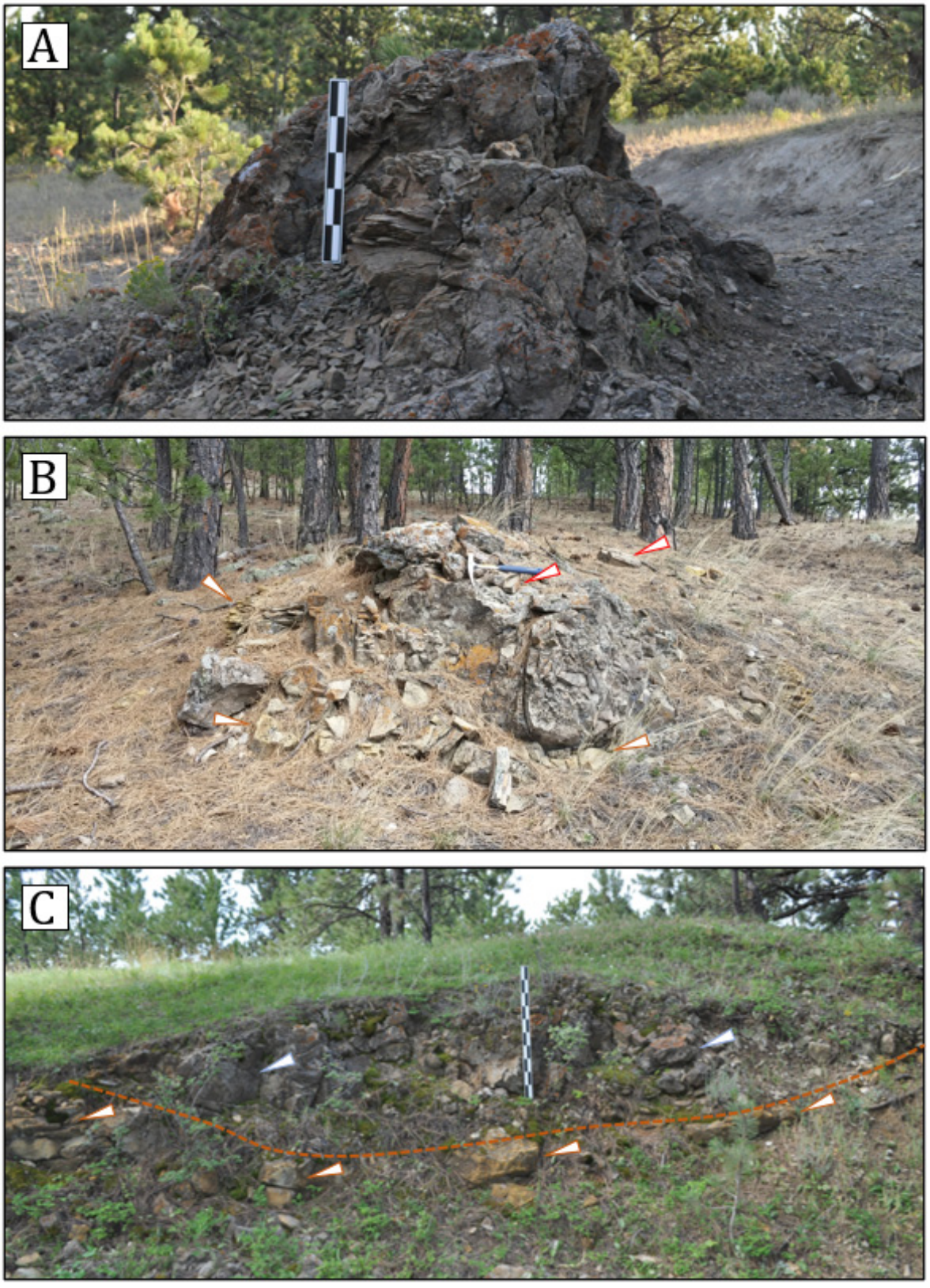
A
B
C

Figure 8. Field images of carbonate buildups. **A**. Carbonate buildup CM 13 exposed in the field. The buildup had a partial petrified log of *Circoporoxylon* encased. In the background is the encasing illitic mudstone. 50 cm scale. **B**. Carbonate buildup CM 52 exposed in the field. A partial petrified log of *Xenoxylon* is encased atop the mound. Some surface wood fragments are visible (red arrow). Peripheral siderites are visible at the base and sides of the carbonate buildup (orange arrows). Hammer for scale. **C**. Carbonate buildup CM 40 exposed in the field. The hemispherical shape of the carbonate buildup is clearly visible. The carbonate buildup (blue arrows) also displays peripheral and underlying siderites (orange line and arrows). Meter scale.

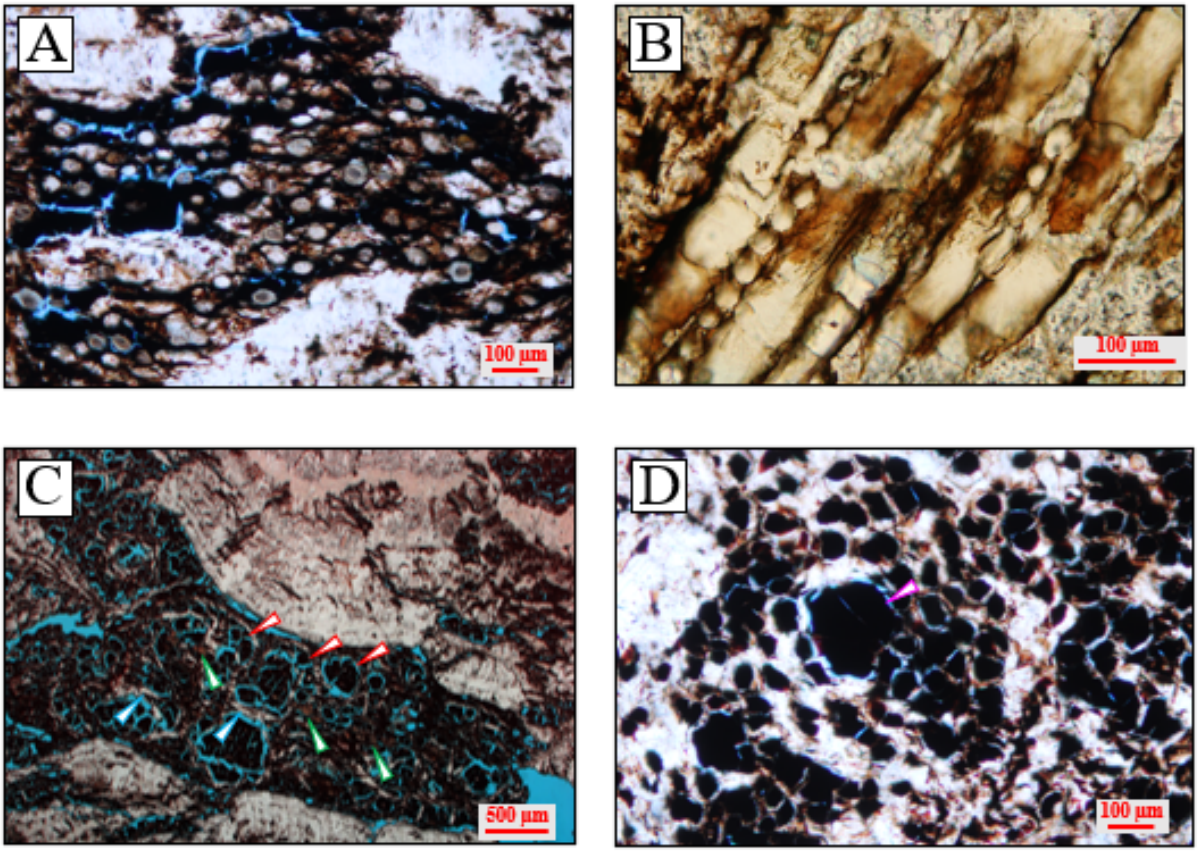

Figure 9. Photomicrographic images of organic material found in some carbonate buildups. **A**. An unknown woody debris in thin section. **B**. The tangential view of a homoxylous woody plant. **C**. A partial bryophyte (liverwort) leaf. The circular chambers (red arrows) are filled with cyanobacteria and bounded by the spongy mesophyll (blue arrows). Collenchymatous cells (cluster of brown cells) present in the midline of the leaf (green arrows) are common in extant liverworts. **D**. The circular pores resemble the features of *Oocardium stratum*, a green alga that is commonly associated with modern tufa deposits. The mean pore diameter is ≈ 30 µm. The large pore (pink arrow) may represent the stem of a hydrophyte.

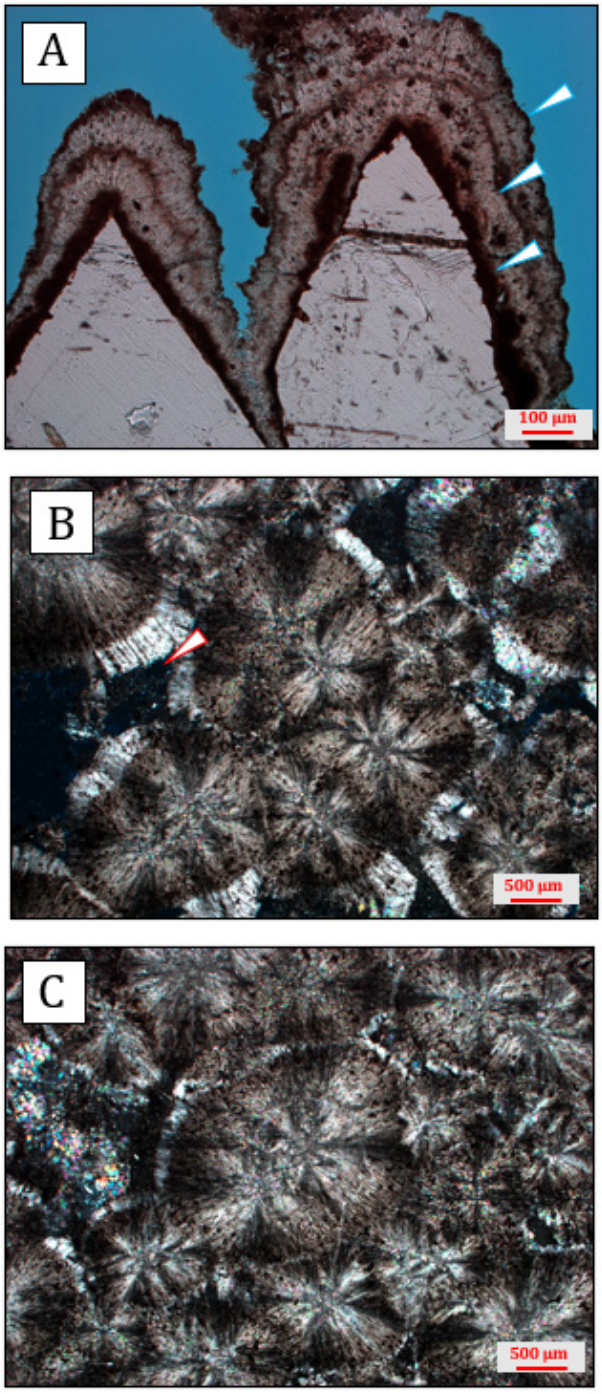

Figure 10. **A**. Photomicrograph of dogtooth calcite crystals with cyanobacterial rinds (blue arrows) suggesting that crystals grew uninterrupted into a subaerial, carbonate-rich pool and the cyano-bacteria had access to sunlight. **B** and **C**. Photomicrographs of spherulites. The spherulites are interpreted to be bacteria derived. Refer to text for information on the bacteria. Primary porosity is evident (red arrow; dark blue epoxy). The dark spots scattered throughout the spherulites are fossil remnants of the bacteria.

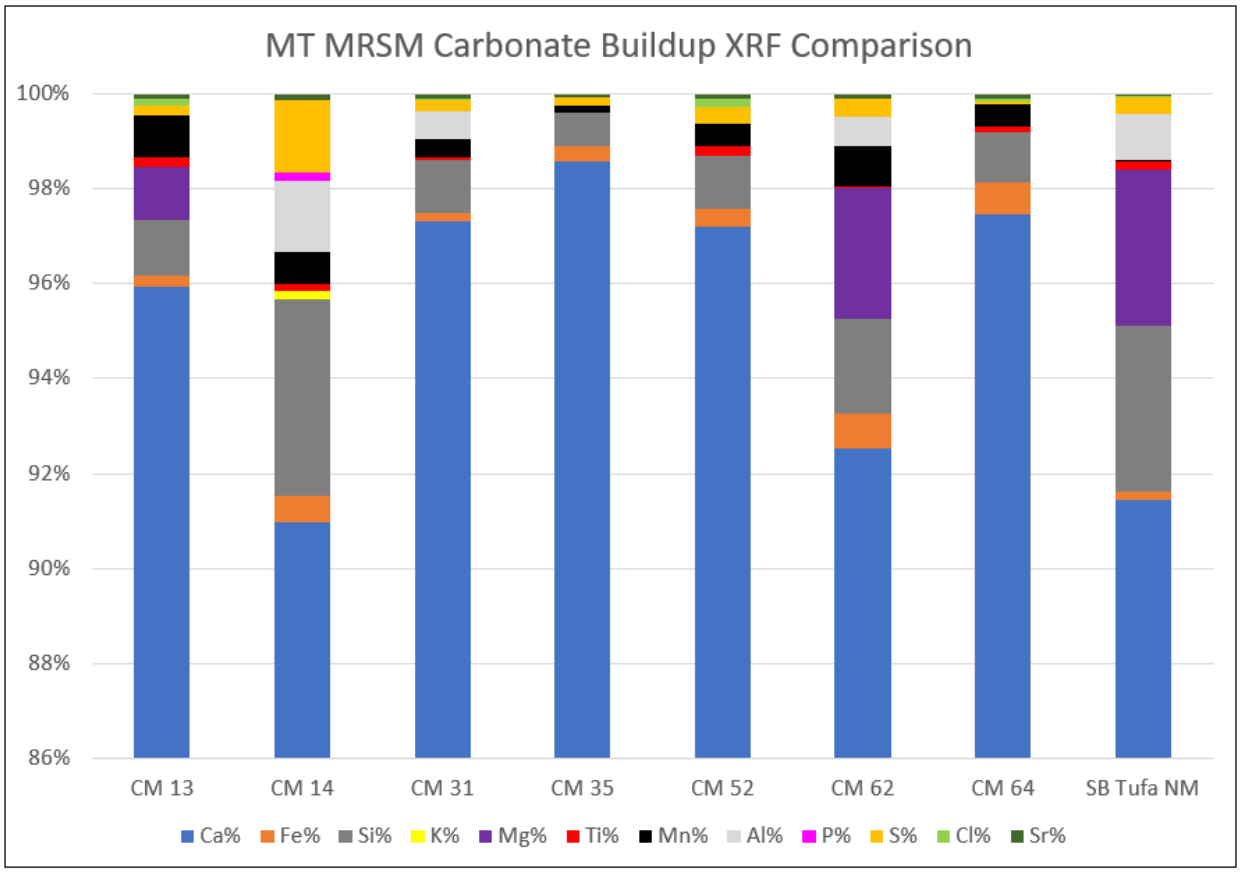

Figure 11. XRF comparison of several Morrison Formation carbonate buildups. The changes in mineralogical composition are likely a result of groundwater interaction with local strata and soils. The carbonate buildup data represent different stratigraphic positions in the formation. No XRF measurements were made on fractures. The bar at the far right is data from the modern cascade Sitting Bull Tufa in Carlsbad, New Mexico.

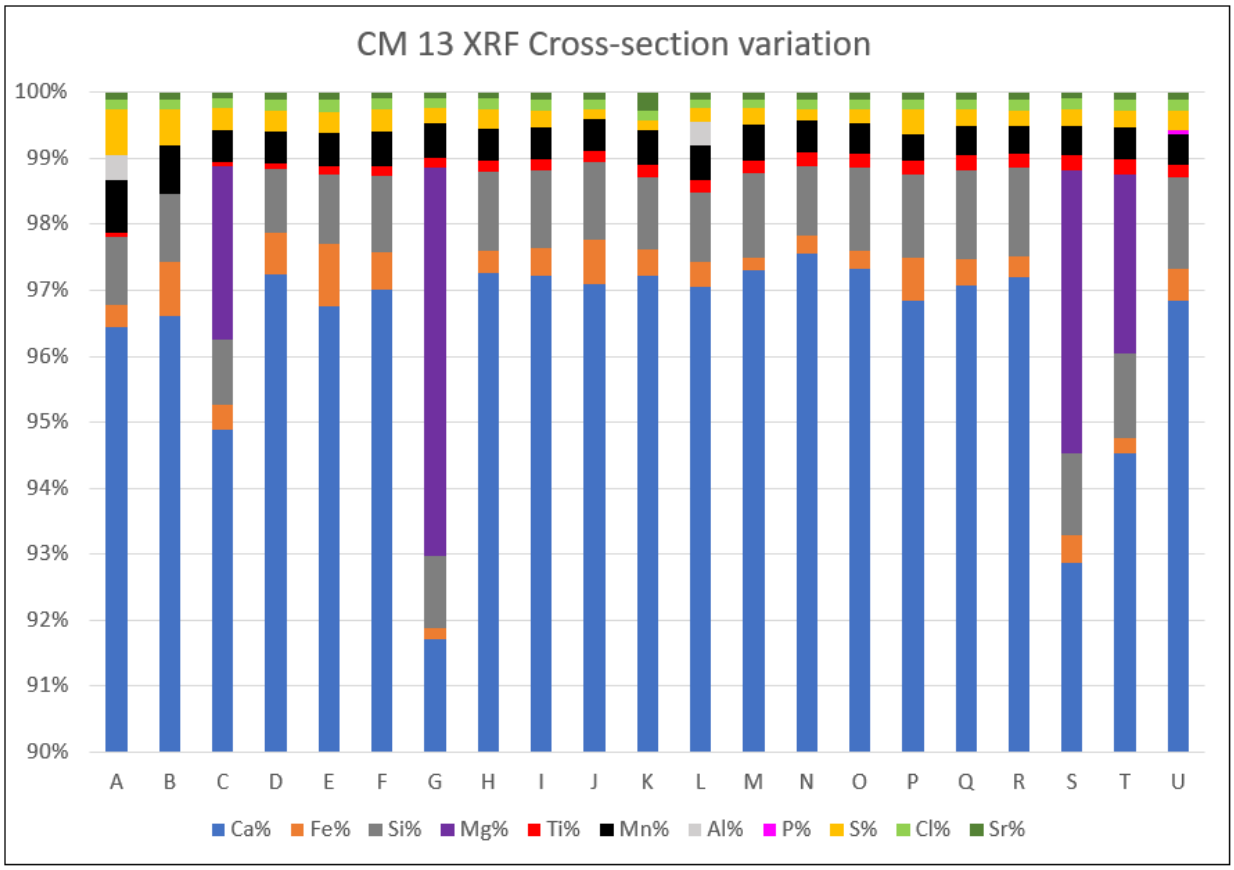

Figure 12. XRF data of CM 13 sampled at 1 cm increments. A large slab of the buildup was cut with measurement A at the bottom and moving upward. The most notable variation during the development of CM 13 is the increase in the percentage of magnesium (Mg). No XRF measurements were made on fractures.

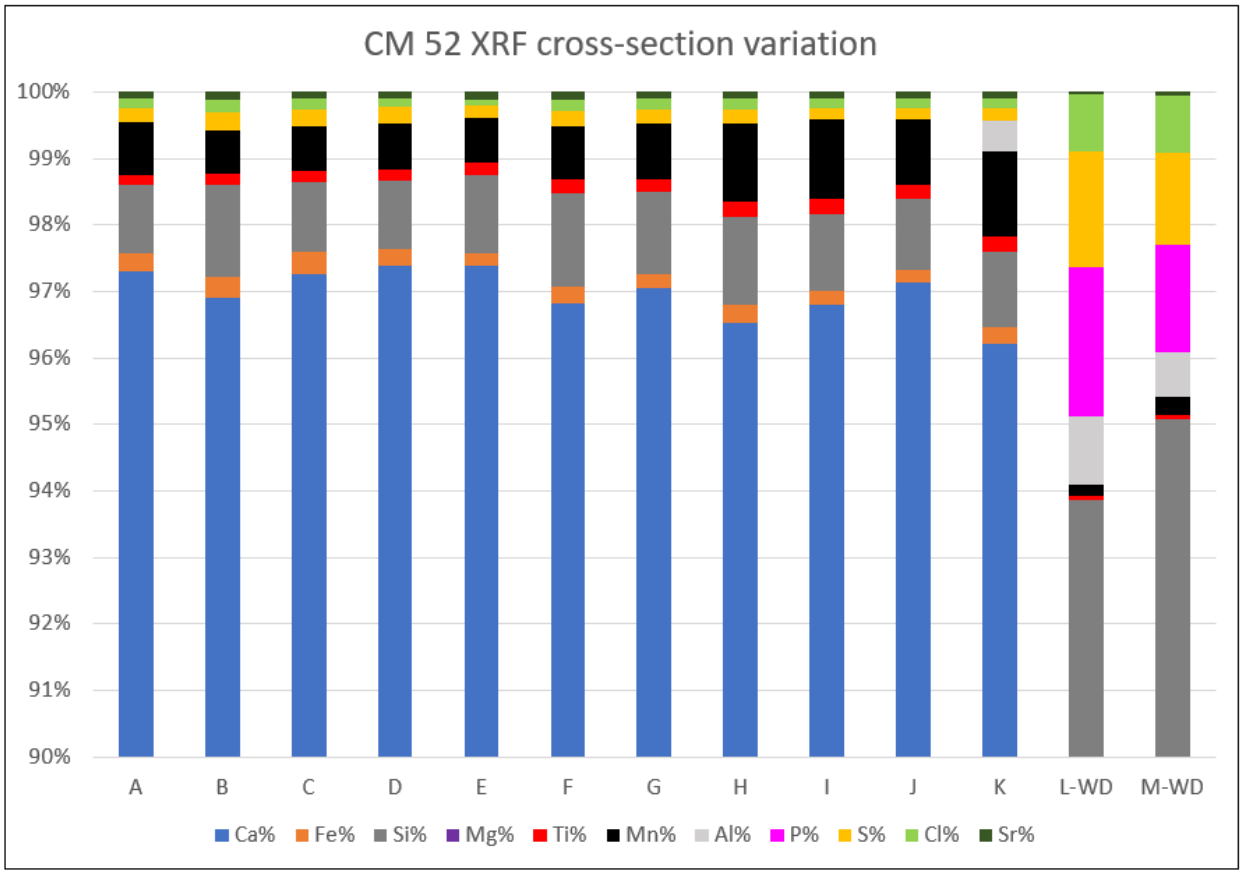

Figure 13. XRF data of CM 52 sampled at 1 cm increments. A large slab of the buildup was cut with measurement A at the bottom and moving upward. Sample CM 52 shows less variability in mineral percentages. Measurements L and M include petrified wood encased at the top of the carbonate buildup. The unique chemical signature of the petrified wood implies preservation may involve Si, P, S, and Cl.

Oxygen and carbon isotope data from carbonate buildups

Sample	$\delta^{13}C$ (‰VPDB)	$\delta^{18}O$ (‰VPDB)
MT MRSN CM13	– 4.27	– 15.48
MT MRSN CM13	– 4.28	– 15.61
MT MRSN CM13	– 4.32	– 15.49
MT MRSN CM35	– 5.02	– 15.97
MT MRSN CM35	– 5.04	– 16.00
MT MRSN CM35	– 5.10	– 15.95
MT MRSN CM52	– 6.45	– 16.89
MT MRSN CM52	– 6.50	– 16.88
MT MRSN CM52	– 6.51	– 16.82

Table 1. Table of the standard isotopic data for three carbonate buildups. Each sample analysis was run three times to ensure consistent values.

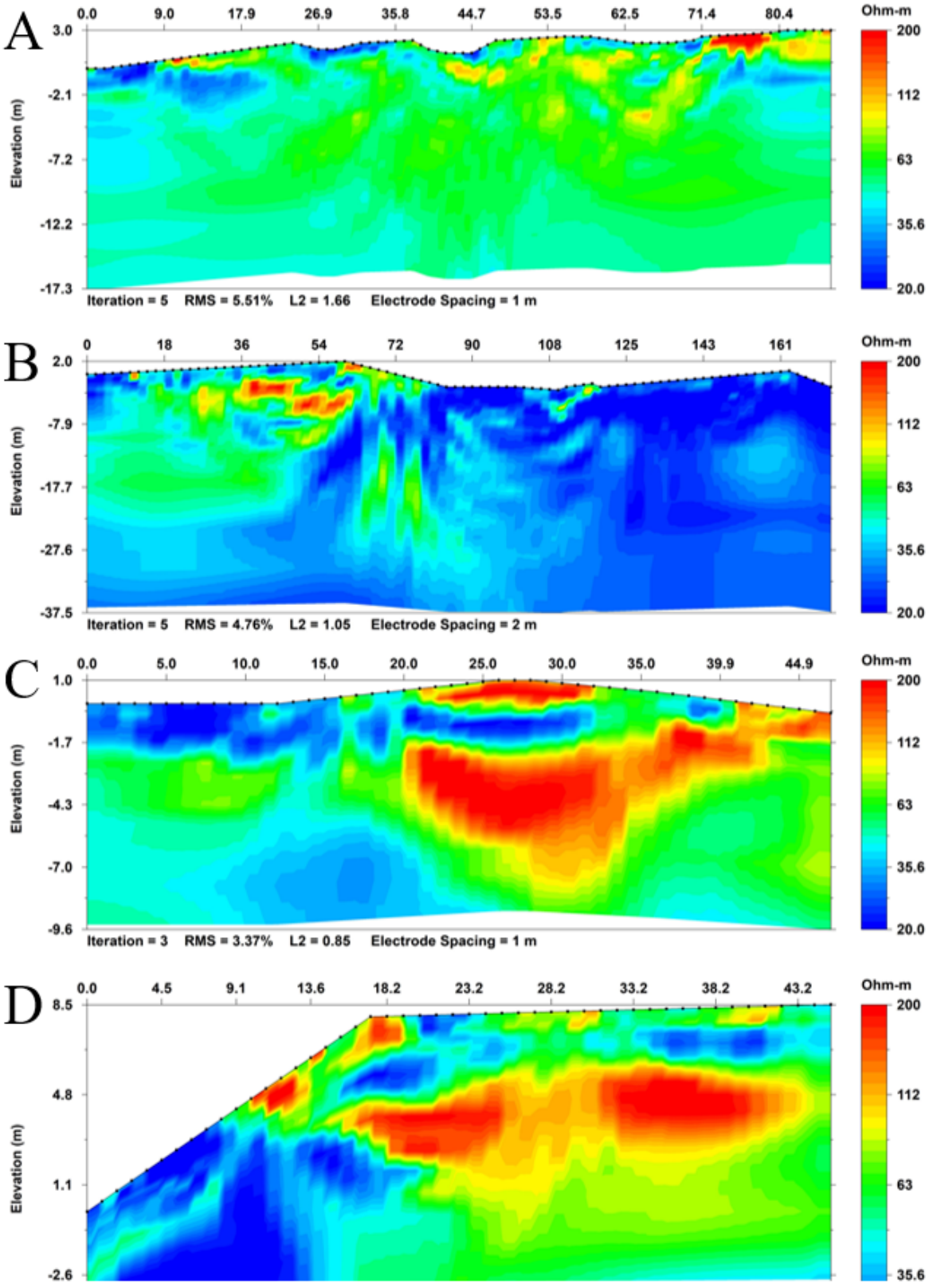
A
0.0 9.0 17.9 26.9 35.8 44.7 53.5 62.5 71.4 80.4
3.0
-2.1
-7.2
-12.2
-17.3
Elevation (m)
Iteration = 5 RMS = 5.51% L2 = 1.66 Electrode Spacing = 1 m
Ohm-m
200
112
63
35.6
20.0
B
0 18 36 54 72 90 108 125 143 161
2.0
-7.9
-17.7
-27.6
-37.5
Elevation (m)
Iteration = 5 RMS = 4.76% L2 = 1.05 Electrode Spacing = 2 m
Ohm-m
200
112
63
35.6
20.0
C
0.0 5.0 10.0 15.0 20.0 25.0 30.0 35.0 39.9 44.9
1.0
-1.7
-4.3
-7.0
-9.6
Elevation (m)
Iteration = 3 RMS = 3.37% L2 = 0.85 Electrode Spacing = 1 m
Ohm-m
200
112
63
35.6
20.0
D
0.0 4.5 9.1 13.6 18.2 23.2 28.2 33.2 38.2 43.2
8.5
4.8
1.1
-2.6
Elevation (m)
Ohm-m
200
112
63
35.6

Figure 14. Electrical Resistivity Tomography (ERT) profiles (A–D). Refer to Figure 4 for profile lines.

A. ERT Profile *A–A'* was run parallel to Prairie Dog Dam (PDD) eastern array. The ERT profile shows high resistivities (> 150 Ω-m) at the distal ends of the profile. The northeastern buildup is about 6 meters across. The profile does not show any additional high resistivity carbonates in the subsurface.

B. ERT profile *B–B'* at Prairie Dog Dam was oriented perpendicular to profile *A–A'* trending northwest across the western, central, and eastern arrays. The ERT profile crosses several siderite buildups of the PDD central array between 86–100 m. This profile section displays low resistivities (< 25 Ω-m) and the siderite buildups are not discernible in the profile. In contrast, the profile does differentiate a small carbonate buildup from the PDD western array at 116–118 m. In the sub-surface, between 36–60 m, is a high resistivity (110–200 Ω-m) zone, interpreted to be a large buildup or possibly two buildups separated stratigraphically.

C. ERT profile *C–C'* was run parallel to the East Blue Dam cluster over the largest observed surface carbonate buildup (CM 40). This buildup is underlain by a thin siderite bed. The hemispherical buildup is 13 m long and 2 m thick. Underlying the buildup is a low resistivity zone (28–15 Ω-m) interpreted to be a ≈ 2 m thick mudstone bed. Beneath this mudstone bed is a high resistivity zone (150–300 Ω-m) interpreted to be a significantly sized carbonate buildup in the subsurface. The lateral extent of this buildup may be as long as 15 to 41 m. The estimated minimum thickness is 1.5 m. Near the end of the profile, the high resistivities appear disjointed and stratigraphically higher and may represent another buildup.

D. ERT profile *D–D'* was oriented perpendicular to profile *C–C'*. High resistivities (150–200 Ω-m) at profile marker 18.2 m represent a small surface buildup. Underlying the high resistivity zone is a lower resistivity zone (30–20 Ω-m). Similar to profile *C–C'*, beneath the lower resistivity zone is a high resistivity zone (150–200 Ω-m). This zone is interpreted to represent a significantly sized buildup. The lateral extent of this buildup is at least 24 m and may extend beyond the profile. The estimated thickness is 1 to 1.5 m. It should be noted that the large *D–D'* profile subsurface buildup(s) has a different subsurface elevation than the large *C–C'* profile subsurface buildup. They are therefore not stratigraphically equivalent.

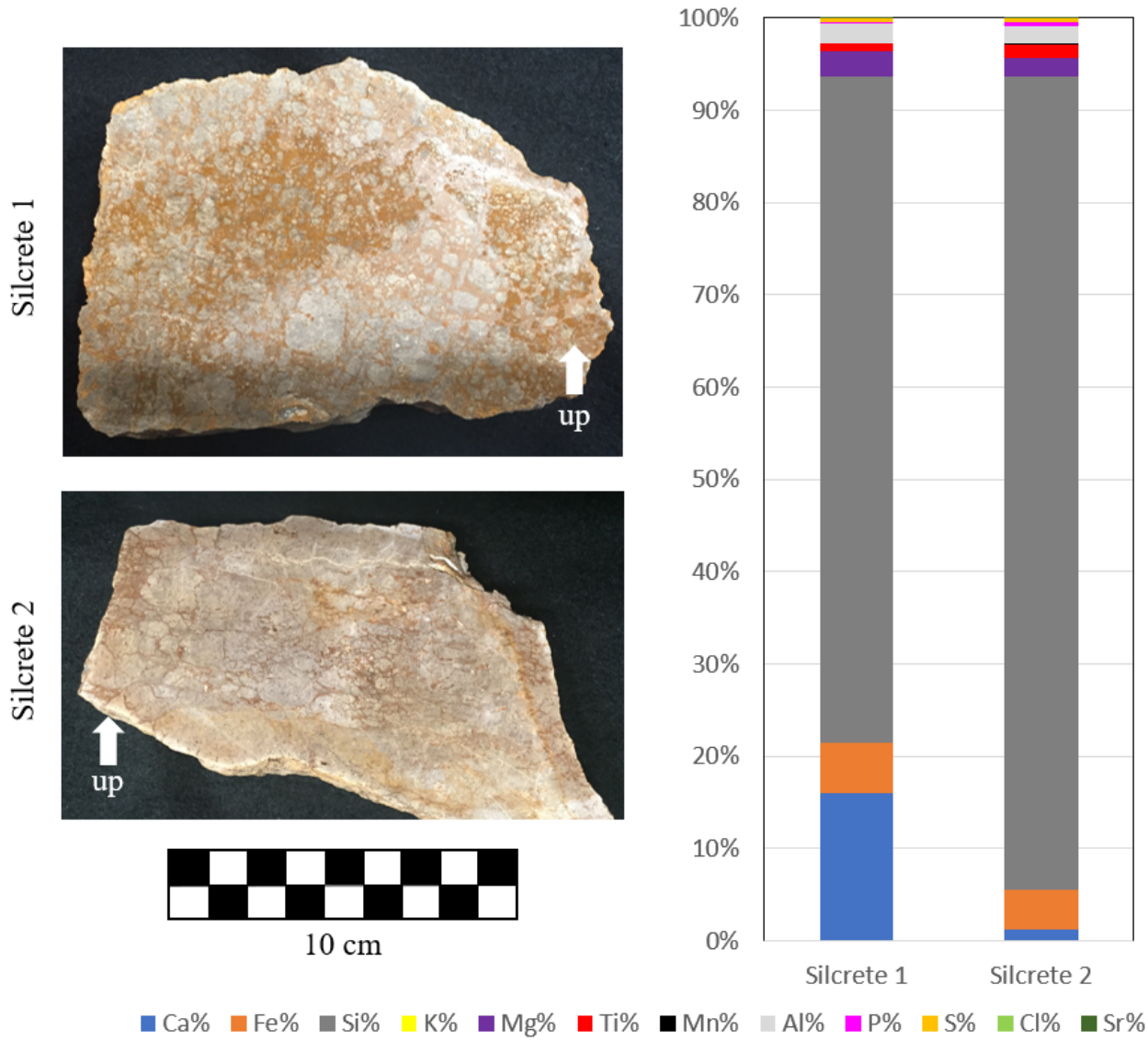

Figure 15. Images of hand samples and XRF data of a Morrison silcrete. This is the only duricrust observed in the formation study area and is stratigraphically 23 m above the Swift Formation. The silcrete shows an established B soil profile. The silcrete layer may also represent a silica-replaced calcrete.

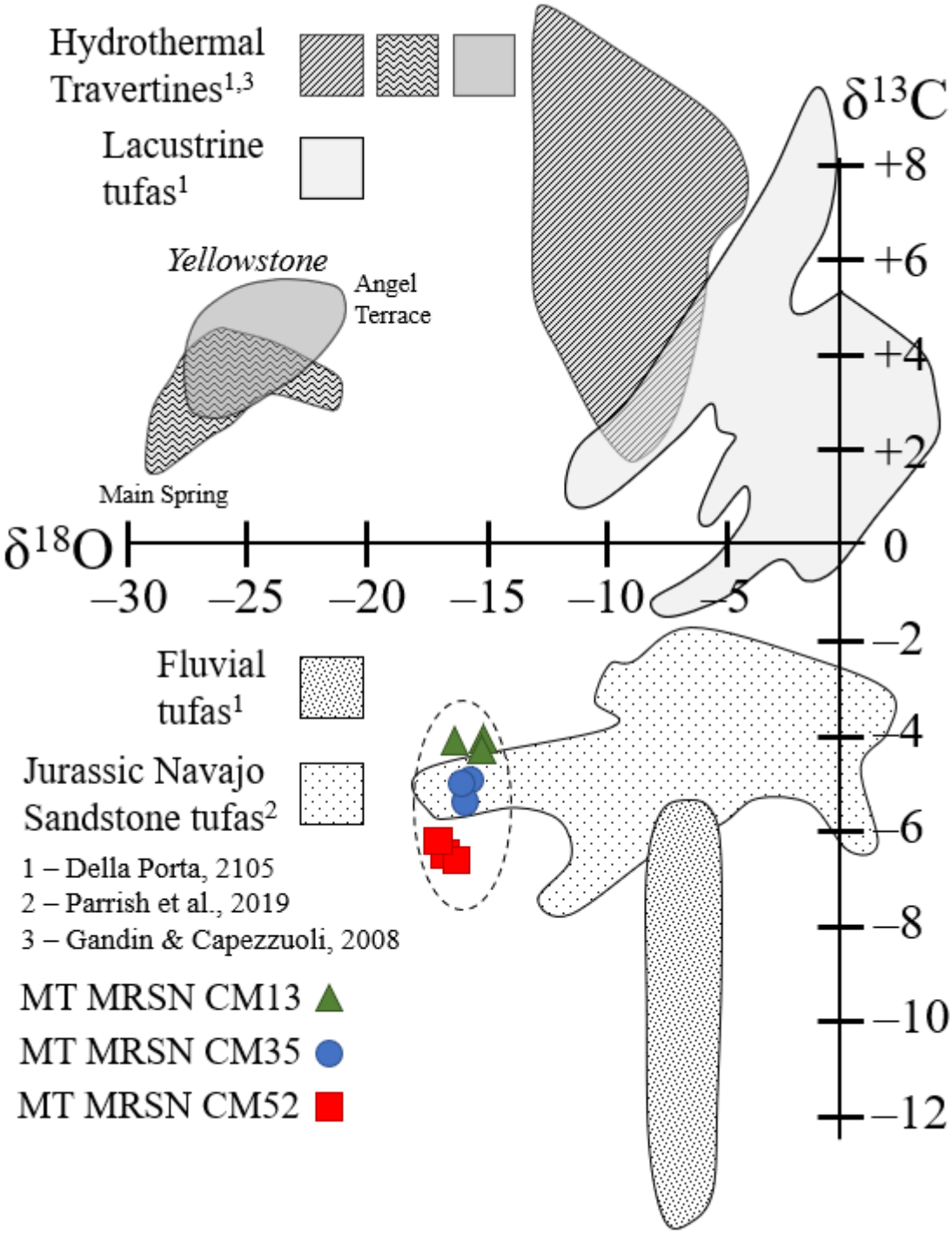

Figure 16. Plot of published standard isotopic data of tufas and travertines and the isotopic data from the central Montana Morrison Formation mound springs. Plotted data indicates that the mound springs are freshwater tufa deposits.

Figure 17. Idealized Morrison Formation carbonate mound spring with a small fracture allowing groundwater flow to the surface. The lack of associated fluvial or lacustrine facies and the formation of the mound suggest low flow rates. The drawing is modified from an image from Great Australian Basin Friends of Mound Springs. Drawing by Serena Celestino.

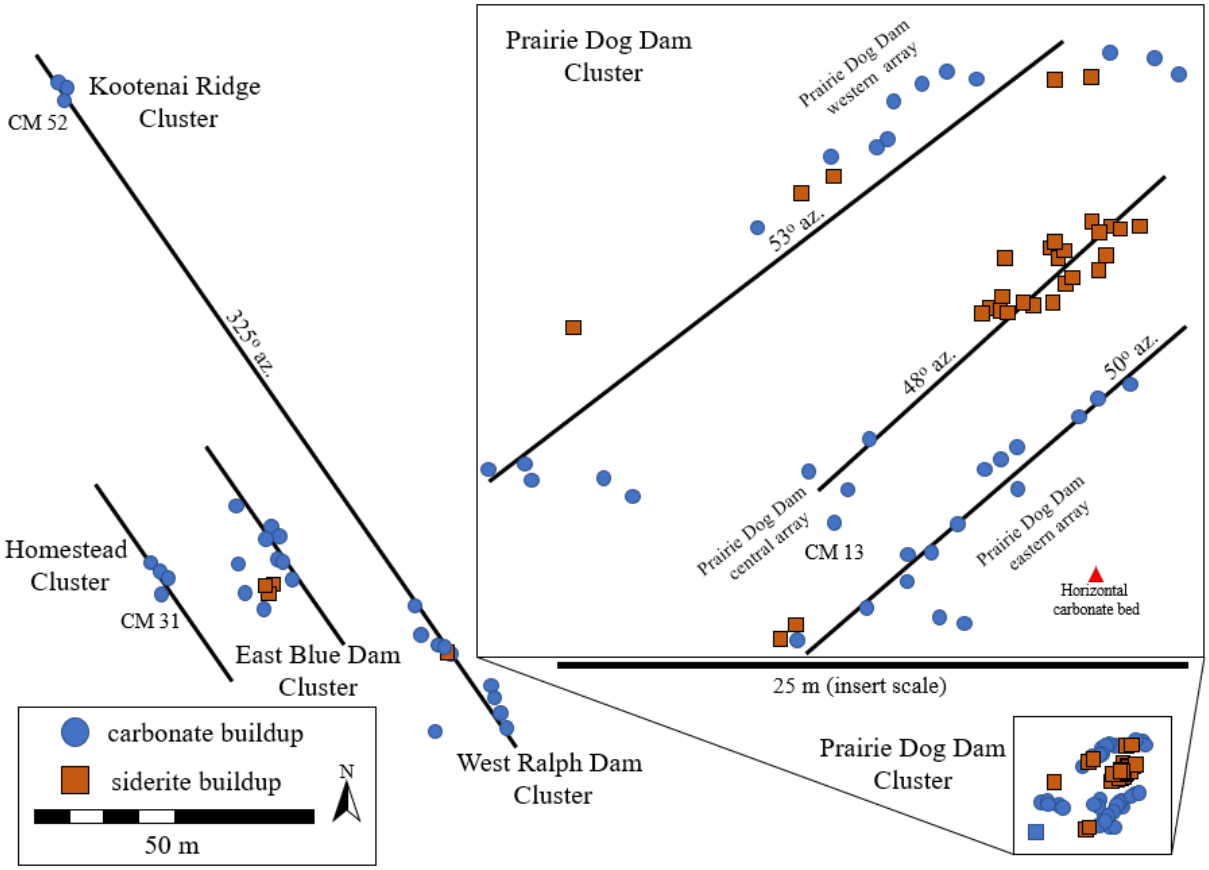

Figure 18. Spatial map of the carbonate and siderite buildups. The buildups are divided into clusters. The insert shows the Prairie Dog Dam Cluster arrays. Lines of best fit for the respective arrays and clusters are shown. The azimuth bearing of each line is similar to the strike of the regional lineaments of Montana, suggesting a correlation between the buildups and the structural lineaments.

CHAPTER 4

Stratigraphy and sedimentology of the Morrison Formation in the western panhandle of Oklahoma with reference to the historical Stovall dinosaur quarries

Dean R. Richmond [a], Tyler C. Hunt [b], Richard L. Cifelli [c]

[a] *School of Geosciences, University of Oklahoma, Sarkeys Energy Center Suite 710, Norman, Oklahoma 73019, USA*
[b] *Department of Biological Sciences, Florida State University, 319 Stadium Drive, Tallahassee, Florida 32304, USA*
[c] *Sam Noble Oklahoma Museum of Natural History, University of Oklahoma, 2401 Chautauqua Avenue, Norman, Oklahoma 73072, USA*

ABSTRACT

New investigations of the Morrison Formation in the western panhandle of Oklahoma reveal that previous stratigraphic measurements are incorrect, and that the formation is approximately 60 m thick in the Kenton, Oklahoma area. Results of previous investigations, together with newly acquired field measurements and well log data from Oklahoma and the surrounding states, provide the basis for a new isopach map of the Morrison Formation. We divide the formation into three new members (Cimarron, Boise, and Kenton members), based on geological, geochemical, petrographic, and paleontological characteristics. Each member is defined by unique depositional facies recording a variable climatic signal and the eventual progradation of the distributive fluvial system to the basin margin. The analogous depositional facies and lithologies of the three newly described members suggest they are lateral facies successions of the well-established members of the Colorado Plateau. The Cimarron Member is comprised of numerous small, ephemeral, clastic lakes at the distal margin of the alluvial braid plain of the Tidwell Member. The Boise Member consists of numerous perennial limestone lakes at the edge of the Salt Wash Member distributive fluvial system. These perennial lakes later coalesced into a

large, single, extensive water body at the top of the member, herein termed Lake Stovall. The Kenton Member records the progradation of the Brushy Basin Member distributive fluvial system to the basin margin in Oklahoma. The first occurrence of fluvial deposition is represented by small, isolated, anastomosing fluvial channels and their associated splays. Stratigraphically near the top of the member is a large, sandy, braided fluvial channel with a basal conglomerate. This large, sandy, braided fluvial channel recorded a major seismic event at the basin margin. The gradual progradation of facies to the basin margin signify that deposition in the foreland basin was geographically extensive and protracted.

Dinosaur fossils excavated under the direction of Stovall during the 1930s are placed into a stratigraphic framework. All the vertebrate quarries are found in a 6-m stratigraphic section at the basal portion of the Kenton Member. The depositional facies and taphonomic data imply the dinosaurs died during a series of severe droughts. Bone dispersal and burial resulted from ephemeral flood splay events.

1. Introduction

Terrestrial sediments of the Upper Jurassic Morrison Formation were deposited in a back-bulge depocenter of a retroarc foreland basin (DeCelles, 2004). The depositional facies of the formation consist of fluvial (Peterson, 1984; Miall and Turner-Peterson, 1989; Robinson and McCabe, 1997; Heller et al., 2015; Owen et al., 2015), lacustrine (Lockley et al., 1984; Turner and Fishman, 1991; Dunagan and Turner, 2004; Demko et al., 2005; Small et al., 2007; Gorman et al., 2008), eolian (Szigeti and Fox, 1981; Peterson, 1988), and coastal sabkha (Anderson and Lucas, 1997) environments that extend across a million square kilometers of the intermountain west of the United States (Dodson et al., 1980). The formation has been intensely studied for its famous

paleobiota including dinosaurs, non-dinosaurian vertebrates, invertebrates, and plant fossils (Chure et al., 2006) and mineral deposits of uranium (Lee and Brookins, 1978; Peterson and Turner-Peterson, 1980; Hansley, 1986; Turner-Peterson and Fishman, 1986). Much of the research on the formation has been conducted on the Colorado Plateau where the formation is well exposed (Stokes, 1944; Keller, 1962; Cadigan, 1967; Peterson, 1984; Peterson and Turner-Peterson, 1987; Turner and Fishman, 1991; Demko et al., 2004; Demko et al., 2005; Dickinson and Gehrels, 2008). However, the stratigraphy, sedimentology, and depositional facies of the Morrison Formation at the basin margins have received scant attention from researchers. Eighty-eight years have passed since the first recorded discovery of Jurassic dinosaurs from the western Oklahoma panhandle (Stovall, 1932). Stovall (1938a) completed a preliminary review of the Morrison Formation in the area but did not attempt to place the dinosaur quarries into a stratigraphic framework. At present, the Morrison Formation in Oklahoma remains undifferentiated.

The purpose of this paper is multifold: (1) To document the stratigraphy, sedimentology, including the depositional facies and petrology, and mudstone geochemistry of the Morrison Formation at the basin margin. (2) To separate the Morrison Formation into stratigraphic members to facilitate correlation with the Morrison Formation on the Colorado Plateau. Variation in depositional facies prompted the establishment of three formally named members. (3) To ascertain how Morrison Formation at the eastern basin margin relates to the formation of the Colorado Plateau. And (4), to place the historical dinosaur quarries in a stratigraphic framework and to understand the depositional facies and vertebrate taphonomy of the quarries.

2. Methods

Stratigraphic measurements were made using standard geological methods and surveyed using a Nikon DTM-322 total station. In this report we follow the stratigraphic nomenclature for Oklahoma as defined by the Oklahoma Geological Survey (Suneson, 2012; 2020). Regional stratigraphic sections were measured from the ground surface through the basal formation through the J5 and K1 unconformities to the top of the Dakota Sandstone. Following the usual practice, we define the Morrison Formation as the strata between the J5 unconformity (top surface of the Jurassic Exeter Sandstone) and K1 unconformity (the basal surface of the Lower Cretaceous Cheyenne Sandstone).

A review of all the thousands of well logs from the Oklahoma panhandle and the surrounding counties from adjacent states yielded 44 logs that logged the Morrison Formation section. Most modern exploration wells drill and set surface casing through the Morrison Formation, which limited the data available for use to create an isopach map of the formation at the eastern basin margin.

Thin sections were prepared by Wagner Petrographic (Lindon, Utah) and were examined under a Zeiss petrographic microscope. Grain size measurements for the well-cemented sandstones were produced using JMicroVision v1.27 from scaled digital thin section images. A 300-framework grain mineral point count was performed on each sandstone thin section to determine mineralogy and sandstone classification according to Dott (1964). A second 300-grain count was measured for each sandstone from which grain size distribution and sorting were calculated using standard petrology equations (Folk and Ward, 1957). Sandstone grain rounding was determined by a random 100-grain count from digital thin section images. Grains were allocated to a rounding class as follows: 0-very angular, 1-angular, 2-subangular, 3-subrounded and 4-rounded. The

average grain roundness was calculated. Carbonates are designated using Folk's classification scheme (Folk, 1959).

The Morrison Formation north of Kenton at SE ½, Sec 8, T6N, R1E was sampled at 3-m increments from the J5 unconformity to the K1 unconformity (Cheyenne Sandstone). Several additional samples were collected from the SE ¼, NE ¼, Sec 16, T5N R5E, north of Boise City. These mudstone samples were prepared for X-ray diffraction (XRD) using standard methods (Moore and Reynolds, 1997). Powder XRD analyses were performed at the University of Oklahoma School of Geosciences using a Rigaku Ultima IV diffractometer that utilizes Cu-K-alpha radiation (40 kV, 44 mA) with a scintillation detector. Data analysis was completed using Jade 2010 software with the ICDD (International Centre for Diffraction Data) PDF4+ database. The XRD 2Ɵ method was used to determine the percentage of illite and smectite in the mudstone samples (Moore and Reynolds, 1997).

3. Regional stratigraphic overview and previous work

Surficial exposures of Mesozoic strata are rare in Oklahoma. Deposits of this age are found only in the southeastern portion of the state and in the extreme northwestern section of the Oklahoma panhandle (fig. 1). The panhandle strata contain the only exposures of Jurassic-age rocks in the state. The stratigraphic nomenclature of this area has a varied history. Numerous historical studies have extended different formation names from adjacent states to define the lithostratigraphic units of the Oklahoma panhandle (Gould, 1905; Rothrock, 1925; DeFord, 1927; Stovall, 1938a, b; 1942; Schoff and Stovall, 1943; Conrad et al., 1987; Hunt and Lucas, 1987; Suneson and Luza, 1999). The lowest strata exposed belong to the Late Triassic Dockum Group, which includes several terrestrial formations initially described in Union County, New Mexico.

Formations included in the group, in ascending order, are the Baldy Hill, Travesser, Sloan Canyon, and Sheep Pen Sandstone (Parker, 1933; Baldwin and Muehlberger, 1959; Conrad et al., 1987; Lucas et al., 1987a, b). The Triassic Formations continue eastward into Oklahoma essentially in subsurface. Only the uppermost section of the Sloan Canyon Formation and the overlying Sheep Pen Sandstone have limited surface exposure in Oklahoma. Overlying the Triassic-age strata is the J0 unconformity (Pipiringos and O'Sullivan, 1978), on which rests the Middle Jurassic Exeter Sandstone. This eolian sandstone (Mankin, 1958b; Snoparsky, 1982; 1986; 1987) has been considered the lithostratigraphic equivalent to the eolian Entrada Sandstone of the San Rafael Group in the Colorado Plateau (Schoff and Stovall, 1943; Johnson, 1959; Irwin and Morton, 1969; Lucas et al., 1998). However, in eastern New Mexico the Exeter Sandstone has been alternately regarded as a member of the Entrada Sandstone (Lucas et al., 1987c). In Oklahoma, the J5 unconformity (Pipiringos and O'Sullivan, 1978) marks the contact between the underlying Middle Jurassic Exeter Sandstone and the overlying Upper Jurassic Morrison Formation. The K1 unconformity (Pipiringos and O'Sullivan, 1978) defines the upper contact of the Morrison Formation with the Lower Cretaceous Cheyenne Sandstone. The Cheyenne Sandstone is the oldest Cretaceous sedimentary stratum in Oklahoma and is interpreted to be of fluvial origin defined by conglomeratic sandstone beds with a fining-upward sequence and trough cross-stratification (Brake, 1982). The initial sediments of the Aptian-age transgression of the epicontinental seaway into the Western Interior are characterized by intercalated sandstone, shale, and limestone beds of the Kiowa Shale. Overlying the Kiowa Shale and capping the mesas in Cimarron County is the Dakota Sandstone (fig. 2). Its depositional systems include a variety of shallow marine clastic facies deposited during a progradation sequence associated with marine regression in the Western Interior Seaway (Atalik and Manfield, 1984). The youngest Mesozoic units in the Oklahoma

panhandle are the Graneros Shale and Greenhorn Formation deposited during the Cenomanian-age marine transgression. Locally at Black Mesa (Kenton, Oklahoma), the Miocene Ogallala Formation unconformably overlies the Cretaceous Greenhorn Formation and is capped by the Pliocene Black Mesa Basalt. The 30 m thick Black Mesa Basalt is a Pliocene-age vesicular alkali olivine basalt (Shead, 1923; Suneson, 2012).

3.1 Upper Jurassic Morrison Formation

The Morrison Formation name was first used to define the sequence of clay, sandstone, and shale beds near the town of Morrison, Colorado that superimpose the marine Sundance Formation and underlie the capping Cloverly or Lakota Sandstones (Mook, 1916). At the beginning of the 20th century, Lee (1901) journeyed through southeastern Colorado and to the Cimarron River in the Oklahoma Territory, but only briefly described and measured the Morrison Formation in southeastern Colorado. Lee (1901) defined the Morrison Formation as the strata between the Red Beds and the Dakota Sandstone. The following year Lee (1902) traveled through southern Colorado and northern New Mexico and passed through the most western portion of the panhandle of Oklahoma. In his report, Lee (1902) redefined the Morrison Formation for the sediments stratigraphically between the newly named Exeter Sandstone and the Dakota Sandstone. He briefly mentioned the existence of the formation in Oklahoma. Darton (1905) visited the Two Buttes area of southeastern Colorado and observed that the area's stratigraphy included the Exeter Sandstone, Morrison Formation, and Dakota Sandstone. Gould (1905) completed an overview of the geology and water resources of Oklahoma. In his report, Gould stated that he did "not desire to express an opinion as to whether or not the Morrison may be found in the region of Kenton." Stanton (1905) in his overview of the Morrison Formation recognized the presence of the formation in the

Oklahoma panhandle. The first worker to measure the Morrison Formation in Oklahoma was Rothrock (1925). He measured the formation west of North Carrizo Creek north of Black Mesa and reported the formation to be only 17 m thick. DeFord (1927) agreed with Lee's (1902) assessment that the formation was present in the Dry Cimarron region of New Mexico and Oklahoma. Regional evaluations of Jurassic formations by Baker et al. (1936) and Oriel and Mudge (1956) showed that the Morrison Formation thins eastward from the Colorado Plateau.

The Morrison Formation, long famous for its dinosaur fossils, yielded the first bones from Oklahoma in 1931 (Stovall, 1932; Kenton quarry 1, 12 km east of Kenton; Stovall, 1938a, b). In 1935, the federal government provided funds for excavation, collection, and preparation of the bones (Langston, 1989). Stovall (1938a) reported that over 3,500 bones had been excavated since the discovery of a large "brontosaur" (*Apatosaurus*) and four other genera represented from the site, including a large carnivore (*Saurophaganax,* Chure, 1995). In his brief report to the Oklahoma Academy of Science, Stovall (1937) also extended the Morrison Formation eastward to north of Boise City, Oklahoma. Stovall proceeded to complete his doctoral degree from the University of Chicago with his dissertation on the "Geology of the Cimarron River Valley in Cimarron County, Oklahoma" (Stovall, 1938a; Hunt and Lucas, 1987).

For his dissertation research, Stovall incorrectly calculated the thickness of the Morrison Formation. He summed measured sections from three different locations to determine the formation thickness. His first section was measured along the North Carrizo Creek at Labrier (Tate) Butte (SE ¼, SE ¼, Sec 21, T6N, R1E; fig. 3). Stovall (1938a) stated that the measured section was in the SW ¼ of Sec 21; however, only the Exeter Sandstone is exposed in this quarter section. Stovall's measurement at this locality is 48 m. The second measurement was at Robber's Roost (NE ¼, SE ¼, Sec 34, T6N, R1E) 3 km southeast of Labrier Butte (fig. 3). His measurement

for this section is 67 m. The exact location of his last measurement in Section 11 (T5N, R1E) is unknown (fig. 3); he measured 27.5 m of the upper portion of the formation in this section. He used a green mudstone bed to correlate between the stratigraphic sections, making his cumulative Morrison section between 142 m (465 ft; Stovall, 1938a, b) and 139 m (456 ft; Stovall, 1941a, which may represent a numerical transposition). Stovall stated that the formation thickened 94 m over 4 km; he evidently added the measurements of the sections. This error has been perpetuated in many publications (Stovall, 1938a, b; 1941a, b; 1942; McLaughlin, 1954; Schoff and Stovall, 1943; Abbott, 1979; Hart et al., 1976; West, 1978; Hunt and Lucas, 1987).

There are several explanations for Stovall's error. First, his measurement (48 m) at Labrier Butte seems to have been incomplete. Our measurement across North Carrizo Creek at Latimer Butte is 60 m (fig. 3). Second, his measurement at Robber's Roost is problematic. A graben fault block is present at Robber's Roost and only 20 m of the uppermost portion of the Morrison Formation is present above the valley floor. At Robber's Roost the Cheyenne Sandstone consists of three accretionary fluvial sandstone channels. The white lower fluvial sandstone bed is 11 m thick. The lower and middle fluvial sandstone beds are separated by 7.5 m of floodplain mudstone. The white middle fluvial sandstone bed is 10 m thick. Down cutting into this white middle sandstone bed is the buff colored upper fluvial sandstone bed, which is about 17 m thick. The Cheyenne Sandstone is 35 m thick at the southwestern section of Robber's Roost. In the Kenton area, west of the Cimarron River, there is usually one fluvial sandstone bed. East of the Cimarron River, at some locations there are two, sometimes three fluvial channel sandstone beds present. The entire Mesozoic section at Robber's Roost from the valley floor to the top of the Dakota Sandstone is 80 m. Stovall (1938a, b) must have included the Morrison, Cheyenne, and Kiowa in his

measurement of 67 m. The exact location of his last measurement in Section 11 (T5N, R1E) is unknown, but exposures of Cretaceous strata dominate the surface area of the section (fig. 3).

McLaughlin (1954) measured two partial Morrison sections in southern Baca County Colorado. He measured from the Morrison Formation limestone beds in the middle of the formation to the Cheyenne Sandstone and questioned his shorter measurements based on Stovall's 142 m thickness made several years earlier. Hart et al. (1976) stated the maximum thickness for the Morrison Formation in the western part of Cimarron County as 143 m. No explanation for this value was provided; it is likely simply cited from Stovall's measurement. West (1978) described the lacustrine facies of the Morrison in Cimarron County; he agreed with Stovall's (1938a, b) measurement for the Morrison Formation. Abbott (1979) contoured the thickness of the Morrison Formation in northwestern New Mexico and western Cimarron County, Oklahoma, with a thickness shown between 122 and 152 m. He does not state how the information was derived; he too likely used Stovall's thickness. Hunt and Lucas (1987) reviewed Stovall's research in the Morrison Formation of Oklahoma, citing Abbott (1979) on the thickness of the unit. This historical review serves to underscore the pervasiveness of Stovall's Morrison measurements as the ultimate source for thickness of the Morrison Formation in the Oklahoma panhandle, a literary tradition that warrants evaluation after 81 years without new data.

3.2 Western Kansas Morrison Formation thickness

In Kansas, the Morrison Formation is almost exclusively in the subsurface, with shallow depths (30 m) in Morton County and deepening northward along the Colorado state line to > 600 m. The Morrison has a small surface exposure along the Cimarron River north of Elkhart, Kansas (Kume and Spinazola, 1984; fig. 4, J). Information pertaining to the Morrison Formation in

Kansas is restricted to well log data and cuttings from the subsurface (Doveton, 2007). The environmental interpretation indicates the presence of ephemeral fluvial systems and shallow freshwater and evaporitic lakes (Doveton, 2007). McLaughlin (1942) measured 12 m of Morrison sediments in the subsurface at Test Hole 4 in the southeast corner of Section 36 (T31S, R42W; fig. 4, D) in Morton County. Merriam (1955) mapped the Morrison Formation of Kansas from log data and groundwater tests. He mapped a zero edge in Morton county, and a maximum thickness of 60 m in Hamilton County (fig. 4, G). In Greeley County, approximately 165 km north of the Oklahoma-Kansas state line, the Morrison Formation thins to 37 m in the Amoco Rebecca Bounds #1 well as measured in core (Joeckel et al., 2007; fig. 4, K). The formation increases in thickness northward to 107 m in Sherman County (Merriam, 1955). Kume and Spinazola (1984) also mapped the Upper Jurassic rocks in Kansas but did not differentiate Triassic and Jurassic rocks in the southwestern part of the state.

3.3 Southeastern Colorado Morrison Formation thickness

Stanton (1905) indicated the Morrison Formation to be about 61 m thick in north-central Las Animas County and near Higbee, Otero County (fig. 4, A). McCarn et al. (1982) specified the Morrison Formation averages between 40 and 60 m in Las Animas County. Sanders (1934) stated the Morrison is 49 m thick in the Two Buttes, Colorado area (fig. 4, C). Doumit (2005) measured the stratigraphy of the Morrison Formation in the Picket Wire Canyonlands southwest of Junta, Colorado at about 87 m (fig. 4, L). McLaughlin (1954) measured two partial sections of the Morrison Formation from the limestone beds near the middle of the formation to the Cheyenne Sandstone in southern Baca County, Colorado just north of the Oklahoma state line. These sections are particularly relevant due to being close to our study area. By adding the lower Morrison

thicknesses from the limestone bed to the formation base from our Baca County section 3 km to the southwest, we calculate a total thickness of the Morrison Formation for the McLaughlin (1954) sections as 52 and 46 m respectively (fig. 4, E).

3.4 Eastern New Mexico Morrison Formation thickness

Lee (1902) reported a Morrison Formation measurement of 63 m at Long Canyon along the Dry Cimarron River in Union County, New Mexico. Parker (1933) measured thicknesses between 80–113 m for Union County. Cooley (1956) measured eight regional sections starting northeast of Folsom, New Mexico and moving eastward along the Dry Cimarron Canyon of northern Union County toward Kenton, Oklahoma. He subdivided the lower strata of the Morrison into the "Wanakah Formation" but the "Wanakah" is no longer recognized in New Mexico (Baldwin and Muehlberger, 1959). Cooley's (1956) sections show thicknesses of the Morrison Formation varying from 110 m in the western Dry Cimarron Valley to 66 m at Shiprock Butte, New Mexico, and are instructive in that they document eastward thinning of the formation (fig. 4, F). Baldwin and Muehlberger (1959) also reported eastward thinning of the Morrison Formation from 107 to 61 m along the Dry Cimarron River Valley. In Harding County, New Mexico, Mankin (1972) measured the thickness of the formation as varying from 170 to 102 m (fig. 4, I). Abbott (1979), modified Mankin's (1958a; fig. 4, H) isochore map displaying a maximum thickness 163 m in western Harding County. He contoured the thickness of the Morrison Formation in the western Oklahoma panhandle having values ranging from 120–150 m.

3.5 The "Brown-Silt" and Bell Ranch Members

The "Brown-Silt Member" as defined by Baldwin and Muehlberger (1959) is a distinctive lower part of the Morrison Formation. The proposed base interbedded with the Exeter Sandstone and its top was purported to be 3 m below a laterally pervasive agate (chert) bed. This member was also once considered the upper part of the Wanakah Formation (Bachman, 1953; Wood et al., 1953; Cooley, 1956). This same section has also been lithostratigraphically correlated to the Summerville Formation of western Colorado (McLaughlin, 1954). This distinctive "Brown-Silt Member" was recognized in Union, Colfax, Mora, and Harding counties in New Mexico (Baldwin and Muehlberger, 1959) and Baca County, Colorado (McLaughlin, 1954). However, the "Brown-Silt Member" designation has not been formally accepted in the literature.

The Bell Ranch Formation was first proposed by Griggs and Read (1959) for sediments which conformably rest on the Entrada Sandstone and are conformably overlain by the Morrison Formation northwest of Tucumcari, New Mexico. The formation was more fully described by Lucas et al. (1985). The Bell Ranch Formation consists of laterally extensive lacustrine beds that interfinger with the Entrada Sandstone and the Exeter Member of the Entrada and may represent the regressive facies of the Todilto Formation. In New Mexico, where the Exeter Member of the Entrada Sandstone is absent, the Todilto Formation is in contact with the Morrison Formation (Lucas et al., 1985). Conrad et al. (1987) incorrectly correlated the lower portion of the Morrison Formation in Oklahoma to the Bell Ranch Formation, New Mexico by placing the Bell Ranch Formation atop the Exeter Sandstone. The Bell Ranch Formation and lower portion of the Morrison Formation in Oklahoma are not stratigraphically equivalent as the Bell Ranch Formation underlies the J5 unconformity (Lucas et al., 1985), whereas the Morrison Formation overlies the unconformity.

3.6 Lower Morrison agate (chert) beds

Lee (1901, 1902), who explored the Morrison Formation in southern Colorado and northern New Mexico, noted agate (chert) beds in the lower portion of the Morrison Formation. Ogden (1954) discussed the use of chert beds as stratigraphic markers throughout the intermountain west including the Ralston Formation of the Colorado Front Range but did not mention the Morrison Formation. Cooley (1956) mentioned the presence of agate beds in the Morrison Formation along the Dry Cimarron Canyon in Union County, New Mexico. Stratigraphically, the chert beds of Union County are between 19.5 and 21 m above the Exeter Sandstone and consist of one, two, or three units in a section ranging in thickness from 10–30 cm. These stratigraphic measurements of Cooley (1956), which include the agate beds are between 67–51 km west of the current Kenton study area. Baldwin and Muehlberger (1959) also referred to an agate bed in the lower portion of the formation in Union County, New Mexico and commented that the intermittent layer is consists of clear, red and blue nodular chalcedony, usually a meter above their "Brown-Silt Member." Mankin (1972) also reported a regional chert layer, with associated gypsum beds at some localities in northeastern New Mexico. He proposed further that the cherts could be used as a stratigraphic marker for the lower part of the Morrison Formation. Prior researchers of the Morrison Formation of Cimarron County, Oklahoma did not previously recognize the presence of chert beds (Stovall, 1938b; Abbott, 1979).

Magadi cherts were first described for chert beds discovered in the East African Rift Lake Magadi (Eugster, 1967). The cherts form in endorheic shallow lacustrine basins with a high pH and are usually associated with volcanic sediments. The precursor minerals of magadiite and kenyaite are formed during early diagenesis. There is usually cracking and sediment deformation of the magadiite due to compaction. Shrinkage occurs as magadiite is transformed to chert. Chert is

formed inorganically by the leaching of the sodium either by lake waters or groundwater during diagenesis (Eugster, 1967, 1969; Schubel and Simonson, 1990). Magadi-type cherts, which form in association with sodic evaporites, have been reported from the Morrison Formation in Wyoming (Surdam et al., 1972) and east of the Colorado Front Range (Dunagan et al., 1997; Dunagan, 1998).

3.7 Morrison Formation clay mineralogy

An investigation of the clay mineralogy of the Morrison Formation in Oklahoma was undertaken to learn if there was a noticeable change in clay minerology from illite to smectite. On the Colorado Plateau, a widespread noticeable change in color and clay mineralogy from reddish illitic mudstones to variegated smectitic mudstones is present in the Brushy Basin Member of the Morrison Formation. This clay change is stratigraphically in the lower portion of the member. This stratigraphic marker has been widely used throughout the Morrison basin for placement of dinosaur quarries in the Morrison Formation (Peterson and Turner, 1993; Richmond and Stadtman, 1996; Richmond and Morris, 1998; Turner and Peterson, 1999) and correlation of depositional facies (Demko et al., 2004).

4. Western Oklahoma Morrison Formation

Mesozoic strata in the western Oklahoma panhandle are well exposed on buttes that are usually capped by the pervasive and highly weathering-resistant Cretaceous Dakota Sandstone. The Morrison Formation is usually exposed in its entirety but is commonly occluded by erosional debris of the Cheyenne and Dakota Sandstones. Stovall (1938a, b) proposed an angular unconformity between the Morrison and Cheyenne Formations; however, no angular unconformity was observed by us in any of the sections evaluated in Oklahoma, Colorado, or New Mexico. Our

exact measurements on Black Mesa itself are problematic due to formation slumping and a substantial amount of talus from the capping basalt. On the southeastern flank of Black Mesa several listric faults have rotated individual blocks away from the mesa into the valley. Each of these fault blocks (FB5, FB6, FB8; fig. 3) have historical quarries associated with them. Fortunately, the internal strata remain intact, although only partial Morrison sections and the capping Cretaceous strata are preserved. North of Black Mesa, there are fewer structural complexities, with the Triassic to Cretaceous strata exposed. Therefore, our regional sections were measured north of Black Mesa (fig 3). At Latimer Butte (SW ¼, SE ¼, Sec 20, T6N, R1E) the first complete regional stratigraphic section was measured (RS1). The Morrison Formation is 60 m thick at this location (RS1; figs. 3, 5) A second stratigraphic measurement (RS2; figs. 3, 5) was made at a small butte near the Oklahoma-New Mexico state line (NW ¼, SW ¼, Sec 18, T6N, R1E). The Morrison Formation at this location is slightly thinner at 54 m. A third section (RS3; figs. 3, 5) was measured at a butte on the eastern side of the North Carrizo Creek near the Oklahoma-Colorado state line (SE ¼, SE ¼, Sec 8, T6N, R1E). The Exeter Sandstone is not present in this section (RS3; figs. 3, 5), nor is it present in many outcrops west of the North Carrizo Creek. At this location, the Morrison Formation is 66 m thick and lies unconformably on the Sheep Pen Sandstone (Parker, 1933). A fourth complete section (RS4; figs. 3, 5) was measured at a small butte north of the Oklahoma-Colorado state line (SE ¼, SW ¼, Sec 12, T35S, R50W) and the formation is 52 m thick. However, based on correlations with other nearby sections, the lower part of the formation is likely faulted, with some of the section missing. We estimate the formation to be 55 m thick at this location. Variability in regional thickness is due to the unconformities at the base and top of the formation. In general, the Morrison Formation in the western panhandle of Oklahoma is 60 m, 82 m thinner than Stovall's 142 m thickness.

To verify our field sections (fig. 5), we compared our outcrop measurements to both historical and well log data. The Morrison Formation is present in the shallow subsurface (< 200 m depth) east of the study area and in the surrounding states. In the subsurface, the formation thins eastward to a zero edge (McKee et al., 1956, This study). The historical, newly acquired stratigraphic measurements, and log data of Oklahoma and the surrounding states were contoured (fig. 4). The isopach thicknesses corroborate a thinning trend eastward as it approaches the zero edge in the subsurface, where the formation cannot be discerned in the well logs. Further eastward Cretaceous strata rest on Triassic and Permian strata. The thinning of the formation eastward can be seen in the log cross section A–A' (figs. 4, 6). The isopach map shows variability in formation thickness likely due to erosional profiles of the J5 and K1 unconformities. In summary, the Morrison Formation as exposed at the surface and in the subsurface in the western Oklahoma panhandle is about 60 m thick and thins eastward (e. g. Bullard, 1928; fig. 4, B and proximal well log data, fig. 6). The formational thickness of surrounding states coincides with the thickness found in Oklahoma. These measurements correct those provided by Stovall (1938a, b; 1941a) and replicated throughout the published literature for more than 80 years.

5. Newly described members of the Morrison Formation of Oklahoma

5.1 Cimarron Member description

A tripartite division of the Morrison Formation in the western Oklahoma panhandle is recognizable. Herein we define three new Morrison Formation members for Oklahoma based upon numerous discernible lithologic criteria (table 1). The base of the lowest stratigraphic section of the formation is defined by the J5 unconformity (Pipiringos and O'Sullivan, 1978). Where the Exeter Sandstone is absent, as in places on the east side of the North Carrizo Creek, the member

rests unconformably on the Triassic Sheep Pen Sandstone (fig. 7A). The upper boundary of the Cimarron Member is defined by the top of the uppermost evaporite-associated chert bed (discussed below). There are relatively few locations where this lower stratigraphic section is well exposed, as it is usually covered by rock debris and vegetation. An exposed section, located several meters north of the Cimarron River at SE ¼, Sec 8, T5N, R1E is here defined as the type section for this member. For this reason, we name this lower unit the Cimarron Member of the Morrison Formation. A second section of the member is exposed 1 km north of the Oklahoma-Colorado border (SW ¼, Sec 7, T35N, R49E; fig. 7A). The Cimarron Member is similar to, and is in part stratigraphically similar to, the "Brown-Silt Member" of Union County, New Mexico.

The Cimarron Member is mudstone dominated with an average sandstone:mudstone ratio of 8.4. The predominately moderate brown mudstones are illitic. Kaolinite is also present throughout the member (fig. 8). The illite clay is not an illite/smectite (I/S) mixed clay as there is little smectite present. There is a color change from moderate brown to variegated mudstone in the Cimarron Member; however, there is no change in mineralogy.

All of the siltstone and sandstone beds of the member share the same moderate brown color. The siltstone and sandstone beds have a limited lateral extent and are thin-bedded (5–50 cm). The beds are usually thinly laminated with preserved wave-dominated and nearly symmetrical ripples (figs. 7B, C). The grains in the siltstone and sandstone are very angular (0.45), moderately well sorted (0.56), coarse-grained silt to fine-grained sand (3.96 Φ) quartz arenites (n = 10). A ubiquitous, prominent, 1 m thick, moderate brown sandstone bed is 7 m above the formation base in the Cimarron Member throughout the area. This sandstone is a subangular (1.36), well sorted (0.44), very fine-grained (2.97 Φ) quartz arenite. Grains often exhibit no grain-to-grain contact, with a sparry calcite cement signifying rapid cementation during deposition (figs. 9A, B).

5.1.1 Cimarron Member fossils and ichnofossils

No vertebrate or invertebrate fossils have been reported from the Cimarron Member. Ichnofossils are common for the Morrison Formation (Hasiotis and Kirkland, 1998; Hasiotis, 2004). Only one ichnofabric was observed on a ripple-laminated sandstone surface, consisting of small burrows of *Treptichnus*, a dipteran fly larva (Getty et al., 2016; Hogue, 2018). There are currently no known dinosaur remains from the Cimarron Member. Brown (1941) mentioned a "*Brontosaurus*"-type trackway being found in the Oklahoma panhandle. A sauropod trackway was collected in 1941 from the Cimarron riverbed about 37 km east of Kenton (Langston, 1989). It is likely the same trackway mentioned by Brown (1941). These trackways from north of Boise City were likely from the Cimarron Member, as it is the lowest unit exposed in the area along the Cimarron River. The collected trackway has since been lost (Langston, 1989). Presently, there are well-known dinosaur trackways exposed in Carrizo Creek, Coopers Arroyo (NE ¼, Sec 28, T6N, R1E) in the lower Morrison Formation (Mulvany and Mulvany, 1989; Hammond, 2013). These trackways are of the dinosaur ichnogenus *Gypsichnites*, a small herbivorous dinosaur (Conrad et al., 1987); and the theropod track, *Megalosauripus* (Hammond, 2013). These trackways are stratigraphically in the Cimarron Member.

5.1.2 Evaporite–associated chert beds

The upper boundary of the Cimarron Member is delineated by the top of the uppermost chert bed in the section. In the western Oklahoma panhandle, the evaporite-associated chert beds are stratigraphically between 14–17 m above the base of the Morrison Formation. The formation chert beds usually occur as a doublet, but can also occur as a single bed, and are between 10–20 cm thick. A 5-cm thick bedded dolomite is usually associated with the chert beds (fig. 7D, 7E). The

cherts are white with red or gray-blue chalcedony spherules, and occasionally mimic chicken-wire anhydrite. They consist of silica and authigenic minerals including dolomite, barite, and celestine. Anhydrite inclusions also occur. Rosettes of dolomite and barite are present at the base of the cherts. The silica fabric consists of euhedral quartz (> 2 mm), megaquartz grains, chalcedony spherules, length-slow and zebraic chalcedony, and "primrose" quartz. These silica structures form by infilling anhydrite dissolution cavities (Warren, 2016). The large euhedral grains, megaquartz, and length-slow chalcedony indicate a high silicon concentration in the phreatic brines during crystallization. Many of the euhedral quartz, chalcedony spherules, and "primrose" quartz display dust lines, which may signify changes in phreatic water chemistry or pH (fig. 9C). The chert is fractured, with sheared grains and chalcedony with sparry calcite cement later infilling voids and fractures (fig. 9D).

Similar to Magadi-type cherts, the cherts of the Oklahoma Morrison Formation are evaporite-associated cherts. These form in a shallow basic (pH > 9) phreatic zone as a result of silicification of sulfate evaporites (Warren, 2016). The member is about 17 m thick although variations in thickness may occur due to the erosional surface of the J5 unconformity and the specific evaporite-associated chert bed that is locally present.

5.1.3 Cimarron Member interpretation

The Cimarron Member represents deposition on a well-drained, low-lying planation surface dotted with small endorheic shallow clastic ephemeral lakes. The well sorted, very fine-grained, thin sandstone beds have limited lateral continuity and preserve symmetrical ripples and laminae (table 1). The siltstone and sandstone beds are interpreted to represent small endorheic shallow ephemeral clastic lakes. Closed lake basins experience expansion and contraction during climatic

fluctuations. The thin laminae of wave-dominated ripples indicate the lakes were shallow (< 100 cm). The clastic source for these small (< km^2 in size) shallow lakes was likely wind-blown sand and loess. Numerous ephemeral lakes and ponds were present during deposition of the Morrison Formation (Dunagan, 1999). Small clastic ephemeral lakes have been described previously for the Salt Wash Member (Owen, 2014; Owen et al., 2015).

As there is no evidence of a nearby elevated watershed or connective fluvial channels for the lakes of the Cimarron Member, the lakes probably represent paleotopographic depressions filled by local rainfall or regional aquifer groundwater. In general, lakes represented in the Morrison Formation appear to have formed in paleotopographic lows as a result of groundwater more than meteoric input (Dunagan, 1998). Groundwater fluctuations may have been common during deposition of the Morrison Formation (Demko et al., 2004) and would have been regulated by local tectonic settings, drainage patterns, seasonal precipitation, and temperature variations (Dubiel and Smoot, 1994). Freshwater springs are not considered to have been a key source to the hydrologic input (Dunagan, 1998). At least one laterally extensive, 1-m thick sandstone bed indicates the presence of a larger, longer-term shallow lake. In the Morrison Formation, shallow lakes are typically characterized by a varied aquatic invertebrate biota (Dunagan, 1998; 1999). Organismal diversity and distribution in the lacustrine environment are controlled by numerous factors including pH, salinity, oxygen, sediment texture, and drainage. Typical aquatic vertebrates of the Morrison Formation include crocodiles, turtles, amphibians, lungfish, and bony fish (e. g. Kirkland, 1998). Invertebrates include mollusks (pelecypods, gastropods, ostracods), crustaceans, semiaquatic and terrestrial insects (Scott et al., 2012).

The lack of evidence for even a depauperate aquatic biota suggests the shallow lakes may have been inhospitable. The preservation of the thin laminae and ripples indicates that the

sediments were not burrowed. The lakes may have been strongly alkaline, saline, too warm, or too muddy to support freshwater invertebrates (ostracods, gastropods, bivalves) or plants and algae (Dubiel and Smoot, 1994). If water is too warm, it will not hold sufficient oxygen for aquatic organisms to survive. The lakes may have occasionally dried completely, although no bioturbation or mudcracks were observed during the course of this study. Except for the evaporite-associated cherts that mark the upper boundary of the Cimarron Member, no evaporites have been reported for the Morrison Formation in Cimarron County, Oklahoma (Stovall, 1938b; Schoff and Stovall, 1943). McLaughlin (1954) mentioned gypsum in the Morrison Formation in eastern Las Animas County, Colorado. The well-drained lowlands and the shallow clastic ephemeral lakes suggest a seasonal semiarid climate with a highly variable rainfall (Dodson et al., 1980; Dunagan, 1998; Bernier and Chan, 2006). The antecedent lacustrine evaporites indicate a period of increased evaporation, due to either increased temperature or decreased precipitation or groundwater influx. The precipitation of gypsum and elevated alkalinity also indicate hydrologically closed lakes.

Sediments of the Cimarron Member were deposited at the distal margin of the foreland basin far from distributive fluvial sedimentation. Based on the member's stratigraphic position overlying the J5 unconformity and its lithologic similarities, the Cimarron Member may represent the distal alluvial plain depositional facies of the Tidwell Member. The Cimarron Member is similar lithologically to the Tidwell Member siltstone facies of Bernier and Chan (2006; fig. 2).

5.2 Boise Member description

The middle stratigraphic section of the Morrison Formation in the Oklahoma panhandle is dominated by mudstone, intercalated with thin limestone beds. The lower contact is defined as the uppermost evaporite-associated chert bed. The upper contact is characterized by a regionally

extensive 50-cm thick limestone bed overlain by a 1-m thick sandstone bed. This member is present in the Kenton area and in the surrounding states; however, because the capping lacustrine sandstone bed crowns the mesas north of the Cimarron River, north of Boise City, this stratigraphic section of related depositional facies is named the Boise Member of the Morrison Formation. An exposed section can be seen in the bluffs along E50 road at NW ¼, Sec 4, T5N, R5E and is defined as the type section for this member. A second section of the member is exposed at an isolated butte north of Boise City along highway 385 at SE ¼, Sec 16, T5N, R5E. The Boise Member can also be seen in the strata north of Kenton but resides in the fault blocks near Black Mesa or is occluded by Cretaceous rock debris. The variegated mudstones of the Boise Member are dominantly illitic. Kaolinite is also present throughout the member (fig. 8). The illite clay is not an illite/smectite (I/S) mixed clay as there is little smectite present.

The member includes numerous thin bedded (< 20 cm) limestone beds. Most of the limestone beds have a limited lateral extent. The limestone strata are thin-bedded microbial pelmicrites or pelsparites (fig. 10A). To demonstrate the variation of limestone beds, several limestone beds from the Kenton area are described in stratigraphic order. The stratigraphically lowest limestone bed is from the fault block at quarry 8 (OMNH V97; fig. 3), 18 m above the formation base. The limestone bed is a pelsparite with a small percentage of ooids having concentric bands of radial fabric. The peloids average 0.34 mm in diameter and are therefore medium-grained (1.66 Φ) and moderately sorted (0.55). Subrounded, very fine- to fine-grained quartz grains are scattered throughout the sparry calcite matrix and are likely eolian sourced. Some peloids envelop one or more quartz grains. Invertebrate fossils are rare consisting only of isolated thin-shelled bivalve fragments. Thin-shelled bivalves are usually autochthonous; this ecophenotype is typical of a lentic environment (Richmond et al., 2017; fig. 10B).

The limestone bed from the recent Homestead quarry (OMNH V1694; fig. 3) is 23 m above the formation base. This limestone bed is an ostracodal micrite. The ostracod shell rims are occasionally preserved with an infilling of dark, organic-rich micrite, whereas other ostracods were diagenetically replaced with sparry calcite. Some charophyte oogonia are also present (fig. 10C). From thin section neither the ostracods, nor charophytes can be identified taxonomically.

The fault block section of quarry 6 (OHMN V95; fig. 3) has two proximal limestone beds; the first at 28 m and the second at 32 m above the formation base. The stratigraphically higher limestone bed is a microbial pelsparite with both fine-grained (2.36 Φ), rounded peloids and thick platy microbial laminae (< 1 mm, fig. 10D). Subrounded, very fine- to fine-grained quartz is scattered throughout the sparry calcite matrix and is likely eolian-sourced.

The fault block section of quarry 5 (OHMN V94; fig. 3) has three closely spaced, thin-bedded limestones, each separated by a thin mudstone bed. The beds are about 32 m above the base of the formation and are capped by a thin sandstone bed. The lowest lacustrine limestone bed is a pelsparite similar to the pelsparite found at the quarry 8 locality, with a small percentage of ooids that have concentric bands of radial fabric. The average peloid diameter is 1.88 mm; they are medium-grained (1.85 Φ) and well sorted (0.46). There is a high percentage of subrounded, very fine- to fine-grained quartz scattered throughout the matrix, which are likely eolian sourced. Some peloids envelop one or more quartz grains. No invertebrate fossils or charophyte oogonia were observed (fig. 10E). The middle limestone bed is a 20-cm thick micrite with random circular *Skolithos*-like burrows that have a diameter of 0.185μ, a perimeter 0.573μ, and an area of 0.026μ^2. The burrows are likely from a subaqueous annelid. The upper limestone bed is a 20-cm thick sandy pelsparite with numerous subangular (1.37), well sorted (0.41), fine-grained (2.11 Φ) quartz grains. The peloids are either circular or oblong, medium-grained (1.98 Φ) and moderately well sorted

(0.55). No ooids or bivalves are present (fig. 10F). The 35-cm thick capping sandstone bed is a subangular (1.68), well sorted (0.42), fine-grained (2.40) quartz arenite and may be correlative to the other laterally extensive sandstone beds.

The limestone beds north of Boise City are different from the pelmicrites and pelsparites of the Kenton area. The limestone beds that cap the mesas north of Boise City are unfossiliferous, finely laminated, organic-rich micrites with scattered silt-sized quartz grains (fig. 10G). Also present are 2.6-mm thick laminae of peloids with intercalated lens of fine- to very fine-grained sand (fig. 10H).

The top of the Boise Member is defined by a regionally extensive couplet of a 50-cm thick microbial limestone bed (fig. 11A) that is capped by 1-m thick, subangular (1.56), well sorted (0.41), fine-grained (2.38 Φ) quartz arenite (n = 3) sandstone bed (fig. 11B).

5.2.1 Boise Member fossils and ichnofossils

Limestone beds themselves show a low species diversity of invertebrate fossils; the story is quite different for strata near the base of the Boise Member. A small accumulation of invertebrate fossils were collected by Stovall (Schoff and Stovall, 1943, p. 69) from a railroad cut (Sec 28 T5N, R5E) north of Boise City. We were unable to relocate the site during a recent field examination of the area due to modern grading of the railbed. However, based on a review of the local stratigraphy, the invertebrate site was likely from the lowest portion of the Boise Member. All specimens from the collection have been lost. The invertebrate fossils reported by Schoff and Stovall (1943) include the pelecypod *Vetulonaia whitei*, a thick-shelled ecophenotype bivalve, interpreted to have preferred a lotic environment. *V. whitei* is only known from the Morrison Formation (Evanoff et al., 1998). The gastropods from the collection included *Liratina jurassica*, a

prosobranch gastropod. Prosobranchs of the Morrison Formation are postulated as having lived in perennial well-oxygenated lentic environments (Evanoff et al., 1998). Another member of the assemblage, *Gyraulus veternus*, was a pulmonate gastropod and presumably tolerated both perennial and oxygen-poor lentic environments. Neither of these gastropod genera has any biostratigraphic significance for the Morrison Formation (Evanoff et al., 1998). Schoff and Stovall (1943) reported several taxa of ostracods, which they classified on the basis of a study by Roth (1933). Without the specimens in hand, taxonomic appraisal is problematic (B. Sames writ. comm., 2019). Two types of charophyte oogonia were found: *Aclistochara lata* and *Peckisphaera verticillata*. *A. lata* was a freshwater charophyte, whereas the environment for *P. verticillata* has not been established. Neither charophyte taxon has any biostratigraphic significance for the Morrison Formation (Schudack et al., 1998). Summing up, this collection of invertebrate and plant fossils found in the lower part of the Boise Member indicates the presence of a warm, clear, perennial, well-oxygenated pond, or lake.

The recently discovered Homestead quarry (OMNH V1694) located on the east side of Black Mesa. The quarry is associated with an ostracodal micrite which also represents a freshwater palustrine environment or small pond. The quarry has slumped Morrison and Cheyenne sediments nearby, but the quarry itself is in stratigraphic position 23 m above the J5 unconformity. This is the lowest dinosaur locality in the Morrison Formation of Oklahoma and the only quarry in the Boise Member. No vertebrate fossils from the site have been published to date, but the Homestead quarry is currently being worked.

Recently, three fossil wood genera were discovered from the Boise Member near Kenton, Oklahoma (Richmond et al., 2018a). These petrified woods are the first reported for the Morrison

Formation of Oklahoma. The stratigraphic position of the specimens is 30 m above the J5 unconformity.

The first fossil wood, *Xenoxylon meisteri* (OMNH 31654–31663), is the second regional occurrence for the Morrison Formation in North America. *X. meisteri* was first reported from the Morrison Formation of central Montana (Richmond et al., 2019). *X. meisteri* is previously known from Russia, China, and Japan. Its fossil distribution indicates that *Xenoxylon* grew in a cool, wet boreal climate (Philippe et al., 2013; Philippe et al., 2017) and its presence in Oklahoma is currently the southernmost North American occurrence of the genus. The second fossil wood genus, *Cupressinoxylon* (OMNH 31664–31676), is common in the Cretaceous of North America, but only one named Jurassic species has been recognized from the continent, *Cupressinoxylon jurassica* from South Dakota (Lutz, 1930). The Oklahoma specimen is similar to the South Dakota taxon. Some growth rings display disrupted growth, strongly suggestive of damage due to a surface fire. Extant Cupressaceae reside primarily in warm temperate regions. The third fossil wood genus is *Agathoxylon* (OMNH 31677–31695). Araucarians are known from other localities in the Morrison Formation (Scott, 1961; Tidwell and Medlyn, 1993; Gee and Tidwell, 2010; Gee et al., 2019). *Agathoxylon* is also known from the Jurassic of Europe (Philippe et. al., 1998; Philippe et al., 2015; Philippe et al., 2017), Mexico (Ríos-Santos and Cevallos-Ferriz, 2019), Cuba, (Haczewski, 1976), and Argentina (Kloster and Gnaedinger, 2018) and Chile (Torres and Philippe, 2002). Extant Araucariaceae grow in warm, humid climates with limited seasonal fluctuations (Tidwell and Medlyn, 1993). Due to their differing presumed climatic preferences, *Xenoxylon*, *Cupressinoxylon*, and *Agathoxylon* are very rarely associated in the fossil record (M. Philippe writ. comm., 2019).

Langston (1989) recalled seeing an additional set of collected dinosaur trackways between the years 1948–1953 assembled on the lawn of the University of Oklahoma Stovall Museum. He reported that the trackway was comprised of "pieces of limestone". The Boise Member contains numerous limestone beds, suggesting the trackway was from the Boise Member. The trackway, and any associated information have been lost, and with them, any possibility of verifying their stratigraphic position.

5.2.2 Boise Member interpretation

Carbonates are sensitive to environmental conditions. We interpret the limestone beds to have formed in perennial shallow endorheic lakes. Therefore, the Boise Member marks a transition from clastic lakes of the Cimarron Member to carbonate lakes, indicating the basin margin was starved of clastic input during deposition (Platt and Wright, 1991). Unlike the sandstone beds representing the ephemeral lakes of the Cimarron Member, the limestone beds of the perennial lakes of the Boise Member recorded a variety of depositional environments (table 1). The limestone beds frequently have algal fenestrae, which may be from cyanobacterial mats. Peloids, ooids, and thin-shelled bivalves are common allochems. The presence of the ooids, which may take thousands of years to form (Neese and Pigott, 1987), indicate low rates of clastic sedimentation at the time of formation (Swirydczuk et al., 1979; Dunagan, 1998) and a long-lasting presence to the lakes. The aragonitic radial and banded radial ooids form on peloids, indicating a hypersaline depositional setting (Medwedeff and Wilkinson, 1983). There are no associated deep-water or turbidite facies. The allochems and the lack of profundal facies indicate that the lakes were shallow (< 10 m).

The member's pelsparites signify sufficient wave activity to disperse mud-sized particles. The disruption of the algae laminae, rounded peloids and sparry calcite indicate high wave energy. Some pelsparites have a high sand grain percentage in a sparry calcite cement, indicating high wave energy, possibly from storms which destroyed cyanobacterial laminae or stromatolites, rounded the peloids, and transported fine-grained sand. In some pelsparites the majority of the sand grains are encased in a thin algal rind that likely formed after the passage of a storm event (fig. 9F). The carbonate petrology of the limestone beds north of the Boise City area indicate the beds were nearer to the depocenter of a large lake. The 2.6-mm thick laminae of peloids intercalated lens of fine- to very fine-grained sand is likely from storm events (figs. 9G, H).

There are no associated fluvial facies to indicate a watercourse input. Endorheic lakes are controlled by climate governing the net-water budget of the lake. Inflow is from either precipitation, groundwater, or springs with outflow solely from evaporation (Platt and Wright, 1991; Scott et al., 2012). Springs are not considered to have been a contributing aspect of the paleolakes (Dunagan, 1998). No subaerial biogenetic structures have been preserved indicating shoreline oscillations. There are no interbedded evaporites or subaerial exposure surfaces such as calcretes or desiccation cracks to indicate the lakes were ephemeral.

The abundant small, closed lakes on a low-gradient plain (Brady, 1969; Taylor, 1980; Tanner et al., 2014) were distal to the distributive fluvial system of the foreland. At the distal margin of the distributive fluvial system of the Salt Wash Member (Morrison Formation) are numerous small lakes (Owen et al., 2015). Similar lateral facies differentiation is found in the modern Brazilian Pantanal Basin (Assine and Silva, 2009; Assine et al., 2016).

The presence of numerous perennial endorheic carbonate lakes has tectonic and climatic implications, suggesting the basin periphery was sediment-starved during deposition and that

precipitation and/or groundwater influence exceeded the evaporation rate. The thinness of the limestone beds indicates the lakes formed in shallow paleotopographic depressions without substantial accommodation space, and yet were likely long-lived.

5.2.3 Lake Stovall

The limestone-sandstone bed couplet extends eastward from the Kenton to north of Boise City, westward to eastern New Mexico and northward to southeastern Colorado and may correlate to other reported lacustrine beds of southeastern Colorado and northeastern New Mexico (Frazier et al., 1983; Lockley et al., 1984; Lockley, 1986; Lockley et al., 1986; Neuhauser et al., 1987; Dunagan, 1998; Dunagan and Turner, 2004). West (1978) postulated that these lacustrine facies extended over 240 km^2. For comparison, Lake T'oo'dichi' a large alkaline, saline, paleolake identified in the Brushy Basin Member of the Morrison Formation of southwestern Colorado and northwestern New Mexico, had an aerial extent of approximately 170 km^2 (Turner and Fishman, 1991). Herein, we refer to the regionally extensive lacustrine strata of the Boise Member of the Oklahoma panhandle and the surrounding states as Lake Stovall in honor of the historical paleontologist who worked this remote area of Oklahoma.

The presence of Lake Stovall has climatic and tectonic implications. The large areal extent of the lake indicates sufficient precipitation or groundwater influx to overcome evaporation, filling the antecedent smaller lakes and leading to coalescence into a single waterbody. The transition from a microbial carbonate bed to a large clastic sandstone bed signals a dramatic increase in the sediment input to the basin margin. Sediment input could result from an increase in foreland tectonism (weathering and sediment supply), an increase in regional precipitation, the progradation of fluvial facies to the basin margin, or from a combination of all these factors. Formation of Lake

Stovall indicates a prolonged period of increased precipitation or groundwater. The large carbonate lake was then overwhelmed by clastic sediment and its accommodation space filled with the capping sandstone bed.

5.3 Kenton Member description

The Kenton Member records the transition from clastic and carbonate lakes of the two underlying members to fluvial deposition (table 1). The Kenton Member is a mud-dominated section with a low sandstone:mudstone ratio and with stratigraphically isolated sandstone beds (fig. 12A). The variegated mudstone shows variability in the percentage of illite, with several samples having a high percentage of smectite (fig. 8). Only a single thin limestone bed was observed in the member.

The sandstone beds of this member are best observed in the Kenton area; therefore, this stratigraphic section is referred to as the Kenton Member of the Morrison Formation. The section located at SE ½ Sec 8, T6N, R1E is defined as the type section for the Kenton Member. The lower contact of the Member is defined by the top of the regionally extensive lacustrine limestone/ sandstone bed couplet. The upper member boundary is the K1 unconformity (Pipiringos and O'Sullivan, 1978) and the overlying Lower Cretaceous Cheyenne Sandstone.

The small sandstone beds of the Kenton Member have a width:thickness ratio of 5.6 (n = 5) and are subangular (1.50), well sorted (0.41), fine-grained (2.33 Φ) quartz arenites (n = 7, fig. 9E). Associated with these small sandstone beds are flat-bottomed, laterally limited, thin, single story sandstone beds that are subangular (1.36), very well sorted (0.32), fine-grained (2.60 Φ) quartz arenites (n = 8, fig. 9F). Stratigraphically near the top of the Morrison Formation in the member is a thick amalgamated sandstone bed with a low width:thickness ratio (13). The sandstone is a

subrounded (2.03), well sorted (0.39), medium-grained (1.63 Φ) quartz arenite (*n* = 11, fig. 9G). The basal sandstone sediments consist of pebble, granule, very coarse- and coarse-grained sediments (0.60 Φ, 100-grain count). Most of the coarser grained fraction consists of well-rounded monocrystalline quartz; however, the largest subrounded grains including those of pebble and granule size are reworked sedimentary clasts (fig. 9H).

The small sandstone beds, showing a channel geomorphology, having a low width:thickness ratio, generally lacking lateral accretion sets, having abrupt lithofacies transitions, and consisting of finer-grained sediments are interpreted to be ephemeral anastomosing fluvial channels (Morris and Richmond, 1992; Hunt and Richmond, 2018). The flat-bottomed, single story sandstone beds are interpreted to be crevasse splays. In general, the splay sandstone beds are more fine-grained, better sorted, and slightly more angular than the fluvial sandstone beds.

Herein we distinguish between flood and crevasse splays. During normal flood stages, water tops the channel's levees bringing silt and clay sized particles to be deposited onto the floodplain (Fisher et al., 2008; Burns et al., 2019). This repeated flooding results in the aggradation of the floodplain (Shen et al., 2015). A recent study of the Late Holocene stratigraphic record of Mississippi delta sediments confirms that 95% of the splay deposits onto the floodplain are comprised of mud (Esposito et al., 2017). Frequent splay deposition impedes the formation of paleosols on the floodplain (Burns et al., 2019). In contrast, a crevasse splay occurs during an excessive flood stage where the levee wall is breached, cutting down to the channel bottom to release sand-size sediment onto the floodplain. Morrison Formation crevasse splay deposits are commonly thin (0.9 m average), single-story, structureless, sandstone beds (Burns et al., 2019). The average length of a crevasse splay sand bed from the Salt Wash Member of the Morrison Formation is 280 m (Burns et al., 2019). Flood energy and entrainment capacity on a low-lying

gradient are dissipated on the floodplain and quickly reduces the flood's competence to transport sediment. Kenton Member crevasse splay sandstone deposits are present but are not common.

The thick sandstone bed represents the amalgamation of several sandy, braided fluvial channels. The sandstone bed has large trough cross-sets indicating an eastward flow direction. This sandy, braided sandstone bed has numerous soft sediment deformation features including convolute and recumbent beds, sills, gas fluidization rings, fluid escape conduits, and possibly small sand volcanoes. The sandstone bed consists of two juxtaposed lithologic types: a hematitic sandstone and a chalcedony-cemented sedimentary quartzite. A sharp contact always segregates the two lithologic types although their positions in the sandstone bed are indiscriminate (fig. 12B). The undisturbed hematitic sandstone frequently displays protruding iron nodules and, in thin section, hematite grain rims and intergranular cement. At the top of the sandstone bed are small, coalescing hematitic rings, signifying gas fluidization. The chalcedony-cemented quartzite recumbent beds and concordant sills are mostly devoid of hematite. Occasionally, there are remnants of hematitic cement preserved. Various small fluid escape tubes and a 2.5-m long vertically oriented 6-cm diameter pipe signify a substantial amount of upward fluid migration by liquefaction or fluidization. Cumulatively, these structures are interpreted to be seismites (Richmond et al., 2018b).

5.3.1 Kenton Member fossils and ichnofossils

All of the Kenton area historical dinosaur quarries are stratigraphically within the Kenton Member and are bracketed within a 6 m section near the base of the member. In the Morrison Formation, it is a common occurrence for dinosaur bones to be incorporated into fluvial sandstone beds (Richmond and Stadtman, 1996; Morris et al., 1996; Richmond and Morris, 1998; Evanoff

and Carpenter, 1998; Heckert et al., 2003; Myers and Storrs, 2007; Mathews et al., 2009; Brezinksi and Kollar, 2018). However, to date no dinosaur bones have been observed or reported from the fluvial sandstone beds of the Morrison Formation in Oklahoma. All of the historical dinosaur quarries of Oklahoma are contained within mudstone strata. The stratigraphy, sedimentology, and taphonomy of the quarries is discussed more fully below.

No invertebrate fossils have been discovered. However, several ichnofossils have been discovered in the member (fig. 13). Ephemeral channel sandstone beds (quarry 8) show circular traces of *Cylindricum antiquus*, a burrowing beetle (Coleoptera) that constructed vertical tubes for shelter. Modern tiger beetles and their larvae shelter in subaerial portions of exposed channel bars where the capillary fringe is below the sand surface (Hasiotis and Demko, 1996). *Cylindricum* is thought to have preferred a moderately moist, subaerially exposed soil (Hasiotis et al., 2007). Another insect trace in the sandstone channel bed is interpreted to be a shallow termite nest. The nest's presence and size also indicate that the sand was moist at the time of formation (Hasiotis et al., 2007).

5.3.2 Kenton Member interpretation

Kenton Member sediments record a climate shift to a drier climate compared to the two lower members. It also marks the progradation of the distributive fluvial system to the backbulge basin margin (table 1). This is evidenced by the infilling of Lake Stovall with clastic sediment. After a period of time (during which the Kenton area dinosaurs died) deposition of crevasse splay and anastomosing fluvial channels occurred at the basin margin.

Anastomosing channels are relatively narrow and deep, with fine-grained sand carried along as bedload in the channel thalweg. Analysis of channel geomorphology and channel fill can

be used to determine the climatic regime under which the anastomosing fluvial systems were deposited; however, the strongest signal is given by the associated floodplain facies. In humid regions, there are higher rates of aggradation resulting in amalgamated channels. Anastomosing sandstone channels in this climatic regime typically have width:thickness ratios up to 30. Channel-fill sediments are organic-rich and have numerous associated crevasse splay sandstone beds. The interfluve sediments consist of lacustrine and palustrine deposits; coals are often present (Smith and Smith, 1980; North et al., 2007). In arid environments, there is a low rate of aggradation and channels are stratigraphically isolated. Channel width:thickness ratios are low and channel fill consist of finer grained sediments (e.g. mud or sand). There is a general absence of levees. Crevasse avulsions, lacustrine, palustrine, and organic deposits are largely absent from the floodplain (Rust, 1981; Nanson et al., 1986; North et al., 2007). The small anastomosing fluvial channel sandstone beds, the paucity of crevasse splay sandstone beds, and lacustrine and palustrine floodplain facies indicate a significantly drier climate than during the deposition of the Cimarron and Boise Members.

The fluvial channel geomorphology, sedimentology, and floodplain facies of the Kenton Member are similar to those of the Brushy Basin Member of the Colorado Plateau. It is reasonable to suggest that the Kenton Member is a continuation of the Brushy Basin distributive fluvial system prograding to the basin edge. Typically, there is a progression in fluvial geomorphology from the alluvial plain to the distributary channels consisting of braided (bedload), meandering (mixed load) to anastomosing (suspended load) fluvial channels (Galloway, 1979; Morris and Richmond, 1992). However, in the Kenton Member deposition rapidly transitioned from distributary anastomosing channels to a relatively large, sandy, braided channel without a record of the intermediate meandering fluvial channel geomorphology. This rapid change in fluvial geomorphology suggests

either an overfilled foredeep, an erosional breach or burial of the forebulge, allocating coarse grained alluvial sediments to the backbulge basin margin (Demko et al., 2004). This coarser grained material marks the first occurrence of this grain size to the basin margin of Oklahoma. Although the Kenton Member is likely correlative to the Brushy Basin Member on the Colorado Plateau, there is no definitive clay mineralogy change seen in the Morrison Formation of Oklahoma (fig. 8).

6. Stratigraphy, sedimentology, and vertebrate taphonomy of the historical Stovall dinosaur quarries

In 1931, Stovall was researching Pleistocene mammals in the Oklahoma panhandle when he was apprised of Jurassic dinosaur bones near Kenton, Oklahoma. When the Federal government instigated Depression relief programs, Stovall sought and received funding from the Works Progress Administration (WPA) to collect and prepare vertebrate fossils in Oklahoma. Excavation at the original discovery site (quarry 1) about 12 km east of Kenton and along the road linking that town to Boise City began in 1935. A concrete cast of a dinosaur femur, erected by a crew from the Sam Noble Museum, now marks the location of the quarry. Field crews worked the Kenton area until the WPA project was terminated in early 1942 (Langston, 1989), with the entry of the U.S. into WWII. According to the compilation of historical documents by Langston (1989), there were 12 fossil vertebrate localities identified in the Morrison Formation of Cimarron County, Oklahoma, at that time. Of these, some appear to have been prospects from which nothing recognizable was collected. Identifiable fossil material was recovered from five of the localities: Kenton quarries 1, 5, 6, 8, and 9 (OMNH localities V92, V94, V95, V97, and V98, respectively; see fig. 3). Unfortunately, the material housed in the collections at the Sam Noble Museum of Natural History (OMNH) may represent only some of the fossil taxa originally present in the quarries. According to

Wann Langston Jr. (1989), who was present at the time of collection, multiple collecting biases may have been introduced, most notably, a bias towards the collection of larger, more complete material. Additionally, many of the bones when found were encased in concretions and this may have obscured the collection of smaller fossils. Furthermore, geologic and taphonomic information was not recorded using modern collection practices. These biases make it difficult to look back through the decades and make confident inferences about the taphonomy and geology of the quarries and the bones therein.

To fill in some of the important contextual information concerning the fossils collected at the Kenton quarries under Stovall's direction, a stratigraphic re-evaluation of the Kenton area was undertaken, and the original Kenton quarries were placed in a stratigraphic context. All the known historical quarries that yielded fossils now present in the OMNH collection (Kenton quarries 1, 5, 6, 8, and 9) are from a 6 m stratigraphic section ranging from 33–39 m above the base of the formation. This mudstone-dominated stratigraphic section is between the laterally extensive sandstone bed that marks the top of the Boise Member and the first sandstone beds of the Kenton Member. This transition section records the change from the algal carbonate and sandstone lacustrine depositional facies (Boise Member; infilling of Lake Stovall) to the initial progradation of the distributive fluvial facies (Kenton Member) to the basin margin. All of the historical Stovall quarries are found within a mudstone matrix and each is topped by flood or crevasse splay deposits. The majority of these quarry-associated splay deposits are subsequently overlain by fluvial channel sandstone beds.

6.1 Quarry depositional environments and vertebrate taphonomy

To understand why the vertebrate quarries are restricted to this mudstone-dominated transition section, a review of the sedimentology and taphonomy of each quarry is presented. The data also provide additional information toward interpreting the paleoclimate during this interval.

Postmortem, prior to burial, a fleshy carcass rots resulting in skeletal disarticulation. An African elephant carcass requires three years to completely disarticulate (Coe, 1976; Hill and Behrensmeyer, 1984). The disarticulation of a large-sized dinosaur carcass, without the aid of scavenging, may have been a slower process. The rate of bone decomposition is dependent on duration of exposure, soil, and climate (Behrensmeyer, 1978). Based on bone weathering observations in Kenya, Behrensmeyer (1978), divided the process into 6 stages (0–5). The weathering stages are: unweathered bone (0); cracking, fat and skin may be present (1); flaking, ligaments cartilage and skin may be present (2); rough fibrous texture, tissue rarely present (3); cracks and splintering (4); and deep cracking and splintering with trabecular bone exposed (5). The bone may be difficult to identify at stage 5. Large and robust bones require a longer surface exposure to completely decompose. Bone weathering experiments in east Africa by Behrensmeyer (1978) demonstrated that in seven to eight years mammal bones were nearly decomposed. However, bones of large animals are identifiable after 35 years (Behrensmeyer and Miller, 2012). In temperate zones, bones can survive on the surface for over 100 years without burial (Miller, 2011). Severely weathered bones break during transport as they are dispersed (Behrensmeyer and Miller, 2012). This process results in numerous partial and fractured bones and also accounts for unrecognizable bone fragments. It should also be noted that many specimens in the OMNH collection with trabecular bone exposed may have been damaged during fossil preparation by

untrained laborers, who often could not distinguish between bone and rock matrix. However, this damage is usually easily recognized by tool marks.

Voorhies' (1969) flume experiment of disarticulated sheep and coyote skeletons has become the standard for bone dispersal studies in fluvial systems. Through repeated experimentation, Voorhies (1969) defined three bone dispersal sets. These sets are now commonly referred to as Voorhies Groups. Group 1 contains axial elements (vertebrate and pelvis), Group 2 comprises the appendicular skeleton (scapulae, limb bones, manus, and pes), whereas Group 3 elements include the skull and teeth. The presence of all three Voorhies Groups in a deposit indicates an autochthonous thanatocoenosis, or a low velocity hydrologic system incapable of winnowing the more mobile Group 1 elements. A fossil deposit skewed toward Groups 1 and 2 indicates a transported bone assemblage. Whereas a fossil deposit comprising of one Group represents a hydrologically sorted assemblage. The number of unique bone elements present in a fossil assemblage can be used to determine the minimum number of individuals (MNI) present in the thanatocoenosis. The numerical difference between the MNI present, the individual total bone count based on the genera, and number bones recovered during the excavation, can also provide insights into bone transport.

Hydrologic bone entrainment and transport is dependent on numerous complex variables of the bone interacting with the ground surface, the entrainment fluid, and the bone's properties. In short, the gradient and the grain size of the sediment surface will affect fluid flow velocities and turbulent flow. The main fluid properties are flow velocity and density. The higher the fluid velocity and density the greater the entrainment capacity. Fluid density is increased by a high suspended load. Bone properties such as bone volume, shape, density, age of the individual (juveniles have more trabecular bone and are less dense), bone freshness, wetness or dryness, and

bone fractures are just a few important factors which may affect entrainment. To simplify the variables and their complicated interactions, bone volume and density can be equated to a quartz grain size equivalent (Behrensmeyer, 1975). Using a modified flow velocity equation of Malde (1968) the minimum flow velocity for bone entrainment can be calculated (Richmond and Morris, 1998). Using a bone density of 1.47 g/cm^3 (Richmond and Morris, 1998), and the bone volume for a sauropod femur, the maximum flow velocity for each quarry deposit can be estimated. A concentrated suspended sediment load and a muddy bed surface can reduce the required fluid velocity to move large bones. Movement of large bones can also occur because flow is turbulent and instantaneous velocities exceeding the mean flow velocity can cause the intermittent movement of these elements (Hansen, 1980).

Quarry 9 (OMNH V98) is the stratigraphically lowest historical quarry, at 33 m above the J5 unconformity. The bones were excavated from a red illitic mudstone sandwiched between two sandstone beds. Below the quarry, 135 cm, is a 120-cm thick trough cross-bedded sandstone bed. A meter above the quarry mudstone bed is a laterally continuous, 100-cm thick, ripple-laminated sandstone bed. The lower bed is an angular (0.81), well sorted (0.42), fine-grained (2.16 Φ) quartz arenite, whereas the upper sandstone bed is a subangular (1.48), well sorted (0.39), fine-grained (2.68 Φ) quartz arenite, Both sandstone beds are interpreted to be a crevasse splay deposits. The trough cross-sets and the ripple laminae show a northeast flow direction. WPA crews collected a small number of specimens (n = 34) from the quarry; these have been identified only as Testudines indet., Archosauria indet., Crocodilia indet., and Sauropoda indet. No quarry map, if one was drawn, has been found in the archives and therefore no taphonomic interpretation can be provided. The aquatic elements of the fauna suggest that animals died at, or near, a waterhole. The majority of bones from quarry 9 show pronounced bone distortion and stage 5 bone weathering. Bone

distortion was likely caused by the dissolution of the bone's hydroxyapatite during residence in the local waterhole. After the evaporation of the waterhole, the bone had a prolonged surface duration and became highly weathered prior to transport and burial. Based on the estimated bone volume (3978 cm^3) for the largest sauropod pubis (OMNH 1778) and using the bone entrainment velocity equation, the estimated flow velocity was 159 cm/s. Based on the depositional facies of the quarry the bones were transported by a flood splay(s). Bone transport distance was limited.

Quarry 8 (OMNH V97), historically known as the "gator quarry", is located at 34 m above the J5 unconformity. The bone-bearing horizon at quarry 8 consists of a 20-cm thick, fossiliferous lacustrine smectitic mudstone, which grades vertically to a 50-cm thick, paludal mudstone facies. Capping the paludal facies locally is a 50-cm thick, 5-m wide, silty mudstone splay distributary channel. A 10-cm thick floodplain mudstone bed overlies the silty splay mudstone bed and grades into banded mudstone paleosols, indicating the complete desiccation of the waterhole.

Several multistory anastomosing fluvial channel sandstone beds overlie the waterhole desiccation sequence and many of the stacked sandstone beds are separated by 10-cm thick mudstone drapes. Mudcracks at the base of the sandstone beds were formed by the subaerial exposure of the point bar from ephemeral fluvial deposition. Southward migration of several lateral accretion sets suggests an eastward flow direction (fig. 12C). Several sandstone beds exhibit the ichnofossil *Cylindricum antiquus* formed on the upper surface of the abandoned channels.

Many fossils from quarry 8 are incomplete and display bone weathering . Bone weathering ranges from stage 1 to 4 with the majority of bones exhibiting stage 1 weathering features. More than half the specimens display distortion from the dissolution of bone hydroxyapatite after decomposing at the pond bottom. The exposed bones likely weathered for several years prior to burial by the silty mudstone flood splay deposit.

Unlike dinosaurs, aquatic vertebrates of the Morrison Formation rarely achieve local abundance, owing to their narrower original habitat requirements. The goniopholidid *Amphicotylus stovalli* (Mook, 1964) is well represented at quarry 8 (MNI 6). Using femur calculations and total length estimates for *Alligator mississippiensis* (Farlow et al., 2005), total length estimates for *A. stovalli* averaged 2.3 m, with one larger individual measuring 3.1 m. The aquatic fauna also includes the chelonids *Glyptops plicatulus* (3), and *Dinochelys whitei* (2), the lungfish *Ceratodus guentheri* and *C. frazieri*?, a small unidentified piscivorous osteichthyan (Hunt and Richmond, 2018) and an amiiform fish (Kirkland, 1987). Unidentified turtle remains are nearly as abundant as crocodilian teeth and scutes. The dinosaurian assemblage of quarry 8 includes one or more small ornithopods comprising of a *Camptosaurus*, an unidentified theropod (Bomberger, 2007), and a small basal tetanuran (Larsen, 2007).

The digital quarry map recreated from the original by Bomberger (2007) shows complete disarticulation and a seemingly random bone distribution with negligible association. All three Voorhies Groups are present. The thanatocoenosis is interpreted to be an attritional allochthonous deposit. Bone dispersal in the waterhole may have been from wave energy or faunal activity.

Quarry 1 (OMNH V92) is stratigraphically 38 m above the J5 unconformity. A period photograph shows the quarry matrix to consist of mudstone (Langston, 1989, fig. 56). One and half meters above the current quarry floor are two capping 20-cm thick sandstone beds separated by a 35-cm thick mudstone bed. The sandstone beds are interpreted to be crevasse splay sandstone deposits and are subangular (1.15), very well sorted (0.30), fine-grained (2.45 Φ) quartz arenites.

The majority of quarry 1 bones show stage 4 bone weathering from a prolonged surface duration prior to transport and burial. In at least one case, bone distortion of a large sauropod rib (OMNH 1554) from quarry 1 is interpreted to be the result of trampling by another large dinosaur.

Trampling of unburied or shallowly buried bones by dinosaurs has been documented elsewhere (Jennings and Hasiotis, 2006).

Quarry 1 was the most prolific quarry and yielded an estimated 3,500 bones (Stovall, 1937). The vast majority of these were unidentifiable fragments, however; the WPA workers were instructed to collect any and all pieces of bone. Of the 696 specimens from quarry 1 currently in the collection, Langston (1989) estimates that about 300 are informative. The minimum number of individuals represented from the quarry is 12. The genera include *Saurophaganax* (2), *Brachiosaurus* (1), *Apatosaurus* (4), *Camarasaurus* (2), a *Camptosaurus* and a *Stegosaurus*, and an extremely large apatosaurine with an estimated body mass of 36–80 tonnes (Wedel et al., 2002; Bonnan and Wedel, 2004; Bomberger, 2007; Wedel, 2013). Two of the apatosaurs and a camarasaur were juveniles. Given the genera present, and 12 individuals, the estimated bone count for the thanatocoenosis is 3,539. Only 696 bones (20%) are registered in the Oklahoma Museum of Natural History (OMNH) collection. As many as 2,843 bones and teeth are missing or remain unexcavated. Collection techniques and lost material may account for a small percentage of the loss, but more likely the variance represents bone dispersal. The quarry bones were likely mapped by the WPA workers, but the map has unfortunately been lost. Without the quarry map displaying bone associations, dispersal patterns cannot be determined. Based on the percentages of the Voorhies Groups, the bones underwent hydrologic sorting (fig. 14A). Based on the estimated bone volume (5094 cm3) for the largest sauropod femur (OMNH 1668) and using the bone entrainment velocity equation, the estimated flow velocity was 164 cm/s. The depositional facies of the quarry suggest that the bones were transported by a flood splay(s). Bone transport distance was limited.

Quarry 6 (OMNH V95) is 13.7 km northwest of quarry 1, along the southeastern margin of Black Mesa (fig. 3) but is stratigraphically equivalent at 38 m. Similar to quarry 9, the quarry 6

horizon is in an illitic mudstone is between several thin sandstone beds. Underlying the quarry is a 50-cm thick sandstone bed. Overlying the quarry mudstone is a 50-cm thick sandstone bed followed by a green 40-cm thick mudstone bed. Capping the 40-cm thick mudstone bed is a second 60-cm thick sandstone bed. The top sandstone is a subangular (1.62), well sorted (0.42), fine-grained (2.43 Φ) quartz arenite. The sandstone and mudstone beds are interpreted to be floodplain and crevasse splay deposits.

The MNI for the quarry is nine individuals including *Saurophaganax* (2), *Apatosaurus*, *Diplodocus* (2), *Camarasaurus, Stegosaurus*, *Camptosaurus*, and an unidentified archosaur (Bomberger, 2007). Given the genera present and the MNI, the expected quarry bone count is 2,743. Only 118 bones (4.3%) are registered in the OMNH collection. As many as 2,625 bones are missing or remain unexcavated. A review of the quarry 6 bone map (Bomberger, 2007) shows that bones are scattered into three areas of concentration over a distance of 48 m. Association of elements referable to the same individual is rare. The percentages of the Voorhies Groups show a transported thanatocoenosis with bones from only Groups 1 and 2 represented (fig. 14B). The majority of quarry 6 bones show stage 4 bone weathering from a prolonged surface exposure prior to transport and burial. Based on the estimated bone volume (4988 cm^3) for the largest sauropod femur (OMNH 1991) and using the bone entrainment velocity equation, the estimated flow velocity was 163 cm/s. Based on the depositional facies of the quarry the bones were transported by a flood splay(s). Bone transport distance was limited.

Quarry 5 (OMNH V94) is 39 m above the J5 unconformity and stratigraphically is the highest dinosaur locality in the Morrison Formation of Oklahoma Quarry. The quarry is located 0.8 km northeast of quarry 6 along the southeastern margin of Black Mesa (fig. 3).

The quarry consists of an illitic floodplain mudstone. Overlying the quarry floor is a 400-cm thick mudstone bed, topped by a crevasse splay complex consisting of a 60-cm thick, planar-laminated, sandstone bed, a 15-cm thick mudstone interval, and a second 30-cm thick sandstone bed. The sandstones are subangular (1.62), well sorted (0.42), fine-grained (2.43 Φ) quartz arenites. The capping, amalgamated, 130-cm thick, trough cross-bedded, fluvial channel sandstone bed is a subangular (1.59), well sorted (0.44), fine-grained (2.44 Φ) quartz arenite.

The MNI for quarry 5 is 14 individuals with genera including *Saurophaganax*, *Ceratosaurus*, *Apatosaurus* (3), *Diplodocus* (3), *Camarasaurus* (3)*, Stegosaurus*, *Camptosaurus*, and an unidentified sauropod (Bomberger, 2007). Given the genera present and the MNI, the predicted bone count is 4,414. Only 378 bones are registered in the OMNH collection. An estimated 4,036 bones are missing or remain unexcavated. A review of the quarry 5 map (Bomberger, 2007) shows bones are scattered over 9 bone concentrations over a distance of 44 m. Several of the bone concentrations show genus-associated elements (Bomberger, 2007). The remaining two areas have a minimal bone count.

The percentages of the Voorhies Groups show a transported thanatocoenosis with only Groups 1 and 2 represented (fig. 14C). The majority of quarry 5 bones show stage 4 bone weathering from a prolonged surface exposure prior to transport and burial. Based on the estimated bone volume (1357 cm^3) for the largest sauropod femur (OMNH 1815) and using the bone entrainment velocity equation, the estimated flow velocity was 138 cm/s. Based on the depositional facies of the quarry, the bones were transported by a flood splay(s). Bone transport distance was limited.

6.2 Taphonomic summary

The scattered bone concentrations, the lack of associated sand-sized sediments, and the Voorhies Group distributions indicate the bones were only transported a short distance and therefore represent autochthonous thanatocoenoses. The MNI and variation of genera represented indicate either an attritional death assemblage or a cataclysmic event. The disappearance of Lake Stovall, and the desiccation of the quarry 8 pond, suggest a drier climatic trend.

Isotopic data from quarry 8 and quarry 1 show a variable precipitation input and elevated temperature. Brundridge (2013) sampled $\delta^{18}O_{phosphate}$ from crocodile teeth (n = 25) and scutes (n = 2) and turtle carapace scutes (n = 16) from quarry 8. The average values for the fossils (–7.88 ± 2.11‰ $\delta^{18}O$ VSMOW) is within the range estimates of precipitation between –9‰ to –17‰ $\delta^{18}O$ VSMOW generated from pedogenic carbonates from the Morrison Formation (Dunagan and Turner, 2004). However, the quarry 8 crocodile and turtle $\delta^{18}O_{phosphate}$ data display large variabilities ranging from –2‰ to –12‰ $\delta^{18}O$ VSMOW. The considerable variations in $\delta^{18}O$ VSMOW values suggest seasonal variation in precipitation. The data can also be explained by more than one source of moisture (i.e. the Pacific Ocean and the newly formed Gulf of Mexico) (Brundridge, 2013). Using stable hydrogen and oxygen isotope values of pedogenic phyllosilicates from quarry 1 and a location near Dalhart, Texas, Myers et al. (2018) derived paleotemperatures ranging between 40 to 50º C. This high temperature range during the deposition of the Kenton Member transition interval complements the taphonomic evidence for the occurrence of droughts.

Droughts are common occurrences in modern (Weigelt, 1989) and ancient environments (Rogers and Sampson, 1989; Rogers, 1990; Richmond and Morris, 1998; Sankey, 2005; Jeffery et al., 2006). Shipman (1975) categorized the severity of drought into three progressive phases. Phase I is a mild drought where rainfall is less than normal. Seasonal waterholes and water courses dry

up. Large migratory animals relocate in search of food and water. Juvenile animals may succumb to drought-related stresses and exhibit increased mortality rates. Phase II is a severe drought. Precipitation continues to be deficient. Mobile animals move out of the area, whereas local animals become concentrated along waterways and at waterholes. Phase III is an extreme drought. Waterbodies dry completely, killing aquatic species, and terrestrial animals congregate at the last remaining water sources, ultimately dying of starvation and dehydration. An example of a Phase III drought in the Morrison Formation can be found at the Dry Mesa dinosaur quarry (Richmond and Morris, 1998). Here 30 genera of vertebrates, including juveniles from several genera of sauropods, were found in a single bone bed (Curtice and Wilhite, 1996; Richmond and Morris, 1998). Juvenile sauropods are rare in the Morrison Formation (Carpenter and McIntosh, 1994; Bonnan and Wedel, 2004). Only the Dry Mesa dinosaur quarry and quarry 1 contain juveniles of more than one sauropod genus (Curtice and Wilhite, 1996; Bonnan and Wedel, 2004).

The dinosaurs of the Kenton area quarries likely died from several recurring Phase I or Phase II droughts. Varying genera of dinosaurs congregated to local remaining waterholes and died. Interestingly, quarries 1 and 6 are stratigraphically equivalent and are separated spatially by 13.7 km. The dinosaurs from each assemblage likely died from the same drought event. Both sites have similar sized apatosaurs based on femora (180 and 181 cm).

Postmortem, the carcasses rotted, resulting in skeletal disarticulation. Most bones in the OMNH collection are incomplete, have trabecular bone exposed, are fractured (some with infilling sediment), indicating extensive bone weathering from a prolonged surface exposure prior to transport and burial. Post-drought bone transport and burial were from flood splay deposition. Splay flood energy and entrainment capacity are quickly dissipated on the floodplain and reduce the flood's competence to transport sediment and bone. Transport may have been accomplished by

single or multiple flood splay events. Therefore, the thanatocoenoses were relatively proximal to their present depositional sites.

7. Conclusions

The original stratigraphic measurement and interpretation by Stovall (1938a, b; 1941a) were incorrect and new stratigraphic measurements and well log data show the formation is approximately 60 m thick in the Kenton, Oklahoma area and rapidly thins to a zero-edge east of Boise City, Oklahoma. Prior to this study the Morrison Formation of this area was undifferentiated; we divide it herein into three newly described members (in ascending order: Cimarron, Boise, and Kenton Members), established by geological, geochemical, petrographic, and paleontological characteristics. Each member is defined by unique depositional facies recording a variable climatic signal and the eventual progradation of the distributive fluvial system to the basin margin. The Cimarron Member consists of numerous small ephemeral clastic lake deposits at the distal edge of the Morrison alluvial plain. The Boise Member consists of numerous perennial limestone lake deposits which, at the top of the member, coalesced into a large lake, called Lake Stovall. The Kenton Member records the progradation of the distributive fluvial system to the basin margin in Oklahoma. The first occurrence of fluvial deposition is represented by small, isolated, anastomosing fluvial channels and their associated splays. Stratigraphically near the top of the Kenton Member is a large sandy braided fluvial channel with a basal conglomerate. The large, sandy, braided fluvial channel recorded a major seismic event at the basin margin. Similar depositional facies suggest the Cimarron, Boise, and Kenton Members correlate to the Tidwell, Salt Wash and Brushy Basin Members of the Colorado Plateau. This indicates that deposition in the foreland basin was geographically extensive and deposition was slow at the basin margin.

All of the historical dinosaur quarries are found in a 6 m stratigraphic section in the basal portion of the Kenton Member. The depositional facies and taphonomic data suggest the dinosaurs died during a series of droughts. After skeletal disarticulation, and prolonged surface exposure, bone dispersal and burial occurred by ephemeral flood splay events.

Acknowledgments

We would like to thank the many ranchers in the Kenton, Oklahoma area who allowed access to their properties to complete this geologic survey. We especially want to express appreciation to Monty Joe and Vickie Roberts of Kenton, Oklahoma for their friendship and support during this project. We are grateful to Nate Murphy of the Judith River Dinosaur Institute, Billings, Montana, for the use of the Nikon total station which allowed for accurate measurements of the stratigraphy of the area. We thank Dr. Doug Elmore (OU) for support and funding for the investigative projects on the evaporite-associated cherts and the seismites. We acknowledge, with thanks, the logistic support of Reggie Whitten and Jeff Hargrave, and the financial support of the Whitten-Newman Foundation. We also thank Dr. Andy Madden (OU) for his instruction on sample preparation and utilization of the XRD for determining clay mineralogy. We thank Dr. Judith Totman Parrish, University of Idaho Professor Emerita, for her careful review of the paper.

References (formatted for submittal to the Journal of Geology)

Abbott, M. M. 1979. A basic evaluation of the uranium potential of the Morrison Formation of northwestern Cimarron County, Oklahoma and adjoining areas of New Mexico and Colorado. MS thesis, Oklahoma State University, Stillwater, OK, 92 p.

Anderson, O. J., and Lucas, S. G. 1997. The Upper Jurassic Morrison Formation in the Four Corners Region. New Mexico Geol. Soc. Guidebook 48:139–156.

Assine, M. L.; Merino, E. R.; Pupim, F. N.; Warren, L. V.; Guerreiro, R. L.; and McGlue, M. M. 2016. Geology and Geomorphology of the Pantanal Basin. *In* Bergier, I., Assine, M. L., eds. Dynamics of the Pantanal Wetland in South America. Handbook Environ. Chem. 37:23–50.

Assine, M. L., and Silva, A. 2009. Contrasting fluvial styles of the Paraguay River in the northwestern border of the Pantanal wetland, Brazil. Geomorph. 113:189–199.

Atalik, E., and Manfield, C. F. 1984. Dakota Sandstone facies, western Oklahoma panhandle. Am. Assoc. Pet. Geol. Bull. 68:449–450.

Bachman, G. O. 1953. Geology of a part of northwestern Mora County, New Mexico. U.S. Geol. Surv. Oil and Gas Invest. Map OM-137.

Baker, A. A.; Dane, C. H.; and Reeside, J. B., Jr. 1936. Correlation of Jurassic formations of parts of Utah, Arizona, New Mexico and Colorado. U.S. Geol. Surv. Prof. Pap. 183, 66 p.

Baldwin, B., and Muehlberger, W. R. 1959. Geologic studies of Union County, New Mexico. New Mexico Bur. Mines Miner. Res. Bull. 63:1–171.

Behrensmeyer, A. K. 1975. The taphonomy and paleoecology of Plio–Pleistocene vertebrate assemblages east of Lake Rudolf, Kenya. Mus. Comp. Zool. Bull. 146:473–578.

Behrensmeyer, A. K. 1978. Taphonomic and ecologic information from bone weathering. Paleobiol. 4:150–162.

Behrensmeyer, A. K., and Miller J. H. 2012. Build links between ecology and paleontology using taphonomic studies of recent vertebrate communities. *In* Louys, J., ed. Paleontology in Ecology and Conservation. Springer Earth Sys. Sci. p. 69–91.

Bernier, J.C., and Chan, M. A., 2006. Sedimentology, depositional environments, and paleoecological context of an early Late Jurassic sauropod, Tidwell Member, Upper Jurassic Morrison Formation, east-central Utah. Mount. Geol. 43:313–332.

Bonnan, M. F., and Wedel, M. J. 2004. First occurrence of *Brachiosaurus* (Dinosauria: Sauropoda) from the Upper Jurassic Morrison Formation of Oklahoma. PaleoBios 24:13–21.

Bomberger, C. N., 2007. Vertebrate fossil associations and taphonomy in the Morrison Formation (Upper Jurassic) Cimarron County, Oklahoma. MS thesis, University of Oklahoma, Norman, OK, 147 p.

Brady, L. L. 1969. Stratigraphy and petrology of the Morrison Formation (Jurassic) of the Canon City, Colorado, area. J. Sediment. Pet. 39:632–648.

Brake, S. S. 1982. Stratigraphic analysis of the Cheyenne Sandstone Member of the Purgatoire Formation (Lower Cretaceous), Northwestern Cimarron County, Oklahoma. Geol. Soc. Am. Abstr. Prog. 14:106.

Brezinski, D. K., and Kollar, A. D. 2018. Origin of the Carnegie quarry sandstone (Morrison Formation, Jurassic) at Dinosaur National Monument, Jensen, Utah. PALAIOS 33: 94–105.

Brown, B. 1941. Age of sauropod dinosaurs. Science 93:594–595.

Brundridge K. 2013. Assessing latitudinal variations in climate of the Jurassic Morrison Formation from oxygen isotopes from aquatic vertebrates. MS thesis, University of Texas, San Antonio, TX, 65 p.

Bullard, F. M., 1928. Lower Cretaceous of western Oklahoma: A study of the outlying area of Lower Cretaceous in Oklahoma and adjacent states. Oklahoma Geol. Surv. 47:7–116.

Burns, C. E.; Mountney, N. P.; Hodgson, D. M.; and Colombera, L. 2019. Stratigraphic architecture and hierarchy of fluvial overbank splay deposits. J. Geol. Soc. 176:629–649.

Cadigan, R. A. 1967, Petrology of the Morrison Formation in the Colorado Plateau Region. U.S. Geol. Surv. Prof. Pap. 556, 113 p.

Carpenter, K., and J. S. McIntosh. 1994. Upper Jurassic sauropod babies from the Morrison Formation. *In* Carpenter, K., Hirsch, K., and Horner, J. R., eds. Dinosaur Eggs and Babies. Cambridge University Press, Cambridge, p. 265–278.

Chure, D. J. 1995. A reassessment of the gigantic theropod *Saurophagus maximus* from the Morrison Formation (Upper Jurassic) of Oklahoma, USA. *In* Sun, A.-L., and Wang, Y.-Q., eds. Sixth Symposium on Mesozoic Terrestrial Ecosystems and Biota. China Ocean Press, Beijing. p. 103–106.

Chure, D. J.; Litwin, R.; Hasiotis, S. T.; Evanoff, E.; and Carpenter, K. 2006. The fauna and flora of the Morrison Formation: 2006. *In* Foster, J. R., Lucas, S. G., eds. Paleontology and Geology of the Upper Jurassic Morrison Formation. New Mexico Mus. Nat. Hist Sci. Bull. 36:233–249.

Coe, M., 1976. The decomposition of elephant carcasses in the Tsavo (East) National Park, Kenya. J. Arid Environ. 1:71–86.

Conrad, K.; Lockley, M. G.; and Prince, N. K. 1987. Triassic and Jurassic vertebrate–dominated trace fossil assemblages of the Cimarron Valley region: Implications for paleoecology and biostratigraphy. New Mexico Geol. Soc. Guidebook 38:127–138.

Cooley, B. B. Jr., 1956. Areal geology of Dry Cimarron Canyon, Union County, New Mexico. MS thesis, University of Texas, Austin, TX, 92 p.

Curtice, B. D., and Wilhite, D. R. 1996. A re-evaluation of the Dry Mesa Dinosaur Quarry sauropod fauna with a description of juvenile elements. *In* Huffman, A. C. Jr., Lund, W. R. and Godwin L. H. eds. Geology and Resources of the Paradox Basin, Utah Geol. Assoc. Guidebook 25:328–338.

Darton, N. H., 1905. Discovery of the Comanche Formation in southeastern Colorado. Science 22:120.

DeCelles, P. G., 2004. Late Jurassic to Eocene evolution of the Cordilleran thrust belt and foreland basin system, western U.S.A.: Am. J. Sci. 304:105–168.

DeFord, R. K., 1927. Areal geology of Cimarron County, Oklahoma. Am. Assoc. Pet. Geol. Bull. 11:753–755.

Demko, T. M.; Currie, B. S.; and Nicoll, K. A. 2004. Regional paleoclimatic and stratigraphic implications of paleosols and fluvial/overbank architecture in the Morrison Formation (Upper Jurassic), Western Interior, USA. Sediment. Geol. 167:115–135.

Demko, T. M.; Nicoll, K.; Beer, J. J.; Hasiotis, S. T.; and Park, L. E. 2005. Mesozoic lakes of the Colorado Plateau. *In* Pederson, J., and Dehler, C. M., eds. Interior Western United States: Geol. Soc. Am. Field Guide 6:1–28.

Dickinson, W. R., and Gehrels, G. E. 2008. Sediment delivery to the Cordilleran foreland basin: Insights from U-Pb ages of detrital zircons in Upper Jurassic and Cretaceous strata of the Colorado Plateau. Am. J. Sci. 308:1041–1082.

Dodson, P.; Behrensmeyer, A. K.; Bakker, R. T.; and McIntosh, J. S. 1980. Taphonomy and paleoecology of the dinosaur beds of the Jurassic Morrison Formation. Paleobiol. 6:208–232.

Dott, R. H. Jr. 1964. Wacke, graywacke and matrix–What approach to immature sandstone classification? J. Sediment. Pet. 34:625–632.

Doumit, P. E. 2005. Stratigraphy and paleoecology of the Upper Jurassic Morrison Formation in the Picket Wire Canyonlands, Comanche National Grasslands, southeastern Colorado. MS thesis, University of Northern Colorado, Greeley, CO, 109 p.

Doveton, J. H. 2007. Facies analysis of the Morrison Formation (Upper Jurassic) in Kansas based on petrophysical logs and drill-cuttings records. Am. Assoc. Pet. Geol. Search Discover Art. 90067.

Dubiel, R. F., and Smoot, J. P. 1994. Criteria for interpreting paleoclimate from red beds–A tool for Pangean reconstructions. Can. Soc. Pet. Geol. Mem. 17:295–310.

Dunagan, S. P. 1998. Lacustrine and palustrine carbonates from the Morrison Formation (Upper Jurassic), east-central Colorado, USA: Implications for depositional patterns, paleoecology, paleohydrology, and paleoclimatology. PhD dissertation, University of Tennessee, Knoxville, TN, 275 p.

Dunagan, S. P. 1999. Paleosynecology and taphonomy of freshwater carbonate lakes and ponds from the Upper Jurassic Morrison Formation (Western Interior, U.S.A.). Geol. Soc. Am. Abstr. Prog. 31:365.

Dunagan, S. P.; Driese, S. G.; and Walker, K. R. 1997. Paleolimnological implications of Magadi-type cherts from lacustrine carbonates in the Morrison Formation (Upper Jurassic) Colorado, U.S.A. Geol. Soc. Am. Abstr. Prog. 29:270.

Dunagan, S. P., and Turner, C. E. 2004. Regional paleohydrologic and paleoclimatic settings of wetland/lacustrine depositional systems in the Morrison Formation (Upper Jurassic), Western Interior USA. Sediment. Geol. 167:269–296.

Esposito, C. R.; Shen, Z.; Törnqvist, T. E.; Marshak, J.; and White, C. 2017. Efficient retention of mud drives land building on the Mississippi Delta plain. Earth Surf. Dynam. 5:387–397.

Eugster, H. P. 1967. Hydrous sodium silicates from Lake Magadi, Kenya: Precursors of bedded chert. Science 157:1177–1180.

Eugster, H. P. 1969. Inorganic bedded cherts from the Magadi area, Kenya. Contr. Mineral. Pet. 22:1–31.

Evanoff, E., and Carpenter, K. 1998. History, sedimentology, and taphonomy of Felch Quarry 1 and associated sandbodies, Morrison Formation, Garden Park, Colorado. *In* Carpenter, K., Kirkland, J., and Chure, D., eds. The Upper Jurassic Morrison Formation: An Interdisciplinary Study. Mod. Geol. 22:145–169.

Evanoff, E.; Good, S. C.; and Hanley, J. H. 1998. An overview of the freshwater mollusks from the Morrison Formation. *In* Carpenter, K., Kirkland, J., and Chure, D., eds. The Upper Jurassic Morrison Formation: An Interdisciplinary Study. Mod. Geol. 22:423–450.

Farlow, J. O.; Hurlburt, G. R.; Elsey, R. M.; Britton, A. R. C.; and Langston, W. Jr. 2005. Femoral dimensions and body size of *Alligator mississippiensis*: Estimating the size of extinct mesoeucrocodylians. J. Vert. Paleon. 25:354–369.

Fisher, J. A.; Krapf, C. B. E.; Lang, S. C.; Nichols, G. J.; and Payenberg, T. H. D. 2008. Sedimentology and architecture of the Douglas Creek terminal splay, Lake Eyre, central Australia. Sediment. 55:1915–1930.

Folk, R. L. 1959. Practical petrographic classification of limestones. Am. Assoc. Pet. Geol. Bull. 43:1–38.

Folk, R. L. and Ward, W. C., 1957, Brazos River Bar: A study in the significance of grain size parameters. J. Sediment. Pet. 27:3–26.

Frazier, F.; Houck, K.; Prince, N.; Vest, W.; and Coringrato, V. 1983. Interpretations of some depositional environments and paleoecology in the Morrison Formation of south eastern Colorado. Geol. Soc. Am. Abstr. Prog. 15:333–334.

Galloway, W. E. 1979. Morrison Formation of the Colorado Plateau. Depositional and ground-water flow systems in the exploration for uranium. Univ. Texas Bur. Econ. Geol., p. 214–228.

Gee, C. T.; Sprinkel, D. A.; Bennis, M. B.; and Gray, D. E. 2019. Silicified logs of *Agathoxylon hoodii* (Tidwell et Medlyn) comb. nov. from Rainbow Draw near Dinosaur National Monument, Uintah County, Utah, USA, and their implications for araucariaceous conifer forests in the Upper Jurassic Morrison Formation. Geol. Intermount. West 6:77–92.

Gee, C. T. and Tidwell, W. D. 2010. A mosaic of characters in a new whole-plant Araucaria, *A. delevoryasii* Gee sp. nov., from the Late Jurassic Morrison Formation of Wyoming, U.S.A. *In* Gee, C. T., ed. Plants in Mesozoic Time: Morphological Innovations, Phylogeny, Ecosystems. Indiana University Press Bloomington, Indianapolis, p. 67–94.

Getty, P. R.; McCarthy T. D.; Hsieh S.; and Bush A. M. 2016. A new reconstruction of continental *Treptichnus* based on exceptionally preserved material from the Jurassic of Massachusetts: J. Paleon. 90:269–278.

Gorman II, M. A.; Miller, I. M.; Pardo, J. D.; and Small, B. J. 2008. Plants, fish, turtles, and insects from the Morrison Formation; A Late Jurassic ecosystem near Cañon City, Colorado. Geol. Soc. Am. Field Guide 10:295–310.

Griggs, R. L., and Read, C. B. 1959. Revisions in stratigraphic nomenclature in Tucumcari-Sabinoso area, northeastern New Mexico. Am. Assoc. Pet. Geol. Bull. 43:2003–2007.

Gould, C. N. 1905. Geology and water resources of Oklahoma. U.S. Geol. Surv. Water-Supply and Irrigation Pap. 148, 178 p.

Haczewski, G. 1976. Sedimentological reconnaissance of the San Cayetano Formation; an accumulative continental margin in the Jurassic of western Cuba. Acta Geol. Polonica 26: 331–352.

Hammond, J. S. 2013. A slippery situation: Theropod tracks at Carrizo Creek, Cimarron County, Oklahoma. Geol. Surv. Am. Abstr. Prog. 45:326.

Hansley, P. L. 1986. Regional diagenetic trends and uranium mineralization in the Morrison Formation across Grants Uranium Region. Am. Assoc. Pet. Geol. Stud. Geol. 22:277–301.

Hansen, C. B., 1980, Fluvial taphonomic processes: models and experiments. *In* Behrensmeyer, A. K., and Hill, A. P. eds. Fossils in the making: vertebrate taphonomy and paleoecology: University of Chicago Press, p. 55–67.

Hart, D. L. Jr.; Hoffman, G. L.; and Geomaat, R. L. 1976. Geohydrology of the Oklahoma Panhandle, Beaver, Cimarron, and Texas counties, U.S. Geol. Surv. Water-Res. Invest. 25–75, 62 p.

Hasiotis, S. T. 2004. Reconnaissance of Upper Jurassic Morrison Formation ichnofossils, Rocky Mountain Region, USA: paleoenvironmental, stratigraphic, and paleoclimatic significance of terrestrial and freshwater ichnocoenoses. Sediment. Geol. 167:177–268.

Hasiotis, S. T., and Demko, T. M. 1996. Terrestrial and freshwater trace fossils, Upper Jurassic Morrison Formation, Colorado Plateau. *In* Morales, M. ed. The Continental Jurassic. Mus. N. Arizona Bull. 60:355–370.

Hasiotis, S. T., and Kirkland, J. I. 1998. Crayfish fossils and burrows (Decapoda: Cambaridae) Upper Jurassic Morrison Formation, Colorado Plateau, U.S.A. *In* Carpenter, K., Kirkland, J., and Chure, D., eds. The Upper Jurassic Morrison Formation: An Interdisciplinary Study. Mod. Geol. 22:481–491.

Hasiotis, S. T.; Kraus, M. J.; and Demko, T. M. 2007. Climate controls on continental trace fossils. *In* Miller, W. III, ed. Trace Fossils—Concepts, Problems, Prospects. Elsevier Press, p. 172–195.

Heckert, A. B.; Zeigler, K. E.; Lucas, S. G.; Spielmann, J. A.; Hester, P. M.; Peterson, R. E.; Peterson, R. E.; and D'Andrea, N. V. 2003. Geology and paleontology of the Upper Jurassic (Morrison Formation: Brushy Basin Member) Peterson Quarry, central New Mexico. New Mexico Geol. Soc. Guidebook 54:315–324.

Heller, P. L.; Ratigan, D.; Trampush, S.; Noda, A.; McElroy, B.; Drever, J.; and Huzurbazar, S. 2015. Origins of bimodal stratigraphy in fluvial deposits: An example from the Morrison Formation (Upper Jurassic), western U.S.A. J. Sed. Res. 85:1466–1477.

Hill, A.P.; Behrensmeyer, A. K. 1984. Disarticulation patterns of some modern East African mammals: Paleobiol. 10:366–376.

Hogue, J. D., 2018. Ichnotaxonomy of the Eocene Green River Formation, Soldier Summit and Spanish Fork Canyon, Uinta Basin, Utah: Interpreting behaviors, lifestyles, and erecting the *Cochlichnus* Ichnofacies. MS thesis, University of Kansas, Lawrence, KS, 171 p.

Hunt, A. P., and Lucas, S. G. 1987. J. W. Stovall and the Mesozoic of Cimarron Valley, Oklahoma and New Mexico. New Mexico Geol. Soc. Guidebook 38:139–151.

Hunt, T. C., and Richmond, D. R. 2018. The aquatic vertebrate community of a bone-dry pond: The historic Stovall Quarry 8, Morrison Formation in the panhandle of Oklahoma. Soc. Vert. Paleon. Abstr. Prog. 38:152.

Irwin, J. H., and Morton, R. B. 1969. Hydrogeologic information on the Glorieta Sandstone and the Ogallala Formation in the Oklahoma panhandle and adjoining areas as related to underground waste disposal. U.S. Geol. Surv. Circ. 630:1–26.

Jeffery, D. L.; Bertog, J. L.; and Bishop, J. R. 2006. Forced regression and lacustrine to fluvial transition of a Jurassic lake, Aaron Scott Quarry, San Rafael Swell, Utah. Geol. Soc. Am. Abstr. Prog. 38:388.

Jennings, D. S., and Hasiotis, S. T. 2006. Taphonomic analysis of a dinosaur feeding site using geographic information systems (GIS), Morrison Formation, southern Bighorn Basin, Wyoming, USA. PALAOIS 21:480–492.

Joeckel, R. M.; Ludvigson, G. A.; Wally, K. D.; and Doveton, J. H. 2007. Preliminary analysis of the Upper Jurassic Morrison Formation in the Rebecca Bounds core, western Kansas. Geol. Soc. Am. Abstr. Prog. 39:338.

Johnson, R. B. 1959. Geology of the Huerfano Park area, Huerfano and Custer counties, Colorado. U.S. Geol. Surv. Bull. 1071–D, 119 p.

Keller, W. D. 1962, Clay minerals in the Morrison Formation of the Colorado Plateau. U.S. Geol. Surv. Bull. 1150, 90 p.

Kirkland, J. I. 1987. Upper Jurassic and Cretaceous lungfish tooth plates from the Western Interior, the last dipnoan faunas of North America. Hunteria 2:1–16.

Kirkland, J. I, 1998. Morrison fishes. *In* Carpenter, K., Kirkland, J., and Chure, D., eds. The Upper Jurassic Morrison Formation: An Interdisciplinary Study. Mod. Geol. 22:503–533.

Kloster, A. C., and Gnaedinger, S. C. 2018. Coniferous wood of *Agathoxylon* from the La Matilde Formation, (Middle Jurassic), Santa Cruz, Argentina. J. Paleon. 92:546–567.

Kume, J., and Spinazola, J. M. 1984. Depth and thickness of selected units in Upper Permian, Upper Jurassic, and Lower Cretaceous rocks in southwestern Kansas. U.S. Geol. Surv. Water-Res. Invest. Rep. 83–4095, 7 maps.

Langston W., Jr. 1989. A history of vertebrate paleontology at the University of Oklahoma. Unpublished manuscript, Oklahoma Museum of Natural History, Norman, 107 p.

Larsen, J. M. 2007. Morphology and relationships of a small-medium theropod dinosaur from the Morrison Formation (Kimmeridgian-Tithonian), Cimarron County, Oklahoma. MS thesis, University of Oklahoma, Norman, OK, 43 p.

Lee, M. J., and Brookins, D. G. 1978. Rubidium-Strontium minimum ages of sedimentation uranium mineralization and provenance Morrison Formation (Upper Jurassic), Grants Mineral Belt, New Mexico. Am. Assoc. Pet. Geol. Bull. 62:1673–1683.

Lee, W. T. 1901. The Morrison Formation of southeastern Colorado. J. Geol. 9:343–352.

Lee, W. T. 1902. The Morrison shales of southern Colorado and northern New Mexico. J. Geol. 10:36–58.

Lockley, M .G. 1986. Morrison paleoichnology. Soc. Vert. Paleon. Abstr. Prog. 4:A29.

Lockley, M. G.; Houck, K. J.; and Prince, N. K. 1986. North America's largest dinosaur trackway site: Implications for Morrison Formation paleoecology. Geol. Soc. Am. Bull. 97:1163–1176.

Lockley, M. G.; Prince, N. K.; Houck, K.; and Carpenter, K. 1984. Reconstruction of a Late Jurassic ecosystem. Geol. Soc. Am. Abstr. Prog. 16:228.

Lucas, S. G.; Heckert, A. B.; Anderson, O. J. 1998. Stratigraphy of the Jurassic Entrada Sandstone in New Mexico. New Mexico Geol. 20:54–55.

Lucas, S. G.; Hunt, A. P.; and Hayden, S. H. 1987a. Triassic stratigraphy in the Dry Cimarron Valley, New Mexico, Colorado and Oklahoma. Geol. Soc. Am. Abstr. Prog. 19:316.

Lucas, S. G.; Hunt, A. P.; and Hayden, S. H. 1987b. The Triassic System in the Dry Cimarron Valley, New Mexico. New Mexico Geol. Soc. Guidebook 38:97–117.

Lucas, S. G.; Hunt, A. P.; and Hayden, S. H. 1987c. Type section of Exeter Member of Entrada Sandstone, Jurassic of northeastern New Mexico. New Mexico Geol. Soc. Guidebook 38:17–22.

Lucas, S. G.; Kietzke, K. K.; Hunt, A. P. 1985. The Jurassic System in east-central New Mexico. New Mexico Geol. Soc. Guidebook 36:213–242.

Lutz, H. J. 1930. A new species of *Cupressionoxylon* (Goeppert) Gothan from the Jurassic of South Dakota. Botan. Gaz. 90:92–107.

Malde, H. E. 1968. The catastrophic Late Pleistocene Bonneville flood in the Snake River Plain, Idaho. U.S. Geol. Surv. Prof. Pap. 596, 52 p.

Mankin, C. J. 1958a. Stratigraphy and sedimentary petrology of Jurassic and pre-Graneros Cretaceous rocks, northeastern New Mexico. PhD dissertation, University of Texas, Austin, TX, 208 p.

Mankin, C. J. 1958b. Sedimentary petrology of the Exeter Sandstone, northeastern New Mexico. Geol. Soc. of Am. Bull. 69:1609.

Mankin, C. J. 1972, Jurassic strata in northeastern New Mexico. New Mexico Geol. Soc. Guidebook 23:91–97.

Mathews, J. C.; Williams, S.; Henderson, M.; and Bonnan, M. F. 2009. The Hanksville-Burpee Quarry: A new dinosaur bonebed from the Brushy Basin Member, Morrison Formation (Latest Jurassic) of eastern Utah. Geol. Soc. Am. Abstr. Prog. 41:23.

McCarn, D. W.; Johnson, V. C.; and Theis, N. J. 1982. National uranium resource evaluation La Junta Quadrangle Colorado and Kansas, U.S. Depart. Energy Rep. PGJ/F–100, 27 p.

McKee, E. D.; Oriel, S. S.; Swanson, V. E.; MacLachlan, M. E.; MacLachlan, J. C.; Ketner, K. B.; Goldsmith, J. W.; Bell, R. Y.; Jameson, D. J.; and Imlay, R. W. 1956. Paleotectonic maps, Jurassic system. Misc. Geol. Invest. Map I–0175.

McLaughlin, T. G. 1942. Geology and ground-water resources of Morton County, Kansas. Kansas Geol. Surv. Bull. 40, 126 p.

McLaughlin, T. G. 1954. Geology and ground-water resources of Baca County, Colorado. U.S. Geol. Surv. Water-Supply Pap. 1256, 232 p.

Medwedeff, D. A., and Wilkinson, B. H. 1983. Cortical fabrics in calcite and aragonite ooids. *In* Peryt, T. M., ed. Coated grains. Springer-Verlag, Berlin Heidelberg, p. 109–115.

Merriam, D. F. 1955. Jurassic rocks in Kansas. Am. Assoc. Pet. Geol. Bull. 39:31–46.

Miall, A. D., and Turner-Peterson, C. E. 1989. Variations in fluvial style in the Westwater Canyon Member, Morrison Formation (Jurassic), San Juan Basin, Colorado Plateau. Sediment. Geol. 63:21–60.

Miller, J. H. 2011. Ghosts of Yellowstone: Multi-decadal histories of wildlife populations captured by bones on a modern landscape. PLoS ONE 6:18057.

Mook, C. C. 1916. Study of the Morrison Formation. Annals N.Y. Acad. Sci. 27:39–191.

Mook, C. C. 1964. New species of *Goniopholis* from the Morrison of Oklahoma. Oklahoma Geol. Notes 24:283–287.

Moore, D. M., and Reynolds, R. C. Jr. 1997. X-ray diffraction and the identification and analysis of clay minerals. Oxford University Press, New York, 378 p.

Morris, T. H., and Richmond, D. R. 1992. A predictive model of reservoir continuity in fluvial sandstone bodies of a lacustrine deltaic system, Colton Formation, Utah. *In* Fouch, T. D., and Nuncio, V. F., eds. Mineral and hydrocarbon resources of the Uinta Basin, Utah Geol. Assoc. Guidebook 20:227–236.

Morris, T. H.; Richmond, D. R.; and Grimshaw, S. C. 1996. Orientation of dinosaur bones in riverine environments: Insights into sedimentary dynamics and taphonomy. *In* Morales, M., ed. The Continental Jurassic. Mus. N. Arizona Bull. 60:521–530.

Mulvany, P. S., and Mulvany, J. O. 1989. Geological map revision of the Black Mesa region, Cimarron County, Oklahoma. Oklahoma Geol. Notes 49:4–40.

Myers, T. S., and Storrs, G. W. 2007. Taphonomy of the Mother's Day Quarry, Upper Jurassic Morrison Formation, south-central Montana, USA. PALAIOS 22:651–666.

Myers, T. S.; Tabor, N. J.; Eagle, R.; Bateman, J. B.; May, S.; Jacobs, L. L.; and Weil A. 2018. Paleoclimate of the Upper Jurassic Morrison Formation in Oklahoma and Texas. Geol. Soc. Am. Abstr. Prog. 50:162.

Nanson, G. C.; Rust, B. R.; and Taylor, G. 1986. Coexistant mud braids and anastomosing channels in an arid-zone river: Cooper Creek, central Australia. Geol. 14:175–178.

Neese, D. G., and Pigott, J. D. 1987. Ooid genesis at Brown's Cay, Bahamas: *In situ* diurnal observations. 8th Bathhurst Meet. Carb. Sediment. Liverpool, 31 p.

Neuhauser, K. R.; Lucas, S. G.; de Albuquerque, J. S.; Louden, R. J.; Hayden, S. H.; Kietzke, K. K.; Oakes, W.; and Des Marais, D. 1987. Stromatolites of the Morrison Formation (Upper Jurassic), Union County, New Mexico: A preliminary report. New Mexico Geol. Soc. Guidebook 38:127–138.

North, C. P.; Nanson, G. C.; and Fagan, S. D. 2007. Recognition of the sedimentary architecture of dryland anabranching (anastomosing) rivers. J. Sediment. Res. 77:925–938.

Ogden, L. 1954. Rocky Mountain Jurassic time surface. Am. Assoc. Pet. Geol. Bull. 38, 914–916.

Oriel, S. S., and Mudge, M. R. 1956. Problems of Lower Mesozoic stratigraphy in southeastern Colorado. Rocky Mount. Assoc. Geol. Guidebook to the Geology of the Raton Basin, Colorado, p. 19–24.

Owen, A. 2014. Analyses of the Salt Wash fluvial system; quantification of a distributive fluvial system in the Late Jurassic Morrison Formation, SW USA. PhD dissertation, University of London, UK, 362 p.

Owen, A.; Nichols, G. J.; Hartley, A. J.; Weissmann, G. S.; and Scuderi, L. A. 2015. Quantification of a distributive fluvial system: The Salt Wash DFS of the Morrison Formation, SW U.S.A. J. Sediment. Res. 85:544–561.

Parker, B. H. 1933. Clastic plugs and dikes of the Cimarron Valley area of Union County, New Mexico. J. Geol. 41:38–51.

Peterson, F. 1984. Fluvial sedimentation in a quivering craton: Influence of slight crustal movements on fluvial processes, Upper Jurassic Morrison Formation, western Colorado Plateau. Sed. Geol. 38:21–49.

Peterson, F. 1988. Pennsylvanian to Jurassic eolian transportation systems in the western United States. Sed. Geol. 56:207–260.

Peterson, F., and Turner, C.E. 1993. Relative age of dinosaur quarries in the Upper Jurassic Morrison Formation–a stratigraphic approach. Soc. Vert. Paleon. Abstr. Prog. 13:52A.

Peterson, F., and Turner-Peterson, C. E. 1980. Lacustrine-humate model; sedimentologic and geochemical model for tabular sandstone uranium deposits in the Morrison Formation, Utah, and application to uranium exploration. U.S. Geol. Surv. Open File Rep. 46, 43 p.

Peterson, F., and Turner-Peterson, C. E. 1987. The Morrison Formation of the Colorado Plateau: Recent advances in sedimentology, stratigraphy, and paleotectonics. Hunteria 2:1–18.

Philippe, M.; Pacyna, G.; Wawrzyniak, Z.; Barbacka, M.; Boka, K.; Filipiak, P.; Marynowski, L.; Thévenard, F.; and Uhl, D. 2015. News from an old wood–*Agathoxylon keuperianum* (Unger) nov. comb. in the Keuper of Poland and France. Rev. Palaeobot. Palynol. 221:83–91.

Philippe, M.; Puijalon, S.; Suan, G.; Mousset, S.; Thévenard, F.; and Mattioli, E. 2017. The paleolatitudinal, distribution of fossil wood genera as a proxy for European Jurassic terrestrial climate. Palaeogeo. Palaeoclim. Palaeoecol. 466:373–381.

Philippe, M.; Thévenard, F.; Barale, G.; Ferry, S.; and Guignard, G. 1998. Middle Bathonian floras and phytocoenoses of France. Palaeogeo. Palaeoclim. Palaeoecol. 143:135–158.

Philippe, M.; Thévenard, F.; Nosova, N.; Kim, K.; and Naugolnykh, S. 2013. Systematics of a palaeoecologically significant boreal Mesozoic fossil wood genus, *Xenoxylon* Gothan. Rev. Palaeobot. Palynol. 193:128–140.

Pipiringos, G. N., and O'Sullivan, R. B. 1978. Principal unconformities in Triassic and Jurassic rocks, Wester Interior United States – A preliminary survey. U.S. Geol. Surv. Prof. Pap. 1035–A, 29 p.

Platt, N. H., and Wright, V. P. 1991. Lacustrine carbonates: facies models, facies distributions and hydrocarbon aspects. Spec. Pub. Int. Assoc. Sediment. 13:57–74.

Richmond, D. R.; Hunt, T. C.; and Elmore, D. 2018b. Shake, rattle, and roll: Late Jurassic earthquake recorded in Morrison Formation fluvial sediments of western Oklahoma. Geol. Soc. Am. Abstr. Prog. 50:6.

Richmond, D. R.; Lukens, M. W.; and Celestino, S. M. 2017, Upper Jurassic Morrison Formation clams on the half shell, central Montana. Geol. Soc. Am. Abstr. Prog. 49:4.

Richmond, D. R.; Lupia, R.; Hunt, T. C.; and Philippe, M. 2018a. The first fossil woods from the Upper Jurassic Morrison Formation of western Oklahoma. Geol. Soc. Am. Abstr. Prog. 50:5.

Richmond, D. R.; Lupia, R.; Philippe, M.; and Klimek, J. 2019. First occurrence of the boreal fossil wood *Xenoxylon meisteri* from the Jurassic of North America: Morrison Formation of central Montana, USA. Rev. Palaeobot. Palynol. 267:39–53.

Richmond, D. R., and Morris, T. H. 1998. Stratigraphy and cataclysmic deposition of the Dry Mesa Dinosaur Quarry, Mesa County, Colorado. *In* Carpenter, K., Kirkland, J., and Chure, D., eds. The Upper Jurassic Morrison Formation: An Interdisciplinary Study. Mod. Geol. 22:121–143.

Richmond, D. R., and Stadtman, K. L. 1996. Sedimentology of a *Ceratosaurus* site in the San Rafael Swell, Emery County, Utah. Brigham Young University Geol. Studies 41:117–124.

Ríos-Santos, C., and Cevallos-Ferriz, S.R.S. 2019. Upper Jurassic, Upper Cretaceous and Paleocene conifer woods from Mexico. Earth Environ. Sci. Trans. Royal Soc. Edinburgh 108:399–418.

Robinson, J. W., and McCabe, P. J. 1997. Sandstone-body and shale-body dimension in a braided fluvial system: Salt Wash Sandstone Member (Morrison Formation). Garfield County, Utah. Am. Assoc. Pet. Geol. Bull. 81:1267–1291.

Rogers, R. R. 1990. Taphonomy of three dinosaur bone beds in the Upper Cretaceous Two Medicine Formation of northwestern Montana; evidence for drought-related mortality. PALAIOS 5:394–413.

Rogers, R. R., and Sampson, S. D. 1989. A drought-related mass death of ceratopsian dinosaurs (Reptilia; Ornithischia) from the Two Medicine Formation (Campanian) of Montana; behavioral implications. J. Vert. Paleon. Abstr. Prog. 9:144.

Roth, R. I. 1933, Some Morrison Ostracoda. J. Paleon. 7:398–405.

Rothrock, E. P. 1925. Geology of Cimarron County Oklahoma. Oklahoma Geol. Surv. Bull. 34, 110 p.

Rust, B. R. 1981. Sedimentation in an arid-zone anastomosing fluvial system: Cooper's Creek, central Australia. J. Sediment. Pet. 51:745–755.

Sanders, C. W. 1934. Geology of Two Buttes Dome in southeastern Colorado. Am. Assoc. Pet. Geol. Bull. 18:860–870.

Sankey, J. T. 2005. Drought, fires, dinosaurs, eggs, and babies in the Late Cretaceous of Big Bend National Park, Texas. PaleoBios, 25:101.

Schoff, S. L., and Stovall, J. W. 1943. Geology and ground water resources of Cimarron County, Oklahoma. Oklahoma Geol. Soc. Bull. 64, 317 p.

Schubel, K. A., and Simonson, B. M. 1990. Petrology and diagenesis of cherts from Lake Magadi, Kenya. J. Sediment. Pet., 60:761–776.

Schudack, M. E.; Turner, C. E.; and Peterson, F. 1998. Biostratigraphy, paleoecology and biogeography of charophytes and ostracodes from the Upper Jurassic Morrison Formation, Western Interior, USA. *In* Carpenter, K., Kirkland, J., and Chure, D., eds. The Upper Jurassic Morrison Formation: An Interdisciplinary Study. Mod. Geol. 22:379–414.

Scott, R. A., 1961. Fossil woods associated with uranium on the Colorado Plateau. U.S. Geol. Surv. Prof. Pap. 55: B130–B132.

Scott, J. J.; Buatois, L. A.; and Mángano, M. G. 2012. Lacustrine environments. Develop. Sediment. 64:379–417.

Shead, A. C. 1923. Notes of the Black Mesa basalt. Proc. Oklahoma Acad. Sci. 3:108–113.

Shen, Z.; Törnqvist, T. E.; Mauz, B.; Chamberlain, E. L.; Nijhuis, A. G.; and Sandoval, L. 2015. Episodic overbank deposition as a dominant mechanism of floodplain and delta-plain aggradation. Geol. 43:875–878.

Shipman, P. 1975. Implications of drought for vertebrate assemblages. Nature 257:667–668.

Small, B. J.; Gorman, M. A.; Pardo, J.; and Smith, D. 2007. A Late Jurassic lacustrine biota from the Morrison Formation of Colorado. Geol. Soc. Am. Abstr. Prog. 39:400.

Smith, D. G., and Smith N. D. 1980. Sedimentation in anastomosed river systems: Examples from alluvial valleys near Banff, Alberta. J. Sediment. Pet. 50:157–164.

Snoparsky, M. B. 1982. The Exeter Sandstone (Upper Jurassic) of the Black Mesa area, Cimarron County, Oklahoma. Geol. Soc. Am. Abstr. Prog. 14:136.

Snoparsky, M. B. 1986. Depositional environments and provenance of the Exeter Sandstone of Cimarron County, Oklahoma, and adjacent parts of Union County, New Mexico. MS thesis, University of Tulsa, Tulsa, OK, 106 p.

Snoparsky, M. B. 1987. The Exeter (Entrada) Sandstone of Cimarron County, Oklahoma and adjacent parts of Union County, New Mexico. New Mexico Geol. Soc. Guidebook 38:12–14.

Stanton, T. W. 1905. The Morrison Formation and its relations with the Comanche series and the Dakota Formation. J. Geol. 13:657–669.

Stokes, W. L. 1944. Morrison Formation and related deposits in and adjacent to the Colorado Plateau. Geol. Soc. Am. Bull. 55:951–992.

Stovall, J. W. 1932. The Jurassic in Oklahoma. Science 76:122–123.

Stovall, J. W. 1937. Advance notes on the Geology of Cimarron Valley of western Oklahoma. Proc. Oklahoma Acad. Sci. 17:78–79.

Stovall, J. W. 1938a. Geology of the Cimarron River Valley in Cimarron County, Oklahoma. Unpublished Ph.D. dissertation, University of Chicago, Chicago, IL, 60 p.

Stovall, J. W. 1938b. The Morrison of Oklahoma and its dinosaurs. J. Geol. 46:583–600.

Stovall, J. W. 1941a. The Mesozoic rocks of the Oklahoma panhandle: Including an area in northeastern New Mexico. Oklahoma City Geol. Soc. Field Confer. p. 1–20.

Stovall, J. W. 1941b. Notes on the stratigraphy of Cimarron County, Oklahoma. Oklahoma City Geol. Soc. Field Confer. p. 21–30.

Stovall, J. W. 1942. The Mesozoic of western Oklahoma. Tulsa Geol. Soc. Digest 10:70–71.

Suneson, N. H. 2012. Black Mesa Basalt. J. Oklahoma Geol. Soc. 63:24–32.

Suneson, N. H. 2020. Roadside geology of Oklahoma. Mount. Press Pub. Comp. Missoula, Montana, p. 384.

Suneson, N. H., and Luza, K. V. 1999. A field trip guide to the geology of the Black Mesa State Park area, Cimarron County, Oklahoma. Oklahoma Geol. Surv. Open File Rep. 4-99, 52 p.

Surdam, R. C.; Eugster, H. P.; and Mariner, R. H. 1972. Magadi-type chert in Jurassic and Eocene to Pleistocene rocks, Wyoming. Geol. Soc. Am. Bull. 83:2261–2266.

Swirydczuk, K.; Wilkinson, B. H.; and Smith, G. R. 1979. The Pliocene Glenns Ferry Oolite: Lake-margin carbonate deposition in the southwestern Snake River Plain. J. Sediment. Pet. 49:995–1004.

Szigeti, G. J. and Fox, J. E. 1981. Unkpapa Sandstone (Jurassic), Black Hills, South Dakota: an eolian facies of the Morrison Formation. *In* Ethridge, F. G. and Flores, R. M. eds. Recent and ancient nonmarine depositional environments: models for exploration. SEPM Spec. Publ. 31:331–349.

Tanner, L.H., Galli, K.G., Lucas, S.G., 2014. Pedogenic and lacustrine features of the Brushy Basin Member of the Upper Jurassic Morrison Formation in western Colorado: Reassessing the paleoclimatic interpretations. Volumina Jurassica X11:115–130.

Taylor, A. M. 1980., Depositional environments of the Dakota Sandstone in southeastern Colorado. SEPM Guidebook Trip 3, 69 p.

Tidwell, W. D., and Medlyn, D. A. 1993. Conifer wood from the Upper Jurassic of Utah, Part II: *Araucarioxylon hoodii* sp. nov. Palaeobot. 42:1–7.

Torres, T., and Philippe, M. 2002. Nuevas especies de *Agathoxylon* y *Baieroxylon* del Liásico de La Ligua, Chile, y evaluación de antecedentes paleoxilológicos en el Jurásico de America del Sur. Revista Geol. de Chile 29:151–165.

Turner, C. E., and Fishman, N. S. 1991. Jurassic Lake T'oo'dichi': A large alkaline, saline lake, Morrison Formation, eastern Colorado Plateau. Geol. Soc. Am. Bull. 103:538–558.

Turner, C. E., and Peterson, F. 1999. Biostratigraphy of dinosaurs in the Upper Jurassic Morrison Formation of the Western Interior, U.S.A. Utah Geol. Surv. Misc. Pub. 99-1:77–114.

Turner-Peterson, C. E., and Fishman, N. S. 1986. Geologic synthesis and genetic models for Uranium mineralization in the Morrison Formation, Grants Uranium Region, New Mexico. Am. Assoc. Pet. Geol. Stud. 22:357–388.

Voorhies, M., 1969. Taphonomy and population dynamics of an early Pliocene vertebrate fauna, Knox County, Nebraska. Contrib. Geol. Univ. Wyoming Spec. Pap. 1, 69 p.

Warren, J. K. 2016. Evaporites: A geological compendium. Springer Inter. Pub. 1813 p.

Wedel, M. J. 2013. A giant, skeletally immature individual of *Apatosaurus* from the Morrison Formation of Oklahoma. Symp. Vert. Paleon. Comp. Anat. p. 40.

Wedel, M. J.; Bonnan, M. F.; Sanders, R. K. 2002, Two previously unreported sauropod dinosaurs from the Upper Jurassic Formation of Oklahoma. J. Vert. Paleon. Abstr. Prog. 22:118.

Weigelt, J. 1989. Recent vertebrate carcasses and their paleobiological implications. Univ. Chicago Press, 188 p.

West, E. S. 1978. Biostratigraphy and paleoecology of the lower Morrison Formation of Cimarron County, Oklahoma. MS thesis, Wichita State University, Wichita, KS, 61 p.

Wood, G. H.; Jr.; Northrop, S. A.; and Griggs, R. L. 1953. Geology and stratigraphy of Koehler and Mount Laughlin quadrangles and parts of Abbott and Springer quadrangles, eastern Colfax County, New Mexico. U.S. Geol. Surv. Oil and Gas Invest. Map 141.

Figures

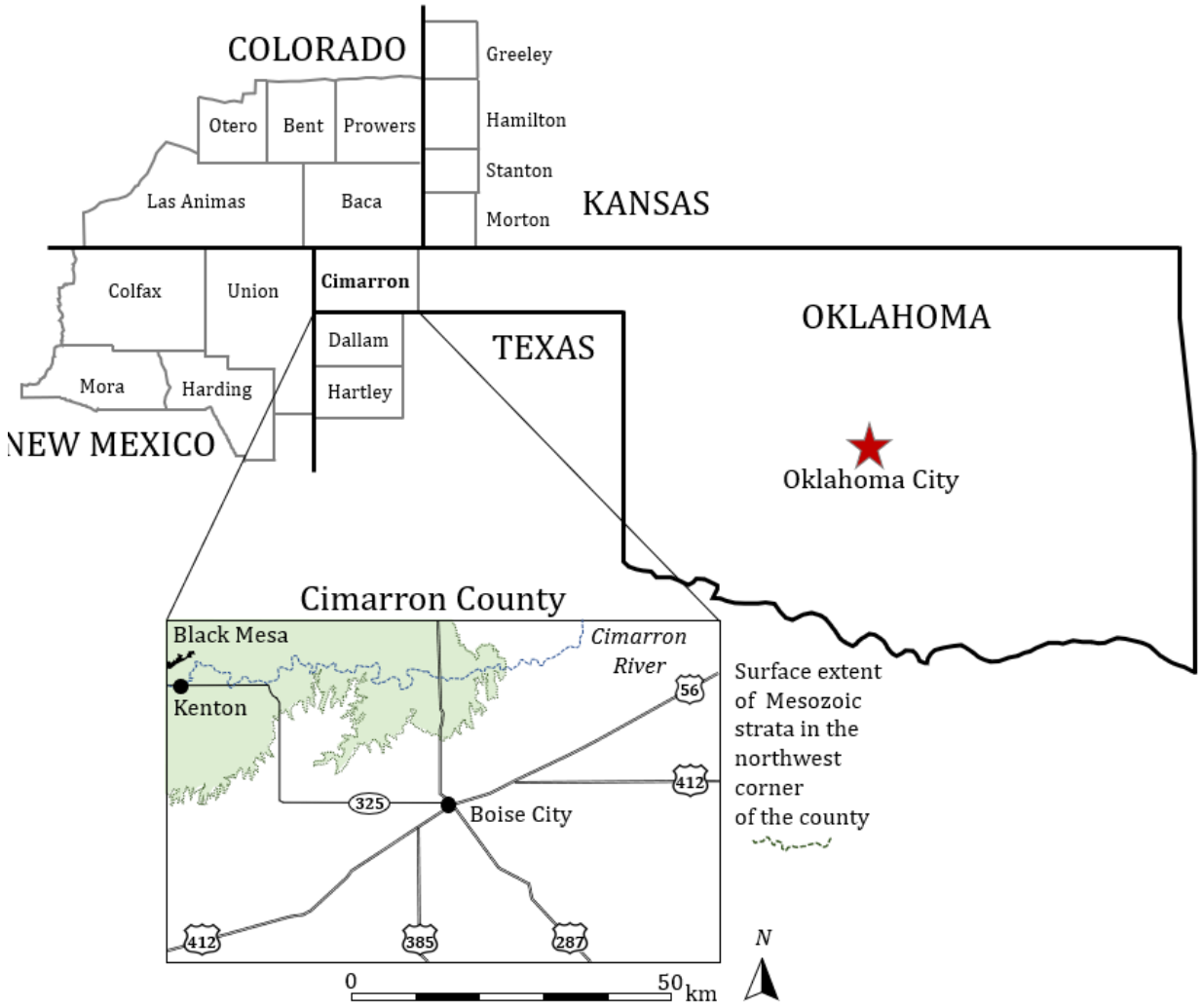

Figure 1. The study area of the Morrison Formation in the western panhandle of Oklahoma. In the northwest portion of Cimarron County, Oklahoma, Mesozoic strata are exposed at the surface. In the remainder of the county, the strata are in the subsurface. Counties of surrounding states are included for information pertaining to the historical references of the Morrison Formation and well log data.

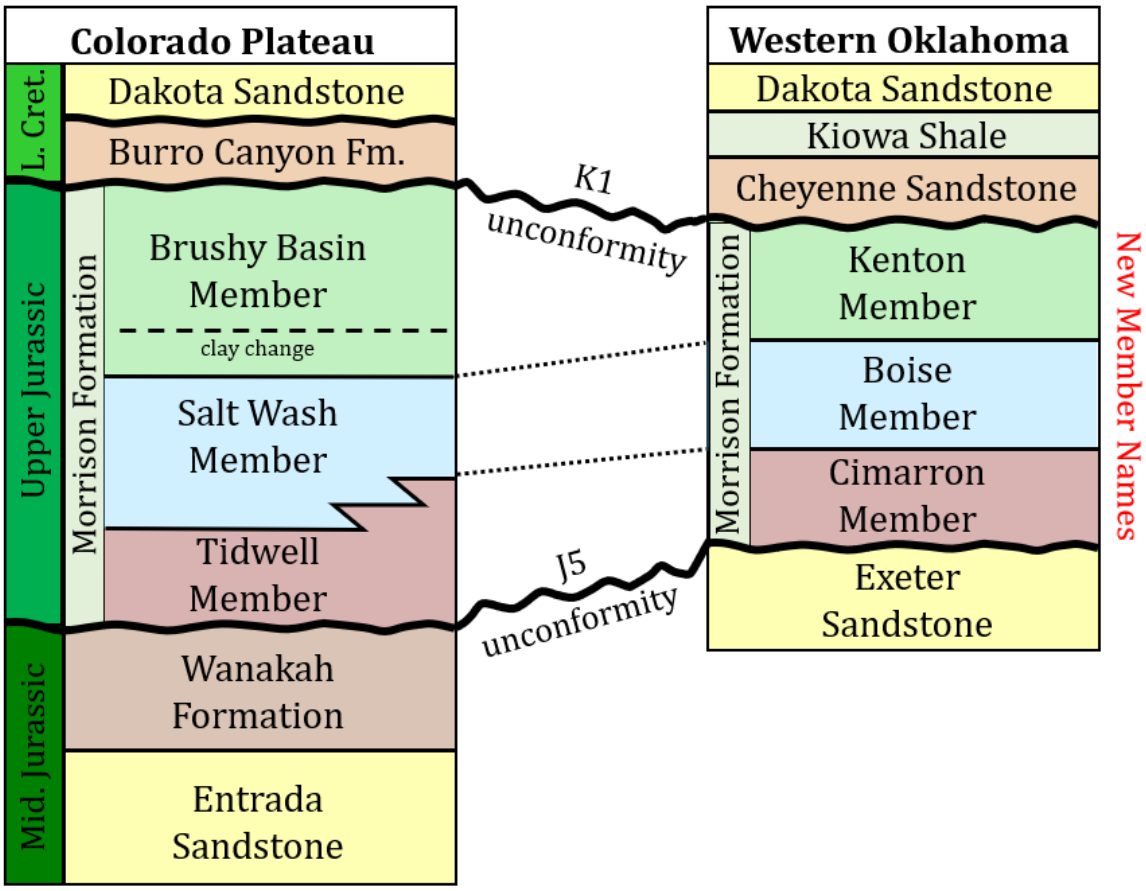

Figure 2. Regional stratigraphic comparison of the Morrison Formation of the Colorado Plateau and the newly named members of the formation in Oklahoma. Nomenclature for the formations in Oklahoma follows the usage by Suneson (2012; 2020). A tripartite division of the Morrison Formation in the western panhandle of Oklahoma is recognizable on the basis of numerous lithologic criteria. Three newly named members, the Cimarron, Boise, and Kenton Members, are described. Based on stratigraphy, depositional facies, and lithology, we propose that the newly named members of the Morrison Formation in Oklahoma correlate to the three well-established members of the Colorado Plateau.

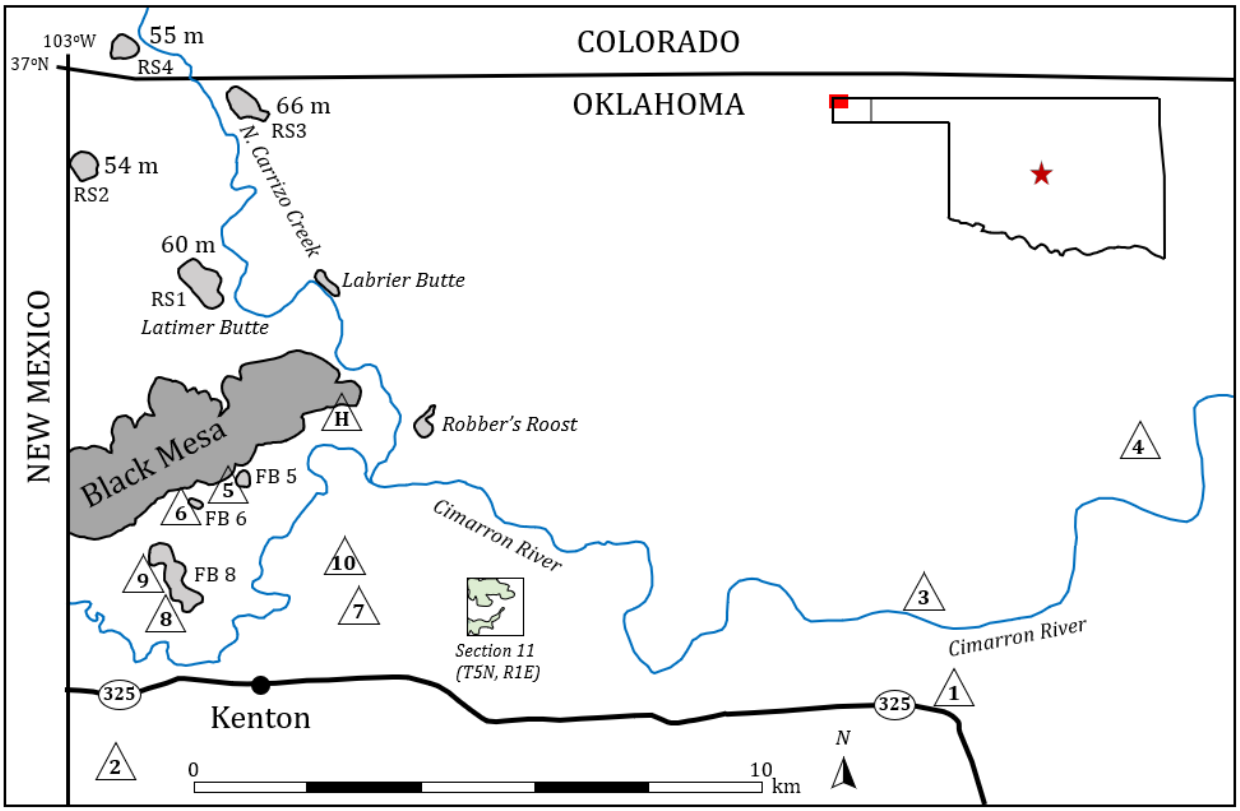

Figure 3. Map of the Kenton study area with current and historical topographical references. Four topographic features north of Black Mesa are outlined where the regional stratigraphic sections (RS 1–4) were measured. Numbers associated with these topographic features refer to the measured thickness (in meters) of the Morrison Formation. The outlined topographic features south of Black Mesa (FB 5, FB 6, FB 8) refer to listric fault blocks which have rotated away from Black Mesa. The numbered triangles denote locations of the historical Stovall quarries; the "H" triangle represents the location of the recently discovered Homestead Quarry. The Section 11 insert indicates where Stovall (1938a) measured his third and final Morrison stratigraphic section. The green area depicts the surface exposures of the Cretaceous strata within Section 11. See text for additional information.

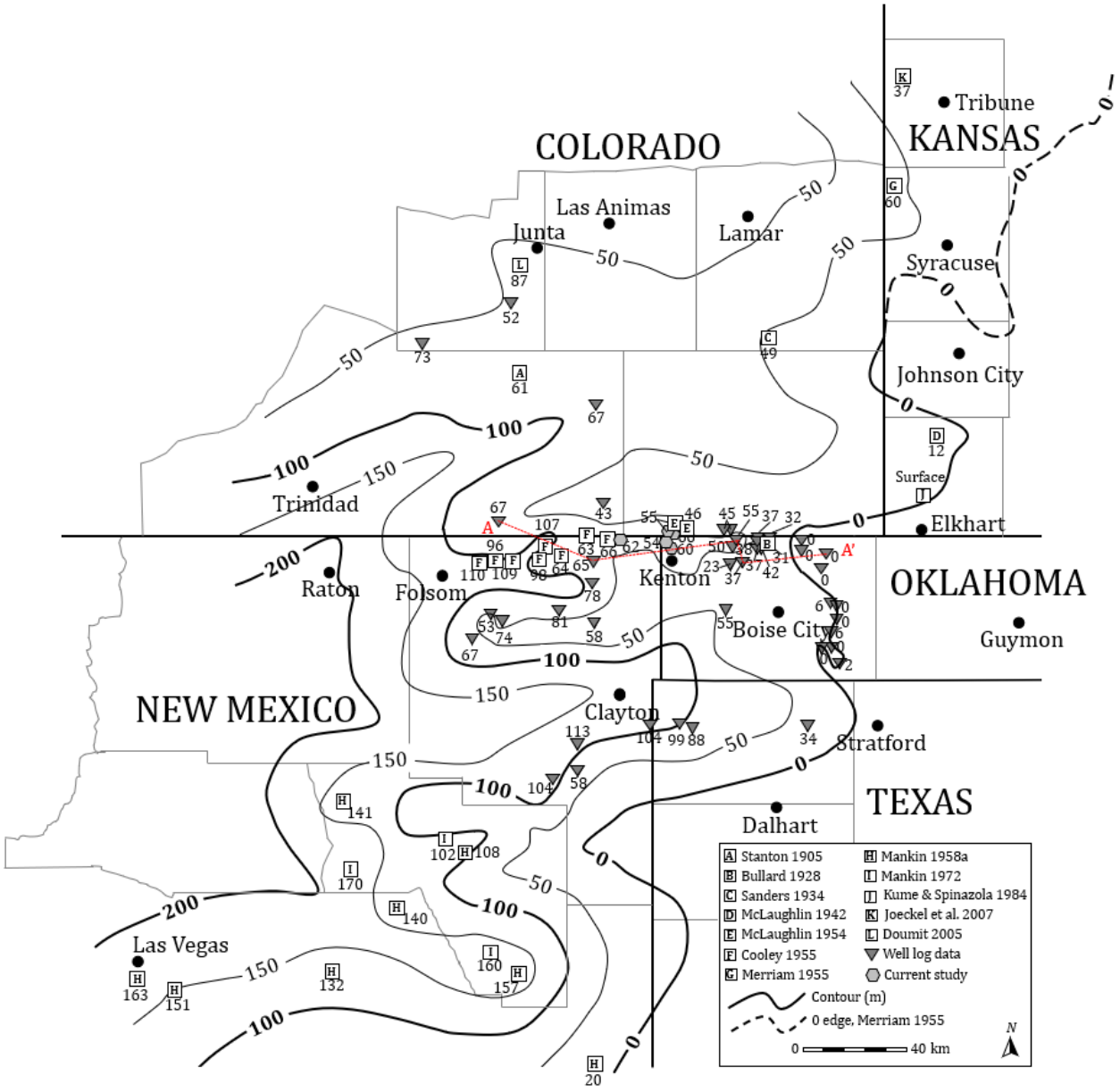

Figure 4. Isopach map of the Morrison Formation in the western panhandle of Oklahoma and surrounding states. Map was created using historical references, five newly measured regional sections, and 44 well logs. The historical references are listed in chronological order A–L. The data and contours indicate an eastward thinning trend with a zero-edge east of Boise City, Oklahoma. The dashed zero-edge contour in western Kansas is from Merriam (1955). Contour interval is 50 m. The red line A–A' show the well log cross-sectional line for Figure 6.

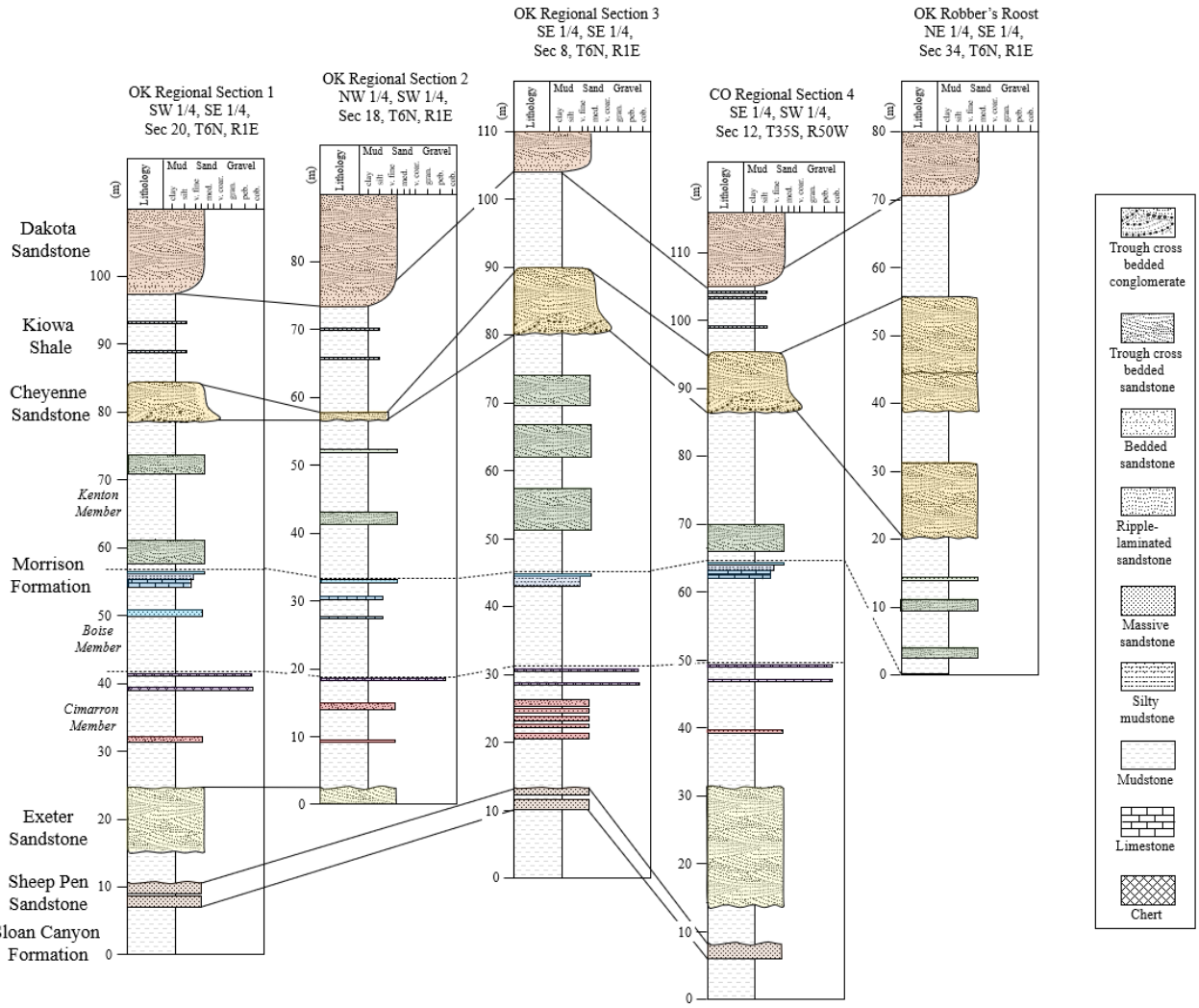

Figure 5. Regional stratigraphic sections of the Morrison Formation measured north of Black Mesa. The sections were measured using standard geologic methods and surveyed with a Nikon DTM-322 total station. The sections are flattened at the base of the Morrison Formation (the J5 unconformity) except for the Robber's Roost section, where the base of the formation is not exposed. The Morrison Formation is divided into the three newly formed members based on geological and paleontological characteristics.

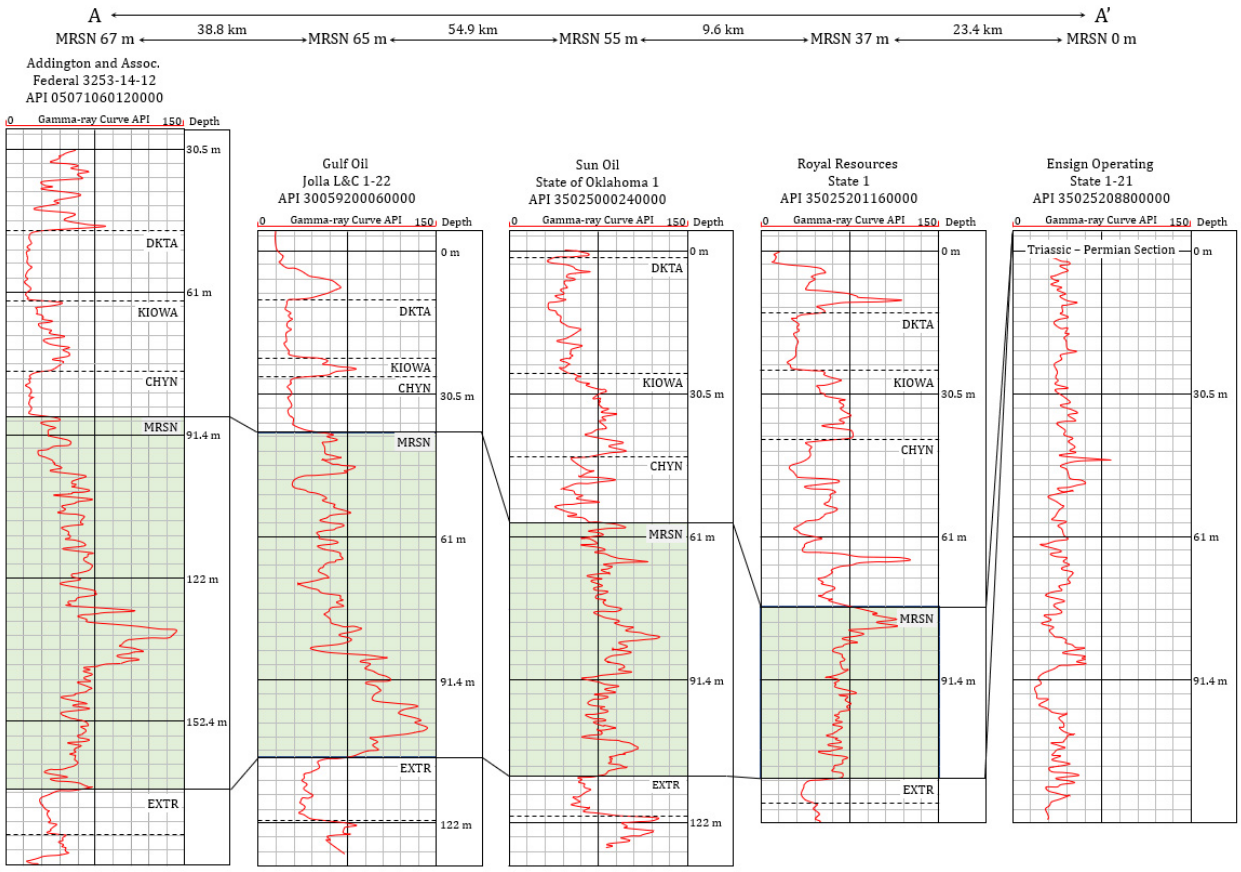

Figure 6. Well log cross-section A–A' from Figure 4. The gamma-ray curve is used to delineate the formations of the Mesozoic section. Log depth from the surface is measured in meters. Morrison Formation thickness for each log is recorded at the top of the figure. The distance between each well log is shown in kilometers. The data shows a thinning of the formation (green shade) eastward to a zero-edge where Triassic-Permian strata are exposed at the surface. Formation codes marked on the logs are as follows: Exeter Sandstone–EXTR, Morrison Formation–MRSN, Cheyenne Sandstone–CHYN, Kiowa Shale–KIOWA, and Dakota Sandstone–DKTA.

Characteristic	Cimarron	Boise	Kenton
Depositional facies	ephemeral lacustrine sandstones	perennial lacustrine carbonates	ephemeral fluvial sandstones (anastomosing & sandy braided)
Bed extent	limited lateral extent	can be regionally extensive	very limited lateral extent (an)
Lithology	siltstone/ sandstone	limestone/ cap sandstone	sandstone
Classification	quartz arenite (predominately granitic quartz)	pelmicrite/ pelsparite quartz arenite (cs)	quartz arenite
Grain size	c. siltstone/ v. fine sandstone	medium (p/o) fine (cs)	fine to medium
Average phi size	3.96 Φ [10]	1.87 Φ [4] p/o 2.38 Φ [3] cs	2.46 Φ [14] an 1.61 Φ [7] sb
Sorting (std. dev.)	mod. well (0.45) [10]	well (0.46) [4] p/o well (0.41) [3] cs	well (0.33) [14] an well (0.39) [7] sb
Rounding (ave.)	v. ang (0.45) [10]	sb ang (1.56) [3] cs	sb ang (1.32) [14] an sb rnd (2.15) [7] sb
Matrix cement	calcite	calcite	calcite, hematite, silica - seismite
Clay mineralogy	illite (98.5%)	illite (89.6%)	illite (75.4%)
Vertebrate fossils	dinosaur trackways	dinosaurs, crocodiles, turtles, fish	none reported
Invert. fossils	none reported	bivalves, ostracods	none reported
Plant fossils	none reported	petrified wood, charophytes	none reported
Soils	poorly drained	v. poorly drained	well drained

Table 1. Table comparing Oklahoma Morrison member characteristics. Numbers enclosed in brackets represent the number of samples used to calculate an average value. Abbreviations are as follows: peloids and ooids–p/o; capping sandstone–cs; anastomosing fluvial sandstones–an; sandy braided fluvial sandstone–sb.

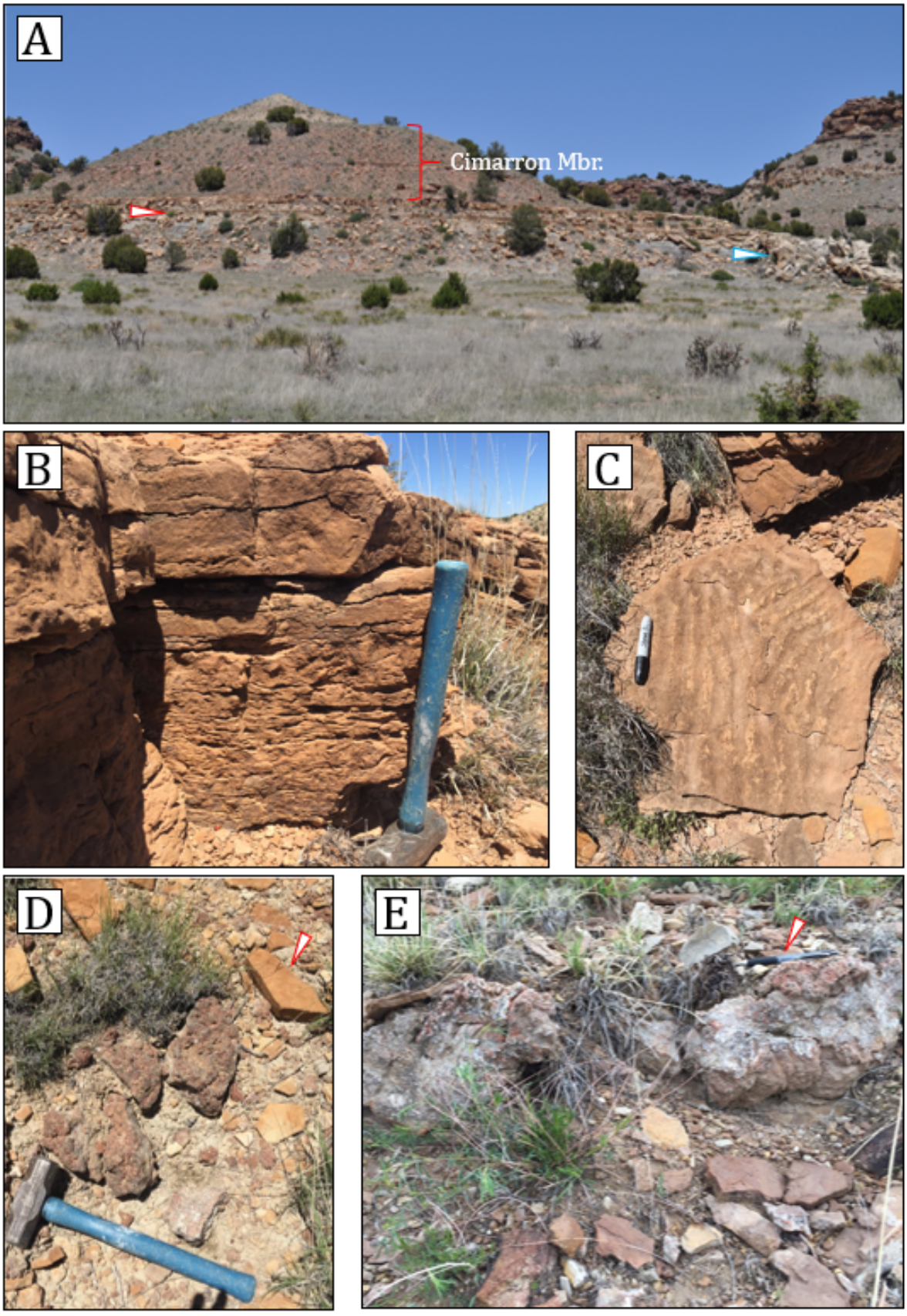
A
Cimarron Mbr.
B
C
D
E

Figure 7. Outcrop views of the lower Cimarron Member of the Morrison Formation.

A. View of the Cimarron Member section 1 km north of the Oklahoma-Colorado border (SW ¼, Sec 7, T35N, R49E) showing the J5 unconformity in contact with the Triassic Sheep Pen Sandstone (red arrow). The Exeter Sandstone can be seen juxtaposed to the Sheep Pen Sandstone (blue arrow) indicating the J5 unconformity is a complex erosional surface. The Exeter Sandstone possibly infilled paleotopographic lows on the erosional surface. No fault was observed, suggesting offset between the two formations. The Cimarron Member is easily recognized by the red illitic mudstone and ripple-laminated sandstone beds.

B. A symmetrical ripple-laminated sandstone bed typical of the Cimarron Member. Thin ripple laminae indicate shallow depositional facies. Sandstone beds are usually thin and not laterally continuous.

C. Symmetrical ripple laminations indicate a shallow clastic lacustrine environment. Marker for scale.

D. Evaporite-associated chert bed (red rocks) with associated thin dolomite bed (buff rocks; red arrow).

E. A thick, amorphous-shaped, evaporite-associated chert bed. The cherts commonly have chalcedony spherules. The chert beds in Oklahoma commonly occur as a doublet. Pen for scale (red arrow).

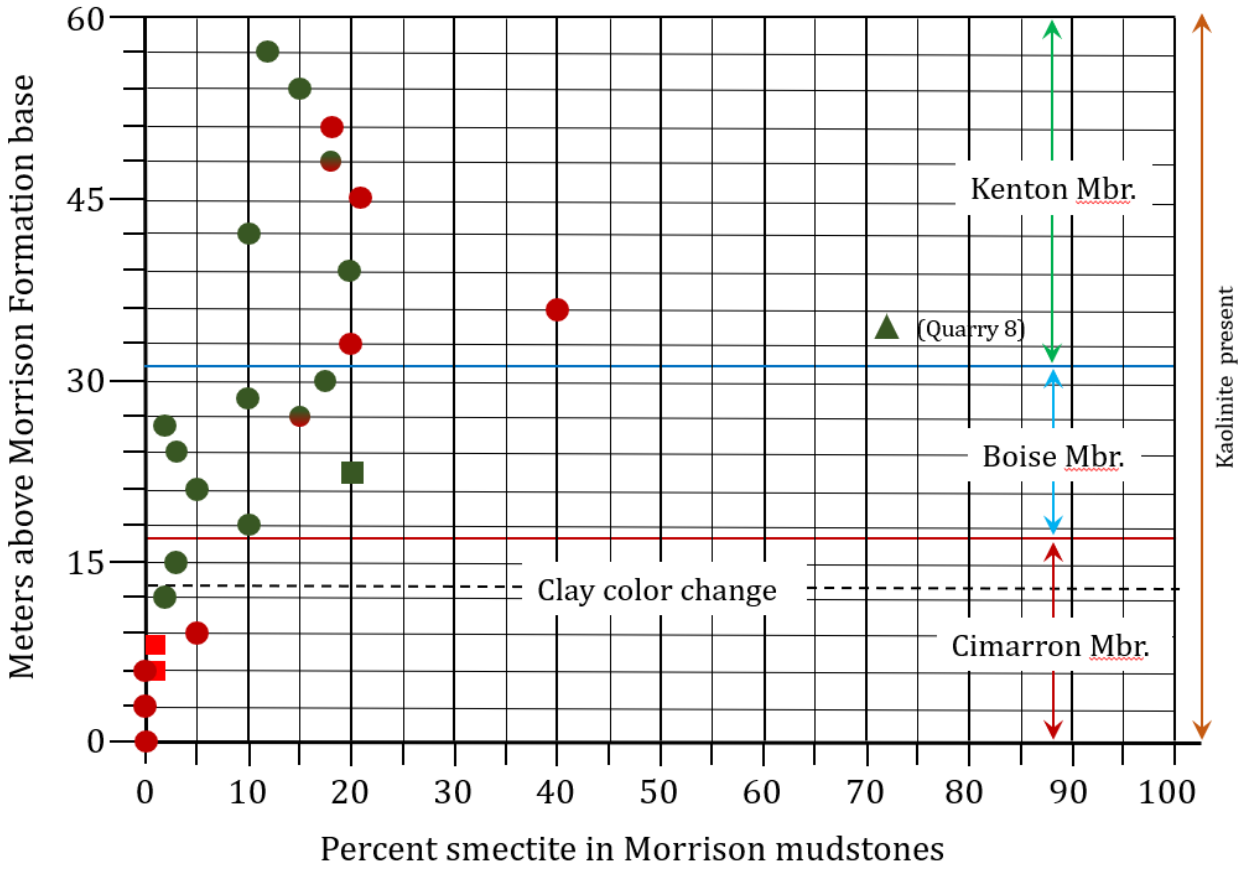

Figure 8. The Morrison Formation of Oklahoma was sampled at 3-m increments for XRD analysis. This sampling was done to determine whether or not a clay change exists, as is characteristic in the Brushy Basin Member in the Colorado Plateau. The colored circles represent samples collected north of Kenton at SE ½, Sec 8, T6N, R1E. The squares represent samples collected north of Boise City at SE ¼, NE ¼, Sec 16, T5N R5E. There is a marked color change from reddish mudstones (red symbols) to variegated mudstones (green symbols) at 13 m. The Cimarron Member mudstones are highly illitic. The Boise and Kenton Members show varying low percentages of smectite. There are two anomalous samples with higher percentages of smectite (quarry 8 and at 36 m). These samples suggest that input of volcanic ash to the basin margin was a rare occurrence.

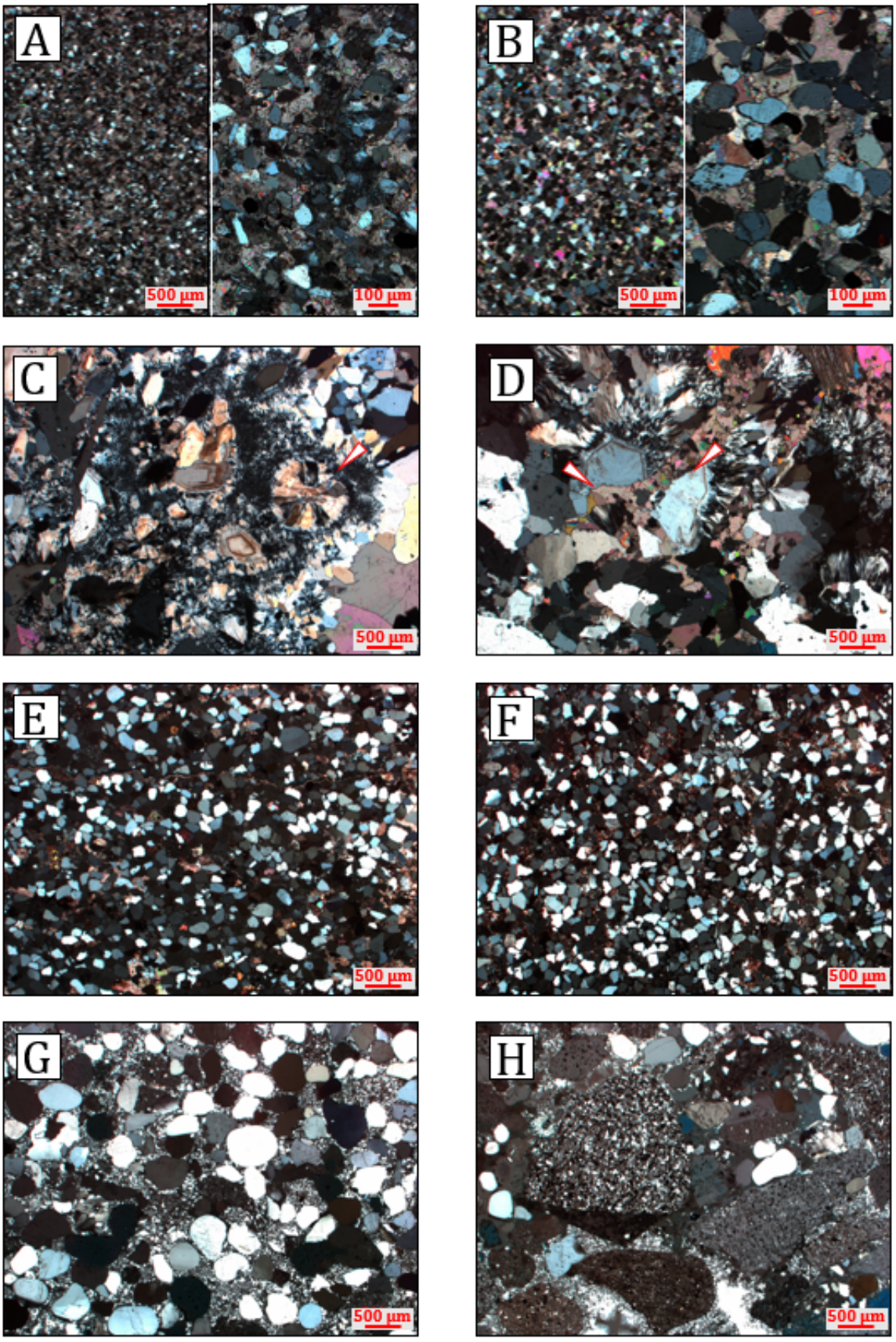
A
500 µm
100 µm
B
500 µm
100 µm
C
500 µm
D
500 µm
E
500 µm
F
500 µm
G
500 µm
H
500 µm

Figure 9. Thin section photomicrographs of Cimarron Member sandstones (**A**, **B**), and the evaporite-associated cherts (**C**, **D**). Also, the Kenton Member anastomosing channel sandstones (**E**, **F**) and the sandy braided sandstone (**G**, **H**).

A. Photomicrograph of a Cimarron Member siltstone (OK MRSN LWR 1) from an exposed section located several meters north of the Cimarron River at SE ¼, Sec 8, T5N, R1E. The siltstone is a very angular (0.29), moderately sorted (0.53), coarse silt (4.24 Φ) quartz arenite. The floating and point grain contacts indicate early calcite cementation and shallow burial.

B. Photomicrograph of a Cimarron Member sandstone (OK MRSN LWR 5), from the same location as the previous sample. The sandstone is an angular (0.62), well sorted (0.45), very fine-grained (3.33 Φ) quartz arenite. The floating and point grain contacts indicate early calcite cementation and shallow burial.

C. Photomicrograph of the Cimarron Member evaporite-associated chert. The cherts consist of large euhedral quartz grains, chalcedony spherules (red arrow), "primrose" quartz, megaquartz grains, length-slow chalcedony (indicating an alkaline environment) and zebraic chalcedony. Many euhedral quartz grains, spherules, and primrose quartz have iron (Fe) dust lines.

D. Photomicrograph of evaporite-associated chert showing late diagenetic fracturing and shearing of euhedral quartz grains (red arrows). The two halves are not from the same euhedral quartz grain. The fracture is infilled with sparry calcite.

E. Photomicrograph of the quarry 8 ephemeral fluvial sandstone. The sandstone is a subangular (1.24), well sorted (0.42), fine-grained (2.46 Φ) quartz arenite. Cement consists of calcite, silica, and hematite. The floating and point grain contacts indicate early cementation and shallow burial.

F. Photomicrograph of quarry 1 splay sandstone. The sandstone is an angular (0.73), very well sorted (0.30), fine-grained (2.33 Φ) quartz arenite. Cement consists of calcite and hematite. The floating and point grain contacts indicate early cementation and shallow burial.

G. Photomicrograph of the Kenton Member sandy braided channel sandstone. The sandstone is a subrounded (2.36), well sorted (0.50), medium-grained (1.27 Φ) quartz arenite. Silica cementation is likely related to the formation of seismites.

H. Photomicrograph of the basal sandy braided channel sandstone. The sandstone is a moderately sorted (0.67), coarse-grained (0.60 Φ) quartz arenite. Silica cementation is likely related to the formation of the seismites. Pebble, granule, very coarse- and coarse-grained sediments found in the sandstone bed are the first occurrence of large sedimentary grains transported to the Morrison basin margin of Oklahoma.

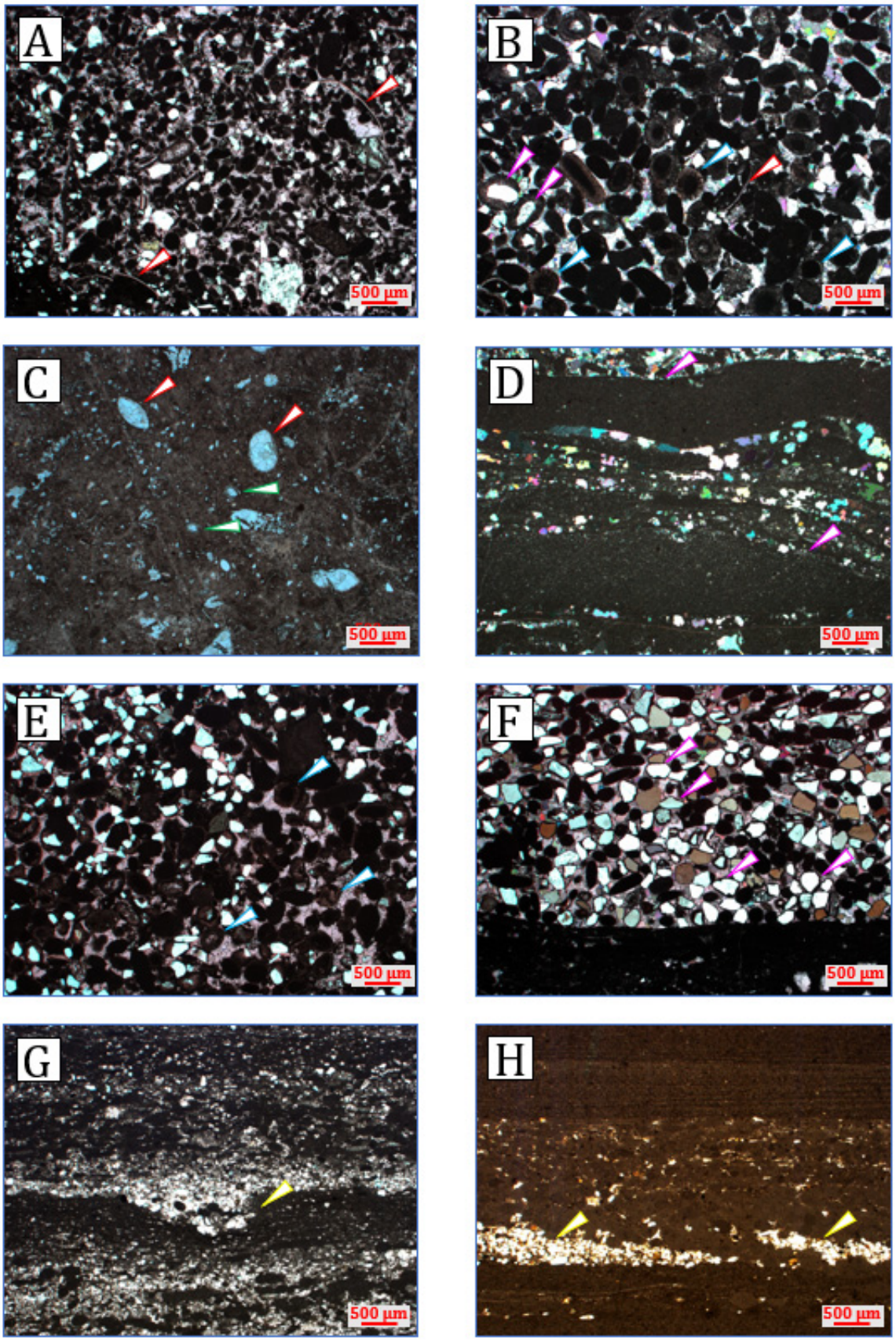
A
500 µm
B
500 µm
C
500 µm
D
500 µm
E
500 µm
F
500 µm
G
500 µm
H
500 µm

Figure 10. Thin section photomicrographs of Boise Member limestones.

A. Photomicrograph of a typical Boise Member lacustrine pelsparite with unpaired thin-shelled bivalve allochems (red arrows). The allochems are in a sparry calcite matrix.

B. Photomicrograph of the stratigraphically lowest limestone bed of the quarry 8 fault block. The limestone is a lacustrine pelsparite with radial ooids (blue arrows) with some peloids incorporating quartz grains (pink arrows). Thin-shelled bivalve unpaired valves are also present (red arrow). The allochems are in a sparry calcite matrix.

C. The Homestead Quarry ostracodal micrite. Ostracod shell rims are either infilled with the dark, organic-rich micrite or sparry calcite (red arrows). Charophyte oogonia are also present (green arrows). Although the taxa cannot be identified, they indicate a freshwater pond or lake.

D. A lacustrine microbial pelsparite from quarry 6 fault block with thick platy microbial laminae (< 1 mm, pink arrows).

E. Lacustrine pelsparite from the quarry 5 fault block. Ooids have concentric bands of radial fabric (blue arrows). The subrounded, very fine- to fine-grained quartz grains are scattered throughout the matrix and are likely eolian sourced.

F. Sandy pelsparite from the quarry 5 fault block. The large peloids and high sand percentage suggest the limestone recorded a storm event. An algal rind encased many of the sand grains (pink arrows) after the passage of the storm.

G. Finely laminated organic-rich lacustrine micrite from north of Boise City, Oklahoma. A scour from a storm event is preserved (yellow arrow) with fine-grained sand fining upward to very fine-grained sand.

H. Another example of a finely laminated organic-rich lacustrine micrite from north of Boise City. Thick laminae of peloids occur with intercalated lenses of very fine-grained sand from storm events. The samples (**G**, **H**) indicate a deeper lacustrine facies suggestive of a large lake north of Boise City, Oklahoma.

Figure 11. The laterally extensive lithologic units which top the Boise Member. **A**. The capping stromatolitic limestone bed of Lake Stovall. Stromatolite mounds are clearly seen in the bed (red arrow). **B**. The Boise Member capping limestone (blue bracket) and the capping sandstone bed (red bracket). The sandstone is a subangular (1.56), well sorted (0.41), fine-grained (2.38 Φ) quartz arenite. Survey rod and hammer for scale. These two beds can be traced throughout the study area and to adjacent states.

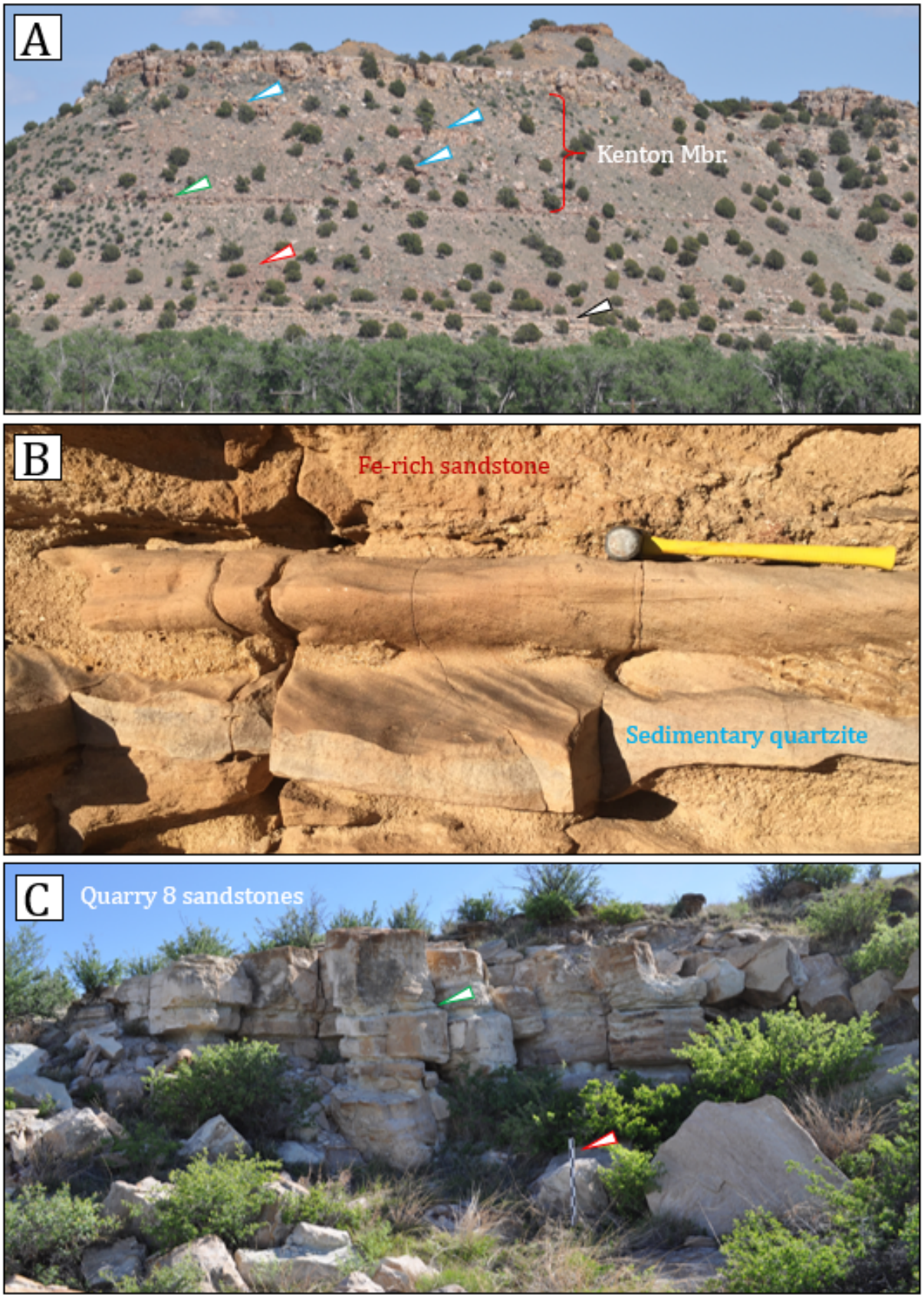
A
Kenton Mbr.
B
Fe-rich sandstone
Sedimentary quartzite
C
Quarry 8 sandstones

Figure 12. **A**. Field photograph of the Morrison Formation to highlight the Kenton Member in outcrop. Cottonwood trees present along North Carrizo Creek at the base of the photograph for scale. The Triassic Sheep Pen Sandstone (black arrow) is visible above the treetops. At this location, the J5 unconformity is between the Sheep Pen Sandstone and the Morrison Formation. The Cimarron Member is the red mudstone at the base of the formation; top is marked with the red arrow. The laterally extensive capping sandstone of the Boise Member (Lake Stovall) is marked with the green arrow. The Kenton Member is marked with the red bracket; blue arrows highlight isolated anastomosing channel sandstone beds. The Morrison Formation is capped by the thick Cheyenne Sandstone, the buff colored Kiowa Shale, and the Dakota Sandstone, which caps the mesa.

B. Field relationship between the iron-rich sandstone and the sedimentary quartzite in the sandy braided fluvial system near the top of the formation. A sharp contact is always present between the two lithologies. The sedimentary quartzite forms amorphous shapes with no discernable pattern. In thin section, the contact between the lithologies is only a few microns. In thin section, the quartzite shows the dissolution of the iron before the infilling of the porosity by the silica cement. The emplacement of the silica is thought to be from hydrothermal fluids related to the tectonic event which created the seismites. Hammer for scale.

C. Amalgamated ephemeral anastomosing fluvial channels in the Kenton Member at quarry 8. The channels are often separated by mudstone drapes (green arrow) indicating waning flow conditions. Paleo-mudcracks are preserved on some bed surfaces. Meter stick for scale (red arrow).

Figure 13. Ichnofossils found in the quarry 8 ephemeral anastomosing fluvial sandstone bed. **A**. Circular traces (red arrow) of *Cylindricum antiquus*, burrowing beetles (Coleoptera) that construct vertical tubes for shelter. *Cylindricum* is thought to have preferred a moderately moist, subaerially exposed soil. **B**. The burrows are interpreted to be a shallow termite nest. The presence and size of the nest indicate that the fluvial sand was moist at the time of formation. Both ichnofossils indicate the ephemeral nature of the fluvial sandstones.

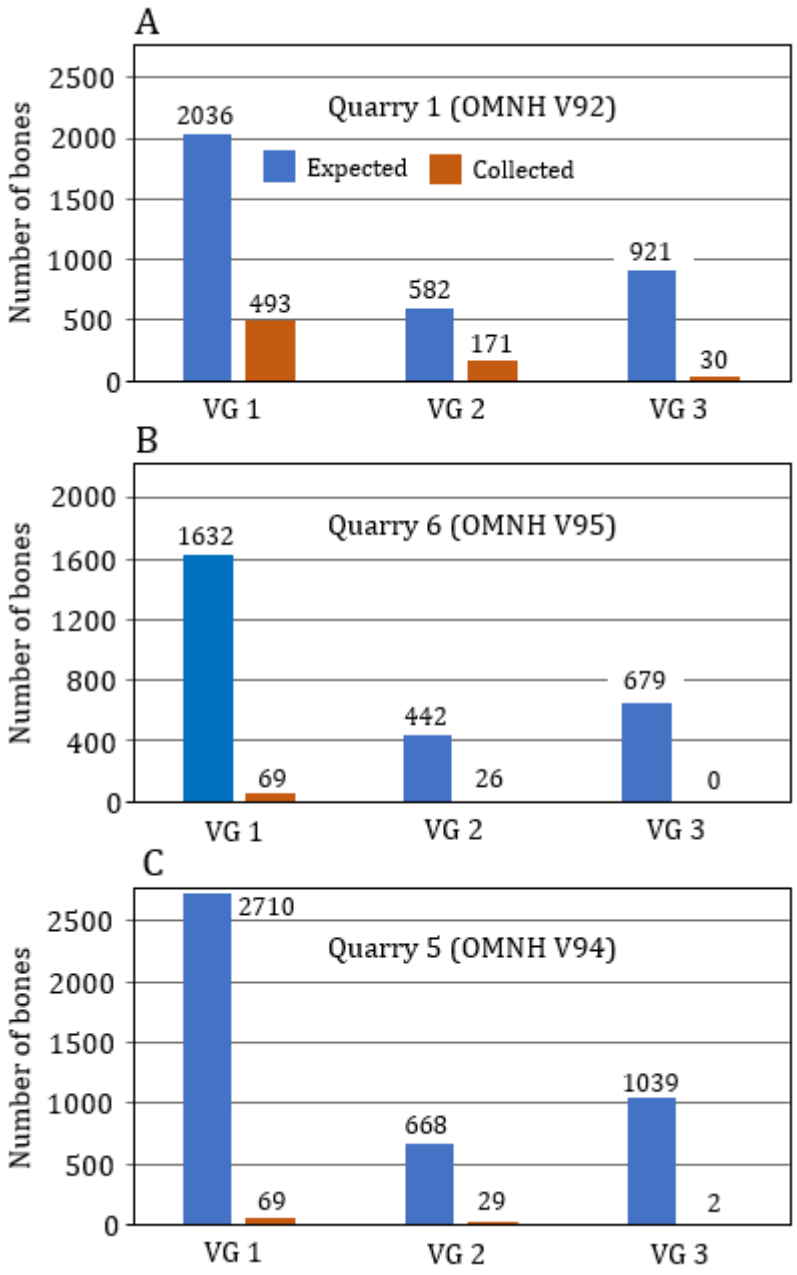

Figure 14. Graphs of Voorhies Groups. Several quarries are represented in stratigraphic order lowest to highest (**A–C**). The minimum number of individuals (MNI) for each representative genera were determined for each quarry. An estimate of the total number of bones per individual was estimated for each representative genera. Using the MNI and genera bone count, a total bone count (assuming complete disarticulation) was projected for each quarry. These bones were assigned to their corresponding Voorhies Group (blue bars). The bones collected from each quarry were placed into their respective Voorhies Group (orange bars). Comparison of the data sets indicate only a small percentage bones were moved a relatively short distance. Each quarry represents autochthonous thanatocoenosis.

CHAPTER 5: CONCLUSIONS

The research projects provide new insights into the geology, paleoecology, and paleoclimate of the northern and eastern periphery of the Morrison foreland basin during the Late Jurassic. The six identified and quantitatively described specimens of *Xenoxylon meisteri* add significant taxonomic information on *Xenoxylon* to the world xylological database. The *Xenoxylon* specimens, together with preliminarily described woods *Circoporoxylo*n and *Piceoxylon*, provide insights into the paleoecology of the Morrison Formation in central Montana. *Xenoxylon* and the other Morrison flora of the area indicate that the region was cooler and wetter, than more southern regions of the formation (fig. 2).

The numerous siderite buildups and carbonate mound springs discovered in central Montana are found in a specific stratigraphic section. The structure of Spindletop Dome resulted in the exposure of these strata along the southern and western flanks. The presence of mound springs implies that sedimentation rates were low during the period of their formation. The siderite buildup and mound springs were sourced by precipitation-fed groundwater that seeped up through Jurassic-age fractures. Standard isotopic data of the mounds confirms the hypothesis that the carbonate-rich waters were sourced from precipitation, with a short subsurface residence time. The interspersed stratigraphic position of the mound springs indicates periods of increased precipitation interspaced with drier intervals. Some mound springs incorporate fossil flora, indicating the close proximity of plants signifying an ambient water temperature for the mound springs.

In the western Oklahoma panhandle, the Morrison Formation depositional facies are an extension of those of the Colorado Plateau. The three newly described members likely correlate to the well-established Tidwell, Salt Wash, and Brushy Basin Members of the Colorado Plateau. The

depositional facies in Oklahoma indicate that sedimentation rates were low at the basin periphery with the first influx of coarse-grained fluvial sedimentation near the top of the formation.

The three members indicate a variable paleoclimate throughout the deposition of the formation at the eastern basin margin. The Cimarron Member consists of numerous small ephemeral clastic lake deposits that formed as the distal facies of the Tidwell alluvial plain. The facies suggest a seasonal climate with marked periods of precipitation. The Boise Member consists of numerous perennial limestone lake deposits at the distal margin of the Salt Wash alluvial plain. The top of the Boise Member is marked by laterally extensive limestone and sandstone beds, called Lake Stovall. The perennial lakes and Lake Stovall indicate a wet climatic trend at the eastern basin margin during this period. Three fossil woods (*Agathoxylon*, *Cupressinoxylon*, and *Xenoxylon*) were discovered in the Morrison Formation of the Oklahoma panhandle (Richmond et al., 2018). The fossil wood climatic proxies correspond with the sedimentology of the Boise Member, indicating a period of increased precipitation. The Kenton Member records the progradation of the distributive ephemeral fluvial systems to the basin margin in Oklahoma and are similar to the fluvial facies of the Brushy Basin Member in Colorado. Interpreted from the taphonomic data of the vertebrate fossils, the basal stratigraphic section of the Kenton Member experienced a series of droughts. In general, the Kenton Member was drier relative to the Boise Member, but there were flood and crevasse splay events, indicating short periods of high rainfall.

The Morrison Formation at the northern (Montana) and eastern (Oklahoma) basin margins are mudstone-dominated with accompanying lacustrine, palustrine, and anastomosing fluvial depositional facies. Both basin margins experienced low sedimentation rates. During the Late Jurassic, the Grass Range central Montana research area was at a paleolatitude of 50º N (Richmond et al., 2019). The modern latitudinal difference between Grass Range, Montana and Kenton,

Oklahoma is 10 degrees. During the Late Jurassic, the Oklahoma panhandle region was at a paleolatitude of 40º N. Both regions were within a Ferrel Cell latitudinal band during the Late Jurassic. In a Ferrel Cell, westerly winds are prevalent and air circulation is from a subtropical high (horse latitudes) to more northern latitudes. The orographic effect from the Sevier orogenic belt and the Mogollon highlands in the western and southwestern provinces of the North American plate had a dominant influence on the climate of the Colorado Plateau. The rain shadow effect likely diminished eastward toward the basin margin in Oklahoma. Therefore, it is likely that the eastern basin margin in Oklahoma experienced a wetter climate than the Colorado Plateau. Moisture input from the newly forming southern Tethys Sea (Gulf of Mexico) might have, at times, contributed seasonal rainfall.

In central Montana, the sedimentary and xylological climatic proxies (e.g. *Xenoxylon* and mound springs) suggest a cool, wet climate. The wet climate suggests that the orographic effect from mountains to the west had minimal impact on precipitation. Moisture input to the region may have been due to continentality from the retreating Sundance Sea. Temperatures may have been cooler in the northern latitudes due to seasonal southerly fluctuations of the polar cell. In summary, although average yearly temperatures in the two regions differed, each region experienced a higher precipitation rate than that of the Colorado Plateau (fig. 2).

Figure 2. Map of western North America during the Late Jurassic. The research focus areas marked by the red (Montana) and green (Oklahoma) dots representing dinosaur quarries. The Morrison basin is shown with a color overlay showing the paleoclimate/precipitation interpretation. The southwest and western regions are interpreted to be hotter and drier than the Oklahoma basin margin. During the Late Jurassic, Oklahoma likely received more precipitation than the Colorado Plateau. The climate was progressively cooler and wetter in the more northern latitudes of central Montana. Image modified from R. Blakey.

CHAPTER 6: CONTINUING RESEARCH

1. Late Jurassic xylology and palynology

Two additional genera have been preliminarily described from the Morrison Formation of central Montana from the OMNH collection; *Piceoxylon* (Richmond et al., 2019a) and *Circoporoxylon* (Richmond et al., 2019b). Initial observations and cell measurements suggests sample MT MRSN 5E PW 4 is a different wood genera from those previously identified. There are numerous samples in the OMNH collection. Each should be reviewed and described to fully understand the forest ecology of the Late Jurassic in central Montana. Additional fossil wood genera should confirm the current climate hypothesis of the northernmost part of the basin.

A manuscript is in preparation to describe three newly discovered fossil woods (*Agathoxylon*, *Cupressinoxylon*, and *Xenoxylon*) from the Morrison Formation of the Oklahoma panhandle (Richmond et al., 2018). The presence of the three wood genera suggests a mixed woodland was present during the deposition of the Boise Member. *Agathoxylon* is known from the Morrison Formation of Utah (Tidwell and Medlyn, 1993; Gee et al., 2019). The interpreted climatic preference for *Agathoxylon* is a warm humid climate with little to no seasonal variation (Gee et al., 2019). *Cupressinoxylon* is a mid-latitude wood with an additional occurrence known from the Morrison Formation of South Dakota (Lutz, 1930). The *Xenoxylon* occurrence in Oklahoma is the southernmost representation of the genus in North America. It is also possible that this southern occurrence of *Xenoxylon* may be the oldest in North America since the Boise Member correlates to the Colorado Plateau Salt Wash Member of the Morrison Formation. The presence of *Xenoxylon* suggests that at times the climate was cool and wet during the Late Jurassic of western Oklahoma. The fossil wood proxies correspond with the sedimentology of the Boise Member, indicating a period of increased precipitation.

A recent xylological field trip to south-central Utah occurred in 2019 at the request of the Bureau of Land Management to collect newly discovered petrified wood in the Morrison Formation. Several fossil woods were collected. Several specimens require identification. The fossil woods were collected near the original site of "*Xenoxylon morrisonense*" Tidwell. A few of these samples might facilitate the reclassification of "*X. morrisonense*".

The Mygatt Moore Dinosaur Quarry of the Morrison Formation in western Colorado is one of the few locations where both dinosaur and plant fossils have been recovered. Petrified wood samples have been collected from the quarry and are currently housed at the Museum of Western Colorado. Since the original thin sections of "*Xenoxylon moorei*" Tidwell are poorly preserved, some of the woods in the Museum of Western Colorado collection may help to redefine "*X. moorei*".

A large diameter tree was discovered in the Stephens-Howe Quarry in the Morrison Formation near Greybull, Wyoming. A previous sampling of the tree during the summer of 2018 showed it to be well preserved. Unfortunately, the samples taken were near the buttress of the tree and did not allow for cellular identification. The tree can be resampled and described. The tree could also be sampled for tree ring data for climatic interpretation.

A small wood fragment was discovered in the Upper Jurassic Knoxville Formation of northern California. The wood has been described and identified as *Protocedroxylon*. An abstract describing the wood has been completed but not yet submitted nor presented.

Comparison of different fossil woods from the *Xenoxylon* project reveal a wide variation in fossil gymnosperm ray height. Ray height may be an additional definitive characteristic of fossil wood genera. Rays may vary in length according to their position in the tree (e.g. basal, mid, or upper trunk, or a branch). Additionally, they might be related to latitude, temperature, or

precipitation. An interesting research project would be to review ray heights from modern gymnosperms to observe and measure any variability from different parts of the tree. Additionally, review the ray heights of modern gymnosperms from different latitudes and climatic zones.

The northernmost surface exposures of the Morrison Formation in Montana contain coal beds. Coal mining was a vast operation in the region during the early 20th century. All commercial coal mines were reclaimed during the 1970's and 1980's. It is now difficult to find coal beds still exposed at the surface. During a 2018 field trip to Great Falls, Montana, permission was given to collect samples from a private mine. A palynology study would provide additional insights into the climate in the northern foreland basin during the Late Jurassic.

2. The carbonate mound springs of central Montana

Additional research for the carbonate mound springs should include the stratigraphic position of each individual mound. This information is known for a number of mounds. The stratigraphic data would help to identify any potential variation in mound geochemistry and isotopic data through time.

There is a slight discrepancy in the geochemical data. XRF analysis suggests that the iron-rich carbonates are siderite, whereas the XRD analysis indicates they are ankerite. Additional sampling and analyses would help resolve these discrepancies.

Three samples were analyzed for standard isotopic data. Samples from additional mound springs could create a meaningful data cluster and show isotopic changes through time. An isotopic data baseline should be established using non-tufa carbonates. A peloidal wackestone, interpreted to represent a shallow waterhole, and paludal limestones could be used for the isotopic baseline.

Clumped isotope analyses should be run to determine paleotemperature of the mound springs and other carbonates.

Several parallel research analyses should be run to determine an age of the Morrison Formation of central Montana. (1) Samples of the siderites could be evaluated to determine if there is sufficient iron to carry a paleomagnetic signature. If so, it would be necessary to obtain oriented samples from the siderite buildups in the field to determine the paleomagnetic stratigraphy. (2) U-Pb dates can be extrapolated from the carbonates if there are sufficient radioactive isotopes in the limestones. (3) Zircon dates have been determined from the underlying marine Swift Formation and the overlying Lower Cretaceous Kootenai Formation but not from the Morrison Formation. Personal observation of the Morrison Formation sandstone petrology indicates the presence of euhedral zircons. If all three analyses yield dates, then a comparison of the data sets should be undertaken.

3. Geology of the Oklahoma panhandle

The first Morrison Formation seismites (Richmond et al., 2018) were discovered during the investigation of the research area. The braided sandstone bed that contains the seismites consists of two different lithologic types: a hematitic sandstone and chalcedony-cemented quartzite. A sharp contact always delineates the two lithologic types. At the top of the sandstone bed are small coalescing hematitic rings, signifying gas fluidization. Soft-sediment deformation structures include convolute and recumbent beds, sills, gas fluidization, fluid escape conduits, and possibly sand volcanoes. Cumulatively, these structures are interpreted to be seismites and have been traced for a total distance of 56 km. The evidence suggests the occurrence a large-scale paleoearthquake. Further research into the seismites and the tectonics at the basin margin should be completed.

The evaporite-associated cherts (Richmond et al., 2019) were noted and reviewed during this research project. In the same Morrison stratigraphic section, additional chert beds have been noted in eastern New Mexico. Field research should be conducted to find additional chert beds in the surrounding states. The antecedent lacustrine evaporites designate a period of increased evaporation, due to either increased temperature or decreased precipitation. A more thorough examination of the cherts, their regional extent, and climatic implications should be completed. This could provide evidence of a distinct arid interval during the Late Jurassic in the southern Colorado Plateau region.

The presence of the large paleo Lake Stovall in the western panhandle of Oklahoma may correlate to other lakes in southern Colorado, where large dinosaur trackways have been noted and described. A regional field study should be undertaken to determine the areal extent of the lake and whether it correlates to other described Morrison paleolakes in the region. The study should include a review of the different lithofacies of Lake Stovall to determine the role of the depositional facies, tectonics, and climate.

Taphonomic evidence indicates that a series of droughts occurred in the lower portion of the Kenton Member in the western panhandle. The Dry Mesa Dinosaur Quarry is the result of a severe drought that occurred in the lower Brushy Basin Member of southern Colorado. It would be interesting to study whether there is a stratigraphic correlation between the drought events. Research should include the taphonomy of any additional dinosaur quarries in this same stratigraphic section to determine if the quarries are drought related. If a correlation could be established, the evidence would suggest a widespread arid period during the Late Jurassic.

Twelve Oklahoma Morrison Formation limestone samples were sent for U-Pb date analysis. At present, three samples have been processed and only one reasonable date has been obtained.

Completion of such analysis would be the first for the Morrison Formation of Oklahoma and could offer insights into sedimentation rates at the basin margin. The information would also allow a comparison with the dates of the formation on the Colorado Plateau.

The Lower Cretaceous Cheyenne Sandstone in Kansas has been well-studied. However, the Cheyenne Sandstone has not been well documented in Oklahoma. An interesting study would include the depositional facies, the amalgamation of fluvial channels in the eastern part of the research area, and its correlation to the Lytle Sandstone of the Colorado Front Range. The Cheyenne Sandstone is well known for its large petrified logs preserved in conglomeratic fluvial beds. Thus far, the fossil wood appears to not be well preserved, but only a few samples have been reviewed. If the fossil wood could be identified, it might provide a climatic contrast to the Morrison Formation.

The Kiowa Formation and Dakota Sandstone in Kansas are well studied, but the formations in Oklahoma have not been described. These formations recorded the first Cretaceous marine transgression-regression cycle. Understanding the depositional facies, vertebrate and invertebrate paleontology, and marine ichnofacies of these formations would provide insights into this marine transgression in Oklahoma, and correlating strata in Texas, Kansas, and New Mexico.